PHOTOCHEMICAL STRATEGIES FOR CARBON–CARBON FORMING PROCESSES

Luca Buzzetti

UNIVERSITAT ROVIRA i VIRGILI

Photochemical Strategies for Carbon–Carbon Forming Processes

LUCA BUZZETTI

DOCTORAL THESIS
2018

UNIVERSITAT ROVIRA I VIRGILI
PHOTOCHEMICAL STRATEGIES FOR CARBON–CARBON FORMING PROCESSES
Luca Buzzetti

UNIVERSITAT ROVIRA I VIRGILI
PHOTOCHEMICAL STRATEGIES FOR CARBON–CARBON FORMING PROCESSES
Luca Buzzetti

Luca Buzzetti

Photochemical Strategies for Carbon–Carbon Bond Forming Processes

Doctoral Thesis

Supervised by Prof. Paolo Melchiorre

ICIQ – Institut Català d'Investigació Química

UNIVERSITAT ROVIRA i VIRGILI

Tarragona
2018

UNIVERSITAT ROVIRA i VIRGILI

ICIQ Institut Català d'Investigació Química

Prof. Paolo Melchiorre, ICREA Research Professor & ICIQ Group Leader

I STATE that the present study, entitled "Photochemical Strategies for Carbon–Carbon Bond Forming Processes", presented by LUCA BUZZETTI for the award of the degree of Doctor, has been carried out under my supervision at the Institut Català d'Investigació Química (ICIQ).

Tarragona, September the 3rd, 2018

Doctoral Thesis Supervisor

Prof. Paolo Melchiorre

UNIVERSITAT ROVIRA I VIRGILI
PHOTOCHEMICAL STRATEGIES FOR CARBON–CARBON FORMING PROCESSES
Luca Buzzetti

Acknowledgements

I would like to thank my supervisor Professor Paolo Melchiorre for giving me the opportunity to join his research group and take part in this exciting trip.

Additionally, I would like to thank all the former and current members of the Melchiorre group for sharing their knowledge and helping me going through my doctoral studies. I want to thank Dr Lorna Piazzi, Maria Checa and Núria Planella for the administrative support.

I would like to express my gratitude to my family and my friends for the support they have provided me along these 4 years.

I would like to thank all the research support units at ICIQ, in particular I am indebted to the NMR-staff, the spectroscopy unit and the chromatography unit. I would also like to acknowledge the financial support from the Institute of Chemical Research of Catalonia (ICIQ) from the European Research Council for the ERC starting grant (278541-ORGA-NAUT) and ERC consolidator grant (681840-CATA-LUX).

Additionally, I am personally grateful to:

- MINECO for a FPI predoctoral fellowship CTQ2013-45938-P
- MINECO for a mobility fellowhip EEBB-I-17-12415

UNIVERSITAT ROVIRA I VIRGILI
PHOTOCHEMICAL STRATEGIES FOR CARBON–CARBON FORMING PROCESSES
Luca Buzzetti

List of Publications

Some of the results presented in this thesis have been published:

- Silvi, M., Verrier, C., Rey, Y. P., Buzzetti, L., and Melchiorre, P., "Visible-Light Excitation of Iminium Ions Enables the Enantioselective Catalytic β-Alkylation of Enals". *Nat. Chem.*, **2017**, *9*, 868-873.

- Buzzetti, L., Prieto, A., Roy, S. R. and Melchiorre, P., "Radical-Based C-C Bond-Forming Processes Enabled by the Photoexcitation of 4-Alkyl-1,4-dihydropyridines". *Angew. Chem. Int. Ed.*, **2017**, *56*, 15039-15043.

- Verrier, C., Alandini, N., Pezzetta C., Moliterno, M., Buzzetti, L., Hepburn, H. B., Vega-Peñaloza, A., Silvi, M. and Melchiorre, P., "Direct Stereoselective Installation of Alkyl Fragments at the β-Carbon of Enals via Excited Iminium Ion Catalysis". *ACS Catalysis*, **2018**, *8*, 1062-1066.

UNIVERSITAT ROVIRA I VIRGILI
PHOTOCHEMICAL STRATEGIES FOR CARBON–CARBON FORMING PROCESSES
Luca Buzzetti

Dai, dai, dai!

(René Ferretti)

UNIVERSITAT ROVIRA I VIRGILI
PHOTOCHEMICAL STRATEGIES FOR CARBON–CARBON FORMING PROCESSES
Luca Buzzetti

Table of Contents

Chapter I: General Overview **1**
1.1 Light and Matter 1
1.2 General Objectives and Summary 5
1.2.1 The Excited-State Reactivity of Iminium Ions 5
1.2.2 Extending the Reactivity of Excited-State Iminium Ions 6
1.2.3 Reactivity of 1,4-Dihydropyridine in the Excited State 7
Chapter II: Introduction **9**
2.1 Light Absorption 9
2.2 Light Absorption and Photochemistry 11
2.3 The Photophysic of Excited States 13
2.4 Unimolecular Processes 15
2.5 Photo-induced Electron Transfer 18
2.6 Energy Transfer 21
2.7 Proton Transfer 24
2.8 Atom Transfer 26
2.9 Mechanistic Considerations 27
Chapter III: The Excited-State Reactivity of Iminium Ions **29**
3.1 Introduction 29
3.2 Iminium Ion Catalysis 31
3.3 Iminium Ion as Chromophore 33
3.4 Target of the Project 35
3.5 The Choice of the Donor 37
3.6 Results and Discussion 39
3.6.1 Bathochromic Shift 40
3.6.2 Preliminary Results and Optimization 41
3.6.3 Designing a New Reaction Set-Up 45
3.6.4 Design of a New Family of Redox Stable Catalysts 46
3.6.5 Scope of the Reaction 50
3.7 Mechanistic Investigations 51
3.7.1 Photophysical Studies of the Iminium Ions 51
3.7.2 Luminescence and Stern-Volmer Quenching Studies 55
3.7.3 Radical-Radical Coupling vs Chain Propagation 58
3.7.4 Effect of the Enal Geometry 60
3.8 Extension of the Scope 61
3.9 Conclusions 63
3.10 Experimental Section 64
Chapter IV: Expanding the Reactivity of Excited-State Iminium Ions **108**

4.1 Introduction 108
4.2 Strategies to Prevent the Back Electron Transfer (BET) 109
4.3 Results and Discussion 112
4.3.1 Oxiranes as Radical Precursors 112
4.3.2 Generation of Alkyl Radicals through C–C Bond Fragmentation 118
4.3.3 Acetals as Radical Sources: a "Half Failed" Approach 118
4.3.4 Alkyl Dihydropyridines as Radical Sources: a Succesful Approach 123
4.3.5 Target of the Project 126
4.3.6 Reaction Optimization 127
4.3.7 Scope of the Reaction 128
4.3.8 Functionalization of Glucosides 129
4.3.9 Reaction Mechanism 130
4.4 Conclusions 131
4.5 Experimental Section 132
Chapter V: Reactivity of 1,4-Dihydropyridine in the Excited State 156
5.1 Introduction 156
5.2 Metalla-photoredox Catalysis 158
5.3 1,4-Dihydropyridine: Ground-State Properties and Reactivity 162
5.4 1,4-Dihydropyridine: Excited-State Properties and Reactivity 167
5.5 Design and Target of the Project 169
5.6 Results and Discussion 171
5.6.1 Photophysical Characterization of 4-alkyl DHPs 171
5.6.2 Proving the Dual Role of 4-alkyl DHPs as Photoreductants and Radical Sources 173
5.6.3 Preliminary Results and Optimization 176
5.6.4 Scope of the Process 178
5.6.5 Mechanistic Considerations 180
5.7 Future Directions 181
5.7.1 Trapping of the Radicals with SOMOphiles 181
5.7.2 Giese-type Radical Conjugate Additions 183
5.7.3 Dihydropyridines for Amidation Reactions 287
5.8 Conclusions 192
5.9 Experimental Section 192
Chapter VI: General Conclusions 216

UNIVERSITAT ROVIRA I VIRGILI
PHOTOCHEMICAL STRATEGIES FOR CARBON–CARBON FORMING PROCESSES
Luca Buzzetti

Chapter I

General Overview

1.1 Light and Matter

Human beings have always been fascinated by light and its intimate interaction with matter. The relation between light and matter stands at the basis of several cultures; for instance, in the Book of Genesis, the creation of light is described right after the creation of matter: *"And God said: Let there be Light, and there was Light. And God saw the Light, that it was good; and God divided the Light from the darkness"*. Similar tales are present in the oldest books of other culture.[1] Light reveals matter and allows the perception of the surrounding world through the sense of sight. Many Greek philosophers, including Empedocles, Plato and Euclid, supported the so called *emission theory* that describes vision as the result of the reflection of beams coming from the eyes. The alternative *intromission theory*, proposed by Aristotle and Galen, and similar to the one accepted nowadays, involves the acquisition of the beams coming from an external source of light and reflected by the objects.

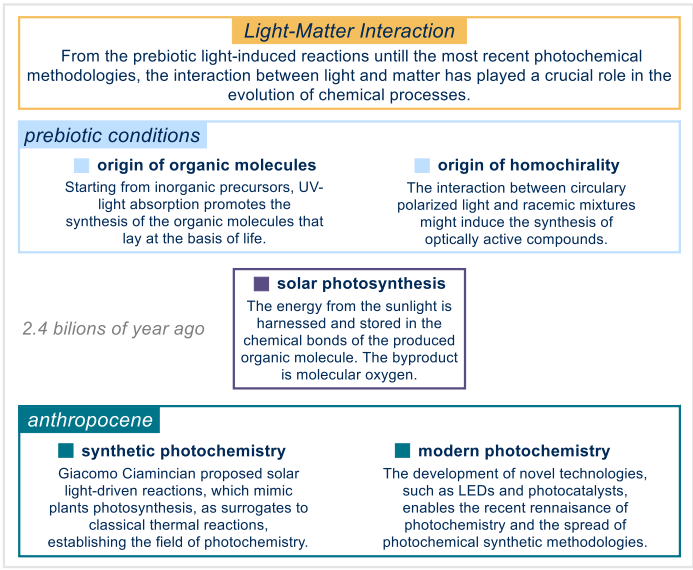

Figure 1.1: The interaction between light and matter has played a crucial role in the evolution of chemical processes.

The interaction between light and matter has been fundamental for the origin of organic molecules that lay at the basis of life. In fact, UV light has been the most important energy source on the primitive Earth. It has been proposed that far ultraviolet irradiation of inorganic

[1] Albini, A., "Photochemistry". 2013; Vol. 41, Springer.

compounds, in the prebiotic environment, allowed the formation of basic organic molecules, nucleobases and amino acids precursors.[2] Moreover, the interaction between circularly polarized light and racemic mixtures is proposed as one of the events that originated homochirality. In principle, polarized light could induce the formation of optically active species starting from racemic precursors.[3] Then, different mechanisms, including selective crystallization and autocatalysis, could have been operative for the amplification of this initial photo-induced enantiomeric enrichment.[4]

Sometime between 2.4 and 2.35 billion years ago a living organism, most probably a cyanobacterium, absorbed visible-light photons and exploited their energy for the fixation of inorganic carbon into organic compounds, using water as source of electrons and releasing molecular oxygen as byproduct.[5] This crucial event started the evolution of one of the most important light-triggered chemical processes that allows life on Earth: *photosynthesis*. Through solar photosynthesis, the energy from the sunlight is harnessed and stored in the chemical bonds of the produced organic molecules. The products of this process represent the principal energy sources of all the heterotrophic organisms including humans. Nowadays, for the production of energy and feedstock, our civilization mainly relies on fossil fuels which primarily derive from solar photosynthetic processes; in fact, they are the result of the action of heat, pressure and anaerobic decomposition on biomass along geological time. Finding alternative, sustainable, abundant and well distributed energy sources is one of the most important challenges of the 21st century.[6] Giacomo Ciamician, the father of synthetic photochemistry, brought the attention of the scientific community attention to this topic in 1912, when he foresaw the crucial role of chemistry in providing novel solutions for a fossil fuel-free society. Within his vision, he proposed solar light-driven chemical transformations, which mimic plants photosynthesis, as valid surrogates to classical thermal reactions, thus laying the foundations for the advent of modern photochemistry.[7] More than 100 years later, photochemistry represents a modern branch of science, at the interface between light and

[2] a) Toupance, G., Bossard, A., Raulin, F., "Far UV irradiation of model prebiotic atmospheres" *Origins of life* **1977**, *8*, 259. b) Barks, H. L., Buckley, R., Grieves, G. A., Di Mauro, E., Hud, N. V., Orlando, T. M., "Guanine, Adenine, and Hypoxanthine Production in UV-Irradiated Formamide Solutions: Relaxation of the Requirements for Prebiotic Purine Nucleobase Formation" *ChemBioChem* **2010**, *11*, 1240. c) Dondi, D., Merli, D., Pretali, L., Fagnoni, M., Albini, A., Serpone, N., "Prebiotic chemistry: chemical evolution of organics on the primitive Earth under simulated prebiotic conditions" *Photochem. Photobiol. Sci.* **2007**, *6*, 1210.

[3] Kagan, H., Moradpour, A., Nicoud, J., Balavoine, G., Tsoucaris, G., "Photochemistry with circularly polarized light. Synthesis of optically active hexahelicene" *J. Am. Chem. Soc.* **1971**, *93*, 2353.

[4] a) Klussmann, M., Iwamura, H., Mathew, S. P., Wells Jr, D. H., Pandya, U., Armstrong, A., Blackmond, D. G., "Thermodynamic control of asymmetric amplification in amino acid catalysis" *Nature* **2006**, *441*, 621. b) Soai, K., Shibata, T., Morioka, H., Choji, K., "Asymmetric autocatalysis and amplification of enantiomeric excess of a chiral molecule" *Nature* **1995**, *378*, 767.

[5] Ward, L. M., Kirschvink, J. L., Fischer, W. W., "Timescales of oxygenation following the evolution of oxygenic photosynthesis" *Orig. Life Evol. Biospheres* **2016**, *46*, 51.

[6] Armaroli, N., Balzani, V., "The future of energy supply: challenges and opportunities" *Angew. Chem. Int. Ed.* **2007**, *46*, 52.

[7] Ciamician, G., "The photochemistry of the future" *Science* **1912**, *36*, 385.

matter and at the crossroad of different disciplines including chemistry, physics, biology, material science, ecology and medicine.

In recent years, a plethora of light-induced chemical reactions has been disclosed studying the properties and the behavior of electronically excited molecules. These chemical entities - extensively discussed in Chapter II - differ fundamentally from the corresponding ground-states species and can unlock reactivities that stand outside the range of classical organic chemistry tools. Undoubtedly, light absorption is the indispensable event of any photochemical reaction and the tendency of a molecule towards absorbing photons is related to its color. A fundamental impediment that has limited the development of photochemical reactions for many years is the inability of most colorless organic molecules to absorb visible wavelengths of light. These molecules generally required high energy photons to be activated, but the UV wavelengths related to these energies are not abundant in the solar spectrum. As a consequence, organic photochemical reactions have been conducted for many years using specialized and purposely designed photoreactors.[8] The recent development and refinement of technologies, such as light-emitting diodes (LEDs) and visible-light absorbing transition-metal complexes, turned the elusive and *niche* field of photochemistry into an accessible and reliable tool for organic chemists. In particular, the seminal works by Yoon,[9] Stephenson,[10] and MacMillan,[11] published almost 10 years ago, started the renaissance of modern *photocatalysis*. This novel approach relies on the ability of transition-metal complexes and organic dyes to absorb visible-light and interact with organic substrates, *via* either single-electron transfer (SET) or energy transfer, providing easy access to open-shell and triplet state reactive species. In the field of *photoredox catalysis*, photons replace other classical redox active reagents and the possibility to access radicals under mild conditions allowed chemists to invent a wide variety of nontraditional and selective bond-construction processes (Figure 1.2a). The high level of robustness provided by this method allowed the merge of radical reactivity with organocatalysis for the asymmetric forging of C–C bonds (Figure 1.2b). MacMillan first reported the enantioselective α-alkylation of aldehydes **1** enabled by the photo-excitation of the transition-metal complex $[Ru(bpy)_3Cl_2]$ **4**. The excited-state photocatalyst **4*** triggers the generation of electrophilic radicals from alkyl bromides **2** through SET reduction. These electrophilic radicals can be subsequently trapped by the transiently-formed chiral enamine **I** in an enantioselective fashion. Inspired by this transformation, our research group has demonstrated that catalytically-generated enamines **I**

[8] Yoon, T. P., Ischay, M. A., Du, J., "Visible light photocatalysis as a greener approach to photochemical synthesis" *Nat. Chem.* **2010**, *2*, 527.
[9] Ischay, M. A., Anzovino, M. E., Du, J., Yoon, T. P., "Efficient visible light photocatalysis of [2+ 2] enone cycloadditions" *J. Am. Chem. Soc.* **2008**, *130*, 12886.
[10] Narayanam, J. M., Tucker, J. W., Stephenson, C. R., "Electron-transfer photoredox catalysis: development of a tin-free reductive dehalogenation reaction" *J. Am. Chem. Soc.* **2009**, *131*, 8756.
[11] Nicewicz, D. A., MacMillan, D. W., "Merging photoredox catalysis with organocatalysis: the direct asymmetric alkylation of aldehydes" *Science* **2008**, *322*, 77.

can be directly activated by visible-light and act as photoreductants.[12] The excited state of these intermediates **I*** triggers the single-electron transfer (SET) reduction of suitable substrates **2**, such as bromomalonates and α-iodosulfones derivatives, generating electrophilic radicals. At the same time, the ground-state chiral enamine provides effective stereochemical induction over the radical trapping event.

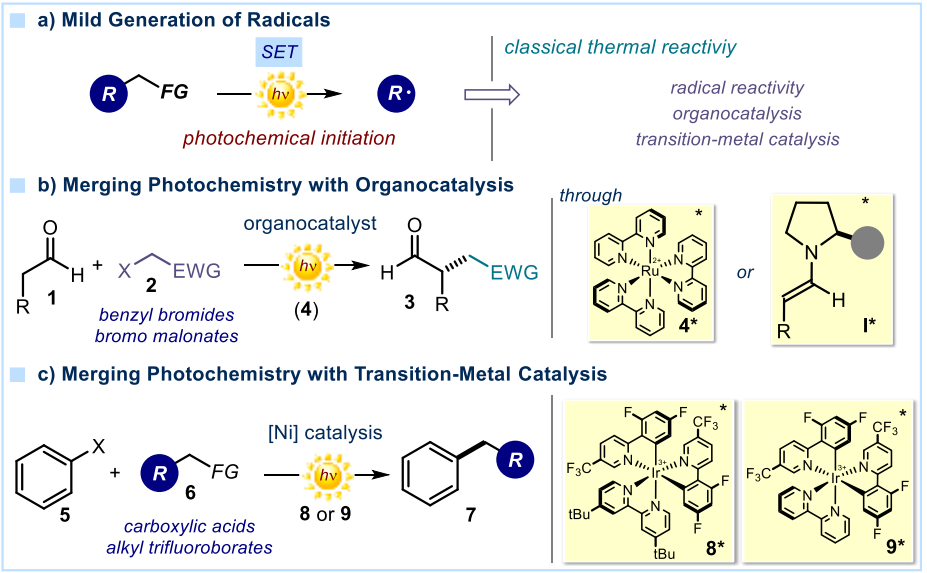

Figure 1.2: a) Photoredox catalysis allows the mild generation of open-shell species that can be used in combination with other powerful tools of organic synthesis, including (b) organocatalysis (c) and transition-metal catalysis.

The recent merger of photoredox catalysis with the widely exploited field of transition-metal catalysis, named *metallaphotocatalysis*, has provided an additional tool for the development of new synthetic methodology allowing the direct coupling of non-traditional reaction partners.[13] In this approach, the light-absorbing photocatalyst plays a dual role: i) it is involved in the mild generation of highly reactive radicals from the substrates, and ii) it modulates the properties (i.e. the oxidation state) of the transition-metal complex through electron or energy transfer processes. Molander[14] and MacMillan and Doyle,[15] independently, first reported the combination of light-absorbing iridium-based photoredox catalysts and a nickel precatalyst for the radical-mediated alkylation of aryl halides **4** (Figure 1.2c). In these works, the

[12] a) Silvi, M., Arceo, E., Jurberg, I. D., Cassani, C., Melchiorre, P., "Enantioselective organocatalytic alkylation of aldehydes and enals driven by the direct photoexcitation of enamines" *J. Am. Chem. Soc.* **2015**, *137*, 6120. b) Filippini, G., Silvi, M., Melchiorre, P., "Enantioselective Formal α-Methylation and α-Benzylation of Aldehydes by Means of Photo-organocatalysis" *Angew. Chem. Int. Ed.* **2017**, *56*, 4447.
[13] Twilton, J., Zhang, P., Shaw, M. H., Evans, R. W., MacMillan, D. W., "The merger of transition metal and photocatalysis" *Nat. Rev. Chem.* **2017**, *1*, 0052.
[14] Zuo, Z., Ahneman, D. T., Chu, L., Terrett, J. A., Doyle, A. G., MacMillan, D. W., "Merging photoredox with nickel catalysis: Coupling of α-carboxyl sp3-carbons with aryl halides" *Science* **2014**, *345*, 437.
[15] Tellis, J. C., Primer, D. N., Molander, G. A., "Single-Electron Transmetalation in Organoboron Cross-coupling by Photoredox/Nickel Dual Catalysis" *Science* **2014**, *345*, 433.

photocatalyst **7** or **8** absorbs visible-light and, from its excited state, triggers the formation of C(sp^3) radicals from ready available trifluoroborate or carboxylic acid derivatives **6**. Concomitantly, the transition-metal catalysts activate the electrophiles **5** and direct their reactivity towards the coupling with the radical intermediates, thus promoting the formation of new chemical bonds and delivering the desired alkylation products **7**. The photocatalyst is also responsible of the modulation of the oxidation states of the transition-metal center helping the organometallic steps of these transformations. The reaction mechanism of metallaphotocatalytic reactions will be extensively discussed in Chapter V.

At the onset of my doctoral studies, the investigation within the Melchiorre group was mainly focused on the combination of organocatalytic strategies with photochemistry for developing novel asymmetric transformation that could not be realized using classical thermal pathways. In particular, the excited-state reactivity of electron donor-acceptor (EDA) complexes[16] and of *in-situ* generated organocatalytic intermediates, such as enamines, was under investigation.

1.2. General Objectives and Summary

The main scientific objective of this doctoral research was to investigate and understand the excited-state reactivity of some organic molecules to develop novel photochemical C–C bond-forming processes. In order to achieve this goal, different tools of organic chemistry were combined. In the first projects (discussed in Chapter III and IV), the merger of organocatalysis and photochemistry enabled the direct asymmetric β-functionalization of enals triggered by the visible-light excitation of *in situ* formed chiral iminium salts.

In the second part of the PhD studies (discussed in Chapter V), the excited-state properties of 4-alkyl-1,4-dihydropyridines (alkyl-DHP) were exploited in combination with transition metal catalysis for the development of nickel-catalyzed radical cross-couplings.

1.2.1. The Excited-State Reactiviy of Iminium Ions

In Chapter III, the asymmetric β-benzylation of enals triggered by visible-light excitation of *in-situ* generated chiral iminium ions is discussed. This transformation does not need any external photocatalyst, but it relies on the excited-state properties of iminium ion salts **II** (Figure 1.3).

[16] Arceo, E., Jurberg, I. D., Álvarez-Fernández, A., Melchiorre, P., "Photochemical activity of a key donor–acceptor complex can drive stereoselective catalytic α-alkylation of aldehydes" *Nat. Chem.* **2013**, *5*, 750.

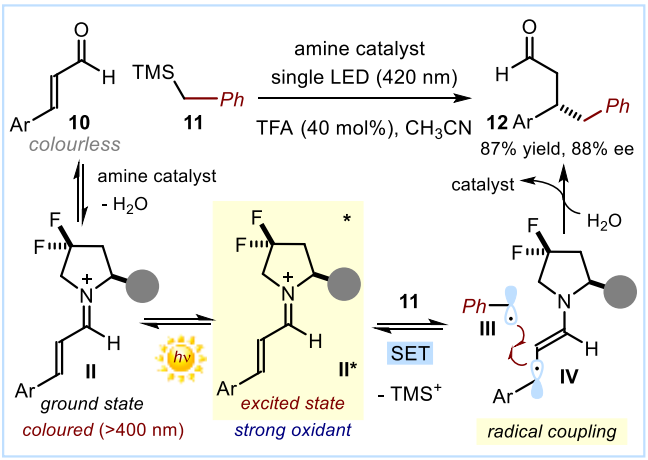

Figure 1.3: Photo-excited iminium-ions trigger the enantioselective β-alkylation of enals.

We demonstrated that selective photo-excitation of coloured chiral iminium-ions **II**, key intermediates in thermal enantioselective organocatalytic processes[17], turns them into strong oxidants (estimated $E(\mathbf{II}^{+*}/\mathbf{II}) \sim +2.4$V). These could trigger the formation of benzylic radicals **III** through SET oxidative fragmentation of ready available organic silanes **11**. The subsequent stereoselective radical coupling led to the direct enantioselective β-benzylation of enals. Crucial to success was the design and the synthesis of a new class of redox-stable chiral secondary amine catalysts with well-tailored electronic properties. These fluorine-containing catalysts could i) generate a photoactive iminium ion, ii) provide the source of stereochemical induction iii) without competing with the substrate in the SET oxidation. The reaction provided access to a variety of β-functionalized enals **12** obtained through the generation of benzyl radical derivatives and other stabilized radicals. Extensive mechanistic investigations proved the involvement of the photo-excited iminium ion in the SET event and disclose the nature of the catalytic cycle.

1.2.2. Extending the Reactivity of Excited-State Iminium Ions

After establishing the synthetic potential of the photoexcited iminium ions, we wondered if this approach could be extended for the direct regio- and enantioselective installation of not-stabilized alkyl fragments at the β position of enals.

[17] a)Lelais, G., MacMillan, D. W., "Modern strategies in organic catalysis: the advent and development of iminium activation" *Aldrichim. Acta* **2006**, *39*, 79. b) Erkkilä, A., Majander, I., Pihko, P. M., "Iminium catalysis" *Chem. Rev.* **2007**, *107*, 5416.

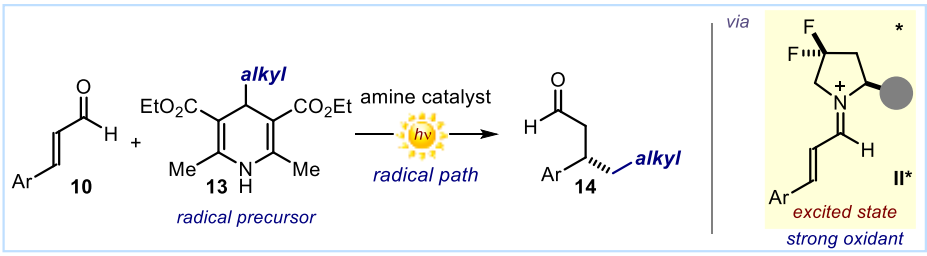

Figure 1.4: Installation of not-stabilized alkyl fragments at the β position of enals through photo-excited iminiu-ion catalysis.

Looking for a suitable radical precursors, characterized by a low oxidation potential and the tendency to release alkyl radicals upon SET oxidation, we identified and selected ready available 4-alkyl-1,4-dihydropyridines **13**[18] (alkyl-*DHPs*), directly obtained from aldehydes. This project is discussed in Chapter IV.

1.2.3. Reactivity of 1,4-Dihydropyridines in the Excited State

After exploiting the ground-state properties of alkyl-DHPs for the generation of open-shell species, we investigated the excited-state chemistry of these compounds. In Chhapter V, we report the results obtained. Visible-light excitation of DHP derivatives **13**, primarily understood as hydride sources in their ground-state, affords strong photo-reductants that can productively engage in SET manifolds and deliver alkyl radicals. We first established, through photophysical investigation and control experiments, the dual ability of photo-excited alkyl-DHPs to generate C(sp^3)-centered radicals and to act as strong reducing agents. We then we demonstrated the possibility to exploit them in photochemical nickel-catalyzed C(sp^2)-C(sp^3) cross-coupling reactions with aryl bromides and acyl chlorides. These transformations provide easy access to a set of alkylated arenes **14** and ketones **15** without the need of any external photoredox catalyst.

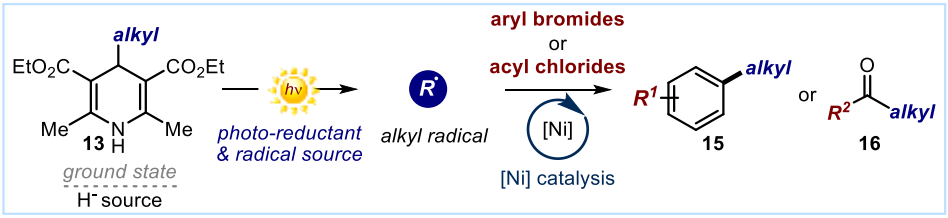

Figure 1.5: Photoexcitation of 4-alkyl DHPs turns them into strong reductants and radical sources capable to engage in nickel-catalyzed radical cross-couplings.

[18] Huang, W., Cheng, X., "Hantzsch Esters as Multifunctional Reagents in Visible-Light Photoredox Catalysis" *Synlett* **2017**, *28*, 148.

We then exploited the peculiar reactivity of excited-state DHPs for the development of other photochemical transformations including a Giese-type radical conjugate addition and a nickel catalyzed radical transfer amidation.

Chapter II

Introduction

Photochemistry deals with the chemical effects of light and with electronically excited-state species. Most of the chemical processes discussed in this thesis are driven by the formation of these chemical entities. Specifically, in the reactions discussed in Chapter III and IV, the excited state of a catalytically generated iminium ion triggers a single-electron oxidation of a suitable substrate to generate a reactive radical intermediate. In Chapter V, the light-excitation of 1,4 dihydropyridine (DHP) derivatives discloses their reductive abilities making them capable to transfer electrons to the reaction partners. Therefore, the main aim of this chapter is to showcase the general characteristics of electronically excited-state molecules. The main aspects of the light-absorption process, along with the photophysical behavior, the unimolecular processes and the modes of interaction of photoexcited species with other substrates will be here highlighted.[1] Particular emphasis will be placed on remarking the difference in reactivity between a molecule in the ground state and in the excited state.

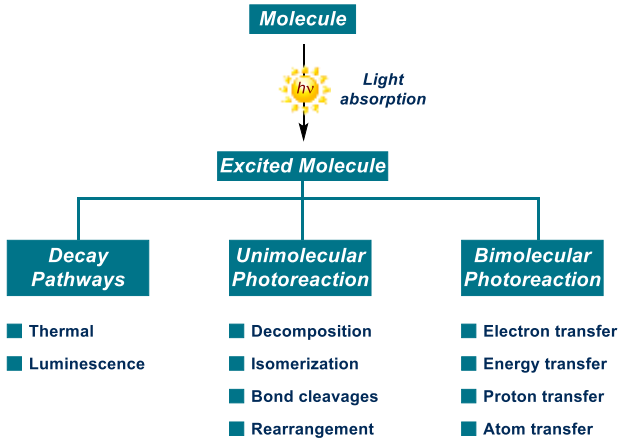

Figure 2.1: Light-absorption generates excited-state molecules that undergo several deactivation pathways.

2.1 Light Absorption

Light-absorption is the key feature that characterizes all the photochemical transformations. This event triggers the formation of electronically excited-state species starting from ground-

[1] For extensive discussion on excited-state species: a) Balzani, V., Ceroni, P., Juris, A., "Photochemistry and photophysics: concepts, research, applications". **2014**; John Wiley & Sons. b) Klán, P., Wirz, J., "Photochemistry of organic compounds: from concepts to practice". **2009**; John Wiley & Sons. c)Wardle, B., "Principles and applications of photochemistry". **2009**; John Wiley & Sons.

state compounds. The importance of this step was well understood at the dawn of the investigations on the interaction between light and matter and it is summarized in the two basic laws of photochemistry:

1) *Only light which is absorbed by a system can cause a photochemical change.* (Grotthuss-Draper Law, 1817-1842)
2) *For every quantum of light (photon) that is absorbed, one molecule of substrate reacts.* (Stark-Einstein Law, 1908-1913)

While the first law establishes the requirement of light-absorption for promoting any photochemical processes, the second law defines an equivalence between the number of photons absorbed and the number of molecules undergoing a photochemical transformation. For this reason, the second law of photochemistry is often referred as "the equivalence law". However, several experiments showed that this equivalence is not always observed and the second law, in its original formulation, does not properly characterize all the photochemical processes. In fact, in some cases, the absorption of photons by the substrate may result in photophysical processes which are not leading to any chemical change. From a quantitative point of view, the absorption of a monochromatic beam of light by an absorber species in solution is governed by the Beer-Lambert law:

$$I = I_0 \times 10^{-\varepsilon l c} \qquad (2.1)$$

Where I the intensity of the transmitted light, I_0 is the intensity of the incident light, ε the molar absorption coefficient, l the optical path and c the concentration of the solution. The equation 2.1 can be rewritten as follows in order to isolate the quantity *absorbance A*:

$$A = \log(I_0/I) = \varepsilon l c \qquad (2.2)$$

Absorbing compounds contain antennae groups, known as *chromophores*, which are responsible for light absorption. The energy of the absorbed photon promotes the transition of one electron from the highest occupied molecular orbital (HOMO) to the lowest unoccupied orbital (LUMO) (Figure 2.2a). This means that the molecule passes from the ground electronic state to an electronically excited state (Figure 2.2b). These states are described by the wave functions Ψ. The effectiveness of the interaction between the chromophores and the electromagnetic radiation is dictated by some conditions. First, there should be a correspondence between the energy of the photons ($h\nu$) and the energy of a pair of electronic energy levels Ψ in the absorber:

$$h\nu = E_f - E_i \qquad (2.3)$$

where E_f and E_i are the energies of the excited-state Ψ_f and the ground-state Ψ_i.

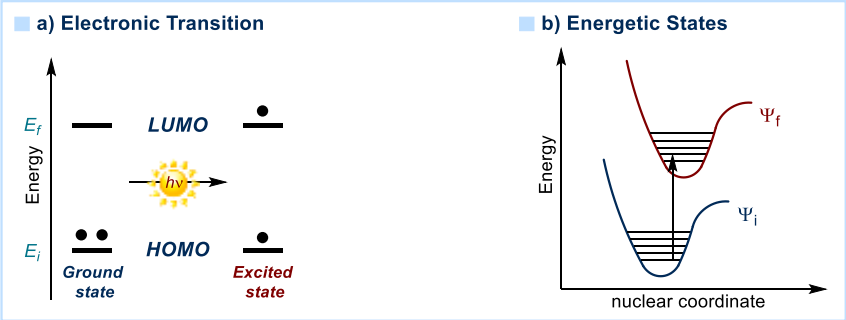

Figure 2.2: a) The energy of the absorbed photon promotes the transition of one electron from the highest occupied orbital (HOMO) to an unoccupied orbital (LUMO) providing access to b) an electronically excited-state Ψ_f.

Furthermore, the intensity of the absorption depends on the similarity between the initial and the final wave functions (Ψ_i and Ψ_f): the strongest absorptions occur when Ψ_f and Ψ_i most closely resemble one another. This is reflected in the selection rules, which predict the magnitude of the electronic transition. The symmetry selection rule states that *electronic transitions involving a large change in the region of space the electron occupies are forbidden*. For this reason $\pi \rightarrow \pi^*$ transitions, where the orbitals lie on the same plane, are *symmetry allowed*. In contrast, $n \rightarrow \pi^*$, with orbitals lying perpendicular one to each other are *symmetry forbidden*. The stricter spin selection rule states that *electronic transition takes place with no change in the spin multiplicity*. Therefore, *singlet→singlet* and *triplet→triplet* transitions are *spin allowed*. On the other hand *singlet→triplet* transitions are *spin forbidden*.

2.2 Light Absorption and Photochemistry

Let's now consider the field of synthetic photochemistry[2], where ground-state compounds can harvest the energy of the photons to initiate photochemical transformations (Figure 2.3). In the simplest case, a reaction substrate **A**, present in stoichiometric amount, directly participates in the light-absorption and triggers the photochemical transformation providing the desired products. This is the case of the venerable Paternò-Büchi reaction where the aldehyde **1** absorbs UV light and reaches an excited state **1*** that reacts with the olefin **2** providing the oxetane **3** (Figure 2.3a).[3] In an alternative scenario, a substoichiometric species, the *photocatalyst* **PC**, absorbs the incident light and, upon excitation, promotes the photochemical transformation interacting with other reaction components and regenerating

[2] a) Albini, A., Fagnoni, M., "Handbook of Synthetic Photochemistry". 2009; John Wiley & Sons. b) Yoon, T. P., Ischay, M. A., Du, J., "Visible light photocatalysis as a greener approach to photochemical synthesis."
[3] Büchi, G., Inman, C. G., Lipinsky, E., "Light-catalyzed organic reactions. I. The reaction of carbonyl compounds with 2-methyl-2-butene in the presence of ultraviolet light" *J. Am. Chem. Soc.* **1954**, *76*, 4327.

itself. This is the field of *photocatalysis*.[4] Stephenson, one of the pioneer of modern visible-light photocatalysis, applied this strategy to achieve the reductive debromination of heterocycles.[5] In this transformation, the transition-metal complex $[Ru(bpy)_3]Cl_2$ reaches an excited state upon visible-light absorption and induces the single-electron transfer (SET) reduction of the bromopyrroloindoline **4** in the presence of tertiary amines as sacrificial electron donors. The resulting cleavage of the C-Br bond provides the debrominated product **5** (Figure 2.3b). Incident light can also be absorbed by a reaction intermediates that is transiently-formed upon aggregation of two or more reaction components (Figure 2.3c). This strategy was applied by our research group to achieve the photocatalyst-free light-induced asymmetric α-alkylation of aldehydes.[6] The electron-rich enamine **I**, generated upon condensation of the aldehyde **6** with the chiral amine catalyst **8**, forms a coloured electron donor-acceptor (EDA) complex[7] with the electron-deficient benzyl bromide derivative **7**. Visible-light excitation of this complex promotes a SET that generates the key benzyl radical intermediate. Stereoselective trapping of this radical by the ground-state chiral enamine, followed by hydrolysis of the catalyst, provided the desired α-alkylation product **9** in an enantioselective fashion.

[4] Schultz, D. M., Yoon, T. P., "Solar synthesis: prospects in visible light photocatalysis" *Science* **2014**, *343*, 1239176.
[5] Narayanam, J. M., Tucker, J. W., Stephenson, C. R., "Electron-transfer photoredox catalysis: development of a tin-free reductive dehalogenation reaction."
[6] Arceo, E., Jurberg, I. D., Álvarez-Fernández, A., Melchiorre, P., "Photochemical activity of a key donor–acceptor complex can drive stereoselective catalytic α-alkylation of aldehydes."
[7] a) Mulliken, R. S., "Molecular compounds and their spectra. II" *J. Am. Chem. Soc.* **1952**, *74*, 811. b) Foster, R., "Electron donor-acceptor complexes" *J. Phys. Chem.* **1980**, *84*, 2135.

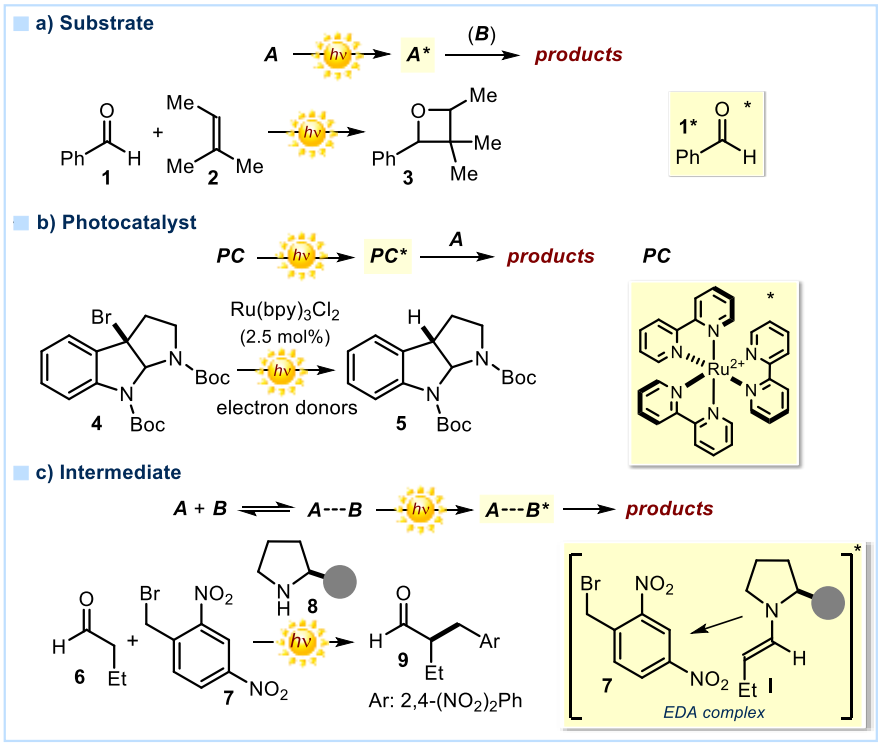

Figure 2.3: Different ground-state species that can harvest the energy of the photons to initiate a photochemical transformation.

2.3 The Photophysic of Excited States

The absorption of light rearranges the electronic structure of the absorbing species and results in the population of an electronically excited states. These species differ fundamentally from the corresponding ground states, mainly for their lifetime, the energy content, and the electronic distribution. For these reasons, they has to be treated not simplistically as "hot" ground-state but as *new* chemical species. Photoexcited molecules are endowed with excess of energy and they have the tendency to lose it, within a very short period, through a variety of deactivation pathways that bring them back to the corresponding ground state. The unimolecular processes that deactivate the excited states, without changing the chemical composition of the light-absorbing species, are classified as *photophysical* processes. These are graphically illustrated in the Jablonski diagrams (Figure 2.4a).[8] In these simplified representations, the electronic states are depicted as thick horizontal lines and the vibrational levels by thin ones, while the electronic transitions are portrayed as arrows. The energy of an excited state is taken to be the energy gap between the lowest vibrational level of the excited

[8] Jablonski, A., "Efficiency of anti-Stokes fluorescence in dyes" *Nature* **1933**, *131*, 839.

state and the corresponding ground state. According to the spin selection rule, light-excitation produce a singlet excited state (S_1). In addition to the higher electronic energy, the excited state is generally associated with an excess of vibrational energy, which is rapidly dissipated through *vibrational relaxation* (*v.r.*) reaching the lowest vibrational level (v_0). S_1 can then decay back to the ground state S_0 through either radiative or radiationless transitions. The former, named *fluorescence*, involves the emission of a photon, while the latter occurs through a combination of *internal conversion* (*i.c.*), the isoenergetic transition between two states with the same multiplicity ($S_1 \rightarrow S_0$), and *vibrational relaxation*. Alternatively, S_1 can undergo *intersystem crossing* (*i.s.c.*) and change the spin multiplicity forming a triplet state (T_1), which decays to the ground state through radiative *phosphorence* or radiationless transition.

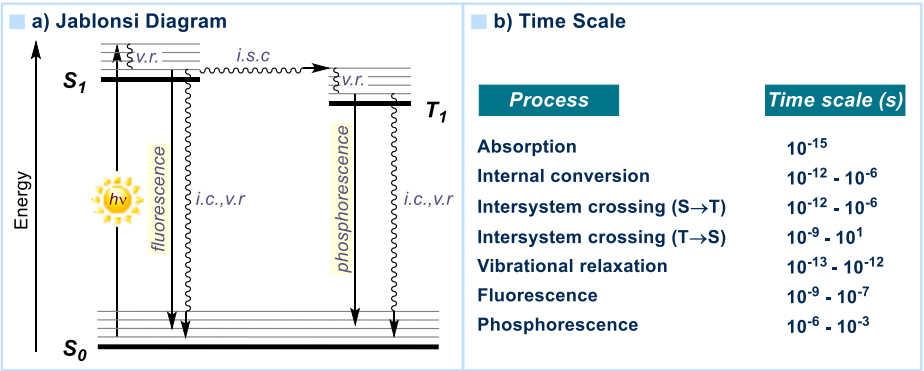

Figure 2.4: Jablonsky diagram and the lifetimes of deactivation processes.

While ground-state species are stable, excited states are short-lived and with a transient character. The lifetime **τ** of these entities depends on the rate of the deactivation processes (Figure 2.4b). These are higher when the spin multiplicity is conserved. In the absence of bimolecular processes, the excited-state lifetime may span from 10^{-12} s, in the case of singlet excited state, to 10 s, in the case of spin-forbidden excited-state species.

Since the molecular geometry is related to the electronic distribution, the photoexcitation of an electron is significantly altering the geometry of the light-absorbing molecules (Figure 2.5). For instance, formaldehyde in the ground state is planar (C_{2v}); upon light excitation, an $n \rightarrow \pi^*$ electronic transition occurs and one electron is promoted from the *n* orbital, located on the oxygen, to the antibonding π^* orbital, overall weakening the C=O double-bond character and increasing the electron density on the carbon. This electronic redistribution results in a rehybridization of the C(sp^2) toward a sp^3 hybridization that confers a pyramidal geometry (C_s) to the excited-state formaldehyde.[9]

[9] Moule, D., Walsh, A., "Ultraviolet spectra and excited states of formaldehyde" *Chem. Rev.* **1975**, *75*, 67.

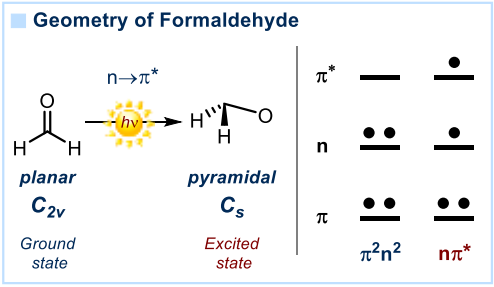

Figure 2.5: variation of the geometry of formaldehyde upon light-absorption.

The energetic content of an electronically excited state is the aspect that influences the most its reactivity. An excited state features an excess of energy from 150 to 600 kJ/mol compared to the corresponding ground state.[10] This extra energy, directly gained from the absorbed photons, turns the excited states in highly reactive intermediates that can engage in a variety of uni- and bi-molecular processes leading to a change in the chemical composition of the species involved. In the next sections, unimolecolar photochemical transformation and the modes of interaction of excited-state with other ground-state molecules will be discussed.

2.4 Unimolecular Processes

The variation of internal energy and electronic distribution associated with photoexcitation perturbs the chemical stability of the light-absorbing molecules. This may result in several unimolecular transformations that change the chemical structure of the chromophore, while dissipating the photonic energy. Among these processes, the most prominent are *isomerisations*, *fragmentations*, and *rearrangements*.

Photoinduced geometric *cis-trans* isomerization is a distinctive photochemical transformation of alkenes. Upon light-absorption, these species undergo a $\pi \rightarrow \pi^*$ electronic transition that does not produce any relevant change in the geometry of the molecule. However, the resulting $\pi\pi^*$ excited states have no net π bonding character. Therefore, the energetic barrier of free rotation of the former C=C bond is significantly decreased, enabling the formation of a lower energy *p-state* (perpendicular) intermediate with a different geometry. The excitation of both geometrical isomers of the olefin gives access to the same p-state intermediate and its relaxation provides a mixture of *cis* and *trans* olefin (Figure 2.6, top). When the rate of formation of each isomer equals the rate of its removal, a *photostationary state* is obtained. In the case of stilbene, irradiation with UV-light of both *cis*/*trans* isomers provides a mixture

[10] These energies are associated with photons in the 200-800 nm wavelength range.

of 93% *cis* and 7% *trans* (Figure 2.6, bottom).[11] The product distribution of the photoisomerization of alkenes is independent from the thermodynamic stability of the products and it is governed by the absorption properties of the two different ground-state isomers (ε_{cis} *vs* ε_{trans}). For this reason, this transformation is synthetically useful for the generation of the thermodynamically disfavored *cis* isomer.

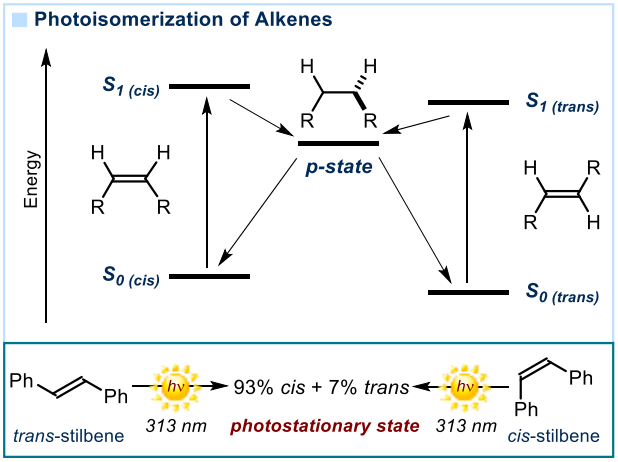

Figure 6.6: Light-induced *cis-trans* isomerization of alkenes.

The magnitude of the photonic energy absorbed by the organic molecules can fall in the same range of common *bond dissociation energy* (BDE) values. Therefore, light absorption may results in a bond cleavage, which forms two open-shell species. This light-induced bond fragmentation (or *photolysis*) occurs when the electronic transition populates a vibrational level of the excited state that lays above the dissociation energy (Figure 2.7). This unimolecular transformation is predominant in compounds which possess relatively weak bonds, including halogenated compounds, peroxides and sulfides. Photolysis is extensively exploited for the mild generation of radicals and several commonly used radical initiators are activated *via* photolytic cleavage.

[11] Hammond, G. S., Saltiel, J., Lamola, A. A., Turro, N. J., Bradshaw, J. S., Cowan, D. O., Counsell, R. C., Vogt, V., Dalton, C., "Mechanisms of photochemical reactions in solution. XXII. Photochemical cis-trans isomerization" *J. Am. Chem. Soc.* **1964**, *86*, 3197.

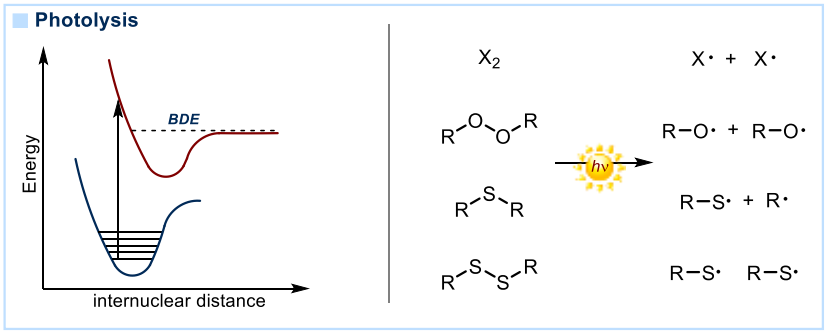

Figure 2.7: Light-induced photolysis.

Finally, light excitation can promote molecular rearrangements that are not achievable through thermal pathway. Electrocyclic processes and sigmatropic rearrangements are examples of unimolecular reactions that can occur photochemically. According to the Woodward-Hoffman orbital symmetry rules,[12] the stereochemical outcome of light-induced electrocyclic processes is opposite compared to the one obtained thermally. In fact, the photoexcitation, and the consequent population of the LUMO, alters the phase of the orbitals involved in the transformation modifying the molecular dynamic of the C–C bond formation (Figure 2.8). For instance, the *4π* electron diene **10** undergoes *conrotatory* electrocyclc ring-closing in the ground state, providing the *anti* cyclobutene **11**. On the other hand, under photochemical conditions, it reacts through a *disrotatory* mode yielding the *syn* product **12**.

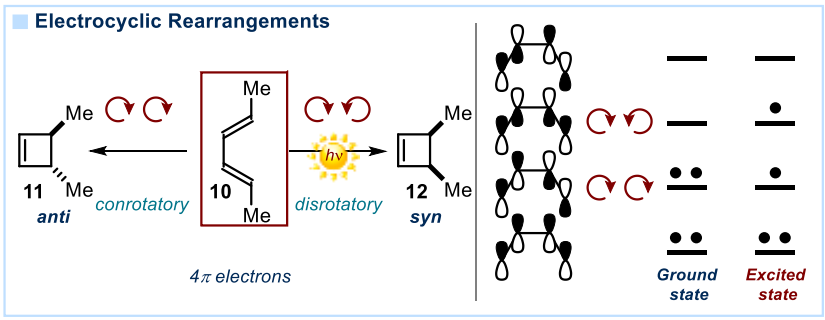

Figure 2.8: Light-induced electrocyclic rearrangement of 4*π* electrons systems.

[12] Woodward, R. B., Hoffmann, R., "The conservation of orbital symmetry" *Angew. Chem. Int. Ed.* **1969**, *8*, 781.

2.5 Photo-induced Electron Transfer

The increased internal energy of the excited-state molecule influences its ability to donate or accept electron, making it a better oxidant and reductant than the ground-state species.[13] This situation is depicted in Figure 2.9, where the ionization potential (IP) and electron affinity (EA) of an excited-state diamagnetic molecule are compared with those of its corresponding ground state. The EA of the excited state is higher than in the ground state, while the IP is lower. From a thermodynamic point of view, the addition of an electron to the half-filled HOMO of the excited molecule is more exothermic compared to its addition to the LUMO of the ground-state species. On the other hand, removing an electron from the excited state is less endothermic than its removal from the ground state.[14]

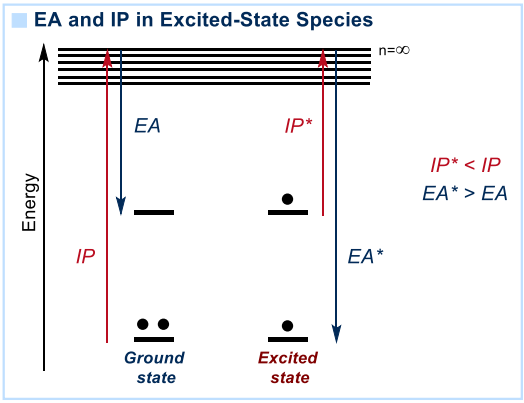

Figure 2.9: Excited-state species has decreased ionization potential (IP) and increased electron affinity (EA) compared to the corresponding ground state.

In the ground state, an electron transfer between a donor (D) and an acceptor (A) generating two charged species is described as:

$$\mathrm{D} + \mathrm{A} \rightarrow D^{+} + A^{-} \qquad (2.4)$$

The thermodynamic feasibility of this reaction can be evaluated by determining the Gibbs free energy of the process (ΔG_{eT}):

$$\Delta G_{eT} = E_{1/2}^{ox}(\mathrm{D}) - E_{1/2}^{red}(\mathrm{A}) + \Delta E_{Coulombic} \qquad (2.5)$$

[13] Kavarnos, G. J. "Fundamentals of photoinduced electron transfer." VCH, Weinheim, New York, **1993**.
[14] Pitre, S. P., McTiernan, C. D., Scaiano, J. C., "Understanding the Kinetics and Spectroscopy of Photoredox Catalysis and Transition-Metal-Free Alternatives" *Acc. Chem. Res.* **2016**, *49*, 1320.

where $E_{1/2}^{ox}(\mathrm{D})$ is the oxidation potential[15] of the donor (D), $E_{1/2}^{red}(\mathrm{A})$ is the reduction potential of the acceptor (A) and $\Delta E_{Coulombic}$ is the parameter that describes the interaction between the charged species formed in the reaction solvent. The electron transfer is thermodynamically favorable when $E_{1/2}^{ox}(\mathrm{D})$ is lower than $E_{1/2}^{red}(\mathrm{A})$. On the other hand, electron transfers involving an excited-state molecule are described as:

$$\mathrm{D}^* + \mathrm{A} \rightarrow D^+ + A^- \tag{2.6}$$

$$\mathrm{D} + A^* \rightarrow D^+ + A^- \tag{2.7}$$

where D^* and A^* are the excited-state donor and the excited-state acceptor respectively.
For these processes, named *photoinduced electron transfers* or PETs, equation 2.5 has to be modified in order to include the increased excited-state free energy. In their seminal work[16], Rehm and Weller showed that the thermodynamic of PETs is described by the following relation:

$$\Delta G_{eT} = E_{1/2}^{ox}(\mathrm{D}) - E_{1/2}^{red}(\mathrm{A}) - E_{00}(\mathrm{D\ or\ A}) + \Delta E_{Coulombic} \tag{2.8}$$

where $E_{00}(\mathrm{D\ or\ A})$ is the excited-state energy of the donor or acceptor. This equation showcases that the higher is the energy of the photoexcited species the more favorable is the electron transfer. $\Delta E_{Coulombic}$ is dependent from the dielectric constant ε and is often negligible in polar solvents. For instance, for an electron transfer producing two charged species in acetonitrile, $\Delta E_{Coulombic} = 0{,}06eV$. Therefore, equation 2.8 can be simplified as:

$$\Delta G_{eT} = E_{1/2}^{ox}(\mathrm{D}) - E_{1/2}^{red}(\mathrm{A}) - E_{00}(\mathrm{D\ or\ A}) \tag{2.9}$$

This equation allows the estimation of the excited-state potentials of the species involved in the electron transfer. In fact, in the case of excited-state donor or excited-state acceptor, the terms can be rearranged as follow:

$$\Delta G_{eT} = [E_{1/2}^{ox}(\mathrm{D}) - E_{00}(\mathrm{D})] - E_{1/2}^{red}(\mathrm{A}) \tag{2.10}$$

$$\Delta G_{eT} = E_{1/2}^{ox}(\mathrm{D}) - [E_{1/2}^{red}(\mathrm{A}) + E_{00}(\mathrm{A})] \tag{2.11}$$

[15] Redox potential (E) can be determined by Cyclic Voltammetry (CV) measurements. In the presence of reversible electron transfers, they can be estimated by averaging the potentials relative to the forward and reverse peaks in the voltammogram ($E_{1/2}$). Conversely, for irreversible voltammograms, E can be approximated either to the maximum peak (E_p) or to the half-peak ($E_{p/2}$). Within this thesis, redox potential values (E) always refer to the reduction reaction of the redox couple expressed in parentheses (D^+/D) or (A/A^-). When the redox couple is not explicitly identified, the apex "red" (E^{red}) is added when an actual reduction is taking place (A/A^-), while, when referring to an oxidation (D/D^+), the apex "ox" (E^{ox}) is used.
[16] Rehm, D., Weller, A., "Kinetics of fluorescence quenching by electron and H-atom transfer" *Isr. J. Chem.* **1970**, *8*, 259.

where $[E_{1/2}^{ox}(\mathrm{D}) - E_{00}(\mathrm{D})]$ represents the oxidation potential of the excited-state donor and $[E_{1/2}^{red}(\mathrm{A}) + E_{00}(\mathrm{A})]$ is the reduction potential of the excited-state acceptor.

$$E_{1/2}^{ox}(\mathrm{D}^*) = E_{1/2}^{ox}(\mathrm{D}) - E_{00}(\mathrm{D}) \quad (2.12)$$

$$E_{1/2}^{red}(\mathrm{A}^*) = E_{1/2}^{red}(\mathrm{A}) + E_{00}(\mathrm{A}) \quad (2.13)$$

It is easy to understand the importance of the evaluation of these potentials in order to predict the thermodynamic feasibility of a photoinduced electron transfer. While the redox potential of the ground-state species can be easily obtained through cyclic voltammetry measurements, the excited-state energy E_{00} corresponds to the energy difference between the lowest vibrational level of the excited state and the corresponding ground state. This value can be assessed spectroscopically: in fact, in the case of singlet excited states, it can be estimated from the position of the long wavelength tail of the UV-Vis absorption spectrum.[17]

Photoinduced electron transfer represents a straightforward strategy to easily access radical intermediates. This is the fundament of photoredox catalysis[18], where a light-absorbing photocatalyst (PC) reaches an electronically excited state (PC*) upon irradiation, enhancing its reductive and oxidative ability. The redox properties of some of the most used photocatalyst are easily available in the literature (and reported in Figure 2.10b), which greatly simplify the choice of a photoredox catalyst for a certain application.[19] In a photoredox protocol (Figure 2.10a), the excited-state photocatalyst may interact with the ground-state species following an oxidative or a reductive quenching cycle. In the oxidative quenching cycle, PC* acts as a reductant, giving an electron to a suitable electron acceptor (A) *via* SET. This event generates the radical anion of the acceptor $A^{\cdot -}$ and the oxidized form of PC ($PC^{\cdot +}$). The latter is an oxidant and may accept an electron from a donor (D), regenerating the ground-state photocatalyst PC and completing the photocatalytic cycle. Alternatively, in the reductive quenching cycle, PC* acts as an oxidant promoting a SET oxidation of a suitable donor (D). This provides the radical cation of the donor $D^{\cdot +}$ and the reduced form of the photocatalyst, which acts as a reductant. Donation of an electron to an acceptor (A) restores the ground state photocatalyst. The radical intermediate generated in the photoredox cycle can be used in further chemical transformations to forge new chemical bonds.

---

[17] Balzani, V., Ceroni, P., Juris, A., "Photochemistry and photophysics: concepts, research, applications". **2014**; John Wiley & Sons.

[18] Shaw, M. H., Twilton, J., MacMillan, D. W., "Photoredox catalysis in organic chemistry" *J. Org. Chem.* **2016**, *81*, 6898.

[19] a) Pitre, S. P., McTiernan, C. D., Scaiano, J. C., "Library of Cationic Organic Dyes for Visible-Light-Driven Photoredox Transformations" *ACS Omega* **2016**, *1*, 66. b) http://chemlabs.princeton.edu/macmillan/wp-content/uploads/sites/6/Merck-Photocatalysis-Chart.pdf

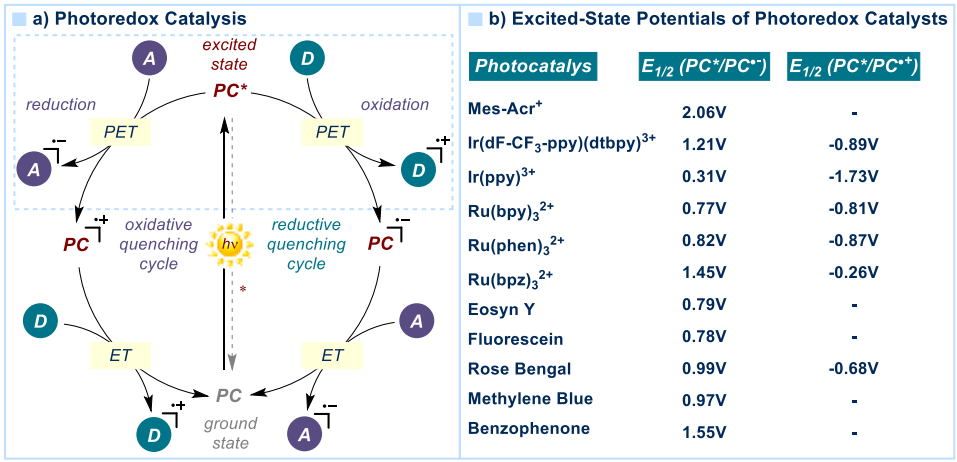

Figure 2.10: a) Quenching cycles in photoredox catalysis and b) excited-state potentials of common photoredox catalysts.

2.6 Energy Transfer

A key feature of excited-state species is their ability to transfer the electronic energy to a neighbouring ground-state molecule. During this energy transfer manifold, the excited state of the donor species (D) is deactivated to a lower electronic state. At the same time, an excited state of the energy acceptor molecule (A) is generated. This process is called *energy transfer* and represents another important bimolecular interaction of excited-state compounds.

$$D^* + A \rightarrow D + A^* \qquad (2.14)$$

Energy transfer, often named *photosensitization*, allows the excitation of molecules which cannot directly absorb incident light. This mechanism plays a crucial role in the photosynthesis process. Here, the light is harvested by chlorophyll molecules that act as antennae and transfer the excitation energy to the photosynthetic reaction centre where the photochemical reactions take place. Energy transfer is an isoenergetic process and the energy lost during the deactivation of the donor is gained in the excitation of the acceptor. If the excitation energy of A is lower compared to the one of D, a higher vibrational level of A is populated and the excess of energy is dissipated through vibrational relaxation. Moreover, during the energy transfer event the electronic spin multiplicity is conserved (*Wigner rule*). For this reason, singlet excited donors $^1D^*$ generate singlet excited acceptors $^1A^*$ while triplet excited donors $^3D^*$ provide triplet excited acceptors $^3A^*$.

Singlet-singlet energy transfer: $$^1D^* + {}^1A \rightarrow {}^1D + {}^1A^* \qquad (2.15)$$

Triplet-triplet energy transfer: $$^3D^* + {}^1A \rightarrow {}^1D + {}^3A^* \qquad (2.16)$$

Energy transfer occurs through *radiative* or *nonradiative* processes, as depicted in Figure 2.11.

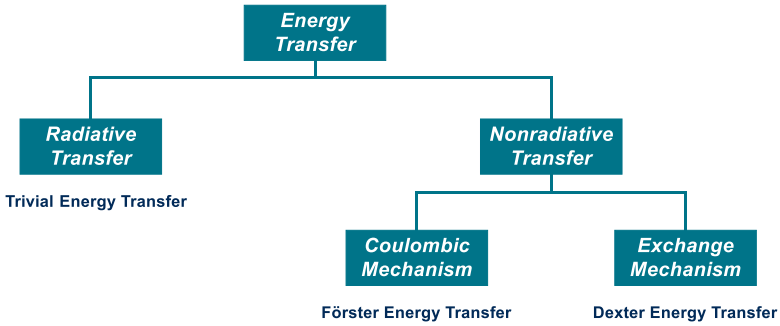

Figure 2.11: The principal mechanisms of electronic energy transfer.

Radiative energy transfer, also called *trivial energy transfer*, proceeds through the spontaneous emission of a photons from the excited-state donor. This is subsequently absorbed by the ground-state acceptor, which reaches an excited state.

$$D^* \rightarrow \mathrm{D} + h\nu \qquad (2.17)$$

$$\mathrm{A} + h\nu \rightarrow A^* \qquad (2.18)$$

Likewise other processes involving light-absorption, this mechanism is governed by the Beer-Lambert law and its effectiveness is strongly dependent on the concentration of the acceptor and on the optical path; however, it is not affected by the distance between A and D. Moreover, in order to take place, radiative energy transfer requires a spectral overlap between the absorption profile of A and the emission profile of D. The multiplicity of the excited species formed *via* radiative energy transfer is dictated by the previously discussed selection rules. As a consequence, this process always generates a singlet excited-state acceptor.

Nonradiative energy transfer occurs without the emission of photons and it is further divided in two mechanisms: the *Coulombic mechanism* and the *electron exchange mechanism*. Coulombic mechanism, also called *Förster resonance energy transfer* (FRET)[20], takes place without contact between D and A. This process is a long-range mechanism and it is operative even at distances that exceed the Van der Waals radius of the species involved. This mechanism is the results of dipole-dipole interaction between the donor and the acceptor and it occurs when the excited-state donor decays to the ground state through a nonradiative process. This transition is accompanied with an electron excitation in the acceptor molecule which provides A* (Figure 2.12). In this process, the spin multiplicity must be conserved for both D and A. In fact, spin-allowed electronic transitions provides high transition dipoles, increasing the effectiveness of the process. Therefore, singlet-singlet energy transfer (eq.

[20] Förster, T., "10th Spiers Memorial Lecture. Transfer mechanisms of electronic excitation" *Discuss. Faraday Soc.* **1959**, *27*, 7.

2.15) may efficiently occurs through this mechanism, while triplet-triplet energy transfers (eq. 2.16), involving a double change of spin multiplicity, are forbidden.

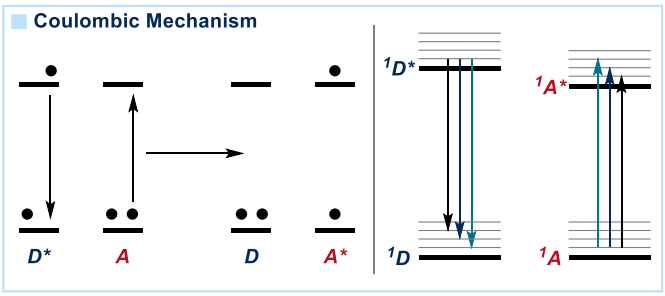

Figure 2.12: The Coulombic mechanism or Förster resonance energy transfer.

Exchange mechanism, also called *Dexter energy transfer*,[21] involves a double electron exchange between the excited-state donor and the ground-state acceptor. The electron in the LUMO of D* is transferred to the LUMO of A while one electron from the acceptor HOMO is transferred to the donor HOMO (Figure 2.13). This mechanism occurs only at short distances, requiring an orbital overlap between the donor and the acceptor. In contrast to the Coulombic mechanism, the exchange mechanism is efficient also in the case of triplet-triplet energy transfer. Consequently, this photosensitization process is often exploited in photochemistry in order to populate triplet states that are not easily accessible *via* direct excitation and intersystem crossing sequence.

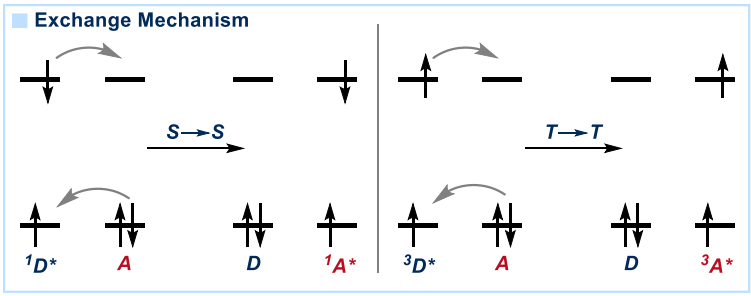

Figure 2.13: The Exchange mechanism or Dexter energy transfer.

Concerning the synthetic aspects, energy transfer was successfully studied and applied by Schenck and Ziegler for photochemical synthesis of the antihelmintic drug Ascaridole (Figure 2.14).[22] In this process, chlorophyll acts as photosensitizer and absorbs visible-light, reaching an electronically excited state. This excited state productively engages in an energy transfer

[21] Dexter, D. L., "A theory of sensitized luminescence in solids" *J. Chem. Phys.* **1953**, *21*, 836.
[22] Schenck, O., Ziegler, K., "Die synthese des ascaridols" *Naturwissenschaften* **1944**, *32*, 157.

with molecular triplet oxygen, providing the highly reactive singlet oxygen $^1O_2$. This undergoes a Diels-Alder cycloaddition with α-terpinene **13** providing Ascaridol **14**. After 1945, this reaction has been adopted by the industry for the large-scale preparation of Ascaridole in Germany, resulting in one of the first example of industrial application of photochemical reactions.

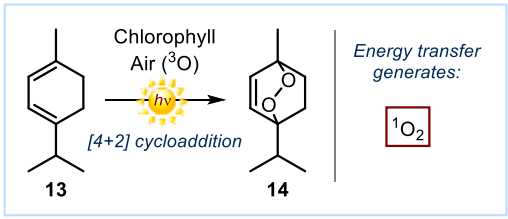

Figure 2.14: Energy transfer-mediated synthesis of Ascaridole.

2.7 Proton Transfer

The charge redistribution associated with photoexcitation can also drastically change the acid-base behavior of the species involved. Excited-state molecules often possess a different acidity compared to the corresponding ground state. For instance, the $n \rightarrow \pi^*$ transition, typical of the photoexcitation of phenol derivatives, decreases the electronic charge on the oxygen atom, which undergoes deprotonation more easily. The fast deprotonation can generate the excited-state conjugated base (eq 2.19).

$$BH + h\nu \rightarrow BH^* \rightleftarrows B^{-*} + H^+ \qquad (2.19)$$

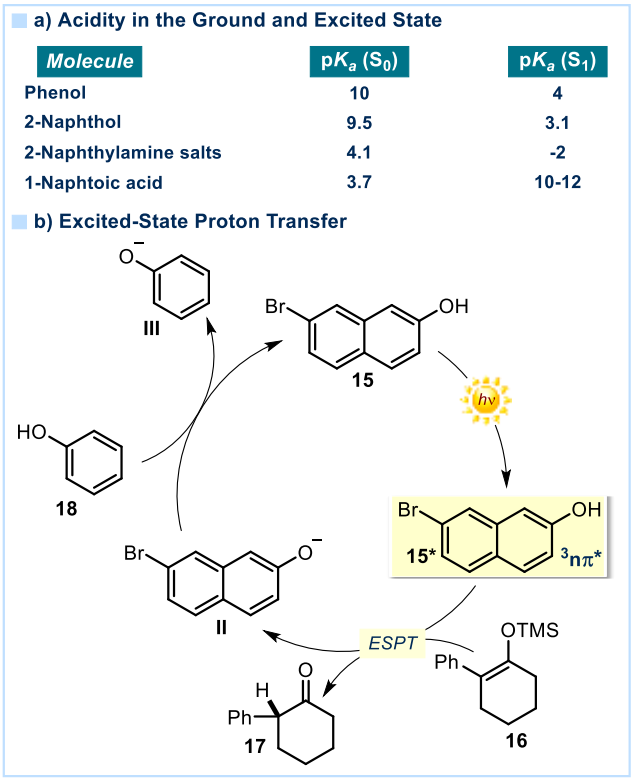

Figure 2.15: a) Acidity of ground-state and excited-state molecules. b) Excited-state proton transfer.

Generally, for phenols and aromatic amines salts, the singlet excited state is 10^5-10^6 more acidic than the corresponding ground state. For aromatic carboxylic acids, this trend is reversed and the acidity of the excited state is decreased compared to the ground state (Figure 2.15a). This is ascribable to the formation of a zwitterionic charge-transfer resonance structure in the excited-state of these species, which increases their basicity. The light-induced increment of acidity in naphtol derivatives was exploited by Hanson to develop an excited-state intermolecular proton transfer (ESPT) photocatalytic methodology (Figure 2.15b).[23] In this transformation, the electronically excited-state of 7-bromo-2-naphtol **15***, generated upon UV light absorption, displays higher acidity and triggers the protonation of the silylenol ether **16** to form the corresponding ketone **17**. Stoichiometric amount of phenol **18** secures the protonation of the conjugated base **II** restoring the naphtol photocatalyst.

[23] Das, A., Banerjee, T., Hanson, K., "Protonation of silylenol ether via excited state proton transfer catalysis" *Chem. Commun.* **2016**, *52*, 1350.

2.8 Atom Transfer

Another important mechanism of photochemical activation involves the generation of radicals through hydrogen atom transfer (HAT) from a ground-state species. This is a peculiar transformation of excited-state carbonyl compounds.[24] These species, which arise from an $n \rightarrow \pi^*$ electronic transitions, are electrophilic and with a radical character in the proximity of the oxygen atom. The triplet $^3n\pi^*$ excited-state of carbonyl compounds can be considered as a biradical species and, in terms of radical reactivity, they behave similarly to alkoxy radicals, abstracting hydrogen atoms from suitable donor compounds.[25] Concerning this mode of interaction of excited-state molecules, one of the most prominent example is the photoreduction of benzophenone in the presence of a hydrogen donors (Figure 2.16). In this reaction, benzophenone **19** absorbs UV light and reaches, after intersystem crossing, a triplet $^3n\pi^*$ excited-state **19***. The biradical character of this species enables the concerted hydrogen atom abstraction from a variety of donors (RH), generating a ketyl radical **III** and the corresponding radical from the donor **IV**. The rate and the feasibility of this process depend on the energy of the excited state involved in the HAT and on the bond dissociation energy of the hydrogen atom donor. Recently, polyoxometalates, like decatungstate ($W_{10}O_{32}^{4-}$), have found many synthetic applications as photocatalysts for HAT reactions.[26]

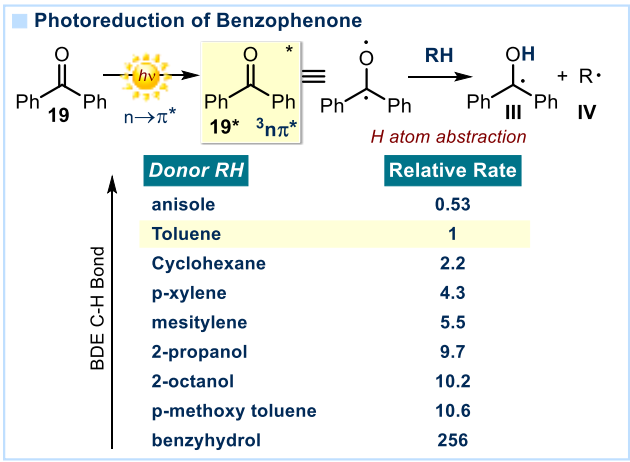

Figure 2.16: Photoreduction of benzophenone.

[24] Scaiano, J. C., "Intermolecular photoreductions of ketones" *J. Photochem.* **1973**, *2*, 81.
[25] Padwa, A., "An alkoxy radical as a model for the n, π excited state" *Tetrahedron Lett.* **1964**, *5*, 3465.
[26] Tzirakis, M. D., Lykakis, I. N., Orfanopoulos, M., "Decatungstate as an efficient photocatalyst in organic chemistry" *Chem. Soc. Rev.* **2009**, *38*, 2609.

2.9 Mechanistic Considerations

The mechanistic investigations of the photochemical processes played a crucial role for the optimization of the synthetic methodologies developed in this doctoral thesis. Understanding the excited-state reactivity and the photophysics of the involved organic intermediates was crucial to implement further transformations. These mechanistic investigations also provided an opportunity for learning important concepts related to the beautiful field of synthetic photochemistry. In this section, some considerations about the classical mechanistic studies of light-driven transformations are discussed.

The short lifetime of the highly reactive species involved in photochemical reactions often hampers the mechanistic investigations. Classical tools use by organic chemists to study polar processes may lack in efficiency when applied to light-driven processes. However, a combination of experiments and instrumental analysis can be carried out in order to elucidate the mechanism of photochemical transformations.

The first event of any photochemical process is the absorption of light from a ground-state molecule to afford an electronically excited state. At the early stage of reaction development, mechanistic investigations should focus on the analysis of the ground-state properties of the light-absorbing molecules. The target is to identify the chromophore (to then achieve its selective and efficient irradiation) and evaluate its redox properties. This requires the chemist to study the chromatic and electrochemical features of the reaction components. This can be easily achieved through *UV-Vis spectroscopy* and *cyclic voltammetry* measurements.

Radiative deactivation *via* fluorescence or phosphorence can be considered the fingerprint of the electronically excited-states. For this reason, the analysis of the emission profile of the excited state involved in the photochemical transformation, and its variations can provide relevant information related to the reaction mechanism. One of the most useful experiments is the Stern-Volmer quenching analysis, which can be performed with a spectrofluorometer. A decrease in intensity of emission (quenching) occurs when an excited-state molecule is deactivated by collision with another species (quencher). Accordingly, emission quenching experiments can be adopted to verify the interactions of photoexcited molecules with other reaction components. These experiments, albeit quantitatively useful, cannot discriminate among different modes of interaction (e.g., energy transfer *vs* electron transfer manifolds).

The detection and identification of transient intermediates involved in a photochemical reaction is usually challenging due to their short lifetime. However, several direct and indirect methods are available for their characterization. The most prominent approach relies on the use of trapping agents which intercept these fleeting and reactive intermediates forming more stable species. The use of classic analytical technologies, including *flash-photolysis*[27] and

[27] Time-resolved absorption spectroscopy (flash-photolysis), can also be used to discriminate between electron-transfer and energy-transfer manifolds. This is possible, for example, when the oxidized or reduced molecule, generated from a SET event, gives rise to a new distinctive absorption signal in the accessible portion of the spectrum.

electron spin resonance (EPR) *spectroscopy*, are also extremely useful for detecting transient and radical species, respectively.

Photochemical reactions often generate radicals that are responsible for product formation. Some processes proceed via a radical-radical coupling mechanism, where open-shell intermediates recombine to afford a closed-shell species. In many cases, radical reactions proceed through self-propagating radical-chain pathways. In such processes, the product is formed through propagation steps that convert the radical, (not necessarily) photochemically generated from the substrate precursor, into the final product while regenerating the chain-propagating radical. In chain process, the photochemical step would therefore serve as initiation event that generates the original radical. The determination of the *quantum yield* (Φ) of a photochemical reaction allows the discrimination between these two pathways. This is defined as:

$$\Phi(\lambda) = \frac{mol\ of\ product\ formed}{mol\ of\ photons\ absorbed}$$

When $\Phi > 1$, a chain propagation radical process is likely taking place. Whilst, fractional values for the quantum yields ($\Phi < 1$) can suggest the occurrence of radical-radical coupling scenarios.

Chapter III

The Excited-State Reactivity of Iminium Ions

Target

Investigation of the excited-state properties of catalitically generated chiral iminium ion and development of a methodology for the light-driven enantioselective β-benzylarion of enals.

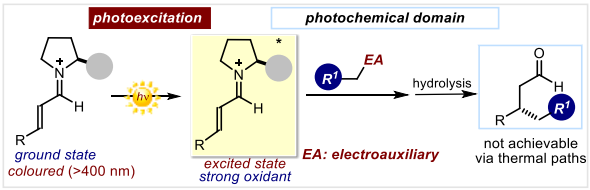

Tool

Use of the oxidative power of excited-state iminium ions to generate alkyl radicals from ready available precursors.[1]

3.1 Introduction

Chiral iminium ions, generated upon condensation of amine catalysts with α,β-unsaturated carbonyl compounds, have been widely used by chemists to make chiral molecules in an enantioselective fashion. Since the first report by MacMillan,[2] the iminium ion activation served to develop a variety of organocatalytic protocols. In contrast, the ability of chiral iminium ions to absorb light and promote photochemical reactions remained unexplored. This is despite the fact that visible-light absorption by iminium ions is an efficient naturally occurring event that initiates the mechanism of vision in higher organisms.

Recently, the Melchiorre group demonstrated that visible-light irradiation of transiently generated *electron-rich* enamines **I**, primarily understood as nucleophiles in their ground states, provides strongly reducing excited states **I*** (Figure 3.1a). These are capable to trigger the SET reduction of suitable acceptors **1**, such as bromomalonates and α-iodosulfones, generating electrophilic alkyl radicals. Stereoselective trapping of these radicals by the chiral enamine provides the desired α-alkylation products **2**.[3] In analogy to this precedent, we

[1] The project discussed in this Chapter has been conducted in collaboration with Dr. Mattia Silvi, Dr. Charlie Verrier and Dr. Yannick Rey. Part of the work has been published, see: Silvi, M., Verrier, C., Rey, Y. P., Buzzetti, L., Melchiorre, P., "Visible-light excitation of iminium ions enables the enantioselective catalytic β-alkylation of enals" *Nat. Chem.* **2017**, *9*, 868. .

[2] Ahrendt, K. A., Borths, C. J., MacMillan, D. W., "New strategies for organic catalysis: the first highly enantioselective organocatalytic diels− alder reaction" *J. Am. Chem. Soc.* **2000**, *122*, 4243.

[3] a) Silvi, M., Arceo, E., Jurberg, I. D., Cassani, C., Melchiorre, P., "Enantioselective organocatalytic alkylation of aldehydes and enals driven by the direct photoexcitation of enamines." b) Filippini, G., Silvi, M., Melchiorre, P., "Enantioselective Formal α-Methylation and α-Benzylation of Aldehydes by Means of Photo-organocatalysis."

surmised that the photoexcitation of catalytically generated *electron-deficient* iminium ion **II**, mainly acting as electrophiles in polar reactions, would provide highly oxidazing excited states **II***, capable to trigger the SET oxidation of suitable electron donors **3**, while generating alkyl radicals. In this case, the stereoselective trapping of these radicals would give access to the enantioenriched β-alkylation product **4.** As for the enamine case, the presence of a suitable fragmenting group within the donor substrate would avoid a back electron transfer (BET) leading to the irreversible and productive formation of radicals. (Figure 3.1b).

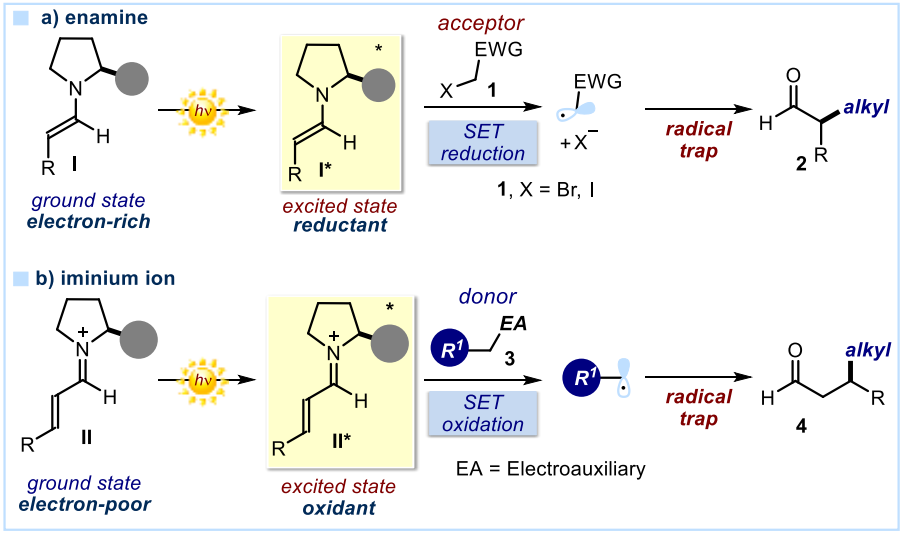

Figure 3.7: a) The photoexcitation of electron-rich enamines provides a strongly reducing excited state that can trigger the radical-mediated α-alkylation of aldehydes. b) In analogy, light-excitation of electron-poor iminium ions may provide an oxidizing excited state.

Following this idea, we could develop a methodology for the synthesis of enantioenriched β-benzylated aldehydes using readily available alkyl silane derivatives as radical sources. These substrates are poor nucleophiles and therefore recalcitrant to classical iminium ion-mediated conjugate addition manifolds. The reaction proceeds under violet light irradiation and provides the desired products in good yields and stereoselectivity. Crucial to success was (i) the design of a proper reaction set-up, which ensured perfect reproducibility, and (ii) the synthesis of a family of chiral amine catalysts with well-tailored electronic properties, which could generate a photo-active iminium ion while providing the source of stereochemical induction.

3.2 Iminium Ion Catalysis

Iminium-ion activation relies on the capability of chiral amine catalysts to reversibly condense with α,β-unsaturated carbonyl compounds, forming electron-deficient iminium ions. The electronic redistribution associated with such condensation lowers the energy of the LUMO within the substrate, thus generating a highly electrophilic π system. This mode of activation was first reported by MacMillan in 2000.[2] In this seminal work, the iminium-ion formation was exploited to promote an asymmetric Diels-Alder cycloaddition of α,β-unsaturated aldehydes with dienes (Scheme 3.1). Here, the condensation of the chiral imidazolidinone catalyst **7** with the enal of the type **5** generates the iminium ion intermediate **III** that undergoes [4+2] cycloaddition with cyclohexadiene **6**. The overall process provides the cycloaddition product **8** with good level of diastereo- and enantio-selectivity.

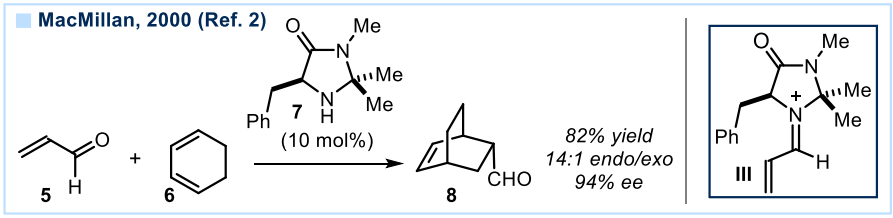

Scheme 3.1: Iminium ion-catalyzed asymmetric [4+2] cycloaddition.

Since this first report, a myriad of transformations, involving the ground-state reactivity of iminium ions, has been developed for the stereoselective β-functionalization of enals (Figure 3.2a).[4] These methodologies often complement the established metal-based asymmetric methods for the conjugate additions to α,β-unsaturated carbonyl compounds.[5] Generally, in these reactions, the iminium ion intermediate undergoes the attack of a soft nucleophile at the β-carbon, providing the enantioenriched β-functionalization product after hydrolysis of the catalyst. The success and the versatility of these organocatalytic transformations is ascribable to the development of efficient chiral amine catalysts. These organocatalysts are generally capable to i) efficiently condense with the enal in a reversible manner, ii) control the iminium-ion geometry and iii) control the discrimination between the two π-faces of the olefin inducing enantioselectivity in the attack of the nucleophile at the β-carbon (Figure 3.2b).

[4] a) Erkkilä, A., Majander, I., Pihko, P. M., "Iminium catalysis." b) MacMillan, D. W., "The advent and development of organocatalysis" *Nature* **2008**, *455*, 304.
[5] Córdova, A., "Catalytic asymmetric conjugate reactions". **2010**; John Wiley & Sons.

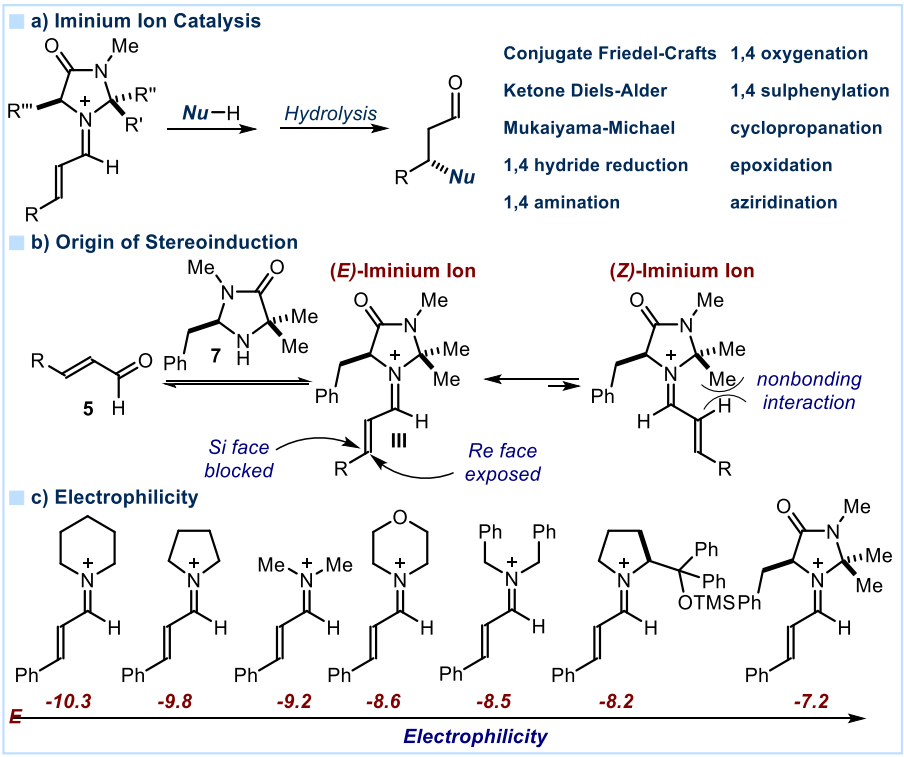

Figure 3.2: a) The iminium ion activation strategy was exploited for the development of a myriad of asymmetric functionalizations of enals. b) Chiral amine catalysts, upon condensation, are capable to control the geometry of the iminium ion and the discrimination between the two π-faces. c) Electrophilicity scale of several iminium ions.

Imidazolidinone and proline derivatives displayed a wide applicability as catalysts for iminium-ion activation. In particular, among the latter, the diarylprolinol silyl ethers, developed by Jørgensen[6] and Hayashi[7], have been widely used as catalysts for the functionalization of enals. Structure-activity studies, conducted by Mayr,[8] defined and compared the electrophilicity parameter E of the iminium ions generated with different secondary amine catalysts (Figure 3.2c). This parameter helps to understand the tendency of these species to undergo the attack of the nucleophiles. The superior reactivity of the imidazolidinone-based and of the diaryl prolinol silyl ether catalysts was confirmed, in fact these organocatalysts provide iminium ion displaying higher electrophilicity.

---

[6] Franzén, J., Marigo, M., Fielenbach, D., Wabnitz, T. C., Kjærsgaard, A., Jørgensen, K. A., "A general organocatalyst for direct α-functionalization of aldehydes: stereoselective C− C, C− N, C− F, C− Br, and C− S bond-forming reactions. scope and mechanistic insights" *J. Am. Chem. Soc.* **2005**, *127*, 18296.

[7] Hayashi, Y., Gotoh, H., Hayashi, T., Shoji, M., "Diphenylprolinol silyl ethers as efficient organocatalysts for the asymmetric Michael reaction of aldehydes and nitroalkenes" *Angew. Chem.* **2005**, *117*, 4284.

[8] Lakhdar, S., Tokuyasu, T., Mayr, H., "Electrophilic Reactivities of α, β-Unsaturated Iminium Ions" *Angew. Chem. Int. Ed.* **2008**, *47*, 8723.

3.3 Iminium Ion as Chromophore

Non-conjugated iminium ions are known to efficiently absorb light and therefore act as chromophores. The electronic characteristics of iminium ions are similar to the ones of alkenes.[9] For example, their absorption profile is similar to the structurally-related olefin (Figure 3.3). Likewise alkenes, iminium ions undergo a $\pi \rightarrow \pi^*$ electronic transition upon light excitation. This transition affords a moderately long-lived singlet excited state that decays to the ground state through fluorescence, with levels of efficiency that vary depending on the substituent.

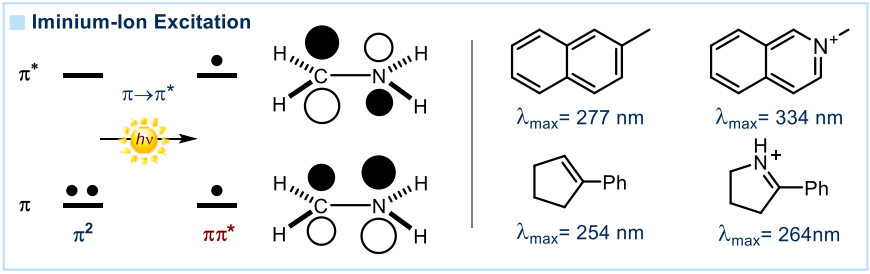

Figure 3.3: Photoexcitation of non-conjugated iminium ions, which display absorption profiles similar to the structurally related olefins.[10]

These $\pi\pi^*$ excited states are characterized by a reduced C=N bond order, due to the population of the antibonding π^* orbital. For this reason, the large energetic barrier for the *cis-trans* isomerization found in the ground state (70-90 kcal/mol) is sensibly decreased in the excited-state manifolds. Moreover, these $\pi \rightarrow \pi^*$ transitions produce excited states with greater electron density on the carbon compared to the ground state. This condition hampers nucleophilic additions, which are peculiar in the thermal reactivity of iminium salts.

As for the α,β-unsaturated iminium ions (ene-iminium ions), the photo-isomerization occurs both at the C=N and at the C=C bond providing photostationary states with up to four geometric isomers (Figure 3.4a). The product distribution is highly influenced by the nature and the steric features of the substituents at the N atom and at the β-C atom.[11] Iminium-ion photoisomerization plays a crucial role in biological system. Nature exploits the iminium ions ability of absorbing visible-light to trigger the mechanism of vision in higher organisms

[9] Mariano, P. S., "The photochemistry of iminium salts and related heteroaromatic systems" *Tetrahedron* **1983**, *39*, 3845.
[10] Kleinfelter, D. C., Schleyer, P. V. R., "Aryl Norbornane Derivatives. I. Preparation of Compounds" *J. Org. Chem.* **1961**, *26*, 3740.
[11] a) Childs, R. F., Dickie, B. D., "Photochemical and thermal stereomutations of 3-aryl-2-propenylideniminium salts" *J. Am. Chem. Soc.* **1983**, *105*, 5041. b) Pankratz, M., Childs, R. F., "Photoisomerization of some N-aryl-α,β-unsaturated Iminium Salts" *J. Org. Chem.* **1988**, *53*, 3278.

(Figure 3.4b).[12] In vertebrates, this is initiated by light excitation of Rhodopsin **IV**, the iminium ion formed upon condensation of 11-*cis*-retinal **9** with the ε-amino group of a lysine residue within the protein opsin **10**. Excited-state Rhodopsin undergoes a cis-trans isomerization at the $C_{11}C_{12}$ bond providing the all-*trans*-state that starts the photo-transduction process. Crucially, 11-*cis*-retinal undergoes a bathochromic absorption shift from ultraviolet (370 nm) to the visible region (> 400 nm) upon formation of **IV**.

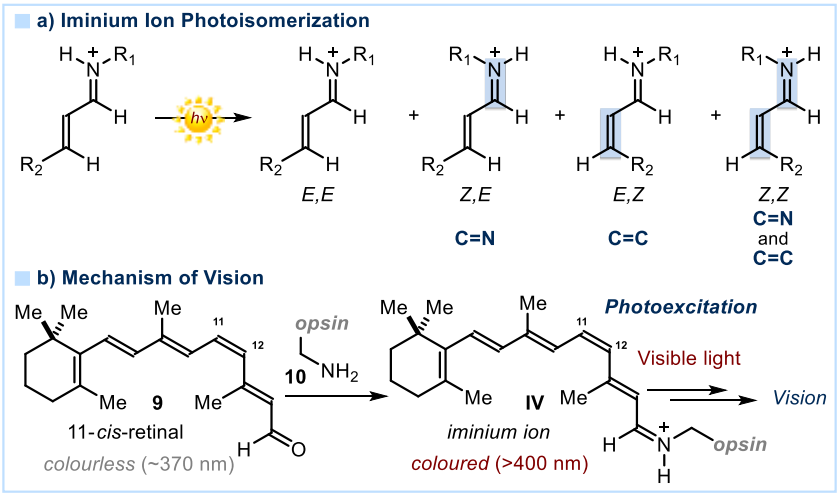

Figure 3.4: a) Photoisomerization of α,β-unsaturated iminium ions provides photostationary states with up to four geometric isomers. b) The mechanism of vision in higher organisms.

Despite the electronic similarity between olefins and non-conjugated iminium salts, the latter present a delocalized positive charge that alters the ground-state and excited-state properties. In the case of iminium ions, this charge lowers the energies of both HOMO and LUMO making them less energetic than the ones of the structurally-related alkenes. The presence of low energy LUMOs in ground-state iminium ions facilitates their single electron reduction, which affords stabilized α-amino radicals. Redox potentials ($E_{1/2}$) for these reductions fall in the range -1.95 and -0.85 V (Figure 3.5). Additionally, the presence of conjugation further lowers the energy of the LUMO; for this reason, α,β-unsaturated iminium ions display more positive redox potentials and are even more prone to SET reductions. The delocalized positive charge, which strongly affects the redox properties of ground-state iminium salts, is also influencing their excited-state reactivity. In fact, considering that excited-state molecules serve as better reductant and better oxidant compared to the corresponding ground states, photoexcited electron-poor iminium ions can enable single electron oxidation.

[12] a) Wald, G., "The molecular basis of visual excitation" *Nature* **1968**, *219*, 800. b) Ernst, O. P., Lodowski, D. T., Elstner, M., Hegemann, P., Brown, L. S., Kandori, H., "Microbial and animal rhodopsins: structures, functions, and molecular mechanisms" *Chem. Rev.* **2013**, *114*, 126.

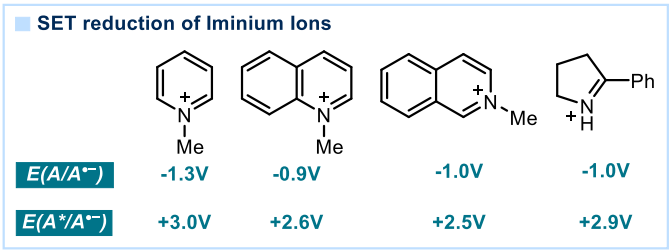

Figure 8.5: The low energy LUMO enables the easy reduction of ground-state iminium ions. Additionally, in their excited states, iminium ions can act as oxidants.

The SET photochemistry of preformed, non-conjugated iminium ions was broadly studied by Mariano in the 1980s.[13] These species, upon light absorption, become powerful oxidants and their redox potential can reach E^{red} > 3V, rendering them capable to oxidize a variety of organic molecules. Mariano demonstrated the wide applicability of excited-state iminium ion in radical-mediated photochemical processes. In its seminal work, the highly oxidant excited state of 2-phenyl-1pyrrolinium perchlorate **11*** (E^{red} = +2.9 V) triggered the thermodynamically feasible SET oxidation of isobutylene **12** (E^{ox} = +2.3 V) forming the two radical intermediates **V** and **VI**. Methanol, which served as solvent for the photochemical reaction, acted as a nucleophile attacking the radical cation **VI** thus providing the more stabilized radical **VII**. Finally, radical recombination of **V** and **VII** yielded the desired product **13** (Scheme 3.2).[14]

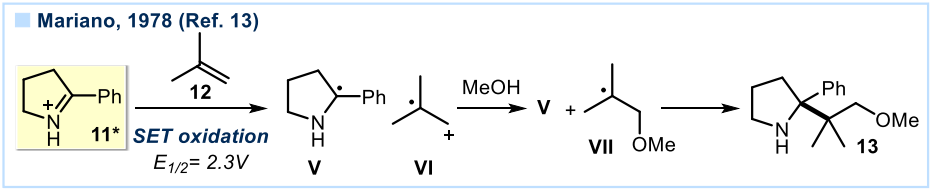

Scheme 3.2: Photoexcited iminium ion enables the SET oxidation of isobutylene and the generation of radicals.

3.4 Target of the Project

Inspired by the excited-state properties of iminium salts, we envisioned the possibility to transfer this SET reactivity to chiral conjugated iminium ions, catalytically generated from α,β-unsaturated aldehydes. We anticipated that this strategy would allow the mild generation

[13] Mariano, P. S., "Electron-transfer mechanisms in photochemical transformations of iminium salts" *Acc. Chem. Res.* **1983**, *16*, 130.
[14] Mariano, P. S., Stavinoha, J. L., Pepe, G., Meyer Jr, E. F., "Novel photochemical addition reactions of iminium salts. Electron transfer initiated additions of olefins to 2-phenyl-1-pyrrolinium perchlorate" *J. Am. Chem. Soc.* **1978**, *100*, 7114.

of open-shell species that could be exploited for the asymmetric construction of C–C bonds. If successful, the approach of combining photochemistry with the classical tool of aminocatalysis would unlock unique reaction manifolds unavailable to classical ground-state iminium ion chemistry, thus providing fresh opportunities for reactions invention. Moreover, this strategy would complement the previously reported excited-state reactivity of enamine by exploiting a different series of radical precursors. In this context, we focused on the development of a visible-light promoted stereoselective β-alkylation of enals.

As depicted in Figure 3.6, we hypothesized that, in analogy with the mechanism of vision, the condensation of a chiral secondary amine catalyst **14** with the enal **15**, in the presence of an acid co-catalyst, would convert an achromatic substrate into a coloured iminium ion **II**. Visible-light excitation would then give access to an electronically excited state **II***, which could serve as strong SET oxidant. Specifically, the SET oxidation of a suitable donor **3** would furnish the 5π-electron β-enaminyl radical intermediate **VIII** along with the radical cation **IX**, which can undergo irreversible fragmentation providing the key alkyl radical **X**. The stereoselective intermolecular coupling of the chiral β-enaminyl radical **VIII** with **X** would form a new C–C bond while forging the stereogenic centre. Hydrolysis of the resulting enamine intermediate **XI** would regenerate the catalyst **14** while liberating the β-functionalized aldehyde **4**.

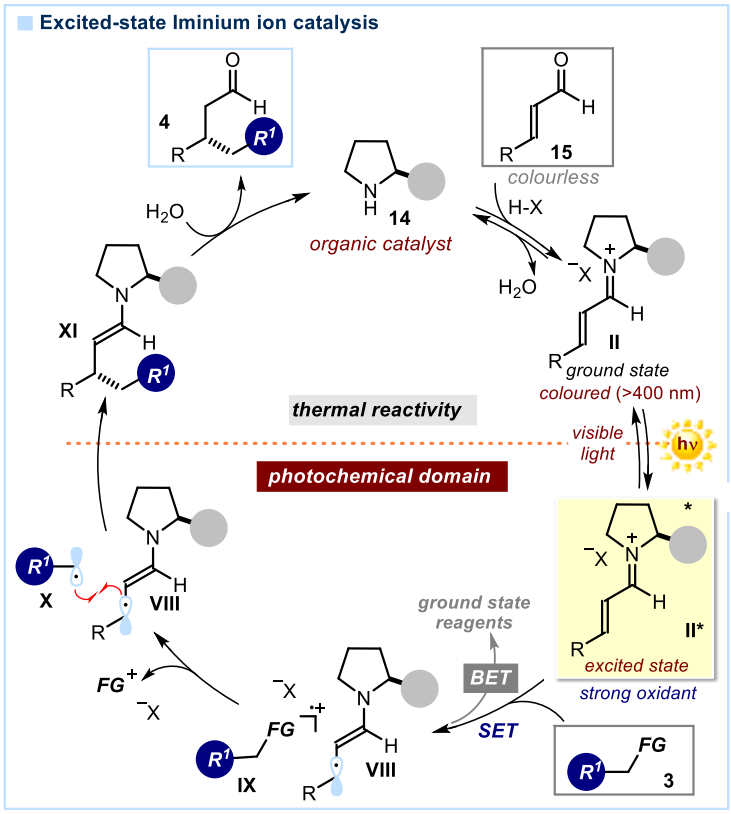

Figure 3.6: Design plan for the light-induced stereoselective β-alkylation of enals.

3.5 The Choice of the Donor

Excited-state iminium ions are very strong oxidant and capable to accept one electron from donor compounds. Seeking for a suitable radical precursor, we focused on the selection of the redox partner **3**. The choice of this substrate is mainly dictated by two requirements: i) the substrate should easily donate an electron to the photoexcited iminium ion and ii) should easily undergo fragmentation after the SET, in order to avoid the unproductive back electron transfer (BET), while providing the desired alkyl radical. We envisioned that the introduction of an electroauxiliary (EA) group within the redox partner would serve to fulfil these requirements.[15] EA groups are moieties that facilitates the electron-transfer in a more selective manner, modulating the redox potentials of the substrates. Moreover, EA groups, undergoing irreversible fragmentation, can help the control of the chemical processes which take place after the ET event.

[15] Yoshida, J.-I., Kataoka, K., Horcajada, R., Nagaki, A., "Modern Strategies in Electroorganic Synthesis" *Chem. Rev.* **2008**, *108*, 2265.

Among EA groups, alkyl silanes have been widely exploited in order to lower the oxidation potential of molecules.[15] The mechanism of action of these groups relies on the interactions between the C–Si σ orbital and other orbitals present within the molecule (Figure 3.7). In the case of substrates containing heteroatoms, the molecular interactions occurs between the C–Si σ orbital and the n orbital, while in the case of conjugate system the interaction of the C–Si bonds takes place with the π orbitals. In both cases, these interactions generate two new molecular orbitals (bonding and antibonding). The raising of the energy of the HOMO, associated with these molecular orbital interactions, facilitates the removal of an electron from the molecule bearing the silyl group. Moreover, the radical cation, which is produced after the SET, possesses two stabilized electrons in the bonding orbital and only one destabilized in the antibonding, thus further decreasing the oxidation potential of these species.

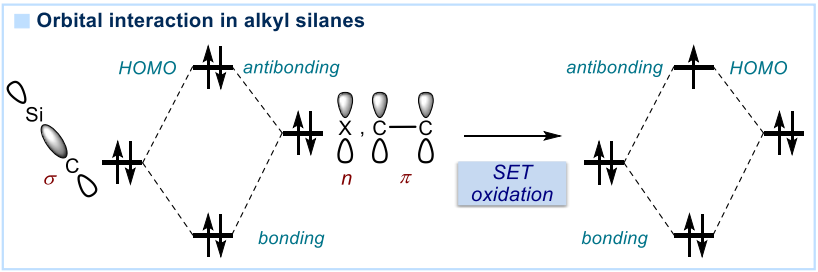

Figure 3.7: Molecular orbital interactions in silyl-group-containing molecules.

The irreversible fragmentation of the radical cation, obtained after SET oxidation, is the key step that provides the desired alkyl radical.[16] The efficiency of this cleavage is fundamental in minimizing the unproductive BET, a thermodynamically favored process that restore the substrates in their ground state. In addition to their role in the modulation of the oxidation potential of the substrates, alkyl silanes rapidly undergo nucleophile-assisted fragmentation in the presence of weak nucleophile, including acetonitrile and water, from the corresponding radical cations.[17] This feature was exploited by Mariano for the development of the photoexcited iminium ion-mediated benzylation reaction depicted in Scheme 3.3.[18] In this protocol, the excited state of a cyclic preformed iminium ion **11*** promoted the SET oxidation of benzyl trimethilsilane **3a** to afford the corresponding radical cations **IX** and the radical intermediate **V**. Nucleophile-assisted fragmentation of the silyl groups gave access to the

[16] Albini, A., Mella, M., Freccero, M., "A new method in radical chemistry: generation of radicals by photo-induced electron transfer and fragmentation of the radical cation" *Tetrahedron* **1994**, *50*, 575.
[17] Dockery, K. P., Dinnocenzo, J. P., Farid, S., Goodman, J. L., Gould, I. R., Todd, W. P., "Nucleophile-assisted cleavage of benzyltrialkylsilane cation radicals" *J. Am. Chem. Soc.* **1997**, *119*, 1876.
[18] Borg, R. M., Heuckeroth, R. O., Lan, A. J., Quillen, S. L., Mariano, P. S., "Arene-iminium salt electron-transfer photochemistry. Mechanistically interesting photoaddition processes" *J. Am. Chem. Soc.* **1987**, *109*, 2728.

stabilized benzyl radical **X**. Radical coupling between **X** and **V** finally led to the desired benzylated product **16**.

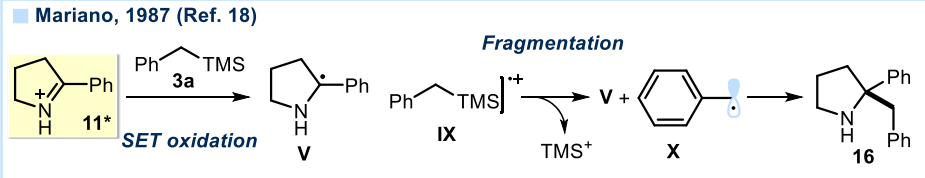

Scheme 3.3: Use of benzyl trimethylsilane as benzyl radical source in a photoexcited iminium ion-mediated benzylation reaction.

Relying on these precedents, we identified benzyl trimethylsilane **3a** as both a suitable donor and benzyl radical source for the proposed light-triggered transformation. We also confirmed the propensity of **3a** towards SET oxidation measuring its oxidation potential by cyclic voltammetry. We measured the fairly low value E^{ox} = 1.74 V (vs Ag/AgCl).

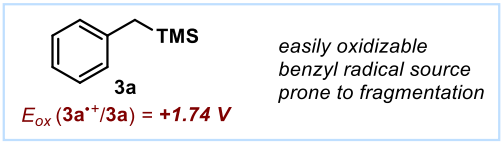

3.6 Results and Discussion

We decided to exploit the excited-state properties of transiently formed iminium ions to achieve the catalytic enantioselective direct β-benzylation of enals. This photochemical transformation would furnish the enantioenriched β-benzylated aldehyde, a synthetically useful chiral compound that cannot be easily accessed by other direct stereoselective methods. In the polar domain, the instability of benzyl-metallic derivatives, along with the competing 1,2-addition manifold, hampered the development of catalytic asymmetric direct metal-catalyzed conjugate additions of benzyl-metallic reagents to α,β-unsaturated aldehydes. However, it is worth mentioning that this transformation has been achieved in non-stereoselective[19] and indirect[20] variants. Additionally, thermal enantioselective iminium ion protocols have been reported for only specific class of highly activated nitro-toluene substrates.[21] In the realm of radical reactivity, the large resonance stabilization of benzyl

[19] Van Heerden, P. S., Bezuidenhoudt, B. C., Steenkamp, J. A., Ferreira, D., "Conjugate addition of benzyl copper reagents to α, α-enoates and-enones" *Tetrahedron Lett.* **1992**, *33*, 2383.
[20] Fañanás-Mastral, M., Feringa, B. L., "Copper-catalyzed regio-and enantioselective synthesis of chiral enol acetates and β-substituted aldehydes" *J. Am. Chem. Soc.* **2010**, *132*, 13152.
[21] a) Dell'Amico, L., Companyo, X., Naicker, T., Bräuer, T. M., Jørgensen, K. A., "Asymmetric Organocatalytic Benzylation of α, β-Unsaturated Aldehydes with Toluenes" *Eur. J. Org. Chem.* **2013**, *2013*, 5262. b) Li, T., Zhu, J., Wu, D., Li, X., Wang, S., Li, H., Li, J., Wang, W., "A strategy enabling enantioselective direct conjugate addition of inert aryl methane nucleophiles to enals with a chiral amine catalyst under mild conditions" *Chem. Eur. J.* **2013**, *19*, 9147. c) Duce, S., Mateo, A., Alonso, I., Ruano, J. L. G., Cid, M. B., "Role

radicals makes their addition to electron-poor olefin difficult. This is why successful strategies for benzyl radical addition to polarized alkenes have largely relied upon reduction of the acceptor partner to form a radical anion, which is a much better trap for benzyl radical.[22]

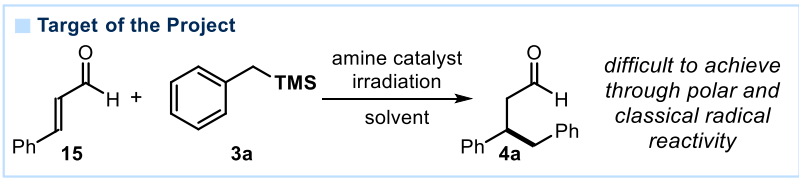

Scheme 3.4: Light-induced enantioselective β-alkylation of cinnamaldehyde.

3.6.1 Bathochromic Shift

We started our investigation with a simple observation: we detected a colour change upon mixing the commercially available imidazolidinone catalyst **A** with cinnamaldehyde **15** in the presence of tetrafluoroboric acid (Figure 3.8). This confirmed that, similarly to the mechanism of vision, the condensation of the colourless enal **15** with the amine catalyst **A** generated a coloured iminium ion **IIa**, capable to absorb visible-light.

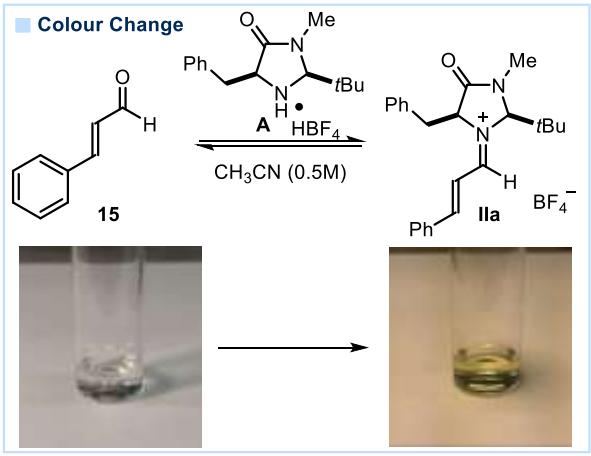

Figure 3.8: The condensation of the colorless cinnamaldehyde with the amino catalyst A induces a bathochromic shift.

of quaternary ammonium salts as new additives in the enantioselective organocatalytic β-benzylation of enals" *Chem. Commun.* **2012**, *48*, 5184.

[22] a) Montanaro, S., Ravelli, D., Merli, D., Fagnoni, M., Albini, A., "Decatungstate as photoredox catalyst: benzylation of electron-poor olefins" *Org. Lett.* **2012**, *14*, 4218. b) Capaldo, L., Buzzetti, L., Merli, D., Fagnoni, M., Ravelli, D., "Smooth Photocatalyzed Benzylation of Electrophilic Olefins via Decarboxylation of Arylacetic Acids" *J. Org. Chem.* **2016**, *81*, 7102.

We confirmed this visual observation by UV-Vis spectroscopy comparing the absorption profile of cinnamaldehyde **15** with the one of the isolated iminium ion **IIa** (for the details related to synthesis and purification of **IIa**, see the Experimental Section). As depicted in Figure 3.9, cinnamaldehyde **15** absorbs only UV fraction of light, while the iminium ion **IIa** presents an absorption band with a tail in the visible region.

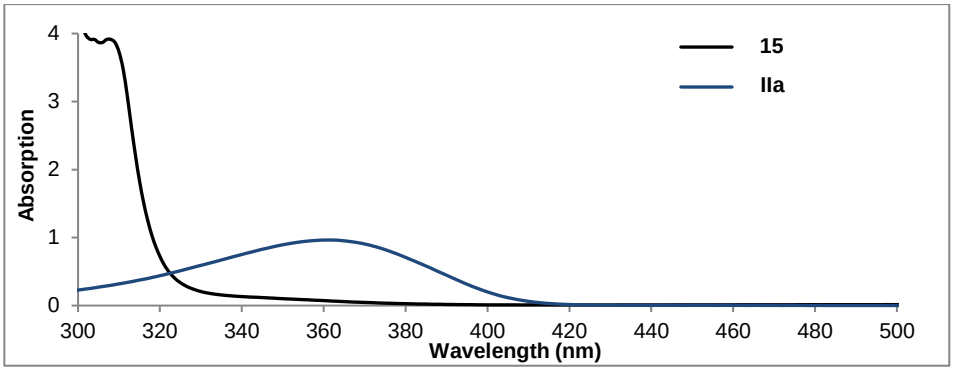

Figure 3.9: UV-Vis absorption spectra of cinnamaldehyde **15** and iminium ion **IIa**.

3.6.2 Preliminary Results and Optimization[23]

The feasibility of our idea was tested against the asymmetric benzylation of cinnamaldehyde **15** in the presence of 20 mol% of the commercially available chiral amine **A**, benzyl silane **3a** and 40 mol% of trifluoroacetic acid as the acid co-catalyst (Scheme 3.5). An excess of cinnamaldehyde (3 Equiv.) and the presence of TFA secured the efficient formation of iminium ion. The reaction mixture was irradiated with a common household 23 W compact fluorescent light (CFL) bulb for 3 days (72 hours) and the desired product **4a** was obtained in 65% isolated yield albeit in an enantiomeric excess as low as 25%.

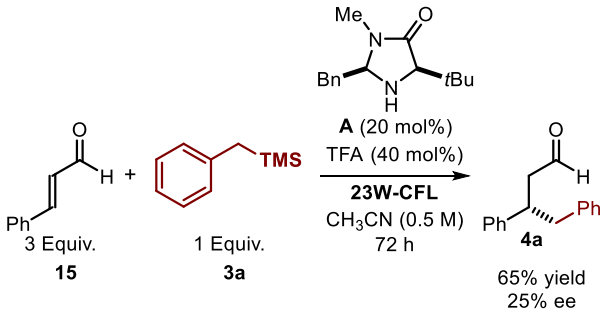

Scheme 3.5: Light-driven conjugate benzylation of cinnamaldehyde: proof of principle.

[23] Preliminary investigations were conducted by Dr Mattia Silvi.

With this promising result in hand, we started the optimization process with the aim of improving the reaction efficiency and stereoselectivity. We first evaluated the importance of the amine catalyst scaffold for this reaction. Therefore, we subjected different organocatalysts, available in our laboratories, to the reaction conditions (Scheme 3.6).

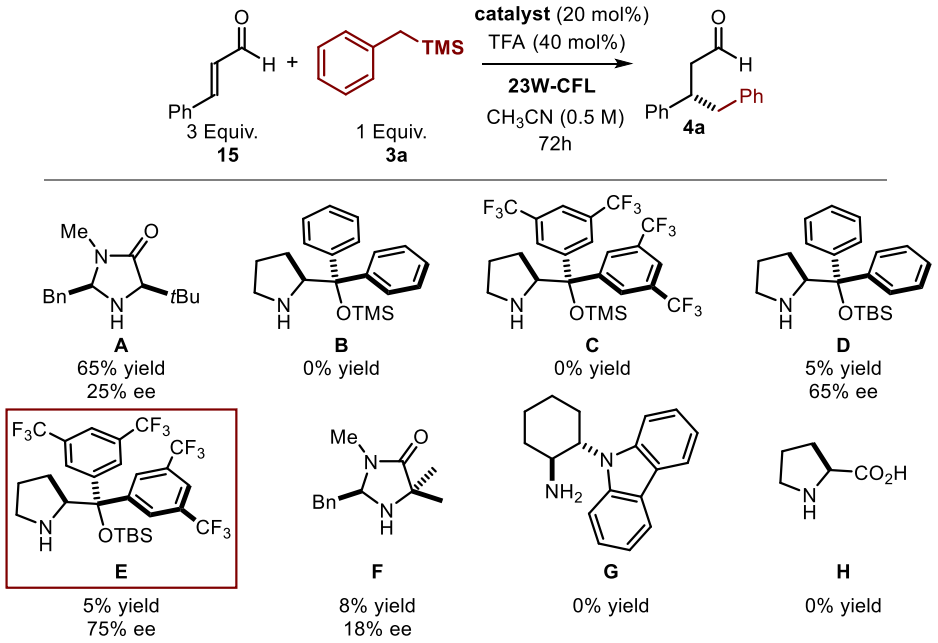

Scheme 3.6: Catalysts used in the preliminary screening.

The highest yield was obtained using the imidazolidinone based catalyst **A**. The use of other chiral amines in the presence of trifluoroacetic acid (TFA) as the acid co-catalyst led to poor reactivity. However, the diarylprolinol based catalysts (**B**-**E**) were effective in terms of stereoselectivity, even though they provided scarce reactivity. In these cases, a suitable bulky silicon protecting group, such as tert-buthyldimethylsilyl TBS, was found to be crucial for improving the catalyst stability in the acidic media and making it competent for this transformation. When the catalyst **D** and **E** were submitted to the reaction conditions, product **4a** was formed in low yield (5%) but with good level of stereoselectivity (65% and 75% ee respectively). This preliminary screening suggested that other imidazolidinone base catalysts **F**, primary amines **G** and proline **H** were not competent catalysts for this methodology.

Motivated by the promising result in terms of enantioselectivity obtained with catalyst **E**, we decided to modulate some other parameters to improve the reaction efficiency. Considering the photochemical nature of this transformation, we evaluated different light sources, since this is a parameter that can drastically affect light-driven reactions.

Table 1: Screening of the light sources for the photochemical β-benzylation of cinnamaldehyde. Reactions performed on a 0.1 mmol scale using 3 Equiv. of enals. NMR yields were determined on the reaction crude using 1 Equiv of trichloroethylene as internal standard.

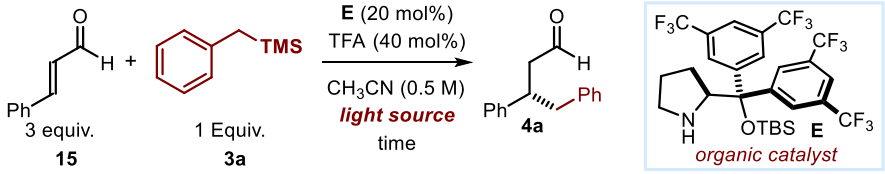

Entry	Light Source	Time (h)	Yield	ee
1	23 W CFL Bulb	72	5%	75%
2	19.2 W White LEDs Strip	72	5%	75%
3	16 W Black CFL Bulb	72	6%	75%
4	Medium Pressure Hg Lamp	11	25%	40%
5	300 W Xe Lamp	16	37%	59%
6	300 W Xe Lamp-380 nm Filter	15	46%	61%
7	7.2 W Black LEDs Strip (400 nm)	40	50%	76%

White LEDs (light emitting diode) strips and phosphorous coated black CFL (entries 2-3) did not affect the reaction outcome, whilst the employment of powerful UV light sources (entries 4-6) improved the yield of the transformation, though with a remarkable erosion of the enantiomeric excess. The use of a commercially available 400 nm LED strip (entry 7) drastically improved the reaction efficiency, furnishing the desired product **4a** after 40 hours in 50% NMR yield and 76% ee.

With the 400nm LED strip as new light source, we evaluated the effect of different silicon protecting groups on the amine catalyst. We prepared a series of diarylprolinol silyl ethers and we subjected them to the photochemical β-benzylation reaction (Scheme 3.7).

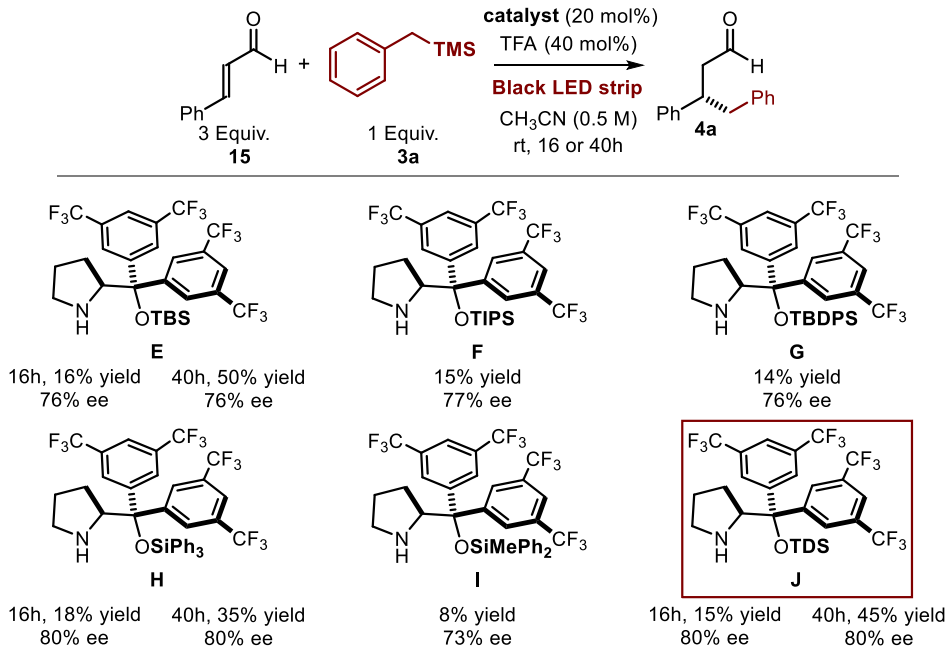

Scheme 3.7: Screening of different silicon protecting group on the diarylprolinol catalysts.

The nature of the silicon group and its steric bulkiness slightly affected the stereoinduction. Running the reaction for 16 hours, the best results in terms of enantiomeric excess were obtained using the triphenylsilyl- and dimthylthexylsilyl (TDS)-protected catalysts **H** and **J**, respectively (18% yield and 80% ee for **H**; 15% yield and 80% ee for **J**). The stability of these two catalysts was then tested over a longer reaction time (40 h). In these conditions, the triphenylsilyl protected catalyst **H** afforded the product in 35% yield without erosion of the enantiomeric excess. However, GC-MS analysis of the crude reaction mixture revealed a complete catalyst degradation. Conversely, the TDS protected catalyst **J** was successfully recovered after the reaction and provided the desired product in 45% yield and 80% ee. For this reason, catalyst **J** was selected for further optimization. Unfortunately, an extensive screening of other standard reaction parameters, including stoichiometry, solvents, acid co-catalysts, and additives, did not lead to any improvement in the reaction outcome.

3.6.3 Designing a New Reaction Set-Up

During the optimization process, we encountered problems in the reproducibility of the results. The reproducibility of an experiment is at the basis of the scientific method,[24] and it is of course a crucial aspect for an experimentalist. We decided to face this situation trying to find a solution and the reason for this inconsistency. In a photochemical reaction, many parameters can significantly affect its efficiency and robustness, including the intensity of the light, the distance of the light source from the reaction vessel and the geometry of the set up. In order to standardize these parameters, we designed a novel reaction set-up for the photochemical β-benzylation of cinnamaldehyde (Figure 3.10).

We first evaluated the light source and we moved from the unreliable 400 nm LEDs strip to a high power (HP) single LED. This commercially available and cheap high-energy LEDs, which can emit at different wavelengths, possess a sharp emission profile. In addition, they can be connected to a power supplier that can be used to finely control the intensity of emission (irradiance, mW/cm^2). The LED was positioned on an aluminum block securing its stability. We then designed and manufactured a 3D-printed vessel holder. This plastic support keeps a constant distance of 1 cm between the light source and the reaction vessel. Before introducing the reaction vessel in the spacer, the light intensity can be easily tuned and measured with a photodiode connected to a simple tester.

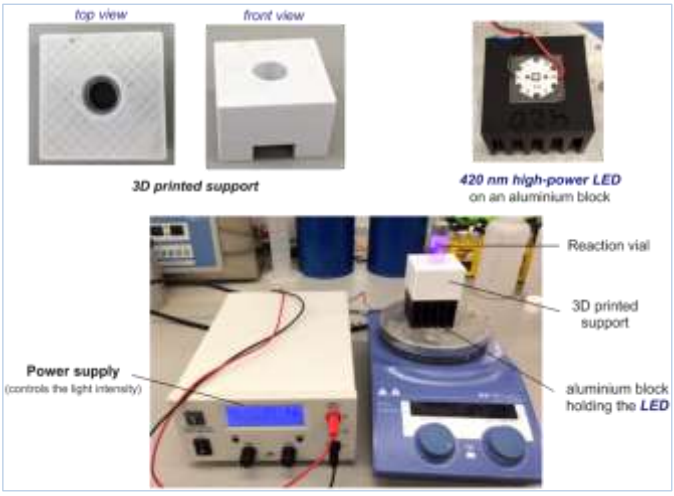

Figure 3.10: Reaction set-up. Top left: 3D printed support; top-right: HP LED on the aluminum block; bottom: the connected reaction set-up.

With the new reaction set up in hand, we tested the best catalyst identified in our previous studies, tuning the wavelength and the light intensity (irradiance) of the LED (Table 2).

[24] a) Baker, M., "1,500 scientists lift the lid on reproducibility" *Nature News* **2016**, *533*, 452. b) Cooper, M. M., "The Replication Crisis and Chemistry Education Research" *J. Chem. Educ.* **2018**, *95*, 1.

Table 2: Tuning of the wavelength and the insensity of the new light source. Reactions performed on a 0.1 mmol scale using 3 Equiv. of enals. NMR yields were determined on the reaction crude using 1 Equiv of trichloroethylene as internal standard.

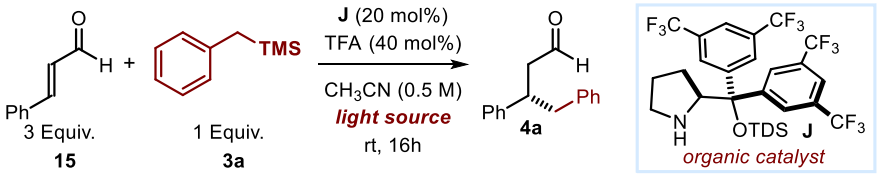

Entry	Wavelength	Irradiance	Yield	ee
1	365 nm	10 mW/cm^2	14%	53%
2	405 nm	40 mW/cm^2	65%	70%
3	415 nm	45 mW/cm^2	63%	78%
4	420 nm	40 mW/cm^2	63%	79%

We identified a 420 nm HP LED as the optimal light source (entry 4). Running the reaction for 16 hours under a 40 mw/cm^2, the desired product **4a** was obtained in 63% yield and 79% ee. Comparable results were obtained using a 415 nm HP LED (entry 3). The use of more energetic wavelengths (365 nm and 405 nm) resulted in a remarkable erosion of the enantiomeric excess (entries 1-2). This effect can be ascribed to a non catalyzed background reaction involving the competitive excitation of cinnamaldehyde when the reaction mixture is irradiated at lower wavelengths.

In addition to the good reaction efficiency, this new reaction set up ensured perfect reproducible conditions, as confirmed by several replication of the results.

3.6.4 Design of a New Family of Redox Stable Catalysts

At this stage, despite extensive efforts, we could not further optimize this photochemical reaction. Since we noticed that the organic catalyst underwent degradation during the process, we evaluated the real effect of this degradation pathway. We first measured the evolution of the catalyst **J** concentration under the optimal reaction conditions. This analysis clearly confirmed the decrease of the catalyst amount during the progression of the reaction (Figure 3.11). After 4 hours, only half amount of catalyst **J** was still present in the reaction mixture.

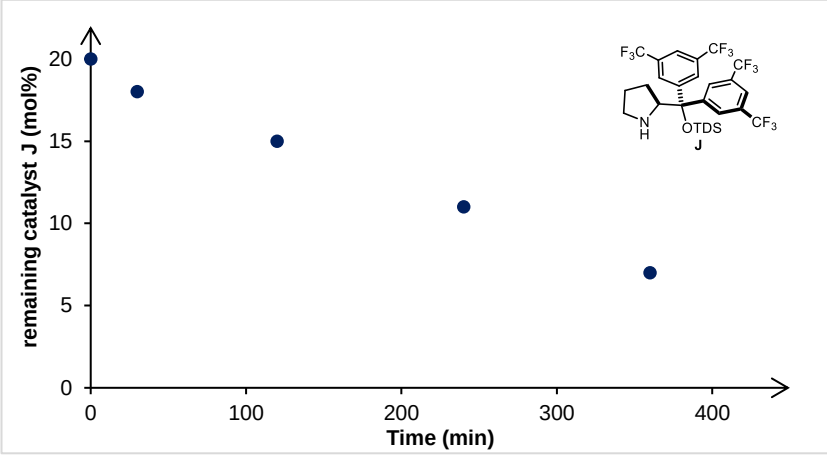

Figure 3.11: Evolution of the catalyst **J** concentration during the model reaction.

Additionally, we detected the formation of several byproducts coming from the degradation of catalyst **J** at the end of the reaction. In particular, we identified the benzophenone derivative **17** as the main degradation product. We reasoned that the degradation of the aminocatalyst **J** could be triggered by its participation in a competitive photoexcited iminium ion-mediated SET. The oxidation of the secondary amine, followed by the β-scission and desilylation of the so-formed radical cation $\mathbf{J}^{\cdot+}$, would provide the observed benzophenone derivative **17** (Scheme 3.8).[25]

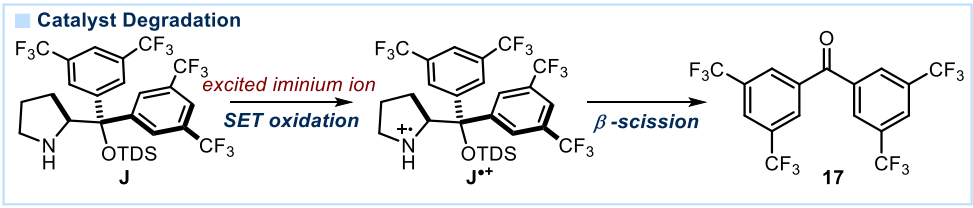

Scheme 3.8: A plausible pathway for the degradation of catalyst **J.**

To confirm the involvement of a SET in the catalyst degradation, we measured the oxidation potential of catalysts **A** and **J** and we evaluated a possible correlation between E^{ox} and the catalytic efficiency of these catalysts. (Scheme 3.9).

[25] Hu, J., Wang, J., Nguyen, T. H., Zheng, N., "The chemistry of amine radical cations produced by visible light photoredox catalysis" *Beilstein J. Org. Chem.* **2013**, *9*, 1977.

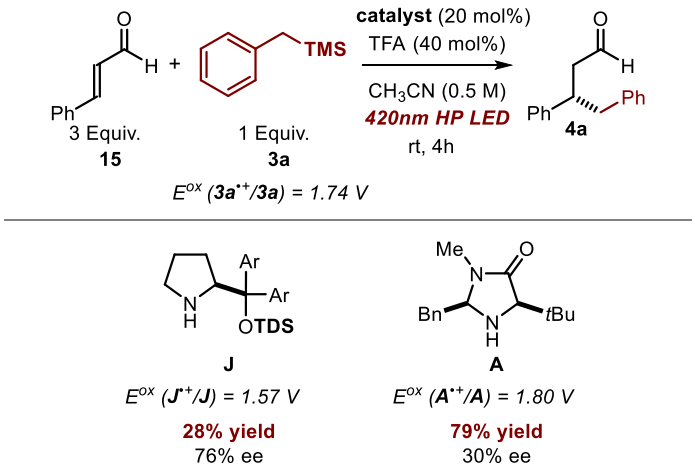

Scheme 3.9: Electrochemical characteristics of amines **A** and **J** and comparison of the catalytic activity.

As expected, we observed a remarkable correlation between the E^{ox} of the chiral amine catalysts A and J and their performance in the benzylation reaction. The electron-rich nature of the diarylprolinol catalyst **J** imparted an oxidation potential of 1.57 V, which is a slightly lower value than the E^{ox} of benzyl silane **3a** (E^{ox} = 1.74 V). This situation turns the catalyst **J** in an alternative suitable electron donor for the photoexcited iminium ion. This indicates that the proposed degradation pathway, which would limit its catalytic ability, is thermodynamically feasible (only 28% of product **4a** was obtained after 4h). On the other hand, the electron-poor imidazolidinone catalyst **A** has a higher oxidation potential of 1.80 V, which secures a better stability under the oxidative conditions. Accordingly, this catalyst provides the desired product **4a** in 79% yield after 4h. Unfortunately, the stereoinduction provided by catalyst **A** is low (only 30% ee).

These observations prompted us to modify the electronic properties of the diarylprolinol catalyst **J** in order to enhance its stability towards oxidation by attenuating its electron-donor ability while maintaining its stereoinduction ability. One of the main strategy used in medicinal chemistry to lower a compound tendency toward enzymatic oxidation relies on the incorporation of electron-withdrawing fluorine atoms in the molecule scaffold.[26] Additionally, it is known that the introduction of fluorine in a substrate backbone strongly reduces amine basicity.[27] In light of these considerations, we investigated the possibility to engineer a diarylprolinol catalyst bearing fluorine atoms within the pyrrolidine scaffold.

[26] Müller, K., Faeh, C., Diederich, F., "Fluorine in pharmaceuticals: looking beyond intuition" *Science* **2007**, *317*, 1881.

[27] Morgenthaler, M., Schweizer, E., Hoffmann-Röder, A., Benini, F., Martin, R. E., Jaeschke, G., Wagner, B., Fischer, H., Bendels, S., Zimmerli, D., "Predicting and tuning physicochemical properties in lead optimization: amine basicities" *ChemMedChem* **2007**, *2*, 1100.

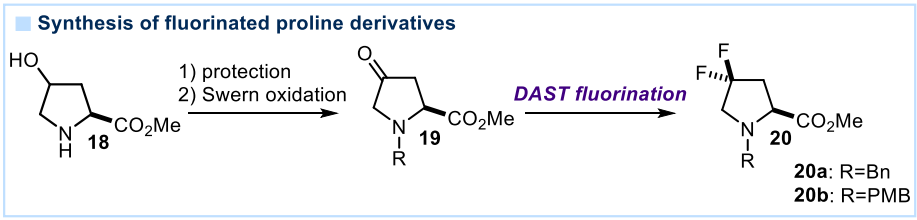

Scheme 3.10: Synthesis of the fluorinated proline derivatives. These intermediates are precursors of the fluorinated secondary amine catalysts.

As depicted in Scheme 3.10, the desired difluorinated pyrrolidine scaffold **20** was successfully obtained through a protection, oxidation, fluorination sequence starting from the commercially available 4-hydroxyproline derivative **18** (see the Experimental Section for details). With these precursors in hand, we could synthesize two novel fluorinated amino catalysts, presenting different aryl groups (**K** and **L**), which were tested in the photochemical β-benzylation reaction (Scheme 3.11).

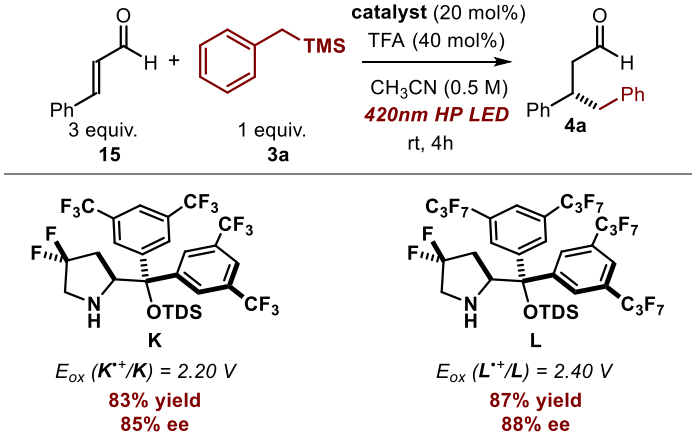

Scheme 3.11: Electrochemical characteristics of catalyst **K** and **L** and their use in the light-driven β-benzylation of cinnamaldehyde.

Both fluorinated catalysts, which displayed a drastically enhanced oxidation potential (E^{ox} > 2 V), offered outstanding results both in terms of yield and enantioselectivity. Catalyst **L**, decorated with bulkier aryl groups, furnished the desired product **4a** in 87% yield and 88% ee after only 4 hours of irradiation. For this reason, it was selected as the best catalyst for this transformation. This experiment concluded the optimization process.

3.6.5 Scope of the Reaction

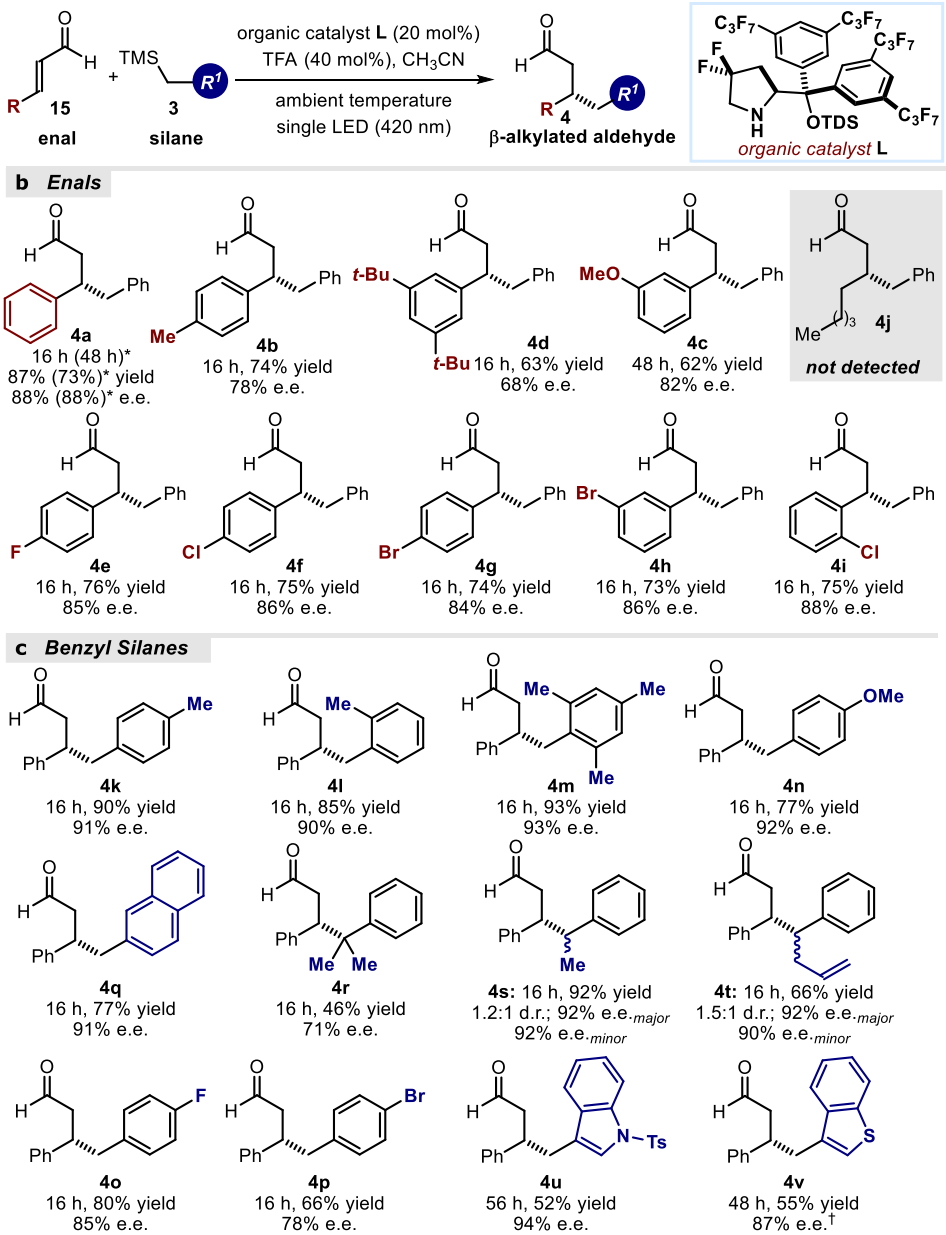

Scheme 3.12: Survey of the α,β-unsaturated aldehydes (products **4a–j**) and the benzylsilane derivatives (products **4k–v**) that can participate in the reaction. Reactions performed on a 0.1 mmol scale using 3 Equiv. of enals. Reaction time, yields and enantiomeric excesses of the isolated products are indicated below each entry (average of two runs per substrate). *Performed on a 1 mmol scale. † Using catalyst **L**. TFA, trifluoroacetic acid; TDS, thexyl-dimethylsilyl; Ts, 4-toluenesulfonyl; TMS, trimethylsilyl.

Adopting the optimized conditions, we demonstrated the generality of the photochemical β-benzylation process by evaluating a variety of enals **15** and benzyl trimethyl silanes **3**. As

shown in Scheme 3.12, different substitution patterns at the aromatic moiety of **15** were well tolerated, regardless of their electronic and steric properties and position on the phenyl ring (products **4a**-**4i**). We were able to scale up the model reaction (product **4a**) up to a 1 mmol scale maintaining a good level of efficiency and without any erosion of the enantiomeric excess. One limitation of the system is that the presence of β-alkyl fragment in the enal completely inhibits the reaction (**4j**). We reasoned that the presence of an enolizable position enables the competitive formation of the more stable dienamine upon deprotonation of the γ proton of the iminium ion. This disables the SET oxidation chemistry. Additionally, the loss of the aryl ring decreases the conjugation within the iminium ion, shifting its absorption profile to the UV-region.

The scope of the benzyl silanes revealed that a wide range of substituents can be tolerated on the aryl ring (product **4k**-**4v**). The presence of a *gem*-dimethyl substituent at the benzylic position gives access to the corresponding product **4r** bearing a quaternary carbon, while monosubstituted benzyl silane provides compound **4s**, having two vicinal stereogenic centres, with high enantiomeric purity (92% for both the diasteroisomers), albeit with a poor diasteromeric ratio (1.2:1). Notably, heteroaryl frameworks can also be included in the product, as shown for the indoyl-and benzohienyl-substituted adduct **4u** and **4v**, respectively.

3.7 Mechanistic Investigations

3.7.1 Photophysical Studies of the Iminium Ions

We started the mechanistic investigations with the photophysical characterization of the iminium ions, the key intermediate of the studied photochemical process. A SET between the photoexcited iminium ion and the benzyl silane is supposed to be the key step. We first focused on the evaluation of the excite-state redox potentials of the iminium ions. Following the Rehm-Weller theory (see Chapter II, Section 1.5), we used a combination of spectroscopic and electrochemical analysis to assign these electrochemical values. We first synthesized and characterized the iminium salts **IIa**, **IIj**, and **IIk**, obtained upon condensation of cinnamaldehyde with the amine catalysts **A**, **J**, and **K**, respectively.[28] The use of TFA provided unstable and hygroscopic iminium salts. Conversely, the use of tetrafluoroboric acid, which was a competent co-catalyst in the β-benzylation process,[29] furnished relatively stable adducts.

[28] **IIa IIj** and **IIk** are intermediates of successful photochemical benzylation reactions, for this reason mechanistic studies can be undertaken on these iminium salts.

[29] Using HBF_4 instead of TFA as acidic co-catalyst, provides the desired product in comparable yield though with lower enantiomeric excess.

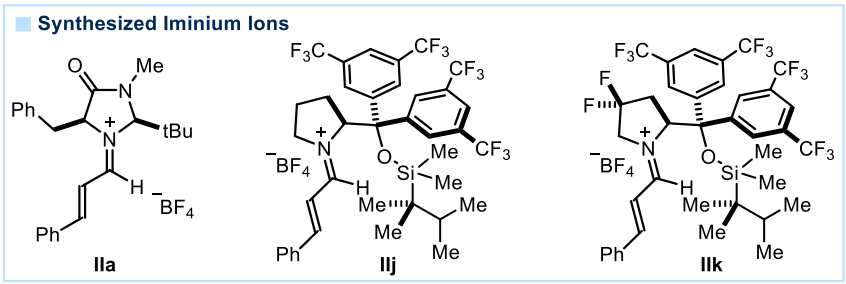

Scheme 3.13: The synthesized iminium ions.

To gain structural information of the iminium ions in the solid state, we obtained a crystal of the iminium ion **IIk** and submitted it to X-ray diffraction analysis (Figure 3.12). Interestingly, the *gem*-difluorine atoms induce a strong conformational control over the pyrrolidine ring, as a consequence of charge-dipole interaction and stereoelectronic effect,[30] which has no counterpart in the structure of iminium ion **IIj**,[31] thus providing a possible rationale for the increased level of stereoselectivity.

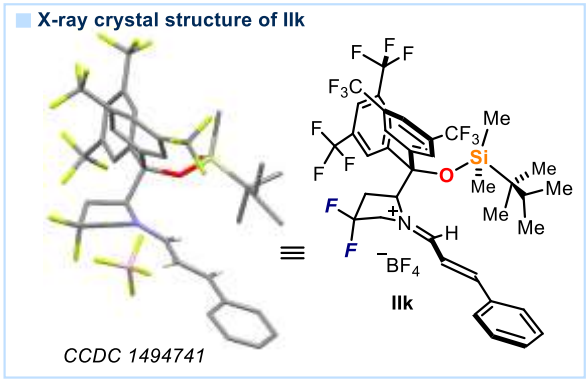

Figure 3.12: X-ray crystal structure of the iminium ion **IIk**.

UV-Vis absorption analysis[32] of these iminium ions revealed a linear Lambert-Beer correlation (Figure 3.13). The linearity of the Lambert-Beer correlation further confirms the stability of these species under the condition of the photophysical investigation.

[30] Zimmer, L. E., Sparr, C., Gilmour, R., "Fluorine conformational effects in organocatalysis: an emerging strategy for molecular design" *Angew. Chem. Int. Ed.* **2011**, *50*, 11860.
[31] The crystal structure of an analogous iminium ion obtained upon condensation of cinnamaldehyde and the catalys **C** is reported in literature and displays an almost flat pyrrolidine ring. CCDC 732053 Grošelj, U., Seebach, D., Badine, D. M., Schweizer, W. B., Beck, A. K., Krossing, I., Klose, P., Hayashi, Y., Uchimaru, T., "Structures of the Reactive Intermediates in Organocatalysis with Diarylprolinol Ethers" *Helv. Chim. Acta* **2009**, *92*, 1225.
[32] For simplicity, here we report only the UV-Vis spectra and the voltammograms related to the iminium ion **IIk**.

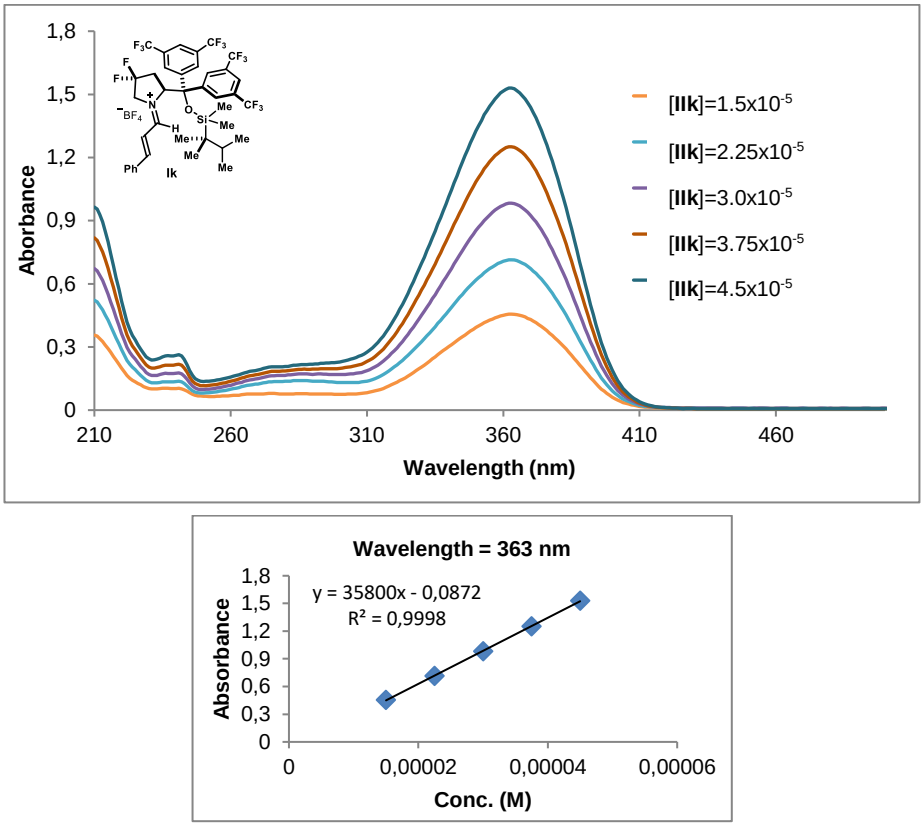

Figure 3.13: UV-Vis absorption spectra of **IIk** at different concentration and Lambert-Beer linear correlation between absorbance and concentration at 363 nm.

The spectroscopic features of the iminium salts **IIa**, **IIj**, and **IIk** are summarized in Table 3. We particularly focused on the absorption maximum λ_{max}, determining the molar extinction coefficients ε of these species at this wavelength. Furthermore, we localized the position of the long wavelength tail λ_{Tail}. This important value can be exploited for the determination of the excited-state energy E_{00} of the species under investigation.

Table 3: Spectroscopic features of the iminium ions **IIa**, **IIj** and **IIk.**

Iminium Ion	λ_{max}	ε_{max} (M^{-1} cm^{-1})	λ_{Tail}	E_{00}
IIa	362 nm	27000	440 nm	2.82 eV
IIj	350 nm	50000	425 nm	2.92 eV
IIk	363 nm	36000	435 nm	2.85 eV

The three iminium ions show very similar absorption profiles. The main difference is related to the significantly higher molar extinction coefficients of **IIj**.

To evaluate the excited-state redox potential of the iminium ions, we characterized them electrochemically. Cyclic voltammetry (CV) measurements inferred their ground-state reduction potentials. In the case of **IIk** (Figure 3.14), a single irreversible reduction peak was observed with $E_p^C = E_{red}$ (**IIk**/**IIk**$^{\bullet-}$) = -0.38 V (vs Ag/AgCl), where E_p^C is the observed cathodic peak potential and E^{red} value describes the electrochemical properties of **IIk**.

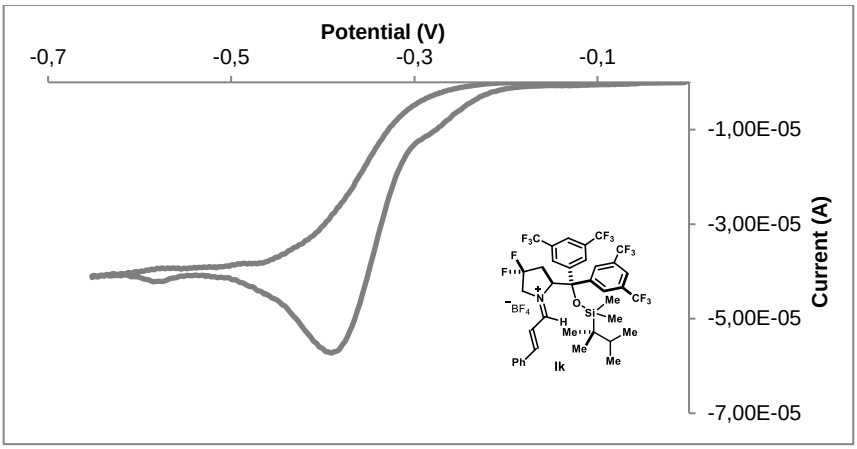

Figure 3.14: Cyclic voltammogram of the preformed iminium ion **IIk** [0.01M] in [0.1 M] $TBAPF_6$ in CH_3CN. Sweep rate: 20 mV/s. Pt electrode working electrode, Ag/AgCl (NaCl saturated) reference electrode, Pt wire auxiliary electrode.

Using the data collected from the cyclic voltammetric studies and from the absorption spectra of the preformed iminium ions **II**, we could estimate the redox potential of the excited iminium salts **II*** using the following Equation 3.1:

$$E^{red}(\mathbf{II^*/II^{\bullet-}}) = E^{red}(\mathbf{II/II^{\bullet-}}) + E_{00}(\mathbf{II^*/II}) \qquad (3.1)$$

(note that **II**$^{\bullet-}$ is the 5π-electron β-enaminyl radical intermediate **VIII** plus the counter-anion in Figure 3.6). The results obtained are summarized in Table 4.

Table 4: Electrochemical characteristics of ground-state and excited-state iminium ions **IIa**, **IIj** and **IIk**.

Iminium Ion	E_{red} (**II/II**$^{\bullet-}$)	E_{00}	E_{red} (**II***/**II**$^{\bullet-}$)
IIa	-0.50 V	2.82 eV	**+2.32 V**
IIj	-0.60 V	2.92 eV	**+2.32 V**
IIk	-0.38 V	2.85 eV	**+2.45 V**

All the studied iminium ions **II** have similar redox potentials, both in their ground states and excited states. As expected, the electron-poor imidazolidinone and the difluorinated amine catalysts impart a lower reduction potential to the ground-state iminium ions **IIa** and **IIk** compared to the diarylprolinol derived **IIj**. The reduction potential of these species in their excited states is exceptionally high ($E^{red} > 2.3V$), securing the thermodynamic feasibility of the SET oxidation of the benzyl silanes, which is crucial for the developed chemistry.

3.7.2 Luminescence and Stern-Volmer Quenching Studies

To unambiguously establish the implication of the photoexcited iminium ion within the photochemical regime and its interaction with the benzyl silane **3a**, we performed a series of Stern-Volmer quenching studies. We first carried out luminescence analysis on the iminium ions **II**, since this technique furnishes information about transient excited species and it is the prerogative starting point of any quenching experiment. After some preliminary attempts, we could detect a considerable emission only in the case of the iminium ion **IIa**. We attribute this behavior to the lower molecular rigidity of **IIj** and **IIk**, which favors other non-radiative relaxation pathways from the excited states.

Irradiation of a degassed solution of iminium ion **IIa**[33] with a 400 nm monochromatic light resulted in a luminescence phenomenon. The normalized emission spectrum of the excited iminium ion **IIa** is shown in Figure 3.15 along with the normalized absorption profile.

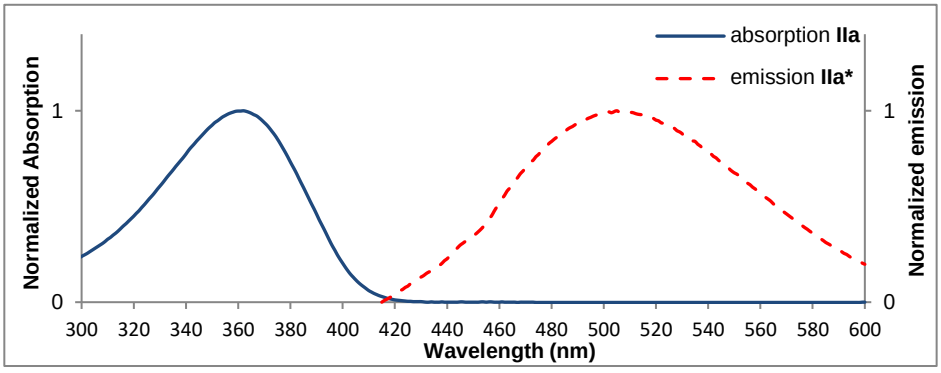

Figure 3.15: Normalized absorption spectrum (blue line) and normalized emission spectrum (red dashed line) of a $3x10^{-5}$ M solution of **IIa** in acetonitrile.

We next decided to carry out luminescence quenching studies to corroborate the electron transfer interaction between the excited-state iminium ion and benzyl trimethylsilane.

[33] **IIa** is able to drive the photochemical reaction with high yield but low ee, this indicates that studying the photophysical beaviour of **IIa** is scientifically relevant.

Importantly, blank experiments revealed that the irradiation of a solution of purified[34] benzyl trimethylsilane **3a** in acetonitrile did not lead to any luminescence phenomenon, which could have hampered the results of the quenching experiments. The addition of increasing amount of **3a** to a solution of iminium ion effectively quenched the iminium ion emission, as shown in Figure 3.16. The analysis of the data, by means of Stern-Volmer plot, showed a linear correlation between the concentration of the quencher **3a** and the ratio I_0/I (insert in Figure 3.16). On the basis of the equation 3.2, it was possible to calculate the Stern-Volmer constant K_{SV}.

$$I_0/I = 1 + K_{SV}[Q] \qquad (3.2)$$

We calculated a Stern-Volmer quenching constant K_{SV} of 2.3 M^{-1}.

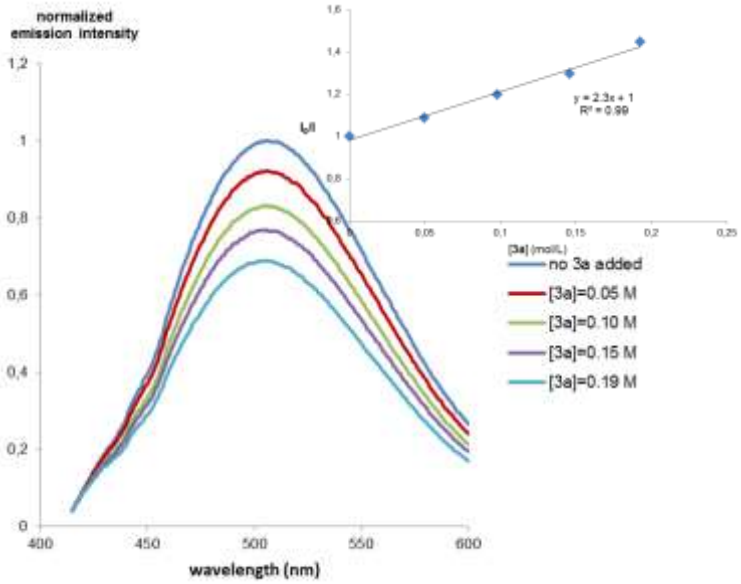

Figure 3.19: Quenching of the iminium ion **IIa** emission ($3 \cdot 10^{-5}$ M in acetonitrile) in the presence of increasing amounts of benzylsilane **3a**. Insert: Stern-Volmer quenching plot.

During the Stern-Volmer studies, we continuously monitored the absorption profile of the iminium ion **IIa** and a small decrease of absorption intensity was noticed upon addition of benzyl silane **3a**. This can be ascribable to different factors: a dilution of the sample upon adding the liquid silane; a minimal hydrolysis of the iminium ion **IIa** over the time; or consumption of **IIa** which participate in the light-driven benzylation within the cuvette in the

[34] The slightly pink commercially available benzyl trimethylsilane was stirred with activated charcoal for 30 min and then filtered over a plug of silica, to afford a completely colourless compound.

presence of **3a**. The small change of normalized absorbance of the iminium ion **IIa** during the quenching experiment is shown in Figure 3.17.

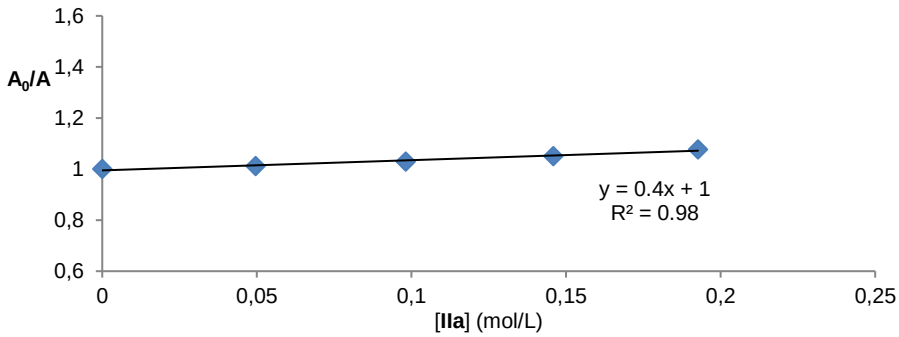

Figure 3.110: Slight decrease in absorption of **IIa** during the quenching experiment.

To account for this minimal variation of iminium ion **IIa** concentration, we recalculated the Stern-Volmer quenching constant, according to Eq. 3.2, taking into account and subtracting the value of the slope of the change in absorbance 0.4 M^{-1}. This correction provided a quenching constant K_{SV} of 1.9 M^{-1}.

A static quenching can occur if a complex is formed in the ground state between the iminium ion **IIa** and the silane **3a**. This association, that can alter the results of the Stern-Volmer experiment, is generally correlated with the appearance of a red-shifted band within the absorption spectrum. In order to exclude this phenomenon, a careful analysis of the absorption spectra of the iminium ion in the presence of increasing amounts of benzyl silane **3a** was carried out. Except for the already discussed minor decrease in absorption, no spectral variations were observed in the area between 300 nm-430 nm, which excluded any ground-state association between **IIa** and **3a**. The raising band below 300 nm is due the absorption of **3a**.

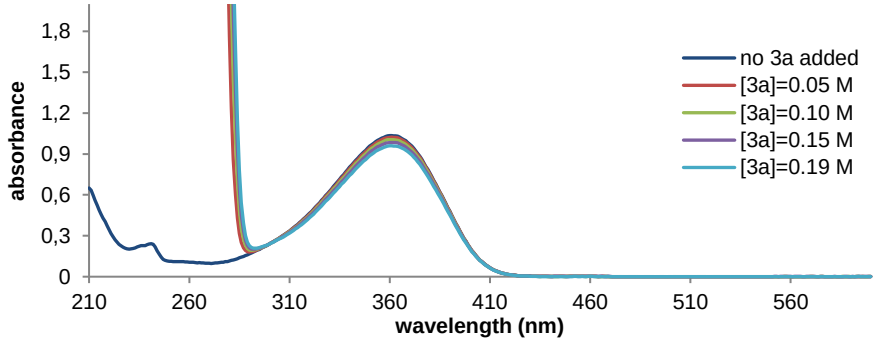

Figure 3.111: Absorption spectra of **IIa** with different amounts of quencher. No spectral variation related to static quenching are observed.

3.7.3 Radical-Radical Coupling *vs* Chain Propagation

As depicted in Figure 3.6, our mechanistic proposal involves a stereoselective intermolecular coupling between the chiral 5π-electron β-enaminyl radical intermediate **VIII** and the alkyl radical **X**, generated upon oxidative fragmentation of the parent benzyl silane **3a**. This *radical-radical coupling* is supposed to forge the new C–C bond. A possible alternative scenario relies on a *chain propagation* manifold, where the photochemical activity of the excited-state iminium ion **II***, by inducing the SET oxidation of benzyl silane **3a**, would serve as the initiation event, generating the benzyl radical **Xa** (Figure 3.19, Top). **Xa** would then escape from the solvent cage and undergo a radical conjugate addition with a ground-state iminium ion providing the 3π-electron α-iminyl radical cation **XII**. In order to propagate the chain, **XII** should be trigger a SET oxidation of another molecule of benzyl silane **3a** forming the enamine intermediate **XI** and another benzyl radical that can re-enter the chain (Figure 3.19, bottom).

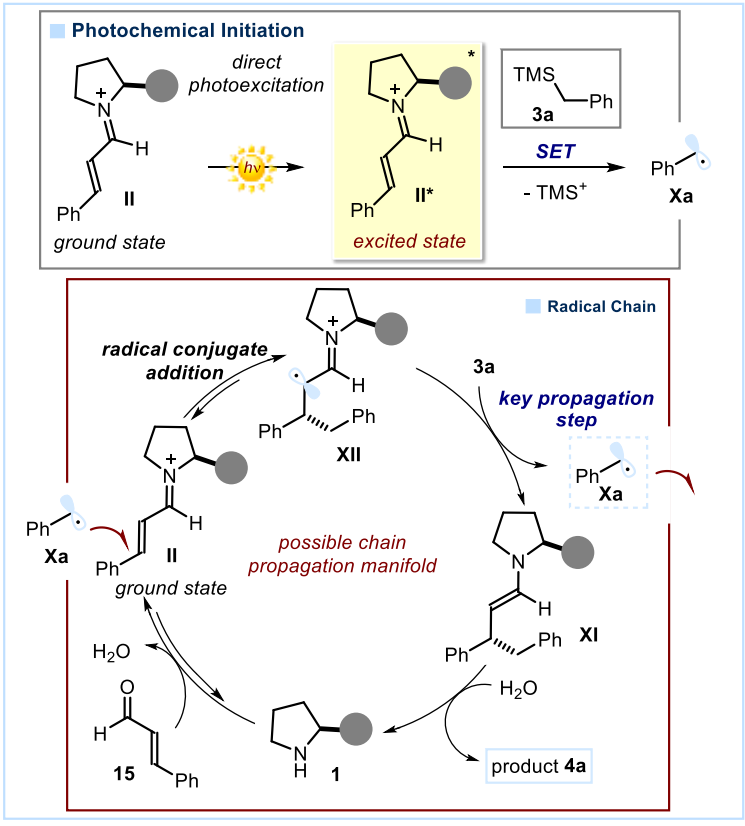

Figure 3.112: Alternative self-propagating radical-chain mechanism for the photochemical enantioselective β-benzylation of cinnamaldehyde.

A variety of data are in accordance with the radical-radical coupling mechanism. First, we never observed the formation of bibenzyl. This product, raising from the dimerization of benzyl radical **Xa**, should be easily formed in an *out-of-cage* scenario. In addition, we measured the quantum yield of the process catalysed by the chiral secondary amine **K**, which was found to be $\Phi = 0.05$ ($\lambda = 400$ nm, in acetonitrile, details about quantum yield determination in the Experimental Section). This fractional value is far lower than the typical ones of chain propagation mechanisms ($\Phi > 1$), suggesting a radical combination manifold as the most plausible. Although these data do not completely rule out a radical-chain process triggered by the conjugate addition of **Xa** to the ground-state iminium ion, a chain propagation mechanism is unlikely for several reasons. The poor nucleophilicity of benzyl radicals affects their propensity towards radical conjugate additions.[35] Moreover, iminium ions displayed a low tendency to trap non-nucleophilic radicals.[36]

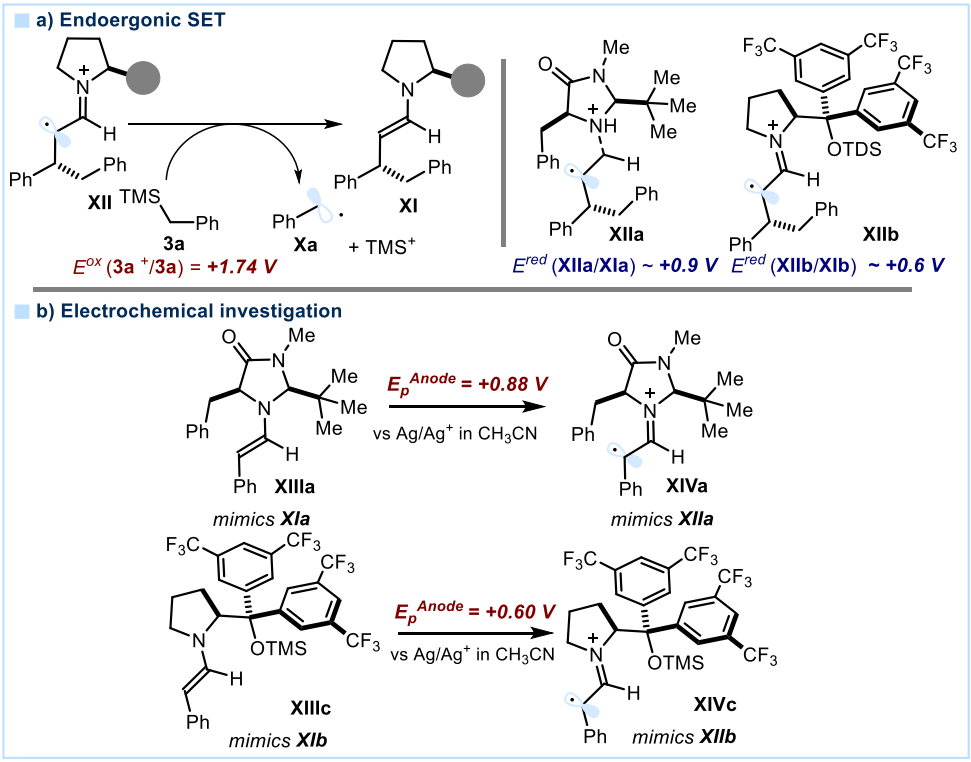

Figure 3.20: a) The key propagation step of an alternative chain propagation manifold is endergonic. b) Electrochemical investigation of the enamines **XIII**, which mimic the reaction intermediate **XI**.

[35] Walbiner, M., Wu, J. Q., Fischer, H., "Absolute Rate Constants for the Addition of Benzyl (PhĊH2) and Cumyl (PhĊMe2) Radicals to Alkenes in Solution" *Helv. Chim. Acta* **1995**, *78*, 910.
[36] Murphy, J. J., Bastida, D., Paria, S., Fagnoni, M., Melchiorre, P., "Asymmetric catalytic formation of quaternary carbons by iminium ion trapping of radicals" *Nature* **2016**, *532*, 218.

Perhaps more importantly, the SET between the α-iminyl radical cation **XII** and the benzyl silane **3a**, which would be essential for a chain propagation manifold, is highly disfavoured when considering the redox potentials of the intermediates (Figure 3.20a).

To evaluate the thermodynamic feasibility of this step, we performed cyclic voltammetry studies on the preformed enamines **XIIIa** and **XIIIc**, which mimic the actual enamine intermediate **XI** involved in the propagation step (Figure 3.20b). Enamine **XI** could not be synthesized because of the instability of enamines lacking aryl substituent. Evaluating the redox properties of **XIIIa** and **XIIIc** is pertinent since their electrochemical oxidation provides access to α-iminyl radical cations of type **XIV**, which mimic **XII**, the key intermediate of the chain propagation. We measured by cyclic voltammetry an oxidation potential $E_p^A = E^{ox}$ of 0.88 V and +0.60 V (vs Ag/AgCl in acetonitrile) for **XIIIa** and **XIIIc**. These values indicate that the α-iminyl radical cation of type **XII** is not capable to oxidize the benzyl silane **3a** which has an E^{ox} = 1.74 V (vs Ag/AgCl in acetonitrile).

3.7.4 Effect of the Enal Geometry

In order to investigate the ability of the newly synthesized difluorinated catalysts to control the geometry of the iminium ion **II**, we performed the photochemical benzylation reaction on the *Z*-isomer of cinnamaldehyde (*Z*)-**15**.

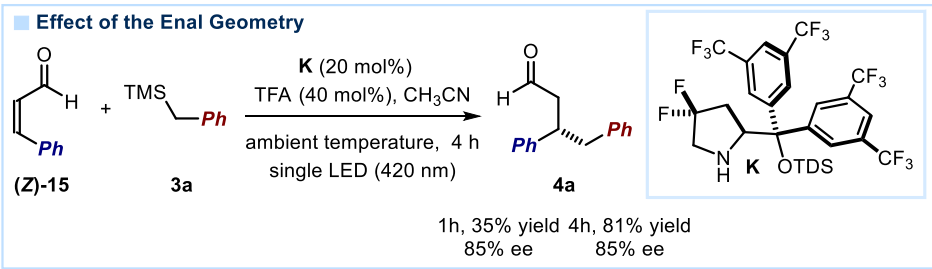

Scheme 3.14: Reaction performed starting from (*Z*)-cinnamaldehyde.

Two reactions were performed in parallel under the same conditions and visible light irradiation, and stirred at ambient temperature for 1 and 4 hours, respectively. These provided 35% NMR yield after 1 hour and 81% NMR yield after 4 hours. In both cases a complete isomerisation of the remaining cinnamaldehyde to the (*E*)-isomer was observed and the product **4a** was obtained in 85% ee. These results, which are in line with the reactions performed using (*E*)-cinnamaldehyde (83% yield, 85% ee after 4 hours), strengthen the argument that this is not a ground-state reaction of the iminium ion.

To better understand the origin of the fast (*Z*) to (*E*) isomerization process, we performed nuclear magnetic resonance studies, which established that the isomerization is a thermally-driven reaction happening in the absence of illumination (Figure 3.21). While the (*Z*)-isomer of cinnamaldehyde is stable in deuterated acetonitrile and in the presence of trifluoroacetic

acid (only traces of (*E*)-isomer were detected after 15 minutes), the addition of the chiral amine catalyst **J** initiates a fast isomerization to give exclusively the (*E*)-isomer (the process was complete 15 minutes after the addition of **K**). This is likely because of a conjugate addition to the iminium ion of either adventitious water or the amine catalyst itself, followed by a retro-reaction, which eventually affords the more thermodynamically stable (*E*)-isomer.

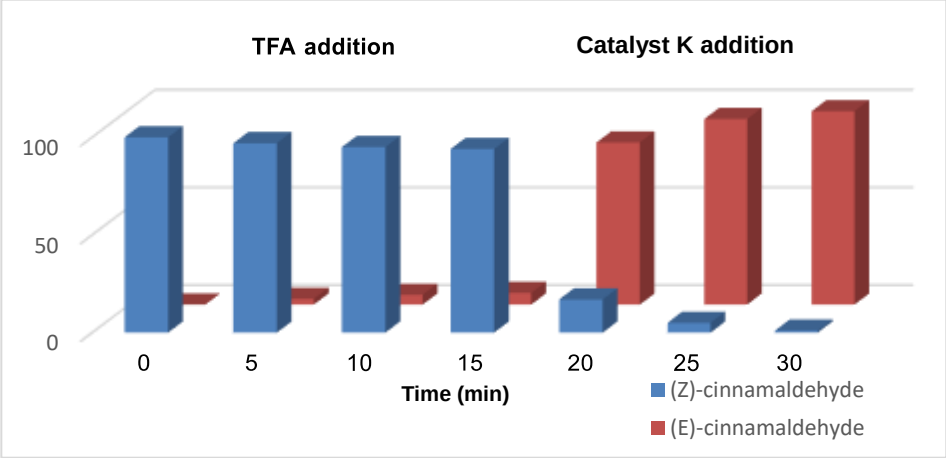

Figure 3.21: (*Z*)-cinnamaldehyde is stable in the presence of TFA (first 15 min). Addition of catalyst **K** initiate a fast thermal isomerization of the (*Z*)-cinnamaldehyde to afford exclusively (*E*)-cinnamaldehyde in the following 15 min.

3.8 Extension of the Scope

We then wondered if the photoexcitation of iminium ions could provide a widely applicable mechanism of substrate activation, suitable for a broad range of stereocontrolled enal β-functionalizations. Relying on our mechanistic investigations, we surmised that the simple analysis of the electrochemical properties, i.e. redox potentials, would provide a rational for the identification of potential substrates that can engage in the iminium-ion-mediated photochemical functionalization of enals. In theory, any organic silane possessing an appropriate oxidation potential ($E^{ox} < 2.3$ V, which is the estimated excited-state potential of the iminium ion), should serve as a suitable reaction partner.

Following this reasoning, we found that α-silyl thioethers, α-silyl amines, and α-silyl ethers could productively participate in the photochemical asymmetric process. In these substrates,

the silyl group at the α-position of the heteroatom imparts an adequately low oxidation potential through a σ→n orbital interaction (Figure 3.21).[15]

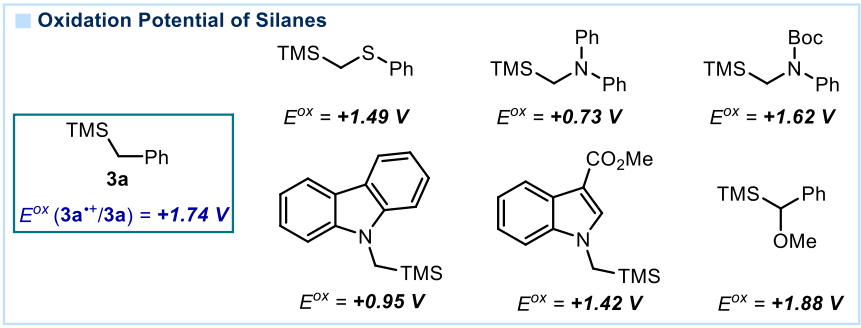

Figure 3.21: Oxidation potential of heteroatom containing alkyl silanes.

After a brief fine tuning of the reaction conditions, we could extend the scope of the light-induced asymmetric β-functionalizations of enals and synthesize chiral aldehydes **22a**-**22h** bearing a methylene heteroatom fragment at the β-position (Scheme 3.14). The desired products were obtained with moderate to high enantiomeric excess. Interestingly, easily oxidizable α-silyl thioethers enable the use of *p*-methoxy and *p*-trifluoromethyl cinnamaldehyde (products **22b** and **21b**), which were recalcitrant to the benzylation procedure.

Crystals from a derivative of compound **22a** were subjected to X-Ray analysis, securing the absolute configuration of the products (see Experimental Section for details).

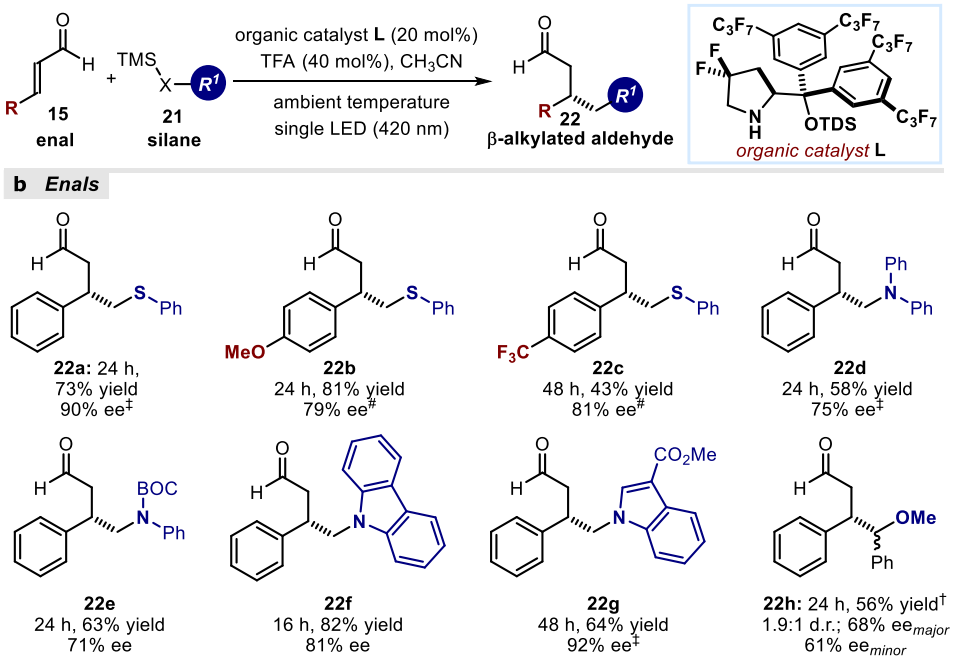

Scheme 3.14: Survey of the the α-silyl thioethers (products **22a–c**), α-silyl amines (products **22d–g**), and α-silyl ethers (product **22h**) that can participate in the reaction. Reactions performed on a 0.1 mmol scale using 3 Equiv. of enals. Reaction time, yields and enantiomeric excesses of the isolated products are indicated below each entry (average of two runs per substrate). † Using catalyst **J**. ‡ Using catalyst **J** in a 3:1 CH3CN/H2O solvent mixture. # Using catalyst **J** in a 3:1 CH3CN/H2O solvent mixture. TFA, trifluoroacetic acid; TDS, thexyl-dimethylsilyl; BOC, tert-butyloxycarbonyl; TMS, trimethylsilyl.

3.9 Conclusions

Our studies led to the development of a novel and simple strategy to control the stereochemical outcome of catalytic photochemical reactions promoted by visible light. In particular, we demonstrated that transiently generated chiral iminium ions, which are key intermediates in polar enantioselective organocatalytic processes, can enable previously inaccessible reactivities when reaching an excited state upon visible-light absorption, while inducing effective stereochemical control over the ensuing C–C bond-forming event. We applied this photochemical mode of substrate activation to develop an enantioselective β-benzylations of enals. The chemistry is driven by the ability of excited-state iminium ions to act as strong oxidants and trigger the generation of benzyl radicals from suitable donors under mild conditions. The reaction protocol is robust and operationally simple, conducted at ambient temperature with readily available substrates, and using a 420 nm high power LED as the light source.

3.10 Experimental Section

General Information. The NMR spectra were recorded at 400 MHz and 500 MHz for ^{1}H, 101 or 126 MHz for ^{13}C and 376 MHz for ^{19}F. The chemical shift (δ) for ^{1}H and ^{13}C are given in ppm relative to residual signals of the solvents ($CHCl_3$ @ 7.26 ppm ^{1}H NMR and 77.16 ppm ^{13}C NMR, and tetramethylsilane @ 0 ppm). Coupling constants are given in Hertz. The following abbreviations are used to indicate the multiplicity: s, singlet; d, doublet; q, quartet; p, pentet; sept, septet; m, multiplet; br, broad signal.
High resolution mass spectra (HRMS) were obtained from the ICIQ HRMS unit on Waters GCT gas chromatograph coupled time-of-flight mass spectrometer (GC/MS-TOF) with electrospray ionization (ESI). X-ray data were obtained from the ICIQ X-Ray unit using a Brucker-Nonius diffractometer equipped with an APPEX 2 4K CCD area detector. Optical rotations are reported as follows: $[\alpha]_D^T$ (c in g per 100 mL, solvent).
UV-vis measurements were carried out on a Shimadzu UV-2401PC spectrophotometer equipped with photomultiplier detector, double beam optics and D_2 and W light sources.
Cut off and band-pass photochemical experiments and quantum yield measurements have been performed using a 300 W xenon lamp (*Asashi* Spectra Co., Ltd.) to irradiate the reaction mixture.
Cyclic voltammetry studies were carried out on a Princeton Applied Research PARSTAT 2273 potentiostat offering compliance voltage up to ± 100 V (available at the counter electrode), ± 10 V scan range and ± 2 A current range.

General Procedures. All reactions were set up under an argon atmosphere in oven-dried glassware using standard Schlenk techniques, unless otherwise stated. Synthesis grade solvents were used as purchased, anhydrous solvents were taken from a commercial SPS solvent dispenser. Chromatographic purification of products was accomplished using force-flow chromatography (FC) on silica gel (35-70 mesh). For thin layer chromatography (TLC) analysis throughout this work, Merck pre-coated TLC plates (silica gel 60 GF_{254}, 0.25 mm) were employed, using UV light as the visualizing agent and Hanessian´s stain solution, ethanol solution of phosphomolybdic acid or basic aqueous potassium permanganate ($KMnO_4$) stain solutions and heat as developing agents. Organic solutions were concentrated under reduced pressure on a Büchi rotary evaporator (*in vacuo* at 40 ºC, ~5 mbar).

Determination of Enantiomeric Purity. HPLC analysis on chiral stationary phase was performed on an Agilent 1200-series instrument, employing Daicel Chiralpak IA, IB, ID, IC and IC-3 chiral columns, or a Waters ACQUITY® UPC^2 instrument, using a Daicel Chiralpak IC-3 chiral column. The exact conditions for the analyses are specified within the characterization section. HPLC/UPC^2 traces were compared to racemic samples prepared performing the reaction in the presence of racemic catalyst **A**.

Materials. Commercial grade reagents and solvents were purchased from Sigma-Aldrich, Fluka, Alfa Aesar, Fluorochem, SynQuest at the highest commercial quality and used without further purification, unless otherwise stated. The chiral secondary amine catalyst **A** is commercially available (Sigma-Aldrich). The preparation of aminocatalysts **J**-**L** is detailed in Section C of the Supplementary Information. Benzyl silanes **3a** and **3p** are commercially available. The preparation of other silane derivatives is here described. Cinnamaldehyde and the majority of enals **15** are commercially available. The preparation of other enal substrates is here described.

Synthesis of the Chiral Amine Catalyst J

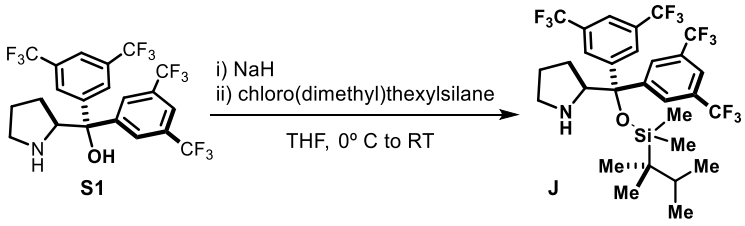

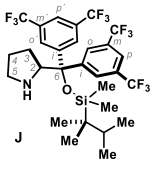

(*S*)-2-(bis(3,5-bis(trifluoromethyl)phenyl)(((2,3-dimethylbutan-2-yl)dimethylsilyl)oxy)methyl)pyrrolidine (J). Commercially available (*S*)-α,α-bis(3,5-dimethylphenyl)-2-pyrrolidinemethanol **S1** (525 mg, 1 mmol, 1 Equiv.) was dissolved in anhydrous THF (5 mL). Sodium hydride (60% dispersion in mineral oil, 3.0 Equiv., 120 mg) was added portionwise over 10 minutes. After stirring for 10 additional minutes, chloro(dimethyl)thexylsilane (2.0 mmol, 2.0 Equiv., 0.4 mL) was added and the reaction stirred for 6 hours. After disappearance of the starting alcohol, as judged by TLC analysis (hexane/EtOAc 90:10), the reaction mixture was poured onto ice and extracted with diethyl ether. The organic phase was washed with water and brine, dried over magnesium sulphate, and concentrated under reduced pressure. The crude residue was purified by column chromatography on silica gel (hexane/CH_2Cl_2, gradient from 100:0 to 85:15), yielding catalyst **J** as a colorless oil, which turned to a white solid after storage at 5 ºC (553 mg, 0.83 mmol, 83% yield); $[\alpha]_D^{26}$ = +9.85 (c = 0.5, $CHCl_3$).

^{1}H NMR (400 MHz, $CDCl_3$): δ 8.09 (s, 2H), 7.86 (s, 2H), 7.75 (m, 2H), 4.31 (dd, *J* = 8.5, 5.3 Hz, 1H), 2.88 (dt, *J* = 10.0, 7.0 Hz, 1H), 2.47 (ddd, *J* = 10.0, 7.0, 5.0 Hz, 1H), 1.93 – 1.69 (m, 3H), 1.48 (dddt, *J* = 14.7, 7.3, 5.2, 3.8 Hz, 2H), 0.93 (dd, *J* = 6.8, 2.0 Hz, 6H), 0.85 (d, *J* = 10.0 Hz, 6H), 0.82-0.70 (m, 1H), -0.15 (s, 3H), -0.46 (s, 3H);

^{13}C NMR (101 MHz, $CDCl_3$): δ 147.8 (*ipso*), 146.1 (*ipso*'), 131.65 (2C, q, J_{CF} = 33.3 Hz, *meta*), 130.6 (2C, q, J_{CF} = 33.3 Hz, *meta'*), 129.4 (4C, apparent s, *ortho*, *ortho´*), 123.6 (2C, q, J_{CF} = 281.0 Hz, ArCF_3), 123.4 (2C, q, J_{CF} = 280 Hz, Ar'CF_3), 121.7 (m, *para*), 121.5 (m,

para'), 83.2 (*C6*), 63.8 (*C2*), 47.4 (*C3*), 33.9 (*C5*), 28.1 (SiC*C*H), 25.8 (Si*C*CH), 20.4 (SiC*C*H$_3$), 20.2 (SiC*C*H$_3$'), 18.6 (2C, SiCCH*C*H$_3$), -0.03 (Si*C*H$_3$), -0.8 (Si*C*H$_3$').
HRMS: Calculated for $C_{29}H_{34}F_{12}NOSi$ 668.2213, found 668.2219.

Synthesis of the Chiral Amine Catalyst K

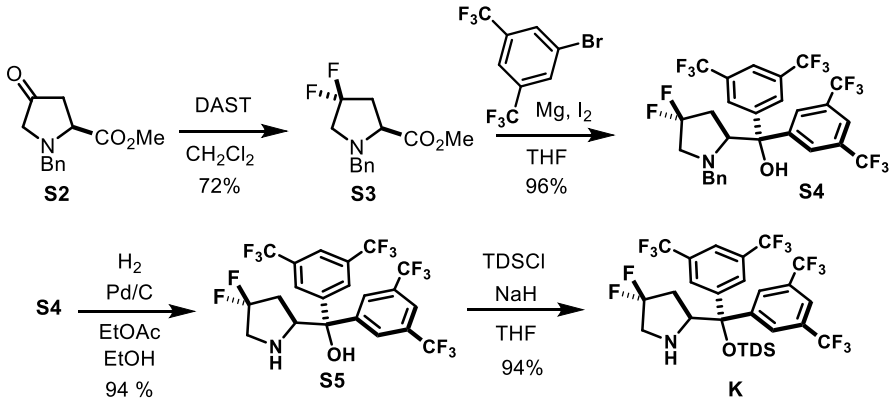

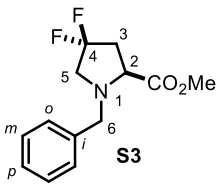

Methyl-(S)-1-benzyl-4,4-difluoropyrrolidine-2-carboxylate S3. Methyl-(*S*)-1-benzyl-4-oxopyrrolidine-2-carboxylate **S2** (3.02 g, 12.95 mmol, 1.00 Equiv.), synthesized according to a procedure reported in the literature[37], was added to an oven dried, argon purged 2-neck round bottomed flask fitted with an argon inlet and septum, followed by the addition of CH_2Cl_2 (130.0 mL). Then, diethylaminosulfur trifluoride (DAST, 4.11 mL, 31.1 mmol, 2.40 Equiv.) was added dropwise at 0 ºC. The resulting yellow solution was allowed to warm slowly up to ambient temperature. After 40 hours stirring, the orange solution was cooled to 0 ºC and $NaHCO_3$ (sat., aq., 200 mL) was carefully added. The mixture was allowed to warm to ambient temperature and vigorously stirred for 15 min. The layers were separated and the aqueous layer was extracted with CH_2Cl_2 (3 x 200 mL). The combined organic layers were dried over $MgSO_4$ and concentrated *in vacuo* to give a dark yellow oil, which was purified by column chromatography (*c*-hexane/EtOAc 20:1) to furnish **S3** as a light yellow liquid (2.38 g; 72% yield). R_f = 0.49 (*c*-hexane/EtOAc 10:1); $[\alpha]_D^{26}$ = -68.3 (c = 0.5, $CHCl_3$).
^{1}H NMR (400 MHz, $CDCl_3$): δ 7.30-7.18 (m, 5H, *Ph*), 3.93 (d, *J* = 13.1 Hz, 1H, C6*H*H), 3.67 (s, 3H, C*H*$_3$), 3.55 (d, *J* = 12.7 Hz, 1H, C6H*H*), 3.53 (d, *J* = 7.8 Hz, 1H, C2*H*), 3.30 (q, *J* = 11.5 Hz, 1H, C5*H*H), 2.79 (dt, *J* = 16.7 Hz, 11.5 Hz, 1H, C5H*H*), 2.61-2.36 (m, 2H, C3*H*$_2$).

[37] Tanaka, K.-i., Sawanishi, H., "Asymmetric syntheses of all four isomers of 4-amino-4-carboxyproline: Novel conformationally restricted glutamic acid analogues" *Tetrahedron: Asymmetry* **1995**, *6*, 1641.

^{13}C NMR (101 MHz, $CDCl_3$): δ 172.0 (*C*O_2Me), 137.1 (*ipso*), 129.0 and 128.6 (4C, *ortho* and *meta*), 128.0 (dd, J_{CF} = 250.1 Hz, 246.5 Hz, *C4*), 127.7 (*para*), 63.2 (t, J_{CF} = 3.8 Hz, *C2*), 60.0 (t, J_{CF} = 29.0 Hz, *C5*), 57.6 (*C6*), 52.2 (*C*H_3), 39.9 (t, J_{CF} = 26.0 Hz, *C3*).
^{19}F NMR (376 MHz, $CDCl_3$): δ -93.0 (dm, J_{FF} = 230.0 Hz), -94.2 (dm, J_{FF} = 230.0 Hz).
HRMS: calculated for $C_{13}H_{16}F_2NO_2$: 256.1144, found: 256.1151.

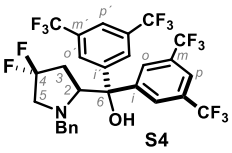

(*S*)-(1-Benzyl-4,4-difluoropyrrolidin-2-yl)-bis-(3,5-bis-(trifluoromethyl)-phenyl)-methanol (**S4**). Magnesium turnings (300 mg, 12.3 mmol, 5.25 Equiv.) were added to a 25 mL 2-neck flask equipped with a condenser and stirred under high-vacuum for 5 hours. THF (10 mL, dry) was then added followed by iodine (15 mg, 59 μmol, 0.025 Equiv.), affording a brown solution. Commercially available 1-bromo-3,5-bis-(trifluoromethyl)-benzene (2.76 g, 9.40 mmol, 4.00 Equiv.) was added to the magnesium-suspension in a first portion of 0.9 g. The speed of addition of the remaining 1.76 g of aryl bromide was controlled to maintain the mixture at reflux. When the exothermic reaction stopped, the reaction mixture was refluxed for 10 additional minutes. The resulting brown mixture was then cooled at 0 ºC and a solution of **S3** (2.35 mmol, 600 mg, 1 Equiv.) in anhydrous THF (2 mL) was added. The mixture was allowed to warm up to ambient temperature. After 15 hours stirring, the mixture was diluted with NH_4Cl (aq., sat., 100 mL) and extracted with CH_2Cl_2 (3 x 100 mL). The combined organic layers were dried over $MgSO_4$ and concentrated *in vacuo*. Purification by column chromatography (*c*-hexane/EtOAc 100:1) afforded **S4** as a white solid (1.47 g, 2.25 mmol, 96% yield). R_f = 0.71 (*c*-hexane/EtOAc 5:1); $[\alpha]_D^{26}$ = +14.0 (c = 0.5, $CHCl_3$).

^{1}H NMR (400 MHz, $CDCl_3$): δ 8.23 (s, 2H, Ar^{ortho}), 8.04 (s, 2H, Ar'^{ortho}), 7.80 (s, 1H, Ar^{para}), 7.77 (s, 1H, Ar'^{para}), 7.32-7.21 (m, 3H, Bn^{para} and Bn^{meta}), 7.01-6.92 (m, 2H, Bn^{ortho}), 5.21 (br. s, 1H, O*H*), 4.45 (t, *J* = 8.3 Hz, 1H, C2*H*), 3.34-3.15 (m, 3H, NCH_2Ph and C5*H*H), 3.05-2.92 (m, 1H, C5H*H*), 2.34-2.19 (m, 1H, C3*H*H), 2.11 (dtd, *J* = 18.0 Hz, 13.5 Hz, 8.7 Hz, 1H, C3H*H*);
^{13}C NMR (101 MHz, $CDCl_3$): δ 148.4 (Ar^{ipso}), 146.5 (Ar'^{ipso}), 136.8 (Bn^{ipso}), 132.6 (2C, q, J_{CF} = 33.6 Hz, Ar^{meta}), 132.5 (2C, q, J_{CF} = 33.5 Hz, Ar'^{meta}), 129.0 (2C, Bn^{meta}), 128.3 (2C, Bn^{ortho}), 128.2 (Bn^{para}), 126.2 (dd, J_{CF} = 251.8 Hz, 245.5 Hz, *C4*), 125.8 (2C, q, J_{CF} = 3.8 Hz, Ar^{ortho}), 125.4 (2C, q, J_{CF} = 4.4 Hz, Ar'^{ortho}), 123.2 (2C, q, J_{CF} = 272.9 Hz, *C*F_3), 123.1 (2C, q, J_{CF} = 273.0 Hz, *C*F_3), 122.2-121.9 (2C, m, Ar^{para} and Ar'^{para}), 76.1 (*C6*), 69.2 (dd, J_{CF} = 4.1 Hz, 2.7 Hz, *C2*), 60.5 (two signals on top of each other: N*C*H_2Ph (s) and C5 (t, J_{CF} = 28.2 Hz)), 38.3 (t, J_{CF} = 25.0 Hz, *C3*).
^{19}F NMR (376 MHz, $CDCl_3$): δ -63.0 (s, 6F, ArCF_3), -63.1 (s, 6F, Ar'CF_3), -98.1 (dp, J_{FF} = 232.4 Hz, J_{HF} = 15.8, 1F, C4*F*F), -100.6 (br d, J_{FF} = 232.1 Hz, 1F, C4F*F*).
HRMS: calculated for $C_{28}H_{20}F_{14}NO$ 652.1313, found: 652.1321.

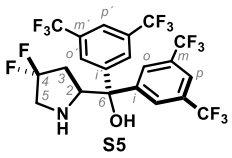

S5

(*S*)-Bis-(3,5-bis-(trifluoromethyl)-phenyl)-(4,4-difluoropyrrolidin-2-yl)-methanol (S5). **S4** (1.40 g, 2.15 mmol, 1.00 Equiv.) was dissolved in a 1:1 mixture of EtOH and EtOAc (12 mL), followed by the addition of Pd/C (10%, wet support, 420 mg). The reaction flask was purged with vacuum/hydrogen cycles (6x). The suspension was vigorously stirred for 26 hours and then filtered over Celite. The plug was washed with CH_2Cl_2 (100 mL) and the solution was concentrated *in vacuo* to give a colorless oil. This was purified by column chromatography (*c*-hexane/EtOAc 5:1) to afford **S5** as colorless oil which solidified as a white solid upon standing (1.14 g; 94% yield).
R_f = 0.54 (*c*-hexane/EtOAc 5:1); $[\alpha]_D^{26}$ = -59.5 (c = 0.5, $CHCl_3$).

^{1}H NMR (400 MHz, $CDCl_3$): δ 8.06 (s, 2H, *ortho*), 7.95 (s, 2H, *ortho'*), 7.83 (s, 1H, *para*), 7.80 (s, 1H, *para'*), 4.70 (s, 1H, O*H*), 4.65 (dd, *J* = 9.5 Hz, 7.1 Hz, 1H, C2*H*), 3.50-3.32 (m, 2H, C5*H*$_2$), 2.26-2.08 (m, 1H, C3*H*H), 2.03-1.88 (m, 1H, C3H*H*), 1.76 (br s, 1H, N*H*).
^{13}C NMR (101 MHz, $CDCl_3$): δ 147.6 (*ipso*), 145.1 (*ipso*'), 132.7 (2C, q, J_{CF} = 33.5 Hz, *meta*), 132.5 (2C, q, J_{CF} = 33.5 Hz, *meta'*), 128.4 (dd, J_{CF} = 252.4 Hz, 245.9 Hz, *C4*), 126.1 (2C, q, J_{CF} = 3.7 Hz, *ortho*), 125.5 (2C, q, J_{CF} = 3.8 Hz, *ortho'*), 123.2 (4C, q, J_{CF} = 272.9 Hz, *C*F_3), 122.3 (apparent p, J_{CF} = 3.7 Hz, *para*), 122.1 (apparent p, J_{CF} = 3.8 Hz, *para'*), 76.3 (*C6*), 62.2 (dd, J_{CF} = 5.5 Hz, 2.1 Hz, *C2*), 54.0 (t, J_{CF} = 29.5 Hz, *C5*), 35.7 (t, J_{CF} = 24.8 Hz, *C3*).
^{19}F NMR (376 MHz, $CDCl_3$): δ -63.0 (s, 6F, ArCF_3), -63.1 (s, 6F, Ar'CF_3), -96.6 (ddq, J_{FF} = 230.7 Hz, J_{HF} = 20.4 Hz, 16.7 Hz, 1F, C4*F*F), -100.6 (ddtd, J_{FF} = 230.8 Hz, J_{HF} = 14.6 Hz, 9.4 Hz, 5.3 Hz, 1F, C4F*F*).
HRMS: calculated for $C_{21}H_{15}F_{14}NO$: 562.0846, found: 562.0851.

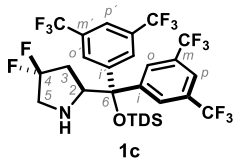

1c

(S)-2-(Bis-(3,5-bis-(trifluoromethyl)-phenyl)-(((2,3-dimethylbutan-2-yl)-dimethylsilyl)-oxy)-methyl)-4,4-difluoropyrrolidine (K). To a colorless solution of **S5** (2.0 g, 3.56 mmol, 1.0 Equiv.) in THF (dry, 18 mL) at 0 ºC was added NaH (60% in mineral oil, 713 mg, 17.8 mmol, 5.0 Equiv.) portionwise. The reaction mixture was stirred for 15 min until gas evolution had ceased, then chloro-(2,3-dimethylbutan-2-yl)-dimethylsilane (1.40 mL, 7.13 mmol, 2.0 Equiv.) was added dropwise and the mixture was allowed to warm up to ambient temperature. After 5 hours stirring, water (50 mL) was carefully added and the mixture was extracted with CH_2Cl_2 (3 x 50 mL). The combined organic layers were dried over $MgSO_4$ and concentrated *in vacuo* to give a yellow oil. Purification by column chromatography (*c*-hexane/EtOAc 100:1) afforded catalyst **K** as a white solid (2.35 g, 94%).
R_f = 0.53 (*c*-hexane/EtOAc 10:1); $[\alpha]_D^{26}$ = +1.9 (c = 0.5, $CHCl_3$).

^{1}H NMR (400 MHz, $CDCl_3$): δ 8.10 (s, 2H, *ortho*), 7.91 (s, 2H, *para* and *para*'), 7.72 (s, 2H, *ortho*'), 4.46 (t, *J* = 8.3 Hz, 1H, C2*H*), 3.15 (td, *J* = 13.9 Hz, 7.2 Hz, 1H, C5*H*H), 2.62 (ddd,

J = 20.2 Hz, 12.9 Hz, 7.9 Hz, 1H, C5H*H*), 2.31-2.08 (m, 2H, C3*H*H and N*H*), 1.95-1.69 (m, 2H, C3H*H* and SiCC*H*), 0.95 (d, *J* = 3.0 Hz, 3H, SiCCHC*H*$_3$), 0.93 (d, *J* = 3.0 Hz, 3H, SiCCHC*H*$_3$'), 0.89 (s, 3H, SiCC*H*$_3$), 0.87 (s, 3H, SiCC*H*$_3$'), -0.14 (s, 3H, SiC*H*$_3$), -0.47 (s, 3H, SiC*H*$_3$).

^{13}C NMR (101 MHz, $CDCl_3$): δ 146.6 (*ipso*), 145.0 (*ipso*'), 132.2 (2C, q, J_{CF} = 33.6 Hz, *meta*), 131.4 (2C, q, J_{CF} = 33.5 Hz, *meta'*), 129.7 (dd, J_{CF} = 254.0 Hz, 246.9 Hz, *C4*), 129.5 (2C, q, J_{CF} = 4.1 Hz, *ortho*), 128.8 (2C, q, J_{CF} = 4.1 Hz, *ortho*'), 123.4 (2C, q, J_{CF} = 272.8 Hz, Ar*C*F_3), 123.2 (2C, q, J_{CF} = 272.9 Hz, Ar'*C*F_3), 122.6 (apparent p, J_{CF} = 3.8 Hz, *para*), 122.4 (apparent p, J_{CF} = 3.8 Hz, *para*'), 82.2 (*C6*), 62.8 (dd, J_{CF} = 6.5 Hz, 1.3 Hz, *C2*), 53.9 (t, J_{CF} = 28.8 Hz, *C3*), 37.6 (t, J_{CF} = 25.0 Hz, *C5*), 33.9 (SiC*C*H), 26.0 (Si*C*CH), 20.4 (SiC*C*H$_3$), 20.2 (SiC*C*H$_3$'), 18.7 (2C, SiCCH*C*H$_3$), -0.03 (Si*C*H$_3$), -0.80 (Si*C*H$_3$').

^{19}F NMR (376 MHz, $CDCl_3$): δ -63.06 (s, 6F, ArCF_3), -63.11 (s, 6F, Ar'CF_3), -97.7 (dp, J_{FF} = 229.6 Hz, J_{HF} = 17.8 Hz, 1F, C4*F*F), -100.6 (br d, J_{FF} = 228.8 Hz, 1F, C4F*F*).

HRMS: calculated for $C_{29}H_{32}F_{14}NOSi$: 704.2024, found: 704.2031.

Catalyst **K** was characterized by X-ray single-crystal analysis.

Synthesis of the Chiral Amine Catalyst L

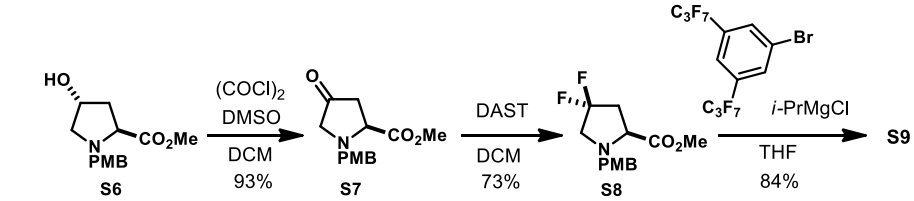

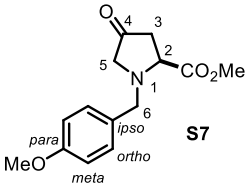

Methyl-(*S*)-1-(4-methoxybenzyl)-4-oxopyrrolidine-2-carboxylate (**S7**). In an oven dried, argon purged, two-neck round-bottomed flask were placed DMSO (323 µL, 4.54 mmol, 2.10 Equiv.) and dry CH_2Cl_2 (7.0 mL). The mixture was cooled at -78ºC, and a solution of oxalyl chloride (241 µL, 2.81 mmol, 1.30 Equiv.) in dry CH_2Cl_2 (7.0 mL) was added over 5 minutes. After 15 min stirring, a solution of methyl-(2*S*,4*R*)-4-hydroxy-1-(4-methoxybenzyl)pyrrolidine-2-carboxylate **S6** (574 mg, 2.16 mmol, 1.00 Equiv.), prepared from commercially available *trans*-4-hydroxy-L-proline according to a procedure reported in

the literature[38], in dry CH_2Cl_2 (7.0 mL), was added over 5 min. The light yellow solution was stirred for 30 min at -78 ºC and then Et_3N (1.45 mL, 10.4 mmol, 4.80 Equiv.) was added to give a turbid solution. The mixture was stirred for 30 min and then allowed to warm up to ambient temperature. The thick suspension was stirred for additional 60 min then water (100 mL) was added and the mixture was extracted with CH_2Cl_2 (3 x 100 mL). The combined organic layers were dried over $MgSO_4$ and concentrated *in vacuo* to give a light yellow oil which was purified by column chromatography (*c*-hexane/EtOAc 2:1) to afford **S7** as a light yellow solid (530 mg, 93% yield).

R_f = 0.44 (*c*-hexane/EtOAc 2:1), $[\alpha]_D^{26}$ = -38.5 (c = 0.5, $CHCl_3$).

^{1}H NMR (500 MHz, $CDCl_3$): δ 7.24-7.20 (m, 2H, *ortho*), 6.88-6.84 (m, 2H, *meta*), 3.85 (d, *J* = 12.9 Hz, 1H, C6*H*H), 3.81 (dd, *J* = 7.7 Hz, 5.9 Hz, 1H, C2*H*), 3.80 (s, 3H, ArOC*H*$_3$), 3.74 (s, 3H, CO_2CH_3), 3.68 (d, *J* = 12.9 Hz, 1H, C6H*H*), 3.33 (d, *J* = 17.2 Hz, 1H, C5*H*H), 2.99 (d, *J* = 17.3 Hz, 1H, C5H*H*), 2.69 (dd, *J* = 18.1 Hz, 7.7 Hz, 1H, C3*H*H), 2.55 (dd, *J* = 18.1 Hz, 5.9 Hz, 1H, C3H*H*).

^{13}C NMR (126 MHz, $CDCl_3$): δ 211.0 (*C4*), 172.6 (*C*O_2Me), 159.2 (*para*), 130.2 (2C, *ortho*), 129.0 (*ipso*), 114.0 (2C, *meta*), 62.2 (*C2*), 59.0 (*C5*), 56.9 (*C6*), 55.4 (ArO*C*H_3), 52.1 (CO_2CH_3), 41.9 (*C3*).

HRMS: calculated for $C_{14}H_{17}NO_4Na$: 286.1050, found: 286.1053.

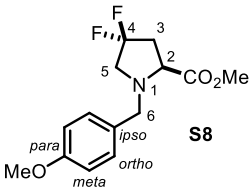

Methyl-(*S*)-4,4-difluoro-1-(4-methoxybenzyl)-pyrrolidine-2-carboxylate (S8). A colorless solution of **S7** (510 mg, 1.94 mmol, 1.00 Equiv.) in CH_2Cl_2 (22 mL) was cooled to 0 ºC and diethylaminosulfur trifluoride (DAST, 768 µL, 5.81 mmol, 3.00 Equiv.) was added dropwise to give a yellow solution. The reaction mixture was allowed to slowly warm up to ambient temperature by leaving it in an ice bath (after 2 hours the ice had melted). After 18 hours stirring, the yellow solution was cooled to 0 ºC, $NaHCO_3$ solution (sat., 50 mL) was carefully added and the mixture was extracted with CH_2Cl_2 (3 x 50 mL). The combined organic layers were dried over $MgSO_4$ and concentrated *in vacuo* to give a brown oil which was purified by column chromatography (*c*-hexane/EtOAc 10:1) to afford S8 as a colorless oil (404 mg; 73% yield).

R_f = 0.62 (*c*-hexane/EtOAc 2:1); $[\alpha]_D^{26}$ = -65.3 (c = 0.5, $CHCl_3$).

^{1}H NMR (400 MHz, $CDCl_3$): δ 7.25-7.19 (m, 2H, *ortho*), 6.90-6.82 (m, 2H, *meta*), 3.91 (d, *J* = 12.9 Hz, 1H, C6*H*H), 3.80 (s, 3H, ArOC*H*$_3$), 3.72 (s, 3H, CO_2CH_3), 3.61-3.50 (m, 2H, C2*H*

[38] Orliac, A., Routier, J., Burgat Charvillon, F., Sauer, W. H., Bombrun, A., Kulkarni, S. S., Gomez Pardo, D., Cossy, J., "Enantioselective Synthesis and Physicochemical Properties of Libraries of 3-Amino-and 3-Amidofluoropiperidines" *Chem. Eur. J.* **2014**, *20*, 3813.

and C6H*H*), 3.33 (q, *J* = 11.7 Hz, 1H, C5*H*H), 2.82 (td, *J* = 14.2 Hz, 11.3 Hz, 1H, C5H*H*), 2.65-2.39 (m, 2H, C3H_2).

^{13}C NMR (101 MHz, $CDCl_3$): δ 172.1 (*C*O_2Me), 159.2 (*para*), 130.3 (2C, *ortho*), 129.1 (*ipso*), 128.0 (dd, J_{CF} = 249.5 Hz, 247.6 Hz, *C4*), 114.0 (2C, *meta*), 63.0 (t, J_{CF} = 3.8 Hz, *C2*), 59.9 (t, J_{CF} = 29.0 Hz, *C5*), 56.9 (*C6*), 55.4 (ArO*C*H_3), 52.2 ($CO_2C$$H_3$), 39.9 (t, J_{CF} = 26.0 Hz, *C3*).

^{19}F NMR (376 MHz, $CDCl_3$): δ -92.6 (dm, J_{FF} = 229.6 Hz), -93.6 (dm, J_{FF} = 229.6 Hz).

HRMS: calculated for $C_{14}H_{17}F_2NO_3Na$: 308.1069, found: 308.1078.

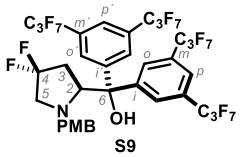

S9

(S)-Bis(3,5-bis-(perfluoropropan-2-yl)-phenyl)-(4,4-difluoro-1-(4-methoxybenzyl)-pyrrolidin-2-yl)-methanol (S9). Isopropylmagnesium chloride (2.0 M in THF, 4.4 mL, 8 .75 mmol, 2.5equiv) was added dropwise at 0 ºC to a solution of 1-bromo-3,5-bis-(perfluoropropan-2-yl)-benzene (4.32 g, 8.75 mmol, 2.5 Equiv.), prepared according to a procedure reported in the literature[39], in anhydrous THF (20 mL). The reaction was stirred for 1 hour at 0 ºC. Then, a solution of **S8** (1g, 3.5 mmol, 1 equiv) in anhydrous THF (10 mL) was added and the reaction mixture was brought to room temperature and stirred for 6 hours. After complete disappearance of S8, as judged by TLC analysis (hexane/EtOAc 90:10), the reaction was quenched by addition of sat. NH_4Cl, and the reaction mixture was extracted twice with ethyl acetate. The combined organic phase were washed with brine, dried over magnesium sulfate and concentrated under reduced pressure. Purification of the crude material by column chromatography (hexane/CH_2Cl_2 gradient form 100:0 to 80:20), provided the tertiary alcohol S9 (3. 165g, 2.94 mmol, 84% yield) as a white solid. R_f = 0.4 (hexane/CH_2Cl_2 9:1); $[\alpha]_D^{26}$ = +18.4 (c = 0.5, $CHCl_3$).

1H NMR (400 MHz, $CDCl_3$): δ 8.21 (s, 2H, Ar^{ortho}), 7.97 (s, 2H, $Ar^{ortho\,'}$), 7.75 (s, 2H, Ar^{para} and Ar^{para}'), 6.85-6.73 (m, 4H, PMB^{ortho} and PMB^{meta}), 5.23 (s, 1H, O*H*), 4.37 (t, *J* = 8.2 Hz, 1H, C2*H*), 3.77 (s, 3H, OCH_3), 3.26-3.06 (m, 3H, NCH_2Ar and C5*H*H), 3.00-2.87 (m, 1H, C5H*H*), 2.28-1.99 (m, 2H, C3H_2).

^{13}C NMR (101 MHz, $CDCl_3$): δ 159.5 (PMB^{para}), 148.7 (*ipso*), 146.7 (*ipso*'), 129.4 (2C, PMB^{ortho}), 129.3 (2C, dd, J_{CF} = 18.5 Hz, 2.0 Hz, *meta*, partially overlaid with PMB^{ortho} and *meta*'), 129.1 (2C, dd, J_{CF} = 18.8 Hz, 2.2 Hz, *meta'*), 128.8 (PMB^{ipso}), 126.1 (dd, J_{CF} = 251.6, 245.5 Hz, *C4*), 125.6 (2C, d, J_{CF} = 10.3 Hz, *ortho*), 125.2 (2C,d, J_{CF} = 10.2 Hz, *ortho*'), 122.9 (t, J_{CF} = 12.6 Hz, *para*, partially overlaid with *para*'), 122.7 (t, J_{CF} = 10.2 Hz, *para*'), 120.4 (8C, qd, J_{CF} = 286.9 Hz, 27.6 Hz, *C*F_3), 114.3 (2C, PMB^{meta}), 91.2 (4C, apparent dp, J_{CF} = 204.7 Hz, 33.5 Hz, CF_3*C*F), 76.1 (*C6*), 68.6 (t, J_{CF} = 3.6 Hz, *C2*), 60.3 (t, J_{CF} = 28.0 Hz, *C5*), 59.7 (N*C*H_2Ar), 55.4 (O*C*H_3), 38.2 (t, J_{CF} = 25.1 Hz, *C3*).

[39] Guin, J., Rabalakos, C., List, B., "Highly Enantioselective Hetero-Diels–Alder Reaction of 1, 3-Bis (silyloxy)-1, 3-dienes with Aldehydes Catalyzed by Chiral Disulfonimide" *Angew. Chem.* **2012**, *124*, 8989.

^{19}F NMR (376 MHz, $CDCl_3$): δ -75.6 - -76.0 (m, 24 F, CF_3), -98.3 (dp, J_{FF} = 232.1 Hz, J_{HF} = 15.6 Hz, 1F, C4*F*F), -99.9 (dp, J_{FF} = 232.1 Hz, J_{HF} = 9.8 Hz, 1F, C4F*F*), -182.1 (sept, J_{FF} = 7.1 Hz, 2F, CF_3C*F*, partially overlaid with CF_3C*F*'), -182.2 (sept, J_{FF} = 7.1 Hz, 2F, CF_3C*F*'). HRMS: calculated for $C_{37}H_{22}F_{30}NO_2$: 1082.1166, found: 1082.1169.

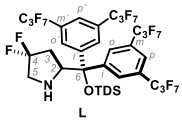

L

***(S)*-2-(Bis-(3,5-bis-(perfluoropropan-2-yl)-phenyl)-(((2,3-dimethylbutan-2-yl)-dimethylsilyl)-oxy)-methyl)-4,4-difluoro-1-(4-methoxybenzyl)-pyrrolidine (L).** Sodium hydride (60% dispersion in mineral oil, 350 mg, 3 Equiv.) was added to a solution of alcohol **S9** (3.14 g, 2.90 mmol) in anhydrous THF (20 mL) at 0 ºC. The reaction mixture was stirred for 10 minutes, then chloro-(dimethyl)-thexylsilane (5.8 mmol, 2.0 Equiv., 1.14 mL) was added. The reaction was warmed up to ambient temperature and stirred for 6 additional hours. After disappearance of the starting alcohol, as judged by TLC analysis (hexane/EtOAc 90:10), the reaction mixture was poured on ice and extracted with diethyl ether. The organic phase was dried over magnesium sulfate and concentrated under reduced pressure. The crude residue was dissolved in CH_2Cl_2 (60 mL) and water (10 mL) was added, followed by the addition of 2,3-dichloro-5,6-dicyano-1,4-benzoquinone (DDQ, 5.8 mmol, 1.32 g, 2 Equiv.) in small portions over 10 minutes. The reaction was stirred at ambient temperature for 1 hour and sat. $NaHCO_3$ was added resulting in a brown color appearance. This mixture was extracted with CH_2Cl_2 twice and the combined organic phases were dried over magnesium sulfate and concentrated under reduced pressure. The crude oil was purified by column chromatography (hexane/CH_2Cl_2 gradient from 100:0 to 95:5), yielding catalyst **L** (2.45 g, 2.22 mmol, 77% yield) as a colorless viscous oil**.** $[\alpha]_D^{26}$ = +10.1 (c = 0.5, $CHCl_3$).

^{1}H NMR (400 MHz, $CDCl_3$): δ 8.06 (s, 2H, *ortho*), 7.88 (s, 1H, *para*), 7.87 (s, 1H, *para'*), 7.70 (s, 2H, *ortho'*), 4.52 (br t, *J* = 7.2 Hz, 1H, C2*H*), 3.11-2.96 (m, 1H, C5*H*H), 2.41-2.21 (m, 2H, C5H*H* and C3*H*H), 2.14 (br s, 1H, N*H*), 1.87 (dtd, *J* = 22.2 Hz, 14.0 Hz, 8.3 Hz, 1H, C3H*H*), 1.75 (sept, *J* = 6.9 Hz, 1H, SiCC*H*),0.92 (d, *J* = 2.4 Hz, 3H, SiCCHCH_3), 0.91 (d, *J* = 2.4 Hz, 3H, SiCCHCH_3'), 0.88 (s, 3H, SiCCH_3), 0.87 (s, 3H, SiCCH_3'), -0.09 (s, 3H, SiCH_3), -0.55 (s, 3H, SiCH_3').

^{13}C NMR (101 MHz, $CDCl_3$): δ 146.7 (*ipso*), 145.0 (*ipso*'), 129.5 (dd, J_{CF} = 254.0 Hz, 245.7 Hz, *C4*), 129.4 (2C, d, J_{CF} = 10.1 Hz, *ortho*), 128.9 (2C, d, J_{CF} = 10.1 Hz, *ortho'*, partially overlaid with *meta*), 128.8 (2C, dd, J_{CF} = 20.9 Hz, 2.1 Hz, *meta*), 127.9 (2C, dd, J_{CF} = 20.7 Hz, 2.3 Hz, *meta'*), 123.5 (t, J_{CF} = 10.8 Hz, *para*), 123.2 (t, J_{CF} = 11.5 Hz, *para'*), 120.6 (4C, qd, J_{CF} = 287.1 Hz, 27.5 Hz, *C*F_3), 120.3 (4C, qd, J_{CF} = 287.3 Hz, 27.3 Hz, *C*F_3'), 91.3 (2C, apparent dp, J_{CF} = 204.5 Hz, 33.6 Hz, CF_3*C*F), 91.2 (2C, apparent dp, J_{CF} = 204.7 Hz, 33.6 Hz, CF_3*C*F'), 82.7 (*C6*), 62.2 (d, J_{CF} = 6.3 Hz, *C2*), 53.4 (t, J_{CF} = 28.8 Hz, *C5*), 37.3 (t, J_{CF} = 25.1 Hz, *C3*), 33.7 (SiC*C*H), 25.7 (Si*C*CH), 20.1 (SiC*C*H_3), 19.9 (SiC*C*H_3'), 18.44 (SiCCH*C*H_3), 18.49 (SiCCH*C*H_3'), -0.3 (Si*C*H_3), -1.5 (Si*C*H_3').

^{19}F NMR (376 MHz, $CDCl_3$): δ -76.1 - -76.3 (m, 18F, C*F*$_3$), -76.3 - -76.5 (m, 6F, C*F*$_3$), -99.2 (dp, J_{FF} = 230.3 Hz, J_{HF} = 18.9 Hz, 1F, C4*F*F), -106.4 (br d, J_{FF} = 222.1 Hz, 1F, C4F*F*), -182.6 (sept, J_{FF} = 7.5 Hz, 2F, CF_3C*F*), -182.7 (sept, J_{FF} = 7.0 Hz, 2F, CF_3C*F*').
HRMS: calculated for $C_{37}H_{32}F_{30}NOSi$: 1104.1769, found: 1104.1792.

Synthesis of the Enals 15

Substrates **15c**, **15d**, **15i** and **15z** were synthesized according to a procedure reported in the literature[40]:

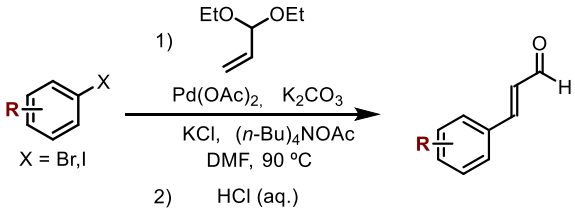

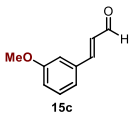

15c

(*E*)-3-(3-methoxyphenyl)-acrylaldehyde (15c). To an oven-dried, argon purged, two neck round-bottomed flask fitted with a condenser was added an orange, cloudy mixture of 3,3-diethoxyprop-1-ene (1.96 mL, 12.8 mmol), $Pd(OAc)_2$ (28.8 mg, 128 μmol), K_2CO_3 (887 mg, 6.42 mmol), KCl (319 mg, 4.28 mmol) (*n*-Bu)$_4$OAc (2.58 g, 8.55 mmol) and 1-bromo-3-methoxybenzene (542 μL, 4.28 mmol) in DMF (20 mL). The reaction mixture was heated to 90 ºC. After 18 hours stirring, the black solution was allowed to cool to ambient temperature. HCl-solution (2 M, aq., 15 mL) was added dropwise and the mixture was stirred for 15 min. Water (100 mL) was added and the mixture extracted with Et_2O (100 mL). The organic layer was dried over $MgSO_4$ and concentrated to give a brown oil, which was purified by column chromatography (*c*-hex/EtOAc 10:1) to afford **15c** as a light yellow oil (621 mg, 89% yield).
^{1}H NMR (500 MHz, $CDCl_3$): δ 9.68 (d, *J* = 7.7 Hz, 1H), 7.43 (d, *J* = 16.0 Hz, 1H), 7.33 (t, *J* = 7.9 Hz, 1H), 7.16-7.12 (m, 1H), 7.06 (dd, *J* = 2.6 Hz, 1.6 Hz, 1H), 6.98 (ddd, *J* = 8.3 Hz, 2.6 Hz, 0.9 Hz, 1H), 6.68 (dd, *J* = 15.9 Hz, 7.7 Hz, 1H), 3.83 (s, 3H).
^{13}C NMR (126 MHz, $CDCl_3$): δ 193.7, 160.1, 152.7, 135.4, 130.2, 128.9, 121.3, 117.1, 113.4, 55.4.

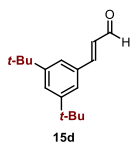

15d

(*E*)-3-(3,5-di-*tert*-butylphenyl)-acrylaldehyde (15d). To an oven-dried, argon purged, two neck round-bottomed flask fitted with a condenser was added an orange, cloudy mixture of 3,3-diethoxyprop-1-ene (1.70 mL, 11.1 mmol), $Pd(OAc)_2$ (25.0 mg, 111 μmol), K_2CO_3 (770 mg, 5.57 mmol),

[40] Battistuzzi, G., Cacchi, S., Fabrizi, G., "An efficient palladium-catalyzed synthesis of cinnamaldehydes from acrolein diethyl acetal and aryl iodides and bromides" *Org. Lett.* **2003**, *5*, 777.

KCl (277 mg, 3.71 mmol) (n-Bu)$_4$OAc (2.24 g, 7.43 mmol) and 1-bromo-3,5-di-*tert*-butylbenzene (1.00 g, 3.71 mmol) in DMF (18 mL). The reaction mixture was heated to 90 ºC. After 14 hours stirring, the black solution was allowed to cool to ambient temperature. HCl-solution (2 M, aq., 30 mL) was added dropwise and the mixture was stirred for 15 min, diluted with water (50 mL) then extracted with Et_2O (2 x 50 mL). The combined organic layers were dried over $MgSO_4$ and concentrated to give a brown oil, which was purified by column chromatography (*c*-hex/EtOAc 30:1) to afford **15d** as a colorless oil (555 mg, 61%).
^{1}H NMR (400 MHz, $CDCl_3$): δ 9.71 (d, J = 7.7 Hz, 1H), 7.53 (t, J = 1.9 Hz, 1H), 7.52 (d, J = 15.9 Hz, 1H), 7.42 (d, J = 1.8 Hz, 2H), 6.75 (dd, J = 15.9, 7.8 Hz, 1H), 1.35 (s, 18H).
^{13}C NMR (101 MHz, $CDCl_3$): δ 194.0, 154.3, 151.9, 133.5, 128.3, 126.0, 123.0, 35.0, 31.5.
HRMS: calculated for $C_{17}H_{24}ONa$ ($M+Na^+$): 267.1725, found 267.1724.

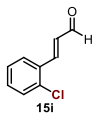

15i

(*E*)-3-(2-chlorophenyl)-acrylaldehyde (15i). To an oven-dried, argon purged, two neck round-bottomed flask fitted with a condenser was added an orange, cloudy mixture of 3,3-diethoxyprop-1-ene (1.88 mL, 12.3 mmol), $Pd(OAc)_2$ (28.0 mg, 123 μmol), K_2CO_3 (849 mg, 6.14 mmol), KCl (305 mg, 4.09 mmol) (n-Bu)$_4$OAc (2.47 g, 8.19 mmol) and 1-chloro-2-iodobenzene (500 μL, 4.09 mmol) in DMF (20 mL). The reaction mixture was heated to 90 ºC. After 17 hours stirring, the black solution was allowed to cool to ambient temperature. HCl-solution (2 M, aq., 15 mL) was added dropwise and the mixture was stirred for 15 min, diluted with water (50 mL) then extracted with Et_2O (100 mL). The organic layer was dried over $MgSO_4$ and concentrated to give a brown oil, which was purified by column chromatography (*c*-hex/EtOAc 20:1) to furnish **15i** as a light yellow solid (654 mg, 96% yield).
^{1}H NMR (400 MHz, $CDCl_3$): δ 9.75 (d, J = 7.7 Hz, 1H), 7.92 (d, J = 16.0 Hz, 1H), 7.65 (dd, J = 7.5 Hz, 1.9 Hz 1H), 7.47-7.42 (m, 1H), 7.38-7.28 (m, 2H), 6.69 (dd, J = 16.0 Hz, 7.7 Hz, 1H).
^{13}C NMR (101 MHz, $CDCl_3$): δ 148.0, 135.3, 132.2, 132.1, 130.6, 130.5, 128.0, 127.4.

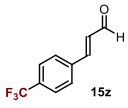

15z

(*E*)-3-(4-(trifluoromethyl)-phenyl)-acrylaldehyde (15z). To an oven-dried, argon purged, two neck round-bottomed flask fitted with a condenser was added an orange, cloudy mixture of 3,3-diethoxyprop-1-ene (1.02 mL, 6.67 mmol), $Pd(OAc)_2$ (15.0 mg, 67 μmol), K_2CO_3 (461 mg, 3.33 mmol), KCl (166 mg, 2.22 mmol) (n-Bu)$_4$OAc (1.34 g, 4.44 mmol) and 1-bromo-4-(trifluoromethyl)benzene (307 μL, 2.22 mmol) in DMF (10 mL). The reaction mixture was heated to 90 ºC. After 16 hours stirring, the black solution was allowed to cool to ambient temperature. HCl-solution (2 M, aq., 15 mL) was added dropwise and the mixture was stirred for 15 min, diluted with water (50 mL) then extracted with Et_2O (50 mL). The organic layer was dried over $MgSO_4$ and concentrated to

give a brown oil, which was purified by column chromatography (*c*-hex/EtOAc gradient from 20:1 to 10:1) to furnish **15z** as a light yellow solid (355 mg, 78% yield).

^{1}H NMR (400 MHz, $CDCl_3$): δ 9.75 (d, *J* = 7.5 Hz, 1H), 7.68 (s, 4H), 7.50 (d, *J* = 16.1 Hz, 1H), 6.77 (dd, *J* = 16.0 Hz, 7.5 Hz, 1H).

^{13}C NMR (101 MHz, $CDCl_3$): δ 193.3, 150.4, 137.4, 132.7 (q, J_{CF} = 32.9 Hz), 130.6, 128.7, 126.2 (q, J_{CF} = 3.8 Hz), 123.8 (q, J_{CF} = 272.4 Hz).

^{19}F NMR (376 MHz, $CDCl_3$): δ -63.1.

Compound **15h** was prepared as shown below

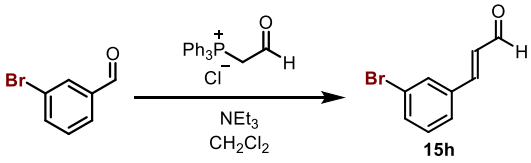

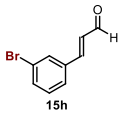

(*E*)-3-(3-bromophenyl)-acrylaldehyde (15h). To a yellow, turbid solution of (2-oxoethyl)-triphenylphosphonium chloride (5.85 g, 17.2 mmol) in dry CH_2Cl_2 (85 mL) was added triethylamine (3.59 mL, 25.7 mmol) to give a brown, clear solution to which was added 3-bromobenzaldehyde (2.00 mL, 17.2 mmol) dropwise. The reaction was stirred for 92 hours, then the mixture was concentrated to afford a brown oil. This was purified by column chromatography (*c*-hex/EtOAc gradient from 20:1 to 10:1) to give **15h** as a light yellow solid (1.18 g, 33% yield).

^{1}H NMR (500 MHz, $CDCl_3$): δ 9.70 (d, *J* = 7.5 Hz, 1H), 7.69 (t, *J* = 1.8 Hz, 1H), 7.55 (ddd, *J* = 8.0 Hz, 2.0 Hz, 1.0 Hz, 1H), 7.48 (dddd, *J* = 7.8 Hz, 1.7 Hz, 1.0 Hz, 0.5 Hz, 1H), 7.38 (d, *J* = 16.0 Hz, 1H), 7.30 (t, *J* = 7.9 Hz, 1H), 6.68 (dd, *J* = 16.0 Hz, 7.6 Hz, 1H).

^{13}C NMR (126 MHz, $CDCl_3$): δ 193.3, 150.7, 136.2, 134.1, 131.3, 130.7, 129.8, 127.0, 123.3.

Data in agreement with the literature.[41]

Synthesis of Benzyl Silanes 3

Many benzyl silanes were synthesized using procedures reported in the literature. The following Scheme depicts the silanes **3** that have been prepared and the corresponding literature references.[42]

---

[41] Kim, E., Koh, M., Lim, B. J., Park, S. B., "Emission wavelength prediction of a full-color-tunable fluorescent core skeleton, 9-aryl-1, 2-dihydropyrrolo [3, 4-b] indolizin-3-one" *J. Am. Chem. Soc.* **2011**, *133*, 6642.

[42] a)Perez, I., Sestelo, J. P., Sarandeses, L. A., "Atom-efficient metal-catalyzed cross-coupling reaction of indium organometallics with organic electrophiles" *J. Am. Chem. Soc.* **2001**, *123*, 4155. b) Bach, R. D., Klix, R. C., "Model studies aimed at the synthesis of Fredericamycin A. A simple o-quinodimethane route to the spiro naphthalene portion" *Tetrahedron Lett.* **1986**, *27*, 1983. c) Maruyama, T., Mizuno, Y., Shimizu, I., Suga,

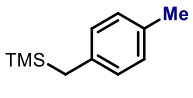

3k (ref. *38a*)

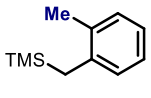

3l (ref. *38b*)

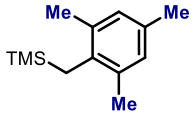

3m (ref. *38c*)

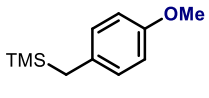

3n (ref. *38d*)

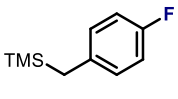

3o (ref. *38c*)

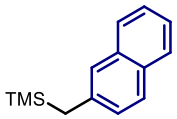

3q (ref. *38e*)

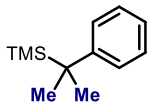

3r (ref. *38f*)

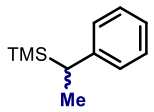

3s (ref. *38f*)

Silanes **3t** and **3u** were prepared from the corresponding benzyl bromides using the procedure detailed in the following scheme:

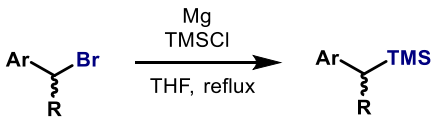

Magnesium turnings (1.2 Equiv.) were added to an oven-dried, argon purged, two neck round-bottomed flask fitted with a condenser and septum, followed by the addition of anhydrous tetrahydrofuran (0.3 M) and chlorotrimethylsilane (3 Equiv.). The reaction mixture was brought to reflux and a THF solution (2 M) of the alkyl bromide (1 Equiv.) was added dropwise over 15 minutes. After additional 10 minutes, the reaction was cooled to ambient temperature and 1M HCl was added. The mixture was extracted with diethyl ether, the organic phase dried over sodium sulfate and concentrated under reduced pressure. The crude oil was purified by column chromatography to yield the silane derivatives **3t** and **3u** as colorless oils.

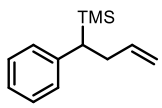

3t

Trimethyl(1-phenylbut-3-en-1-yl)silane (3t). Following the procedure described above, and using magnesium turnings (292 mg, 12 mmol), chlorotrimethylsilane (7 mL), and freshly prepared (1-bromobut-3-en-1-yl)benzene (10 mmol, 2.1 g), prepared according to a procedure reported

S., Yoshida, J.-i., "Reactions of a N-acyliminium ion pool with benzylsilanes. Implication of a radical/cation/radical cation chain mechanism involving oxidative C− Si bond cleavage" *J. Am. Chem. Soc.* **2007**, *129*, 1902. d) Coughlin, D. J., Salomon, R. G., "New synthetic approach to 4-alkylidenecyclohexenes. Reduction-protodesilylation of benzylsilanes" *J. Org. Chem.* **1979**, *44*, 3784. e) Huckins, J. R., Rychnovsky, S. D., "Synthesis of optically pure arylsilylcarbinols and their use as chiral auxiliaries in oxacarbenium ion reactions" *J. Org. Chem.* **2003**, *68*, 10135. f) Georgakilas, V., Perdikomatis, G. P., Triantafyllou, A. S., Siskos, M. G., Zarkadis, A. K., "Friedel–Crafts acetylation and benzoylation of benzylsilanes and xanthenes" *Tetrahedron* **2002**, *58*, 2441.

in the literature[43], silane **3t** (1.7 g, 8.3 mmol, 83% yield) was obtained as a colorless oil after column chromatography (pure hexane).

^{1}H NMR (500 MHz, $CDCl_3$): δ 7.25 – 7.20 (m, 2H), 7.10 – 7.06 (m, 1H), 7.03 – 6.99 (m, 2H), 5.71 (ddt, *J* = 17.0, 10.2, 6.6 Hz, 1H), 4.96 (ddt, *J* = 17.0, 2.0, 1.4 Hz, 1H), 4.86 (ddt, *J* = 10.2, 2.0, 1.4 Hz, 1H), 2.60 – 2.45 (m, 2H), 2.13 (dd, *J* = 11.4, 4.5 Hz, 1H), -0.05 (s, 9H).

^{13}C NMR (101 MHz, $CDCl_3$): δ 143.3, 138.9, 128.2, 127.9, 124.5, 114.9, 37.1, 33.9, -2.7.

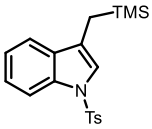

3u

1-tosyl-3-((trimethylsilyl)methyl)-1H-indole (3u). Following the procedure described above, and using 3-(bromomethyl)-1-tosyl-1H-indole (1g, 2.75 mmol), prepared according to a literature procedure[44], magnesium turnings (80 mg), and chlorotrimethylsilane (1.1 mL), silane **3u** (182 mg, 0.51 mmol, 19%) was obtained as a white solid after column chromatography (hexane/CH_2Cl_2 1:1).

^{1}H NMR (400 MHz, $CDCl_3$): δ 7.99 (dt, *J* = 8.3, 0.9 Hz, 1H), 7.72 – 7.66 (m, 2H), 7.37 (ddd, *J* = 7.8, 1.4, 0.7 Hz, 1H), 7.29 (ddd, *J* = 8.5, 7.2, 1.3 Hz, 1H), 7.23 – 7.14 (m, 4H), 2.31 (s, 3H), 2.03 (d, *J* = 1.1 Hz, 2H), -0.04 (s, 9H).

^{13}C NMR (101 MHz, $CDCl_3$): δ 144.6, 135.6, 135.3, 132.0, 129.9, 129.8, 126.9, 126.8, 124.6, 123.0, 121.5, 121.3, 119.9, 114.0, 21.6, 14.3, -1.4.

Silane **(3v)** was prepared by Kumada coupling of trimethylsilyl-methyl Grignard and 3-bromo thiophene as detailed in the following Scheme.

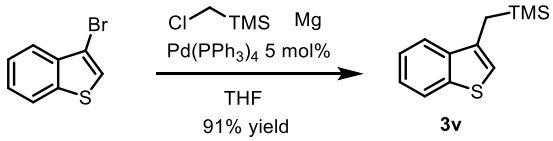

3v

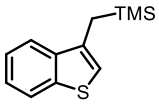

3v

(benzo[b]thiophen-3-ylmethyl)trimethylsilane (3v). To an oven-dried, argon purged two neck round-bottomed flask fitted with a condenser and septum was added magnesium turnings (750 mg, 2.2 equiv) followed by anhydrous tetrahydrofuran (8 mL). Chloromethyl trimethylsilane (20 mmol, 2.8 mL, 3 Equiv.) was added dropwise to maintain reflux. After cooling to ambient temperature, the solution was transferred by cannula into a 50 mL sealable Schlenk tube containing a solution of 3-bromobenzothiophene (1.41g, 6.65 mmol), prepared

[43] Gu, X., Ndungu, J. M., Qiu, W., Ying, J., Carducci, M. D., Wooden, H., Hruby, V. J., "Large scale enantiomeric synthesis, purification, and characterization of ω-unsaturated amino acids via a Gly-Ni (II)-BPB-complex" *Tetrahedron* **2004**, *60*, 8233.

[44] Chen, X., Fan, H., Zhang, S., Yu, C., Wang, W., "Facile Installation of 2-Reverse Prenyl Functionality into Indoles by a Tandem N-Alkylation–Aza-Cope Rearrangement Reaction and Its Application in Synthesis" *Chem. Eur. J.* **2016**, *22*, 716.

according to a procedure reported in the literature[45], and palladium tetrakis-(triphenylphosphine)-palladium (384 mg, 5 mol%) in 10 mL of anhydrous THF. The tube was sealed and the reaction was heated to 80 ºC for 48 hours. After cooling to room temperature, the solution was poured on 50 mL of cold 1M HCl solution. The aqueous phase was extracted twice with pentane and the combined organic phase were dried over magnesium sulfate and concentrated *in vacuo*. The crude mixture was subjected to flash chromatography (hexane 100%) yielding pure **3v** (1.32g. 6 mmol, 91%) as a colorless oil.

^{1}H NMR (400 MHz, $CDCl_3$): δ 7.84 (ddd, *J* = 7.6, 1.5, 0.8 Hz, 1H), 7.69 – 7.62 (m, 1H), 7.39 – 7.28 (m, 2H), 6.85 (apparent q, *J* = 0.9 Hz, 1H), 2.31 (d, *J* = 0.9 Hz, 2H), 0.02 (s, 9H).

^{13}C NMR (101 MHz, $CDCl_3$): δ 140.4, 139.5, 134.4, 123.9, 123.6, 122.9, 122.3, 118.4, 18.8, -1.2.

Synthesis of the α-Heteroatom-Substituted Silanes 21

Many α-heteroatom substituted silanes were synthesized using procedures reported in the literature. The following Scheme depicts the silanes that have been prepared and the corresponding reference.[46]

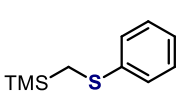

21a (ref. *42a*)

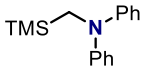

21d (ref. *42b*)

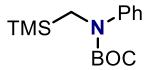

21e (ref. *42b*)

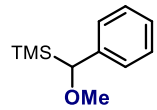

21e (ref. *42c*)

Silanes **21f** and **21g** were prepared from the corresponding carbazole and indole derivative according to the following Scheme:

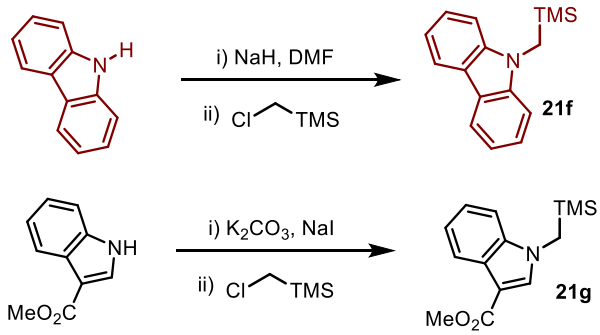

[45] Berens, U., Englert, U., Geyser, S., Runsink, J., Salzer, A., "A flexible approach to different families of bidentate P, P ligands as highly efficient ligands for asymmetric catalysis" *Eur. J. Org. Chem.* **2006**, *2006*, 2100.

[46] a) Ishibashi, H., Nakatani, H., Umei, Y., Yamamoto, W., Ikeda, M., "Reaction of [arylthio (chloro) methyl] trimethylsilanes with arenes and alk-1-enes in the presence of Lewis acid: syntheses of [aryl (arylthio) methyl]-and (1-arylthioalk-3-enyl)-trimethylsilanes" *J. Chem. Soc. Perkin Trans. 1* **1987**, 589. b) Ruiz Espelt, L., McPherson, I. S., Wiensch, E. M., Yoon, T. P., "Enantioselective conjugate additions of α-amino radicals via cooperative photoredox and Lewis acid catalysis" *J. Am. Chem. Soc.* **2015**, *137*, 2452. c) Okajima, M., Suga, S., Itami, K., Yoshida, J.-i., ""Cation Pool" Method Based on C− C Bond Dissociation. Effective Generation of Monocations and Dications" *J. Am. Chem. Soc.* **2005**, *127*, 6930.

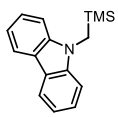

21f

9-((trimethylsilyl)-methyl)-9*H*-carbazole (21f). Sodium hydride (216 mg. 9 mmol, 3 Equiv.) was added to an oven-dried, argon purged two neck round flask equipped with a stirring bar and fitted with a vacuum adaptor and septum, and dissolved in anhydrous DMF (3 mL) The stirred solution was cooled to 0º C and carbazole (0.500 mg, 3 mmol, 1 Equiv.) was added portionwise. The mixture was stirred for 30 min then (chloromethyl)-trimethylsilane (736 mg, 6 mmol, 2 Equiv.) was added dropwise. The mixture was warmed up to ambient temperature and stirring was continued over 30 minutes. The reaction was quenched by the addition of water (15 mL), the mixture transferred to a separatory funnel and extracted with diethyl ether (2 x 20 mL). The organic phase was washed with brine, dried over magnesium sulphate, and concentrated *in vacuo*. The yellow residue was purified by flash chromatography (100% hexanes) to give the title compound **21f** as a white solid, 0.65 g (85% yield). The product was stored at 4 ºC.

^{1}H NMR (300 MHz, $CDCl_3$): δ 8.16 (d, *J* = 7.8 Hz, 2H), 7.51 (ddd, *J* = 8.2, 7.1, 1.2 Hz, 2H), 7.41 – 7.35 (m, 2H), 7.26 (ddd, *J* = 7.9, 7.1, 1.0 Hz, 3H), 3.89 (s, 2H), 0.11 (s, 9H).

^{13}C NMR (101 MHz, $CDCl_3$): δ 140.8, 125.5, 122.6, 120.3, 118.4, 109.0, 34.4, -1.2.

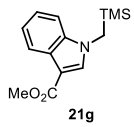

21g

Methyl 1-((trimethylsilyl)-methyl)-1*H*-indole-3-carboxylate (21g). Potassium carbonate (1.4 g. 10 mmol, 2 Equiv.) and sodium iodide (150 mg, 1 mmol, 0.2 Equiv.) were added to an oven-dried, argon purged two neck round flask equipped with a stirring bar and fitted with a vacuum adaptor and septum, and dissolved in anhydrous DMF (4 mL). The stirred solution was cooled to 0 ºC and methyl 1H-indole-3-carboxylate (876 mg, 5 mmol, 1 Equiv.) was added portionwise. The mixture was stirred for 30 min then (chloromethyl)-trimethylsilane (1.2 g, 10 mmol, 2 Equiv.) was added dropwise. The mixture was warmed up to ambient temperature and stirring was continued over 30 minutes. The reaction was quenched by the addition of water (15 mL), transferred to a separatory funnel and extracted with diethyl ether (2 x 20 mL). The organic phase was washed with brine, dried over magnesium sulphate, and concentrated *in vacuo*. The yellow residue was purified by recrystallization from boiling hexane to give **21g** as white needles, 1.2 g (90% yield). The product was stored at 4 ºC.

^{1}H NMR (300 MHz, $CDCl_3$): δ 8.22 – 8.11 (m, 1H), 7.73 (s, 1H), 7.38 – 7.15 (m, 3H), 3.91 (s, 3H), 3.72 (s, 2H), 0.10 (s, 9H).

^{13}C NMR (101 MHz, $CDCl_3$): δ 165.7, 137.3, 134.5, 126.5, 122.5, 121.7, 110.4, 106.6, 100.1, 51.0, 38.4, -2.0.

General Procedure for the β-Benzylation of Enals 15

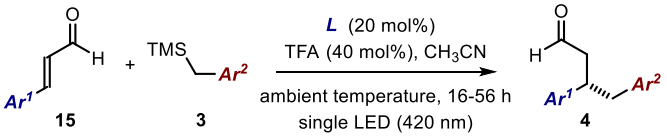

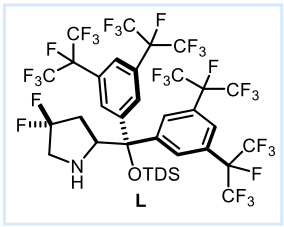

To a 5 mL argon-purged glass vial, containing the amine catalyst **L** (0.02 mmol, 20 mol%), the benzyl silane derivative **3** (0.1 mmol, 1 Equiv.) and the enal **15** (0.3 mmol, 3 Equiv.), was added 200 µL of an argon-sparged 0.2 M acetonitrile solution of TFA (0.04 mmol of TFA). The vial was further flushed with argon, sealed with Parafilm, and then placed into a 3D-printed plastic support mounted on an aluminium block fitted with a 420 nm high-power single LED (λ = 420 nm, irradiance = 41 mW/cm^2, as controlled by an external power supply). This set-up secured a reliable irradiation while keeping a constant distance of 1 cm between the reaction vessel and the light source. The reaction was stirred under visible light irradiation at ambient temperature for the indicated time (generally 16 hours). Then the solvent was evaporated and the crude mixture was purified by column chromatography on silica gel to furnish the product **4** in the stated yield and enantiomeric purity. Conversions were determined by ^{1}H NMR analysis of the crude mixture using trichloroethylene as the internal standard. If not otherwise stated, full consumption of the limiting silane substrate (**3**) was observed at the end of the reaction.

The light source for illuminating the reaction vessel consisted in a 420 nm high-power single LED (OCU-440 UE420-X-T) purchased from OSA OPTO

Characterization of Products 4

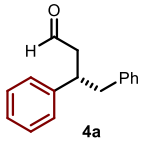

(*S*)-3,4-diphenylbutanal (4a). Prepared according to the general procedure using benzyl trimethylsilane **3a** (0.1 mmol, 19 µL), cinnamaldehyde **15a** (0.3 mmol, 38 µL), aminocatalyst **L** (0.02 mmol, 22 mg), and 200 µL of a 0.2 M acetonitrile solution of trifluoroacetic acid (40 mol%). Time of irradiation: 16 hours. The crude mixture was purified by flash column chromatography (hexane/diethyl ether 92:8, 3 consecutive purifications) to afford the product as a colorless oil (19.5 mg, 87% yield, 88% ee, average of two runs). The enantiomeric excess was determined to be 88% by HPLC analysis on a Daicel Chiralpak IC-3 column: 90:10 hexane/IPA, flow rate 0.6 mL/min, λ = 215 nm: τ_{Major} = 15.1 min, τ_{Minor} = 16.4 min. $[\alpha]_D^{26}$ = -45.8 (c = 0.49, $CHCl_3$, 88% ee). Absolute configuration determined in comparison to compound **22a**.

^{1}H NMR (400 MHz, $CDCl_3$): δ 9.62 (t, *J* = 2.0 Hz, 1H), 7.34 – 7.16 (m, 9H), 7.11 – 7.06 (m, 2H), 3.52 (p, *J* = 7.4 Hz, 1H), 2.99 (dd, *J* = 13.5, 7.1 Hz, 1H), 2.91 (dd, *J* = 13.5, 7.9 Hz, 1H), 2.85 – 2.69 (m, 2H).

^{13}C NMR (101 MHz, $CDCl_3$): δ 201.9, 143.6, 139.6, 129.6, 128.9, 128.6, 127.9, 127.1, 126.7, 49.38, 43.7, 42.4.
HRMS: Calculated for $C_{16}H_{16}NaO$ 247.1093, found: 247.1090.

1 mmol scale reaction. The model reaction was repeated on a more synthetically useful scale using the same light illumination system but a different reaction vessel (see picture to the right). A 50 mL round-bottom flask was used to increase the surface-area-to-volume ratio, which allowed for more efficient irradiation of the reaction mixture. To a 50 mL argon-purged flat bottom flask, containing the amine catalyst **L** (220 mg, 0.2 mmol, 20 mol%), the benzyl silane **3a** (1 mmol, 190 µL, 1 Equiv.) and cinnamaldehyde **15a** (380 µL, 3.0 mmol, 3 Equiv.), was added 2.0 mL of an argon sparged 0.2 M acetonitrile solution of TFA (0.4 mmol of TFA, 40 mol%). The flask was further flushed with argon, and sealed with Parafilm. The reaction vessel was then placed 1 cm above of a 420 nm high-power single LED (λ = 420 nm, irradiance = 41 mW/cm^2, as controlled by an external power supply). The reaction was stirred under visible light irradiation at ambient temperature for 48 hours. Then, the solvent was evaporated and the crude mixture was purified by column chromatography on silica gel (hexane/diethyl ether 92:8, 3 consecutive purifications) to afford product **4a** as a colorless oil (164 mg, 73% yield, 88% ee). 45% of catalyst **L** (99.5 mg) were recovered after column chromatography.

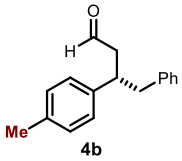

4b

(*S*)-4-Phenyl-3-(*p*-tolyl)-butanal (4b). Prepared according to the general procedure using benzyl trimethylsilane **3a** (0.1 mmol, 19 µL), cinnamaldehyde **15b** (0.3 mmol, 44 mg), aminocatalyst **L** (0.02 mmol, 22 mg), and 200 µL of a 0.2 M acetonitrile solution of trifluoroacetic acid (40 mol%). Time of irradiation: 16 hours. The crude mixture was purified by column chromatography (hexane/diethyl ether 10:1) to give a light yellow oil (17.6 mg, 74% yield, 78% ee, average of two runs). The enantiomeric excess was determined to be 78% by HPLC analysis on a Daicel Chiralpak IC column: 99:1 hexane/IPA, flow rate 0.8 mL/min, λ = 215 nm: τ_{Major} = 15.3 min, τ_{Minor} = 17.1 min. $[\alpha]_D^{26}$ = -42.5 (c = 0.50, $CHCl_3$, 78% ee). Absolute configuration determined in comparison to compound **22a**.
^{1}H NMR (500 MHz, $CDCl_3$): δ 9.58 (t, *J* = 2.0 Hz, 1H), 7.28-7.21 (m, 2H), 7.21-7.15 (m, 1H), 7.12-7.04 (m, 6H), 3.46 (p, *J* = 7.4 Hz, 1H), 2.96 (dd, *J* = 13.5 Hz, 7.0 Hz, 1H), 2.86 (dd, *J* = 13.5 Hz, 8.0 Hz, 1H), 2.78-2.67 (m, 2H), 2.32 (s, 3H).
^{13}C NMR (126 MHz, $CDCl_3$): δ 201.9, 140.3, 139.5, 136.4, 129.43, 129.36, 128.5, 127.5, 126.5, 49.1, 43.5, 41.8, 21.2.
HRMS: Calculated for $C_{18}H_{22}Na$ (M+MeOH+Na^+): 293.1502, found: 293.1512.

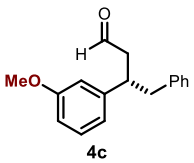

4c

(*S*)-3-(3-Methoxyphenyl)-4-phenylbutanal (4c). Prepared according to the general procedure using benzyl trimethylsilane **3a** (0.1 mmol, 19 μL), cinnamaldehyde **15c** (0.3 mmol, 49 mg), aminocatalyst **L** (0.02 mmol, 22 mg), and 200 μL of a 0.2 M acetonitrile solution of trifluoroacetic acid (40 mol%). Time of irradiation: 48 hours. The crude mixture (87% conversion of **3a**) was purified by column chromatography (hexane/diethyl ether 5:1) to give a colorless oil (15.3 mg, 62% yield, 82% ee, average of two runs). The enantiomeric excess was determined to be 82% by HPLC analysis on a Daicel Chiralpak IC column: 95:5 hexane/IPA, flow rate 0.8 mL/min, λ = 215 nm: τ_{Major} = 12.7 min, τ_{Minor} = 13.4 min. $[\alpha]_D^{26}$ = –41.2 (c = 0.69, $CHCl_3$, 82% ee). Absolute configuration determined in comparison to compound **22a**.

^{1}H NMR (400 MHz, $CDCl_3$): δ 9.59 (t, *J* = 1.9 Hz, 1H), 7.28-7.15 (m, 4H), 7.10-7.05 (m, 2H), 6.79-6.72 (m, 2H), 6.70 (t, *J* = 2.1 Hz, 1H), 3.77 (s, 3H), 3.47 (p, *J* = 7.5 Hz, 1H), 2.96 (dd, *J* = 13.5 Hz, 7.0 Hz, 1H), 2.87 (dd, *J* = 13.5 Hz, 7.9 Hz, 1H), 2.81-2.67 (m, 2H).

^{13}C NMR (101 MHz, $CDCl_3$): δ 201.7, 159.9, 145.1, 139.4, 129.7, 129.4, 128.5, 126.5, 120.0, 113.7, 112.0, 55.3, 49.0, 43.4, 42.2.

HRMS calculated for $C_{18}H_{22}O_3Na$ (M+MeOH+Na^+): 309.1467, found: 309.1461.

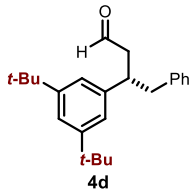

4d

(*S*)-3-(3,5-di-*tert*-butylphenyl)-4-phenylbutanal (4d). Prepared according to the general procedure using benzyl trimethylsilane **3a** (0.1 mmol, 19 μL), cinnamaldehyde **15d** (0.3 mmol, 73 mg), aminocatalyst **L** (0.02 mmol, 22 mg), and 200 μL of a 0.2 M acetonitrile solution of trifluoroacetic acid (40 mol%). Time of irradiation: 16 hours. The crude mixture (95% conversion of **3a**) was purified by flash column chromatography (hexane/toluene 1:1) to afford the product as a colorless oil (21.2 mg, 63% yield, 68% ee, average of two runs). The enantiomeric excess was determined, after sodium borohydride reduction of the isolated aldehyde to afford the corresponding alcohol, to be 68% by HPLC analysis on a Daicel Chiralpak IC column: 99:1 hexane/IPA, flow rate 0.8 mL/min, λ = 215 nm: τ_{Major} = 9.8 min, τ_{Minor} = 10.3 min. $[\alpha]_D^{26}$ = –17.5 (c = 0.69, $CHCl_3$, 68% ee). Absolute configuration determined in comparison to compound **22a**.

^{1}H NMR (400 MHz, $CDCl_3$): δ 9.60 (t, *J* = 2.1 Hz, 1H), 7.28-7.14 (m, 4H), 7.06-7.00 (m, 2H), 6.94 (d, *J* = 1.8 Hz, 2H), 3.49 (p, *J* = 7.3 Hz, 1H), 2.95 (dd, *J* = 13.3 Hz, 6.9 Hz, 1H), 2.89 (dd, *J* = 13.4 Hz, 7.9 Hz, 1H), 2.82-2.69 (m, 2H), 1.29 (s, 18H).

^{13}C NMR (101 MHz, $CDCl_3$): δ 202.2, 150.9, 142.3, 139.6, 129.5, 128.4, 126.4, 121.9, 120.7, 48.9, 43.8, 42.6, 35.0, 31.6.

HRMS calculated for $C_{25}H_{36}O_2Na$ (M+MeOH+Na^+): 391.2613, found: 391.2608.

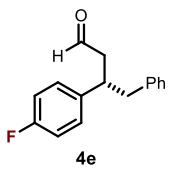

4e

(*S*)-3-(4-Fluorophenyl)-4-phenylbutanal (4e). Prepared according to the general procedure using benzyl trimethylsilane **3a** (0.1 mmol, 19 µL), cinnamaldehyde **15e** (0.3 mmol, 45 mg), aminocatalyst **L** (0.02 mmol, 22 mg), and 200 µL of a 0.2 M acetonitrile solution of trifluoroacetic acid (40 mol%). Time of irradiation: 16 hours. The crude mixture was purified by flash column chromatography (hexane/diethyl ether 10:1) to afford the product as a colorless oil (18.4 mg, 76% yield, 85% ee, average of two runs). The enantiomeric excess was determined to be 85% by HPLC analysis on a Daicel Chiralpak IC column: 99:1 hexane/IPA, flow rate 0.7 mL/min, λ = 215 nm: τ_{Major} = 19.0 min, τ_{Minor} = 20.2 min. $[\alpha]_D^{26}$ = –45.3 (c = 0.69, $CHCl_3$, 85% ee). Absolute configuration determined in comparison to compound **22a**.

^{1}H NMR (400 MHz, $CDCl_3$): δ 9.60 (t, *J* = 1.8 Hz, 1H, C*H*O), 7.27-7.15 (m, 3H, *Bn*^{para} and *Bn*^{meta}), 7.13-7.06 (m, 2H, *Ar*^{ortho}), 7.05-7.00 (m, 2H, *Bn*^{ortho}), 6.99-6.91 (m, 2H, *Ar*^{meta}), 3.49 (p, *J* = 7.4 Hz, 1H, C3*H*), 2.89 (d, *J* = 7.5 Hz, 2H, C4H_2), 2.75 (dd, *J* = 7.3 Hz, 1.9 Hz, 2H, C2H_2).

^{13}C NMR (101 MHz, $CDCl_3$): δ 201.3 (*C*HO), 161.7 (d, J_{CF} = 244.8 Hz, *Ar*^{para}), 139.1 (*Bn*^{ipso}), 139.0 (d, J_{CF} = 3.3 Hz, *Ar*^{ipso}), 129.3 (2C, *Bn*^{ortho}), 129.1 (2C, d, J_{CF} = 8.0 Hz, *Ar*^{ortho}), 128.5 (2C, *Bn*^{meta}), 126.6 (*Bn*^{para}), 115.5 (2C, d, J_{CF} = 21.2 Hz, *Ar*^{meta}), 49.3 (*C2*), 43.5 (*C4*), 41.4 (*C3*).

^{19}F{^{1}H} NMR (376 MHz, $CDCl_3$): δ -116.3.

HRMS calculated for $C_{17}H_{19}FO_2Na$ ($M+MeOH+Na^+$): 297.1261, found: 297.1253.

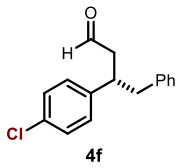

4f

(*S*)-3-(4-Chlorophenyl)-4-phenylbutanal (4f). Prepared according to the general procedure using benzyl trimethylsilane **3a** (0.1 mmol, 19 µL), cinnamaldehyde **15f** (0.3 mmol, 50 mg), aminocatalyst **L** (0.02 mmol, 22 mg), and 200 µL of a 0.2 M acetonitrile solution of trifluoroacetic acid (40 mol%). Time of irradiation: 16 hours. The crude mixture was purified by flash column chromatography (hexane/toluene 1:2) to afford the product as a colorless oil (19.4 mg, 75% yield, 86% ee, average of two runs). The enantiomeric excess was determined to be 86% by HPLC analysis on a Daicel Chiralpak IC column: 99:1 hexane/IPA, flow rate 0.6 mL/min, λ = 215 nm: τ_{Major} = 25.0 min, τ_{Minor} = 28.6 min. $[\alpha]_D^{26}$ = –56.8 (c = 0.69, $CHCl_3$, 86% ee). Absolute configuration determined in comparison to compound **22a**.

^{1}H NMR (400 MHz, $CDCl_3$): δ 9.60 (t, *J* = 1.8 Hz, 1H), 7.26-7.14 (m, 5H), 7.10-6.99 (m, 4H), 3.48 (p, *J* = 7.4 Hz, 1H), 2.88 (d, *J* = 7.5 Hz, 2H), 2.75 (dd, *J* = 7.3 Hz, 1.8 Hz, 2H).

^{13}C NMR (101 MHz, $CDCl_3$): δ 201.1, 141.8, 139.0, 132.5, 129.3, 129.0, 128.8, 128.5, 126.6, 49.1, 43.3, 41.4.

HRMS calculated for $C_{17}H_{14}ClO$ ($M-H^-$): 257.0728, found: 257.0729.

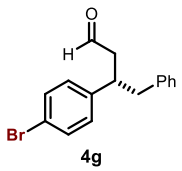

4g

(*S*)-3-(4-Bromophenyl)-4-phenylbutanal (4g). Prepared according to the general procedure using benzyl trimethylsilane **3a** (0.1 mmol, 19 µL), cinnamaldehyde **15g** (0.3 mmol, 63 mg), aminocatalyst **L** (0.02 mmol, 22 mg), and 200 µL of a 0.2 M acetonitrile solution of trifluoroacetic acid (40 mol%). Time of irradiation: 16 hours. The crude mixture was purified by flash column chromatography (hexane/toluene 1:2) to afford the product as a colorless oil (22.4 mg, 74% yield, 84% ee, average of two runs). The enantiomeric excess was determined to be 84% by HPLC analysis on a Daicel Chiralpak IC column: 99:1 hexane/IPA, flow rate 1.0 mL/min, λ = 215 nm: τ_{Major} = 11.6 min, τ_{Minor} = 13.0 min. $[\alpha]_D^{26}$ = –57.0 (c = 0.69, $CHCl_3$, 84% ee). Absolute configuration determined in comparison to compound **22a**.

^{1}H NMR (500 MHz, $CDCl_3$): δ 9.60 (t, *J* = 1.7 Hz, 1H), 7.41-7.37 (m, 2H), 7.26-7.21 (m, 2H), 7.21-7.16 (m, 1H), 7.05-6.99 (m, 4H), 3.47 (p, *J* = 7.4 Hz, 1H), 2.89 (d, *J* = 7.5 Hz, 2H), 2.75 (dd, *J* = 7.3 Hz, 1.8 Hz, 2H).

^{13}C NMR (126 MHz, $CDCl_3$): δ 201.0, 142.4, 139.0, 131.8, 129.4, 129.3, 128.5, 126.6, 120.6, 49.1, 43.2, 41.5.

HRMS: calculated for $C_{17}H_{19}BrO_2Na$ ($M+MeOH+Na^+$): 357.0466, found: 357.0462.

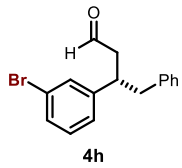

4h

(*S*)-3-(3-Bromophenyl)-4-phenylbutanal (4h). Prepared according to the general procedure using benzyl trimethylsilane **3a** (0.1 mmol, 19 µL), cinnamaldehyde **15h** (0.3 mmol, 63 mg), aminocatalyst **L** (0.02 mmol, 22 mg), and 200 µL of a 0.2 M acetonitrile solution of trifluoroacetic acid (40 mol%). Time of irradiation: 16 hours. The crude mixture was purified by flash column chromatography (hexane/toluene 2:1) to afford the product as a colorless oil (22.1 mg, 73% yield, 86% ee, average of two runs). The enantiomeric excess was determined to be 86% by HPLC analysis on a Daicel Chiralpak IC column: 99:1 hexane/IPA, flow rate 0.6 mL/min, λ = 215 nm: τ_{Major} = 17.3 min, τ_{Minor} = 18.6 min. $[\alpha]_D^{26}$ = –48.7 (c = 0.69, $CHCl_3$, 86% ee). Absolute configuration determined in comparison to compound **22a**.

^{1}H NMR (400 MHz, $CDCl_3$): δ 9.60 (t, *J* = 1.9 Hz, 1H), 7.35-7.29 (m, 2H), 7.28-7.10 (m, 4H), 7.09-7.01 (m, 3H), 3.46 (p, *J* = 7.4 Hz, 1H), 2.92 (dd, *J* = 13.5 Hz, 7.2 Hz, 1H), 2.86 (dd, *J* = 13.5 Hz, 7.8 Hz, 1H), 2.82-2.68 (m, 2H).

^{13}C NMR (101 MHz, $CDCl_3$): δ 200.9, 145.9, 138.9, 130.6, 130.3, 130.0, 129.3, 128.6, 126.7, 126.5, 122.8, 48.9, 43.2, 41.7.

HRMS: calculated for $C_{17}H_{19}BrO_2Na$ ($M+MeOH+Na^+$): 357.0466, found: 357.0463.

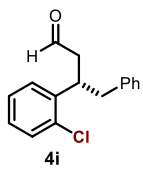

4i

(*S*)-3-(2-Chlorophenyl)-4-phenylbutanal (4i). Prepared according to the general procedure using benzyl trimethylsilane **3a** (0.1 mmol, 19 µL), cinnamaldehyde **15i** (0.3 mmol, 50 mg), aminocatalyst **L** (0.02 mmol, 22 mg), and 200 µL of a 0.2 M acetonitrile solution of trifluoroacetic acid (40 mol%). Time of irradiation: 16 hours. The crude mixture was purified by flash column chromatography (hexane/toluene 1:2) to afford the product as a colorless oil (19.4 mg, 75% yield, 88% ee, average of two runs). The enantiomeric excess was determined to be 88% by HPLC analysis on a Daicel Chiralpak IC column: 99:1 hexane/IPA, flow rate 0.6 mL/min, λ = 215 nm: τ_{Major} = 20.6 min, τ_{Minor} = 22.7 min. $[\alpha]_D^{26}$ = –13.0 (c = 0.69, $CHCl_3$, 88% ee). Absolute configuration determined in comparison to compound **22a**.

^{1}H NMR (500 MHz, $CDCl_3$): δ 9.55 (t, *J* = 2.1 Hz, 1H), 7.37 (dd, *J* = 7.9 Hz, 1.3 Hz, 1H), 7.29-7.10 (m, 8H), 4.11 (p, *J* = 7.4 Hz, 1H), 3.06 (dd, *J* = 13.6 Hz, 6.2 Hz, 1H), 2.82 (dd, *J* = 13.6 Hz, 8.5 Hz, 1H), 2.81-2.71 (m, 2H).

^{13}C NMR (126 MHz, $CDCl_3$): δ 201.2, 140.5, 138.9, 134.0, 130.1, 129.4, 128.5, 128.2, 128.0, 127.2, 126.7, 47.8, 41.8, 37.9.

HRMS calculated for $C_{17}H_{19}ClO_2Na$ (M+MeOH+Na^+): 313.0971, found: 313.0967.

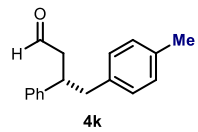

4k

(*S*)-3-phenyl-4-(*p*-tolyl)butanal (4k). Prepared according to the general procedure using *p*-tolyl-trimethylsilane **3k** (0.1 mmol, 17.9 mg), cinnamaldehyde **15a** (0.3 mmol, 38 µL), aminocatalyst **L** (0.02 mmol, 22 mg), and 200 µL of a 0.2 M acetonitrile solution of trifluoroacetic acid (40 mol%). Time of irradiation: 16 hours. The crude mixture was purified by flash column chromatography (hexane/diethyl ether 92:8, 2 consecutive purifications) to afford the product as a colorless oil (23.2 mg, 90% yield, 91% ee, average of two runs). The enantiomeric excess was determined to be 91% by HPLC analysis on a Daicel Chiralpak IC-3 column: 96:4 hexane/IPA, flow rate 0.8 mL/min, λ = 215 nm: τ_{Major} =11.0 min, τ_{Minor} = 11.8 min. $[\alpha]_D^{26}$ = -50.8 (c = 0.69, $CHCl_3$, 91% ee). Absolute configuration determined in comparison to compound **22a**.

^{1}H NMR (400 MHz, $CDCl_3$): δ 9.58 (t, *J* = 2.0 Hz, 1H), 7.31 – 7.26 (m, 2H), 7.23 – 7.15 (m, 3H), 7.07 – 7.02 (m, 2H), 6.98 – 6.93 (m, 2H), 3.47 (p, *J* = 7.5 Hz, 1H), 2.94 (dd, *J* = 13.6, 6.9 Hz, 1H), 2.83 (dd, *J* = 13.6, 8.1 Hz, 1H), 2.79 – 2.67 (m, 2H), 2.30 (s, 3H).

^{13}C NMR (101 MHz, $CDCl_3$): δ 202.1, 143.7, 136.5, 136.2, 129.4, 129.4, 128.9, 127.9, 127.0, 49.3, 43.3, 42.4, 21.4.

HRMS: Calculated for $C_{17}H_{18}NaO$ 261.1250, found: 261.1261.

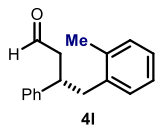

4l

(*S*)-3-phenyl-4-(*o*-tolyl)butanal (4l). Prepared according to the general procedure using *o*-tolyl-trimethylsilane **3l** (0.1 mmol, 17.9 mg), cinnamaldehyde **15a** (0.3 mmol, 38 µL), aminocatalyst **L** (0.02 mmol, 22 mg), and 200 µL of a 0.2 M acetonitrile solution of trifluoroacetic acid (40 mol%). Time of irradiation: 16 hours. The crude mixture was purified by flash column chromatography (hexane/diethyl ether 92:8, 2 consecutive purifications) to afford the product as a colorless oil (20.1 mg, 85% yield, 90% ee, average of two runs). The enantiomeric excess was determined to be 90% by HPLC analysis on a Daicel Chiralpak IC-3 column: 90:10 hexane/IPA, flow rate 0.7 mL/min, λ = 215 nm: τ_{Major} = 9.8 min, τ_{Minor} = 10.9 min. $[\alpha]_D^{26}$ = -22.2 (c = 0.59, $CHCl_3$, 90% ee). Absolute configuration determined in comparison to compound **22a**.

^{1}H NMR (500 MHz, $CDCl_3$): δ 9.58 (t, *J* = 2.0 Hz, 1H), 7.31 – 7.26 (m, 2H), 7.23 – 7.19 (m, 1H), 7.19 – 7.15 (m, 2H), 7.14 – 7.09 (m, 2H), 7.09 – 7.04 (m, 1H), 6.97 (dd, *J* = 7.3, 1.4 Hz, 1H), 3.52 – 3.42 (m, 1H), 2.97 – 2.86 (m, 2H), 2.86 – 2.73 (m, 2H), 2.26 (s, 3H).

^{13}C NMR (126 MHz, $CDCl_3$): δ 201.7, 143.7, 137.7, 136.5, 130.6, 130.3, 128.8, 127.6, 126.9, 126.7, 126.0, 49.1, 41.0, 19.6.

HRMS: Calculated for $C_{17}H_{18}NaO$ 261.1250, found: 261.1263.

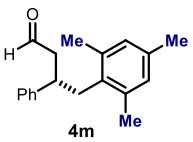

4m

(*S*)-4-mesityl-3-phenylbutanal (4m). Prepared according to the general procedure using trimethyl-(2,4,6-trimethylbenzyl)-silane **3m** (0.1 mmol, 21.5 mg), cinnamaldehyde **15a** (0.3 mmol, 38 µL), aminocatalyst **L** (0.02 mmol, 22 mg), and 200 µL of a 0.2 M acetonitrile solution of trifluoroacetic acid (40 mol%). Time of irradiation: 16 hours. The crude mixture was purified by flash column chromatography (hexane/diethyl ether 92:8, 2 consecutive purifications) to afford the product as a colorless oil (24.4 mg, 92% yield, 93% ee, average of two runs). The enantiomeric excess was determined to be 93% by HPLC analysis on a Daicel Chiralpak IC-3 column: 85:15 hexane/IPA, flow rate 0.5 mL/min, λ = 215 nm: τ_{Major} = 11.7 min, τ_{Minor} = 12.6 min. $[\alpha]_D^{26}$ = -100.69 (c = 0.55, $CHCl_3$, 93% ee). Absolute configuration determined in comparison to compound **22a**.

^{1}H NMR (500 MHz, $CDCl_3$): δ 9.53 (dd, *J* = 2.4, 1.8 Hz, 1H), 7.31 – 7.26 (m, 2H), 7.24 – 7.20 (m, 1H), 7.19 – 7.15 (m, 2H), 6.81 (s, 2H), 3.46 (tt, *J* = 8.8, 6.2 Hz, 1H), 2.99 – 2.80 (m, 3H), 2.71 (ddd, *J* = 16.5, 5.8, 1.8 Hz, 1H), 2.24 (s, 3H), 2.19 (s, 6H).

^{13}C NMR (126 MHz, $CDCl_3$): δ 201.8, 143.8, 136.8, 135.8, 133.3, 129.3, 128.7, 127.5, 126.9, 48.4, 40.4, 37.2, 21.0, 20.4.

HRMS: Calculated for $C_{19}H_{22}NaO$ 289.1563, found: 289.1556.

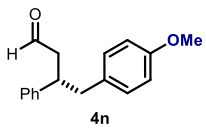

4n

(*S*)-4-(4-methoxyphenyl)-3-phenylbutanal (4n). Prepared according to the general procedure using 4-methoxybenzyl-trimethylsilane **3n** (0.1 mmol, 19.4 mg), cinnamaldehyde **15a** (0.3 mmol, 38 µL), aminocatalyst **L** (0.02 mmol, 22 mg), and 200 µL of a 0.2 M acetonitrile solution of trifluoroacetic acid (40 mol%). Time of irradiation: 16 hours. The crude mixture was purified by flash column chromatography (hexane/acetone 97:3, 2 consecutive purifications) to afford the product as a colorless oil (19.5 mg, 77% yield, 92% ee, average of two runs). The enantiomeric excess was determined to be 92% by HPLC analysis on a Daicel Chiralpak IC-3 column: 85:15 hexane/IPA, flow rate 0.5 mL/min, λ = 215 nm: τ_{Major} = 17.9 min, τ_{Minor} = 16.1min. $[\alpha]_D^{26}$ = -30.2 (c = 0.64, $CHCl_3$, 92% ee). Absolute configuration determined in comparison to compound **22a**.

^{1}H NMR (400 MHz, $CDCl_3$): δ 9.59 (t, *J* = 2.0 Hz, 1H), 7.31 – 7.27 (m, 1H), 7.22 – 7.17 (m, 1H), 7.17 – 7.13 (m, 2H), 6.98 – 6.93 (m, 2H), 6.80 – 6.75 (m, 2H), 3.77 (s, 3H), 3.44 (p, *J* = 7.4 Hz, 1H), 2.90 (dd, *J* = 13.6, 7.3 Hz, 1H), 2.82 (dd, *J* = 13.6, 7.4 Hz, 1H), 2.78 – 2.67 (m, 2H).

^{13}C NMR (101 MHz, $CDCl_3$): δ 202.0, 158.5, 143.7, 131.6, 130.5, 128.9, 127.9, 127.0, 114.1, 55.6, 49.3, 42.8, 42.6.

HRMS: Calculated for $C_{17}H_{18}NaO_2$ 277.1199, found: 277.1195.

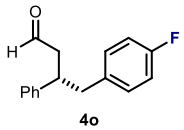

4o

(*S*)-4-(4-fluoroyphenyl)-3-phenylbutanal (4o). Prepared according to the general procedure using 4-fluorobenzyl-trimethylsilane **3o** (0.1 mmol, 18.2 mg), cinnamaldehyde **1a** (0.3 mmol, 38 µL), aminocatalyst **L** (0.02 mmol, 22 mg), and 200 µL of a 0.2 M acetonitrile solution of trifluoroacetic acid (40 mol%). Time of irradiation: 16 hours. The crude mixture was purified by flash column chromatography (hexane/toluene, gradient from 100% hexane to 100% toluene) to afford the product as a colorless oil (19.3 mg, 80% yield, 85% ee, average of two runs). The enantiomeric excess was determined, after sodium borohydride reduction of the isolated aldehyde to afford the corresponding alcohol, to be 85% by HPLC analysis on a Daicel Chiralpak IC-3 column: 90:10 hexane/IPA, flow rate 0.5 mL/min, λ = 215 nm: τ_{Major} = 16.0 min, τ_{Minor} = 15.1 min. $[\alpha]_D^{26}$ = -46.0 (c = 0.63, $CHCl_3$, 92% ee). Absolute configuration determined in comparison to compound **22a**.

^{1}H NMR (500 MHz, $CDCl_3$): δ 9.63 (t, *J* = 1.9 Hz, 1H), 7.30 – 7.25 (m, 2H), 7.22 – 7.18 (m, 1H), 7.14 – 7.10 (m, 2H), 7.00 – 6.94 (m, 2H), 6.92 – 6.87 (m, 2H), 3.45 (p, *J* = 7.4 Hz, 1H), 2.89 (d, *J* = 7.4 Hz, 2H), 2.83 – 2.71 (m, 2H).

^{13}C NMR (126 MHz, $CDCl_3$): δ 201.6, 162.8, 160.9, 143.2, 135.3, 135.2, 131.0, 130.9, 129.0, 127.9, 127.2, 115.5, 115.3, 49.4, 42.7, 42.4.

HRMS: Calculated for $C_{16}H_{15}FNaO$ 265.0999, found: 265.1000.

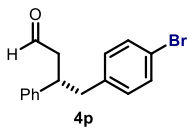

4p

(*S*)-4-(4-bromophenyl)-3-phenylbutanal (4p). Prepared according to the general procedure using 4-bromobenzyl-trimethylsilane **3p** (0.1 mmol, 20.5 µL), cinnamaldehyde **15a** (0.3 mmol, 38 µL), aminocatalyst **L** (0.02 mmol, 22 mg), and 200 µL of a 0.2 M acetonitrile solution of trifluoroacetic acid (40 mol%). Time of irradiation: 16 hours. The crude mixture was purified by flash column chromatography (hexane/toluene, gradient from 100% hexane to 100% toluene, 2 consecutive purifications) to afford the product as a colorless oil (20 mg, 66% yield, 78% ee, average of two runs). The enantiomeric excess was determined to be 78% by HPLC analysis on a Daicel Chiralpak IC-3 column: 95:5 hexane/IPA, flow rate 0.7 mL/min, λ = 215 nm: τ_{Major} = 15.1 min, τ_{Minor} = 13.8 min. $[\alpha]_D^{26}$ = -25.4 (c = 0.43, $CHCl_3$, 78% ee). Absolute configuration determined in comparison to compound **22a**.

^{1}H NMR (500 MHz, $CDCl_3$): δ 9.63 (t, *J* = 1.8 Hz, 1H), 7.35 – 7.31 (m, 2H), 7.30 – 7.24 (m, 2H), 7.23 – 7.18 (m, 1H), 7.13 – 7.09 (m, 2H), 6.90 – 6.86 (m, 2H), 3.44 (p, *J* = 7.4 Hz, 1H), 2.92 – 2.83 (m, 2H), 2.83 – 2.70 (m, 2H).

^{13}C NMR (101 MHz, $CDCl_3$): δ 201.5, 143.0, 138.6, 131.7, 131.3, 129.0, 127.9, 127.2, 120.5, 49.4, 42.9, 42.1.

HRMS: Calculated for $C_{17}H_{19}BrNaO_2$ 357.0461, found: 357.0461.

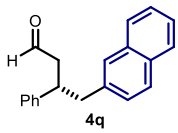

4q

(*S*)-4-(naphthalen-2-yl)-3-phenylbutanal (4q). Prepared according to the general procedure using trimethyl(naphthalen-2-ylmethyl)silane **3q** (0.1 mmol, 21.4 mg), cinnamaldehyde **15a** (0.3 mmol, 38 µL), aminocatalyst **L** (0.02 mmol, 22 mg), and 200 µL of a 0.2 M acetonitrile solution of trifluoroacetic acid (40 mol%). Time of irradiation: 16 hours. The crude mixture (85% conversion of **3q**) was purified by flash column chromatography (hexane/toluene, gradient from 100% hexane to 100% toluene, 2 consecutive purifications) to afford the product as a white solid (21.3 mg, 77% yield, 91% ee, average of two runs). The enantiomeric excess was determined to be 91% by HPLC analysis on a Daicel Chiralpak IC-3 column: 90:10 hexane/IPA, flow rate 0.6 mL/min, λ = 215 nm: τ_{Major} = 16.3 min, τ_{Minor} = 14.9 min. $[\alpha]_D^{26}$ = -78.1(c = 0.61, $CHCl_3$, 91% ee). Absolute configuration determined in comparison to compound **22a**.

^{1}H NMR (400 MHz, $CDCl_3$): δ 9.63 (t, *J* = 1.9 Hz, 1H), 7.83 – 7.78 (m, 1H), 7.77 – 7.71 (m, 2H), 7.56 – 7.50 (m, 1H), 7.50 – 7.41 (m, 2H), 7.33 – 7.28 (m, 2H), 7.25 – 7.18 (m, 4H), 3.63 (apparentp, *J* = 7.4 Hz, 1H), 3.11 (qd, *J* = 13.5, 7.4 Hz, 2H), 2.90 – 2.74 (m, 2H).

^{13}C NMR (101 MHz, $CDCl_3$): δ 201.9, 143.5, 137.1, 133.7, 132.5, 129.0, 128.3, 128.0, 127.0, 127.93, 127.87, 127.82, 127.1, 126.3, 125.8, 49.3, 43.8, 42.2.
HRMS: Calculated for $C_{20}H_{18}NaO$ 297.1250, found: 297.1246.

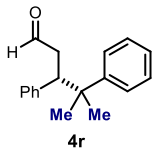

4r

(*S*)-4-methyl-3,4-diphenylpentanal (4r). Prepared according to the general procedure using trimethyl(2-phenylpropan-2-yl)silane **3r** (0.1 mmol, 19.3 mg), cinnamaldehyde **15a** (0.3 mmol, 38 µL), aminocatalyst **L** (0.02 mmol, 22 mg), and 200 µL of a 0.2 M acetonitrile solution of trifluoroacetic acid (40 mol%). Time of irradiation: 16 hours. The crude mixture was purified by flash column chromatography (hexane/diethyl ether 92:8, 2 consecutive purifications) to afford the product as a colorless oil (12.6 mg, 50% yield, 71% ee, average of two runs). The enantiomeric excess was determined to be 71% by HPLC analysis on a Daicel Chiralpak IC-3 column: 90:10 hexane/IPA, flow rate 1.0 mL/min, λ = 215 nm: τ_{Major} = 8.3 min, τ_{Minor} = 12.2 min. $[\alpha]_D^{26}$= -33.0 (c = 0.37, $CHCl_3$, 71% ee). Absolute configuration determined in comparison to compound **22a**.
^{1}H NMR (400 MHz, $CDCl_3$): δ 9.31 (dd, *J* = 2.9, 1.4 Hz, 1H), 7.39 – 7.29 (m, 4H), 7.29 – 7.19 (m, 4H), 7.13 – 7.07 (m, 2H), 3.51 (dd, *J* = 11.2, 4.2 Hz, 1H), 2.79 (ddd, *J* = 16.7, 11.2, 2.9 Hz, 1H), 2.44 (ddd, *J* = 16.7, 4.2, 1.4 Hz, 1H), 1.31 (s, 3H), 1.22 (s, 3H).
^{13}C NMR (101 MHz, $CDCl_3$): δ 202.2, 148.1, 140.4, 130.2, 128.5, 128.2, 127.2, 126.8, 126.5, 51.4, 45.2, 41.4, 29.0, 23.4.
HRMS: Calculated for $C_{18}H_{20}NaO$ 275.1406, found: 275.1398.

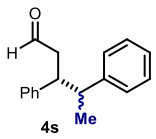

4s

(*3R*)-3,4-diphenylpentanal (4s). Prepared according to the general procedure using trimethyl(1-phenylethyl)silane **3s** (0.1 mmol, 17.8 mg), cinnamaldehyde **15a** (0.3 mmol, 38 µL), aminocatalyst **L** (0.02 mmol, 22 mg), and 200 µL of a 0.2 M acetonitrile solution of trifluoroacetic acid (40 mol%). Time of irradiation: 16 hours. The crude mixture was purified by flash column chromatography (hexane/diethyl ether 92:8, 2 consecutive purifications) to afford the product as a colorless oil (22 mg, 90% yield, 1.2:1 mixture of diastereoisomers, average of two runs). The enantiomeric excess of both diastereoisomers was determined, after sodium borohydride reduction of the isolated aldehyde to afford the corresponding alcohol, to be 92% by HPLC analysis on a Daicel Chiralpak IC-3 column: 97:3 hexane/IPA, flow rate 1.2 mL/min. *Major diastereomer*: λ = 215 nm: τ_{Major} = 24.1 min, τ_{Minor} = 19.9 min. *Minor diastereomer*: λ = 215 nm: τ_{Major} = 17.5 min, τ_{Minor} = 18.6 min. $[\alpha]_D^{26}$= -40.4 (c = 0.42, $CHCl_3$, 1.2:1 dr, 92% ee_{major} / 92% ee_{minor}). Absolute configuration determined in comparison to compound **22a**.
^{1}H NMR$_{major\ diastereomer}$ (400 MHz, $CDCl_3$): δ 9.37 (dd, *J* = 2.5, 1.6 Hz, 1H), 7.39 – 7.32 (m, 2H), 7.29 – 7.13 (m, 6H), 7.04 – 6.98 (m, 2H), 3.33 (td, *J* = 10.2, 4.6 Hz, 1H), 2.92 (dq, *J* = 10.2, 7.0 Hz, 1H), 2.71 – 2.44 (m, 2H), 1.07 (d, *J* = 7.0 Hz, 3H).

^{1}H NMR*minor diastereomer* (400 MHz, $CDCl_3$): δ 9.60 (t, *J* = 2.1 Hz, 1H), 7.39 – 7.32 (m, 2H), 7.29 – 7.13 (m, 6H), 7.04 – 6.98 (m, 2H), 3.49 (q, *J* = 7.3 Hz, 1H), 3.09 (apparent p, *J* = 7.1 Hz, 1H), 2.86 – 2.79 (m, 2H), 1.31 (d, *J* = 7.1 Hz, 3H).
^{13}C NMR*major diastereomer* (101 MHz, $CDCl_3$): δ 201.7, 145.3, 142.8, 128.9, 128.8, 128.3, 127.7, 127.0, 126.9, 49.1, 47.7, 46.2, 20.7.
^{13}C NMR*minor diastereomer* (101 MHz, $CDCl_3$): δ 202.1, 143.9, 141.6, 128.7, 128.22, 128.19, 128.1, 126.7, 126.4, 46.7, 46.3, 45.2, 18.1.
HRMS: Calculated for $C_{17}H_{18}NaO$ 261.1250, found: 261.1252.

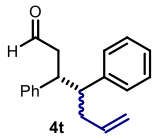

4t

(*R*)-3,4-diphenylhept-6-enal (4t). Prepared according to general procedure using trimethyl-(1-phenylbut-3-en-1-yl)-silane **3t** (0.1 mmol, 20.4 mg), cinnamaldehyde **15a** (0.3 mmol, 38 µL), aminocatalyst **L** (0.02 mmol, 22 mg), and 200 µL of a 0.2 M acetonitrile solution of trifluoroacetic acid (40 mol%). Time of irradiation: 16 hours. The crude mixture was purified by flash column chromatography (hexane/diethyl ether, 92:8, 2 consecutive purifications) to afford the product as a white solid (17.4 mg, 66% yield, 1.5:1 mixture of diastereoisomers). The enantiomeric excess was determined to be 92% for the *major* diastereomer and 90% for the *minor* diastereomer by HPLC analysis on a Daicel Chiralpak IC-3 column: 95:5 hexane/IPA, flow rate 0.5 mL/min, λ = 215 nm. *Major diastereomer*: τ_{Major} =18.5 min, τ_{Minor} = min 23.9. *Minor diastereomer*:: τ_{Major} =15.1 min, τ_{Minor} = min 15.7. $[\alpha]_D^{26}$= -1.7 (c = 0.48, $CHCl_3$, 1.5:1 dr, 92% ee_{major} / 90% ee_{minor}).
^{1}H NMR*major diastereomer* (500 MHz, $CDCl_3$): δ 9.34 (dd, *J* = 2.5, 1.5 Hz, 1H), 7.37 – 7.31 (m, 2H), 7.28 – 7.22 (m, 2H), 7.22 – 7.13 (m, 6H), 5.41 (ddt, *J* = 17.2, 10.3, 7.0 Hz, 1H), 4.81 – 4.67 (m, 2H), 3.40 (td, *J* = 10.3, 4.4 Hz, 1H), 2.89 – 2.82 (m, 1H), 2.59 (ddd, *J* = 16.8, 10.1, 2.5 Hz, 1H), 2.49 – 2.38 (m, 1H), 2.24 – 2.12 (m, 2H).
^{1}H NMR*minor diastereomer* (500 MHz, $CDCl_3$): δ 9.61 (t, *J* = 2.0 Hz, 1H), 7.28 – 7.22 (m, 2H), 7.22 – 7.13 (m, 4H), 6.92 – 6.84 (m, 4H), 5.62 (dddd, *J* = 17.3, 10.2, 7.2, 6.4 Hz, 1H), 5.04 – 4.91 (m, 2H), 3.58 (dt, *J* = 8.9, 6.4 Hz, 1H), 2.99 (dt, *J* = 9.5, 5.9 Hz, 1H), 2.90 – 2.80 (m, 1H), 2.77 (ddd, *J* = 16.8, 8.9, 2.2 Hz, 1H), 2.55 – 2.35 (ddd, *J* = 16.8, 4.4, 1.5 Hz, 2H).
^{13}C NMR*major diastereomer* (126 MHz, $CDCl_3$): δ 201.7, 142.6, 141.0, 136.7, 129.1, 129.0, 128.8, 128.5, 127.3, 127.2, 116.4, 52.3, 49.2, 46.5, 38.7.
^{13}C NMR*minor diastereomer* (126 MHz, $CDCl_3$): δ 202.1, 142.9, 140.8, 137.0, 129.6, 129.3, 128.3, 128.1, 127.0, 126.8, 116.9, 50.8, 47.4, 44.7, 37.3.
HRMS: Calculated for $C_{19}H_{20}NaO$ 287.1411, found: 287.1414.

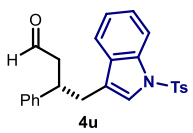

4u

(*S*)-3-phenyl-4-(1-tosyl-1*H*-indol-3-yl)-butanal (4u). Prepared according to the general procedure using 1-tosyl-3-((trimethylsilyl)methyl)-1H-indole **3u** (0.1 mmol, 35.7 mg), cinnamaldehyde **15a** (0.3 mmol, 38 µL), aminocatalyst **L** (0.02 mmol, 22 mg), and 200 µL of a 0.2 M acetonitrile solution of trifluoroacetic acid (40 mol%). Time of irradiation: 56 hours. The crude mixture was purified by flash column chromatography (hexane/acetone, gradient from 95:5 to 85:15) to afford the product as a yellow pale solid (21.9 mg, 52% yield, 94% ee, average of two runs). The enantiomeric excess was determined to be 94% by HPLC analysis on a Daicel Chiralpak IC-3 column: 60:40 hexane/IPA, flow rate 0.8 mL/min, λ = 215 nm: τ_{Major} = 40.5 min, τ_{Minor} = 26.8 min. $[\alpha]_D^{26}$= -13.4 (c =0.49, $CHCl_3$, 94% ee). Absolute configuration determined in comparison to compound **22a**.

^{1}H NMR (500 MHz, $CDCl_3$): δ 9.66 (t, *J* = 1.7 Hz, 1H), 7.92 (dt, *J* = 8.3, 0.9 Hz, 1H), 7.59 – 7.52 (m, 2H), 7.51 – 7.46 (m, 1H), 7.31 – 7.27 (m, 1H), 7.25 – 7.19 (m, 4H), 7.18 – 7.14 (m, 2H), 7.11 – 7.08 (m, 2H), 7.06 (d, *J* = 0.9 Hz, 1H), 3.61 – 3.51 (m, 1H), 3.03 (ddd, *J* = 14.5, 6.4, 1.0 Hz, 1H), 2.95 (ddd, *J* = 14.5, 8.4, 0.9 Hz, 1H), 2.81 (ddd, *J* = 7.2, 1.7, 0.8 Hz, 2H), 2.33 (s, 3H).

^{13}C NMR (126 MHz, $CDCl_3$): δ 201.4, 145.0, 143.3, 135.5, 135.5, 131.2, 130.1, 129.0, 127.7, 127.2, 127.0, 125.0, 124.5, 123.5, 120.4, 119.8, 114.1, 50.0, 40.0, 32.4, 21.9.

HRMS: Calculated for $C_{25}H_{23}NNaO_3S$ 440.1296, found: 440.1281.

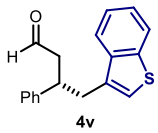

4v

(*S*)-4-(benzo[*b*]thiophen-3-yl)-3-phenylbutanal (4v). Prepared according to the general procedure using (benzo[*b*]thiophen-3-ylmethyl)-trimethylsilane **3v** (0.1 mmol, 35.7 mg), cinnamaldehyde **15a** (0.3 mmol, 38 µL), aminocatalyst **K** (0.02 mmol, 14.5 mg), and 200 µL of a 0.2 M acetonitrile solution of trifluoroacetic acid (40 mol%). Time of irradiation: 48 hours. The crude mixture was purified by flash column chromatography (hexane/toluene, gradient from 100% hexane to 100% toluene) to afford the product as yellow pale oil (15.3 mg, 55% yield, 87% ee, average of two runs). The enantiomeric excess was determined to be 87% by HPLC analysis on a Daicel Chiralpak IC-3 column: 90:10 hexane/IPA, flow rate 0.7 mL/min, λ = 215 nm: τ_{Major} = 13.4 min, τ_{Minor} = 14.6 min. $[\alpha]_D^{26}$= -32.2 (c = 0.49, $CHCl_3$, 87% ee). Absolute configuration determined in comparison to compound **22a**.

^{1}H NMR (400 MHz, $CDCl_3$): δ 9.63 (t, *J* = 1.8 Hz, 1H), 7.82 (dddd, *J* = 17.6, 8.0, 1.3, 0.7 Hz, 2H), 7.43 – 7.32 (m, 2H), 7.32 – 7.26 (m, 2H), 7.24 – 7.16 (m, 3H), 6.88 (d, *J* = 1.0 Hz, 1H), 3.67 (p, *J* = 7.3 Hz, 1H), 3.26 – 3.10 (m, 2H), 2.85 (dd, *J* = 7.2, 1.8 Hz, 2H).

^{13}C NMR (101 MHz, $CDCl_3$): δ 201.6, 143.7, 140.8, 139.2, 134.1, 129.1, 127.7, 127.3, 124.6, 124.4, 123.7, 123.3, 122.0, 49.8, 40.2, 36.3.

HRMS: Calculated for $C_{18}H_{16}NNaOS$ 303.0820, found: 303.0818.

General Procedure for the β-Alkylation of Enals with α-Heteroatom-substituted Organic Silanes 21

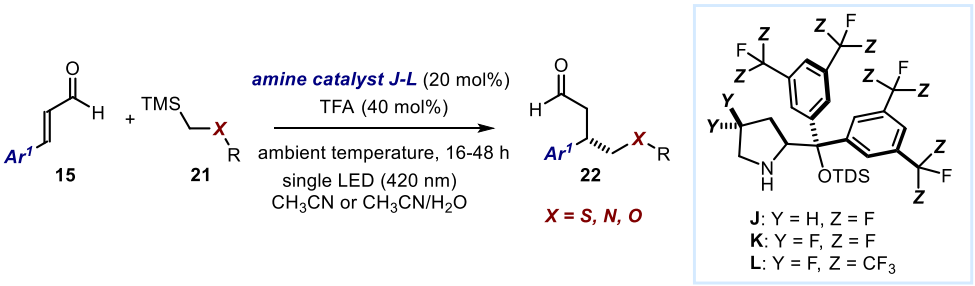

To a 15 mL Schlenk tube containing the amine catalyst **1** (0.02 mmol, 20 mol%), the α-heteroatom-substituted silane derivative **21** (0.1 mmol, 1 Equiv.), and the enal **15** (0.3 mmol, 3 Equiv.), were added the solvent (CH_3CN or CH_3CN/water 3:1, 200 µL) and TFA (0.04 mmol, 3.1 µL). The Schlenk tube was placed under an atmosphere of argon, cooled to – 78 °C, and degassed via vacuum evacuation (5 min), backfilled with argon, and warmed to room temperature. The freeze-pump-thaw cycle was repeated three times, and then the Schlenk tube was sealed with Parafilm and placed into a 3D-printed plastic support mounted on an aluminium block fitted with a 420 nm high-power single LED (λ = 420 nm, irradiance = 41 mW/cm^2, as controlled by an external power supply). This setup secured a reliable irradiation while keeping a distance of 1 cm between the reaction vessel and the light source. The reaction was stirred at ambient temperature for the indicated time (generally 24 hours). The solvent was removed *in vacuo* and the crude mixture was purified by column chromatography on silica gel to give the product **5** in the stated yield and enantiomeric purity. If not otherwise stated, full consumption of the limiting silane substrate (**21**) was observed at the end of the reaction.

Characterization of Products 22

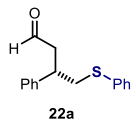

(*S*)-3-phenyl-4-(phenylthio)-butanal (22a). Prepared according to the general procedure using trimethyl-((phenylthio)-methyl)-silane (0.1 mmol, 19.6 mg), cinnamaldehyde (0.3 mmol, 39.6 mg), aminocatalyst **J** (0.02 mmol, 13.4 mg), trifluoroacetic acid (0.04 mmol, 3.1 µL), acetonitrile (150 µL) and water (50 µL). Time of irradiation: 24 hours. The crude mixture (95% conversion of the silane) was purified by flash column chromatography (hexane/toluene, gradient from 100:0 to 0:100, 3 consecutive purifications) to give the product as a yellow oil (18.6 mg, 73% yield, 90% ee, average of two runs). The enantiomeric excess was determined by HPLC analysis on a Daicel Chiralpak IC-3 column, 95:15 hexane/iPrOH, flow rate 0,8 mL/min, λ = 215 nm: τ_{Major} = 15.6 min, τ_{Minor} = 18.7 min, (90% ee); $[\alpha]_D^{26}$= -32.6 (c = 0.54, $CHCl_3$, 90% ee).

Absolute configuration determined by X-ray analysis on a derivative of compound **22a** (see below for details).

^{1}H NMR (500 MHz, $CDCl_3$): δ 9.67 (t, J= 1.8Hz, 1H), 7.35-7.27 (m, 6H), 7.26-7.18 (m, 4H), 3.46 (tt J=8.4, 6.1 Hz, 1H), 3,26(dd, J=13.3, 6.3 Hz, 1H), 3.13 (dd, J=13.3, 8.4 Hz, 1H), 3.08 (ddd, J=17.1, 5.9, 1.6 Hz, 1H), 2.82 (ddd, J= 17.1, 8.4, 2 Hz, 1H).

^{13}C NMR (126 MHz, $CDCl_3$): δ 200.9, 142.4, 135.8, 129.7, 129.2, 129.0, 127.6, 127.4, 126.5, 48.8, 40.6, 39.6.

HRMS: calculated for $C_{16}H_{16}NaOS$ ($M+Na^+$): 279.0814, found: 279.0807.

Product manipulation: product **22a** was converted into derivative **22a'** upon $NaBH_4$ reduction and esterification with pyrene carbonyl chloride. **22a** was dissolved in methanol and stirred at 0 ºC. Sodium borohydride (5 Equiv.) was added and the reaction mixture was allowed to reach ambient temperature and stirred for 3 hours. Solvent was removed under reduced pressure and the crude mixture was filtered on a silica plug (EtOAc). The crude mixture was directly charged on a vial and dissolved in anhydrous CH_2Cl_2. Pyrene carbonyl chloride (1.5 Equiv.), DMAP (0.2 Equiv.) and triethylamine (1.5 Equiv.) were added to the stirred solution at 0 ºC. After 10 minutes, the reaction was allowed to reach ambient temperature and stirring was continued overnight. Then, the solvent was removed under reduced pressure and the crude mixture was purified by column chromatography (hexane/EtOAc, gradient from 100:0 to 95:5).

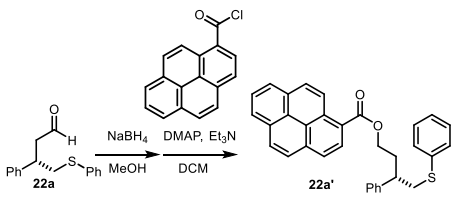

^{1}H NMR (400 MHz, $CDCl_3$): δ 9.24 (d, *J* = 9.4 Hz, 1H), 8.43 (d, *J* = 8.1 Hz, 1H), 8.29 – 8.25 (m, 2H), 8.20 (dd, *J* = 9.2, 4.7 Hz, 2H), 8.14 – 8.03 (m, 3H), 7.44 – 7.03 (m, 10H), 4.45 (ddd, *J* = 11.5, 6.6, 5.3 Hz, 1H), 4.28 (ddd, *J* = 11.0, 8.1, 6.0 Hz, 1H), 3.35 – 3.24 (m, 2H), 3.15 (m, 1H), 2.63 (m, 1H), 2.21 (m, 1H).

Crystals of derivative **22a'**, suitable for X-ray diffraction analysis, were obtained upon slow evaporation of a hexane solution.

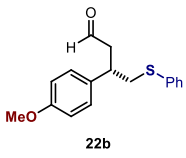

(*S*)-3-(4-methoxyphenyl)-4-(phenylthio)-butanal (22b). Prepared according to the general procedure using trimethyl-((phenylthio)-methyl)-silane (0.1 mmol, 19.6 mg), 4-methoxycinnamaldehyde, (0.3 mmol, 48.7 mg), aminocatalyst **K** (0.02 mmol, 14.1 mg), trifluoroacetic acid (0.04 mmol, 3.1 µL), acetonitrile (150 µL) and water (50 µL). Time of irradiation: 24 hours. The crude mixture was purified by flash column chromatography (toluene, 2 consecutive purifications) to give the product as a yellow oil (23.2 mg, 81% yield, 79% ee, average of two runs). The enantiomeric excess was determined by HPLC analysis on

a Daicel Chiralpak IA-3 column, 95:5 hexane/IPA, flow rate 0.8 mL/min, λ = 215 nm: τ_{Major} = 27.9 min, τ_{Minor} = 32.3 min (79% ee); $[\alpha]_D^{26}$= -43.9. (c = 0.78, $CHCl_3$, 79% ee). Absolute configuration determined in comparison to compound **22a**.

^{1}H NMR (400 MHz, $CDCl_3$): δ 9.65 (t, *J* = 2.1, 1.5 Hz, 1H), 7.35 – 7.26 (m, 4H), 7.23 – 7.17 (m, 1H), 7.15 – 7.08 (m, 2H), 6.88 – 6.82 (m, 2H), 3.79 (s, 3H), 3.41 (tt, *J* = 8.4, 6.1 Hz, 1H), 3.22 (dd, *J* = 13.2, 6.4 Hz, 1H), 3.11 (dd, *J* = 13.2, 8.3 Hz, 1H), 3.04 (ddd, *J* = 17.0, 5.9, 1.6 Hz, 1H), 2.78 (ddd, *J* = 17.0, 8.6, 2.1 Hz, 1H).

^{13}C NMR (101 MHz, $CDCl_3$): δ 201.1, 158.8, 136.0, 134.3, 129.7, 129.2, 128.5, 126.5, 114.4, 55.4, 49.0, 40.8, 38.9.

HRMS: calculated for $C_{17}H_{18}NaO_2S$ ($M+Na^+$): 309.0920, found: 309.0914.

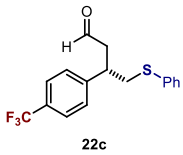

22c

(*S*)-4-(phenylthio)-3-(4-(trifluoromethyl)-phenyl)-butanal (22c). Prepared according to the general procedure using trimethyl-((phenylthio)-methyl)-silane (0.1 mmol, 19.6 mg), 4-trifluoromethylcinnamaldehyde, (0.3 mmol, 60.0 mg), aminocatalyst **K** (0.02 mmol, 14.1 mg), trifluoroacetic acid (0.04 mmol, 3.1 µL), acetonitrile (150 µL) and water (50 µL). Time of irradiation: 48 hours. The crude mixture (67% conversion of the silane) was purified by flash column chromatography (toluene/hexane 4:1, 3 consecutive purifications) to give the product as a yellow oil (13.8 mg, 43% yield, 81% ee, average of two runs). The enantiomeric excess was determined by HPLC analysis on a Daicel Chiralpak IC column, 99:1 hexane/iPrOH, flow rate 0.8 mL/min, λ = 215 nm:, τ_{Major} = 13.3 min, τ_{Minor} = 15.3 min (81% ee); $[\alpha]_D^{26}$= -3.98 (c = 0.32, $CHCl_3$, 81% ee). Absolute configuration determined in comparison to compound **22a**.

^{1}H NMR (400 MHz, $CDCl_3$): δ 9.68 (t, *J* = 1.4 Hz, 1H), 7.57 – 7.54 (m, 2H), 7.34 – 7.26 (m, 7H), 7.25 – 7.17 (m, 1H), 3.53 (m, *J* = 7.9, 6.2 Hz, 1H), 3.26 – 3.14 (m, 2H), 3.14 (ddd, J=17.6, 6.0, 1.6 Hz, 1H), 2.85 (ddd, *J* = 17.6, 8.2, 1.6 Hz, 1H).

^{13}C NMR (101 MHz, $CDCl_3$): δ 200.0, 146.4, 135.4, 130.0, 129.7(q), 129.3, 128.1, 126.8, 125.9(q), , 124.2(q), 48.7, 40.3, 39.4.

HRMS: calculated for $C_{17}H_{16}F_3OS$ ($M+H^+$): 325.0868 found: 325.0873.

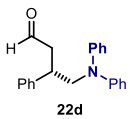

22d

(*S*)-4-(diphenylamino)-3-phenylbutanal (22d). Prepared according to the general procedure using *N*-phenyl-*N*-((trimethylsilyl)-methyl)-aniline (0.1 mmol, 25.5 mg), cinnamaldehyde (0.3 mmol, 39.6 mg), aminocatalyst **J** (0.02 mmol, 13.4 mg), trifluoroacetic acid (0.04 mmol, 3.1 µL), acetonitrile (150 µL) and water (50 µL). Time of irradiation: 24 hours. The crude mixture was purified by flash column chromatography (hexane/toluene, gradient from 100:0 to 0:100, 3 consecutive purifications) to give the product as a yellow oil (18.3 mg, 58% yield, 75% ee, average of two runs). The enantiomeric excess was determined, after sodium borohydride reduction of the

isolated aldehyde to afford the corresponding alcohol, to be 75% by UPC^2 analysis on a Daicel Chiralpak IC-3 column: gradient from 100% CO_2 to 60:40 CO_2/acetonitrile over 4 minutes, curve 6), flow rate 3 mL/min, λ = 294 nm: τ_{Minor} = 3.43 min, τ_{Major} = 3.57 min (75% ee); $[\alpha]_D^{26}$= -39.9 (c = 0.31, $CHCl_3$, 75% ee). Absolute configuration determined in comparison to compound **22a**.

^{1}H NMR (400 MHz, $CDCl_3$): δ 9.62 (t, *J* = 2.0 Hz, 1H), 7.36 – 7.15 (m, 9H), 7.00 – 6.93 (m, 2H), 6.88 (dt, *J* = 7.8, 1.1 Hz, 4H), 3.94 (dd, *J* = 14.6, 8.3 Hz, 1H), 3.86 (dd, *J* = 14.6, 6.7 Hz, 1H), 3.74 (tt, *J* = 8.3, 6.6 Hz, 1H), 2.95 (ddd, *J* = 16.9, 6.4, 1.9 Hz, 1H), 2.83 (ddd, *J* = 16.9, 8.2, 2.0 Hz, 1H). ^{13}C NMR (101 MHz, $CDCl_3$): δ 201.3, 148.5, 141.6, 129.5, 128.9, 127.9, 127.3, 121.9, 121.5, 58.9, 47.7, 38.7.

HRMS: calculated for $C_{22}H_{22}NO$ (M+H): 316.1696, found: 316.1695.

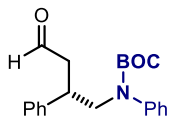

22e

(*S*)-*tert*-butyl-(4-oxo-2-phenylbutyl)-(phenyl)-carbamate (22e). Prepared according to the general procedure using *tert*-butyl 2-phenyl-3-(trimethylsilyl)propanoate (0.1 mmol, 27.9 mg), cinnamaldehyde (0.3 mmol, 39.6 mg), aminocatalyst **L** (0.02 mmol, 22.1 mg), trifluoroacetic acid (0.04 mmol, 3.1 µL), and acetonitrile (200 µL). Time of irradiation: 24 hours The crude mixture (77% conversion of the silane) was purified by flash column chromatography (EtOAc:hex 10:90) to give the product as a yellow oil (21.3 mg, 63% yield, 71% ee, average of two runs). The enantiomeric excess was determined, after sodium borohydride reduction of the isolated aldehyde to afford the corresponding alcohol, to be 71% by UPC^2 analysis on a Daicel Chiralpak IC-3 column with a gradient (100% CO_2 to 60:40 CO_2/IPA over 4 minutes, curve 6), flow rate 3 mL/min, , λ = 215 nm: τ_{Minor} = 3.40 min, τ_{Major} = 3.55 min (71% ee); $[\alpha]_D^{26}$= -18.1 (c = 0.87, $CHCl_3$, 71% ee). Absolute configuration determined in comparison to compound **22a**.

^{1}H NMR (400 MHz, $CDCl_3$): δ 9.63 (t, *J* = 1.9 Hz, 1H), 7.32 – 7.24 (m, 4H), 7.25 – 7.08 (m, 4H), 6.99 (d, *J* = 7.8 Hz, 2H), 4.01 (dd, *J* = 14.0, 7.9 Hz, 1H), 3.82 (dd, *J* = 14.0, 7.6 Hz, 1H), 3.51 (qd, *J* = 7.9, 6.3 Hz, 1H), 2.91 – 2.61 (m, 2H), 1.37 (s, 9H).

^{13}C NMR (101 MHz, $CDCl_3$): δ 201.2, 154.9, 142.2, 141.1, 128.9, 128.8, 128.1, 127.2, 127.2, 126.3, 80.6, 54.9, 47.5, 39.1, 28.4.

HRMS: calculated for $C_{21}H_{25}NNaO_3$ ($M+Na^+$): 362.1727, found: 362.1721.

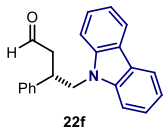

22f

(*S*)-4-(9*H*-carbazol-9-yl)-3-phenylbutanal (22f). Prepared according to the general procedure using 9-((trimethylsilyl)-methyl)-9*H*-carbazole (0.1 mmol, 25.4 mg), cinnamaldehyde (0.3 mmol, 39.6 mg), aminocatalyst **L** (0.02 mmol, 22.1 mg), trifluoroacetic acid (0.04 mmol, 3.1 µL) and acetonitrile (200 µL). Time of irradiation: 16 hours. The crude mixture was purified by flash column chromatography (hexane/Et_2O 92:8) to give the product as a yellow oil (25.6 mg, 82%

yield, 81% ee, average of two runs). The enantiomeric excess was determined by HPLC analysis on a Daicel Chiralpak IC column, 95:5 hexane:iPrOH, flow rate 0.8 mL/min, λ = 215 nm: τ_{Major} = 11.4 min, τ_{Minor} = 22.5 min, (81% ee); $[\alpha]_D^{26}$= -13.8 (c = 0.85, $CHCl_3$, 81% ee). Absolute configuration determined in comparison to compound **22a**.

^{1}H NMR (400 MHz, $CDCl_3$): δ 9.57 (dd, *J* = 1.9, 1.1 Hz, 1H), 8.14 – 8.05 (m, 2H), 7.47 – 7.36 (m, 2H), 7.34 (d, *J* = 0.8 Hz, 1H), 7.32 (d, *J* = 0.9 Hz, 1H), 7.30 – 7.17 (m, 7H), 4.53 (dd, *J* = 14.7, 8.2 Hz, 1H), 4.39 (dd, *J* = 14.7, 6.8 Hz, 1H), 3.98 (tt, *J* = 8.1, 6.6 Hz, 1H), 2.97 (ddd, *J* = 17.5, 8.1, 1.9 Hz, 1H), 2.82 (ddd, *J* = 17.5, 6.5, 1.1 Hz, 1H).

^{13}C NMR (101 MHz, $CDCl_3$): δ 200.4, 140.9, 140.6, 129.1, 127.7, 127.6, 125.9, 123.0, 120.5, 119.3, 108.9, 49.4, 46.9, 39.74.

HRMS: calculated for $C_{22}H_{19}NNaO$ ($M+Na^+$): 336.1359, found: 336.1367.

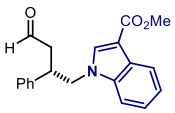

22g

(*S*)-methyl-1-(4-oxo-2-phenylbutyl)-1*H*-indole-3-carboxylate (22g). Prepared according to the general procedure using methyl 1-((trimethylsilyl)-methyl)-1*H*-indole-3-carboxylate (0.1 mmol, 26.1 mg), cinnamaldehyde (0.3 mmol, 39.6 mg), aminocatalyst **J** (0.02 mmol, 13.4 mg), trifluoroacetic acid (0.04 mmol, 3.1 µL), acetonitrile (150 µL) and water (50 µL). Time of irradiation: 48 hours. The crude mixture was purified by flash column chromatography (hexane/EtOAc 60:40) to give the product as a yellow oil (20.4 mg, 64% yield, 92% ee, average of two runs). The enantiomeric excess was determined by HPLC analysis on a Daicel Chiralpak IC-3 column, 60:40 hexane:iPrOH, flow rate 0.8 mL/min, λ = 215 nm: τ_{Minor} = 19.7 min, τ_{Major} = 27.3 min (92% ee); $[\alpha]_D^{26}$= -59.3 (c = 0.66, $CHCl_3$, 92% ee). Absolute configuration determined in comparison to compound **22a**.

^{1}H NMR (400 MHz, $CDCl_3$): δ 9.72 (t, *J* = 1.2 Hz, 1H), 8.17 (ddd, *J* = 6.2, 2.2, 0.8 Hz, 1H), 7.54 – 7.42 (m, 2H), 7.36 – 7.21 (m, 5H), 7.15 – 6.99 (m, 2H), 4.47 (dd, *J* = 14.1, 6.7 Hz, 1H), 4.23 (dd, *J* = 14.1, 8.0 Hz, 1H), 3.89 (s, 3H), 3.84 (q, *J* = 7.3 Hz, 1H), 2.95 (ddd, *J* = 17.9, 6.9, 1.4 Hz, 1H), 2.85 (ddd, *J* = 18.1, 7.4, 1.0 Hz, 1H).

^{13}C NMR (101 MHz, $CDCl_3$): δ 199.9, 165.5, 140.1, 136.6, 134.7, 129.2, 127.9, 127.5, 126.7, 123.1, 122.1, 121.9, 107.4, 52.7, 51.1, 46.8, 40.1.

HRMS: calculated for $C_{20}H_{20}NO_3$ ($M+H^+$): 322.14.38, found 322.1435.

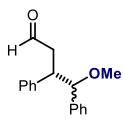

22h

(*S*)-4-methoxy-3,4-diphenylbutanalone (22h). Prepared according to the general procedure using (methoxy-(phenyl)-methyl)-trimethylsilane (0.1 mmol, 19.4 mg), cinnamaldehyde (0.3 mmol, 39.6 mg), aminocatalyst **K** (0.02 mmol, 14.1 mg), trifluoroacetic acid (0.04 mmol, 3.1 µL) acetonitrile (200 µL). Time of irradiation: 24 hours. The crude mixture (95% conversion of the silane; 37% of benzaldehyde was identified as a side product) was purified by flash column chromatography

(hexane/toluene, gradient from 100:0 to 0:100, 3 consecutive purifications) to give the product as a yellow oil (14.2 mg, 56% yield, 1.9:1 mixture of diastereoisomers, 68% ee_{major}, 61% ee_{minor}, average of two runs). The enantiomeric excess was determined by HPLC analysis on a Daicel Chiralpak IC column, 99:1 hexane:iPrOH, flow rate 0.8 mL/min, λ = 215 nm. *Minor diastereoisomer*: τ_{Major} = 12.8 min, τ_{Minor} = 15.2 min (61% ee); *major diastereoisomer*: τ_{Major} = 16.4 min, τ_{Minor} = 18.7 min (68% ee); $[\alpha]_D^{26}$= -13.3 (c = 0.48, $CHCl_3$, 68% ee_{major}, 61% ee_{minor}, 1.9:1 dr).

^{1}H NMR (400 MHz, $CDCl_3$): *Major diastereoisomer*: δ 9.70 (dd, *J* = 2.8, 1.6 Hz, 1H), 7.28 – 7.11 (m, 7H), 7.09 – 6.97 (m, 3H), 4.18 (d, *J* = 8.3 Hz, 1H), 3.49 (q, *J* = 7.4 Hz, 1H), 3.18 (s, 3H), 3.05 (ddd, *J* = 16.4, 7.3, 2.9 Hz, 1H), 2.79 (ddd, *J* = 16.5, 7.0, 1.7 Hz, 1H). M*inor diastereoisomer*: δ 9.56 (t, *J* = 2.0 Hz, 1H), 7.30 – 7.17 (m, 6H), 7.09 – 7.03 (m, 4H), 4.36 (d, *J* = 6.3 Hz, 1H), 3.61 (dt, *J* = 8.4, 6.3 Hz, 1H), 3.16 (s, 3H), 2.77 (ddd, *J* = 17.0, 6.4, 2.0 Hz, 1H), 2.68 (ddd, *J* = 17.0, 8.4, 2.0 Hz, 1H).

^{13}C NMR (101 MHz, $CDCl_3$): *Major diastereoisomer*: δ 201.5, 140.7, 139.7, 128.9, 128.5, 128.4, 128.2, 127.4, 126.9, 88.1, 57.0, 48.5, 46.9. *Minor diastereoisomer*: δ 201.4, 140.2, 139., 128.3, 128.2, 128.0, 127.8, 127.7, 127.0, 86.9, 57.3, 46.8, 45.9.

HRMS calculated for $C_{18}H_{22}NaO_3$ ($M+MeOH+Na^+$): 309.1461, found: 309.1461.

Synthesys and Characterization of the Iminium Ion II

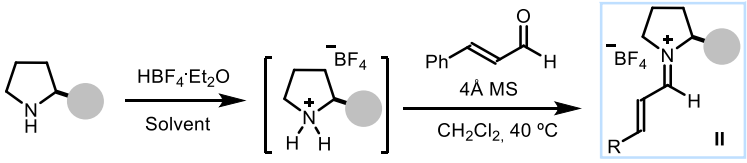

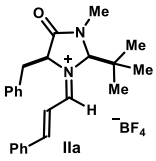

(2*R*,5*S*,*E*)-5-benzyl-2-(*tert*-butyl)-3-methyl-4-oxo-1-((*E*)-3-phenylallylidene)imidazolidin-1-ium (IIa). The chiral amine catalyst **A** (185 mg, 0.75 mmol) was converted into the corresponding tetrafluoroborate salt by treatment with tetrafluoroboric acid diethyl ether complex (125 µL, 0.9 mmol, 1.2 Equiv.) in anhydrous diethyl ether (10 mL). The tetrafluoroborate salt was isolated by filtration under nitrogen flow to yield a hygroscopic white powder, which was dried under high vacuum for one hour. Part of the obtained salt (100 mg, 0.30 mmol, 1 Equiv.) was placed in an oven-dried, argon purged Schlenk tube containing 4Å molecular sieves pellets (50 mg). Anhydrous CH_2Cl_2 (2 mL) was added followed by cinnamaldehyde **15a** (46 µL, 0.36 mmol, 1.2 Equiv.). The mixture was heated to 40 ºC for 4 hours. Then, the bright yellow solution was transferred dropwise into an oven-dried, argon purged 50 mL Schlenk tube containing 30 mL of anhydrous diethyl ether, resulting in the formation of a bright yellow precipitate. The suspension was sonicated for two minutes and

the iminium ion **IIa** (94 mg, 0.21 mmol, 53% yield) was collected by filtration under argon, washed with anhydrous diethyl ether and dried under high vacuum. The salt was stable when stored under an argon atmosphere at 5 ºC.

^{1}H NMR (400 MHz, CD_3CN): δ 8.53 (dd, *J* = 10.9, 1.3 Hz, 1H), 8.07 (d, *J* = 15.0 Hz, 1H), 7.72 – 7.65 (m, 1H), 7.59 – 7.35 (m, 8H), 7.32 – 7.27 (m, 1H), 6.27 (dd, *J* = 15.0, 10.9 Hz, 1H), 5.30 (d, *J* = 0.9 Hz, 1H), 4.89 (dd, *J* = 8.9, 4.7 Hz, 1H), 3.58 (dd, *J* = 14.9, 4.8 Hz, 1H), 3.27 (dd, *J* = 14.9, 9.0 Hz, 1H), 3.14 – 3.09 (m, 3H), 1.27 (s, 9H).

^{13}C NMR (101 MHz, CD_3CN): δ 173.1 ($C=N^+$), 168.1 (C=O), 167.3 (PhCH), 137.1 (Ph), 136.3 (Ph), 134.1 (Ph), 132.3 (Ph), 130.8 (Ph), 130.53 (Ph), 130.46(Ph), 129.2(Ph), 117.9 (PhC=CH), 91,2 (CH-*t*Bu), 65.7 (CH-Bn), 38.4 ($PhCH_2$), 32.6 (NMe), 26.9 (tBu), 25.0 ($C(Me)_3$).

HRMS: Calculated for $C_{24}H_{29}N_2O$ 361.2274, found 361.2275.

UV-VIS: λ_{max} = 362 nm.

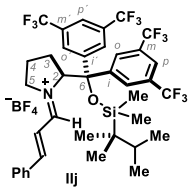

IIj

(*S*,*E*)-2-(bis-(3,5-bis-(trifluoromethyl)-phenyl)-(((2,3-dimethylbutan-2-yl)-dimethylsilyl)-oxy)-methyl)-1-((*E*)-3-phenylallylidene)-pyrrolidin-1-ium tetrafluoroborate salt (IIJ). The chiral amine catalyst **J** (500 mg, 0.75 mmol) was converted into the corresponding tetrafluoroborate salt by treatment with tetrafluoroboric acid diethyl ether complex (125 μL, 0.9 mmol, 1.2 Equiv.) in anhydrous hexane (10 mL). The tetrafluoroborate salt was isolated by filtration under nitrogen flow to yield a hygroscopic white powder, which was dried under high vacuum for one hour. Part of the obtained salt (300 mg, 0.397 mmol, 1 Equiv.) was placed in oven-dried, argon purged Schlenk tube containing 4Å molecular sieves pellets (50 mg). Anhydrous CH_2Cl_2 (2 mL) was added followed by cinnamaldehyde **15a** (53 μL, 0.417 mmol, 1.05 Equiv.). The mixture was heated to 40 ºC for 4 hours. Then, the bright yellow solution was transferred dropwise into an oven-dried, argon purged 50 mL Schlenk tube containing 30 mL of anhydrous hexane, resulting in the formation of a yellowish precipitate. The suspension was sonicated for two minutes and the iminium ion **IIj** (124 mg, 0.16 mmol, 40% yield) was collected by filtration under argon, washed with anhydrous hexane and dried under high vacuum. The salt was stable when stored under an argon atmosphere at 5 ºC.

^{1}H NMR (400 MHz, CD_3CN): δ 8.65 (d, *J* = 10.7 Hz, 1H), 8.20 (ddt, *J* = 7.6, 1.7, 0.8 Hz, 2H), 8.03 (d, *J* = 15.0 Hz, 3H), 7.98 – 7.96 (m, 2H), 7.92 – 7.86 (m, 2H), 7.73 – 7.66 (m, 1H), 7.63 – 7.56 (m, 2H), 7.12 (dd, *J* = 15.0, 10.7 Hz, 1H), 5.57 (dd, *J* = 9.7, 4.5 Hz, 1H), 4.01 – 3.86 (m, 1H), 2.58 (dtd, *J* = 14.5, 9.7, 6.4 Hz, 1H), 2.36 (dt, *J* = 15.6, 8.7 Hz, 1H), 2.19 – 2.06 (m, 1H), 2.01 – 1.88 (m, 1H), 1.76 (p, *J* = 6.8 Hz, 1H), 1.47 – 1.34 (m, 1H), 0.95 – 0.82 (m, 12H), -0.26 (s, 3H), -0.31 (s, 3H).

^{13}C NMR (101 MHz, CD_3CN): δ 169.2 (*C*H=N$^+$), 164.5 (Ph-*C*H), 142.8 (*ipso*), 142.3 (*ipso*'), 135.8 (Ph),134.4 (Ph), 133.0 (2C, q, J_{CF} = 33.0 Hz, *meta*), 132.6 (2C, q, J_{CF} = 33.4 Hz, *meta'*), 131.8 (Ph), 130.8 (Ph,), 130.4 (m, 4C, *ortho*+*ortho´*), 124,9 (1C, m, *para*), 124.7 (1C, m, *para´*), 124.2 (2C, q J_{CF} = 271 Hz, Ar*C*F$_3$), 124.1 (2C, q, J_{CF} = 271 Hz, Ar*C*F$_3$), 84.5 (C6), 77.2 (C2), 54.5 (*C5*), 34.2(SiC*C*H), 27.1 (*C3*), 23.23 (*C4*), 20.85 (SiC*C*H$_3$), 20.0 (SiC*C*H$_3$'), 19.1 (SiCCH*C*H$_3$), 18.6 (SiCCH*C*H$_3$´), -0.2 (Si*C*H$_3$), -0.3 (Si*C*H$_3$');
^{19}F NMR: (376 MHz, CD_3CN) δ -63.49 (6F), - 43.63 (6F), -151.9 (BF_4)
HRMS: Calculated for $C_{38}H_{40}F_{12}NOSi$ 782.2682, found 782.2676.
UV-VIS: λ_{max} = 350 nm.

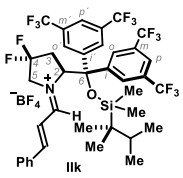

IIk

(*S*,*E*)-2-(bis-(3,5-bis-(trifluoromethyl)-phenyl)-(((2,3-dimethylbutan-2-yl)-dimethylsilyl)-oxy)-methyl)-1-((*E*)-3-phenylallylidene)-pyrrolidin-1-ium tetrafluoroborate salt (IIk). The chiral amine catalyst **K** (500 mg, 0.71 mmol) was converted into the corresponding tetrafluoroborate salt by treatment with tetrafluoroboric acid diethyl ether complex (120 µL, 0.85 mmol, 1.2 Equiv.) in anhydrous hexane (10 mL). The tetrafluoroborate salt was isolated by filtration under nitrogen flow to yield a hygroscopic white powder, which was dried under high vacuum for one hour. Part of the obtained salt (200 mg, 0.25 mmol, 1 Equiv.) was placed in oven-dried, argon purged Schlenk tube containing 4Å molecular sieves pellets (50 mg). Anhydrous CH_2Cl_2 (2 mL) was added followed by cinnamaldehyde **15a** (41 µL, 0.33 mmol, 1.3 Equiv.). The mixture was heated to 40 ºC for 4 hours. Then, the bright yellow solution was transferred dropwise into an oven-dried, argon purged 50 mL Schlenk tube containing 30 mL of anhydrous hexane, resulting in the formation of a yellow precipitate. The suspension was sonicated for two minutes and the iminium ion **IIk** (124 mg, 0.16 mmol, 40% yield) was collected by filtration under argon, washed with anhydrous hexane and dried under high vacuum. The salt was stable when stored under an argon atmosphere at 5 ºC.
^{1}H NMR (500 MHz, CD_3CN): δ 8.68 (d, *J* = 10.8 Hz, 1H), 8.24 (s, 2H), 8.20 (d, *J* = 15.0 Hz, 1H), 8.01 (apparent d, *J* = 5.4 Hz, 4H), 7.95 – 7.90 (m, 2H), 7.79 – 7.73 (m, 1H), 7.64 (t, *J* = 7.7 Hz, 2H), 7.08 (dd, *J* = 15.0, 10.8 Hz, 1H), 5.86 (dd, *J* = 10.6, 4.9 Hz, 1H), 4.41 (t, *J* = 15.4 Hz, 1H), 3.28 (dddd, *J* = 21.9, 16.6, 10.4, 5.7 Hz, 1H), 2.81 (qd, *J* = 15.7, 5.1 Hz, 1H), 2.44 (td, *J* = 18.1, 8.9 Hz, 1H), 1.76 (p, *J* = 6.8 Hz, 1H), 0.94 – 0.83 (m, 12H), -0.25 (s, 3H), -0.30 (s, 3H).
^{13}C NMR (126 MHz, $CDCl_3$): δ 171,6 (*C*H=N$^+$), 168.1 (Ph-*C*H), 141.7 (*ipso*), 141.0 (*ipso*'), 137.0 (Ph),134.3 (Ph), 133.3 (2C, q, J_{CF} = 33.8 Hz, *meta*), 133.0 (2C, q, J_{CF} = 34.2 Hz, *meta'*), 132.6 (Ph), 131.9 (2C, apparent d, J=1.8 Hz, *ortho*), 130.9 (Ph), 130,2 (2C, apparent d, J_{CF} = 2.6 Hz, *ortho*'), 126.14 (dd, J_{CF} = 254.0 Hz, 246.9 Hz, *C4*), 124.14 (2C, q, J_{CF} = 273 Hz, Ar*C*F$_3$), 124.13 (2C, q, J_{CF} = 274 Hz, Ar'*C*F$_3$), 125.3 (2C, m, *para*, *para´*), 84.6 (*C6*), 76.0 (apparent s, *C2*), 60.0 (dd, J_{CF} = 37.2, 34.1 Hz, *C3*), 37.5 (dd, J_{CF} = 28.0, 25.0 Hz, *C5*), 34.2

(SiCCH), 26.5 (SiCCH), 20.9 (SiCCH$_3$), 20.0 (SiCCH$_3$'), 19.1 (SiCCHCH$_3$), 18.7 (SiCCHCH$_3$´), -0.2 (SiCH$_3$), -0.3 (SiCH$_3$').

^{19}F NMR (376 MHz, CD_3CN): δ -63.41 (6F), -63.47 (6F), -87.72 (d, *J* = 237.5 Hz), -97.67 (d, *J* = 237.5 Hz), -151.7.

HRMS: Calculated for $C_{36}H_{36}F_{14}N_4Si$: 818.2480, found 818.2482.

UV-VIS: λ_{max} = 363 nm.

The structure of the iminium ion **IIk** was confirmed by X-ray analysis.

Quantum Yield Measurement

A ferrioxalate actinometer solution was prepared by following the Hammond variation of the Hatchard and Parker procedure outlined in the *Handbook of Photochemistry*[47]. The ferrioxalate actinometer solution measures the decomposition of ferric ions to ferrous ions, which are complexed by 1,10-phenanthroline and monitored by UV/Vis absorbance at 510 nm. The moles of iron-phenanthroline complex formed are related to moles of photons absorbed.

The following solutions were prepared and stored in a dark laboratory (red light):

1. Potassium ferrioxalate solution: 294.8 mg of potassium ferrioxalate (commercially available from Alfa Aesar) and 139 μL of sulfuric acid (96%) were added to a 50 mL volumetric flask, and filled to the mark with water (HPLC grade).
2. Phenanthroline solution: 0.2% by weight of 1,10-phenanthroline in water (100 mg in 50 mL volumetric flask).
3. Buffer solution: 2.47 g of NaOAc and 0.5 mL of sulfuric acid (96%) were added to a 50 mL volumetric flask, and filled to the mark with water (HPLC grade).
4. Model reaction solution: benzyl silane **3a** (2.5 mmol), cinnamaldehyde **15a** (7.5 mmol), amine catalyst **K** (0.5 mmol), and trifluoroacetic acid (1 mmol) were sequentially added to a 5 mL volumetric flask and filled to the mark with acetonitrile (HPLC grade).

The actinometry measurements were done as follows:

1. 1 mL of the actinometer solution and 1 mL of the model reaction (β-alkylation of **15a** with **3a** catalyzed by amine **K**) were added to two identical Schlenk tubes (*diameter* = 12 mm). The Schlenk tubes were placed 10 cm away from the light source. They were irradiated together with a 300 W Xenon Lamp operating at 100% of light intensity with a high transmittance bandpass filter of 400 ± 5 nm without stirring. This procedure was repeated 4 times, quenching the two reactions after different time intervals: 45 sec, 60 sec, 75 sec, and 90 sec for the actinometry solution; 30 min, 60 min, 90 min, and 120 min for the model reaction.

[47] Murov, S. L. Ed. *Handbook of Photochemistry* (Marcel Dekker, New York, 1973).

2. After irradiation, the actinometer solution was removed and placed in a 10 mL volumetric flask containing 0.5 mL of 1,10-phenanthroline solution and 2 mL of buffer solution. This flask was filled to the mark with water (HPLC grade).
3. The UV-Vis spectra of the complexed actinometer samples were recorded for each time interval. The absorbance of the complexed actinometer solution was monitored at 510 nm.

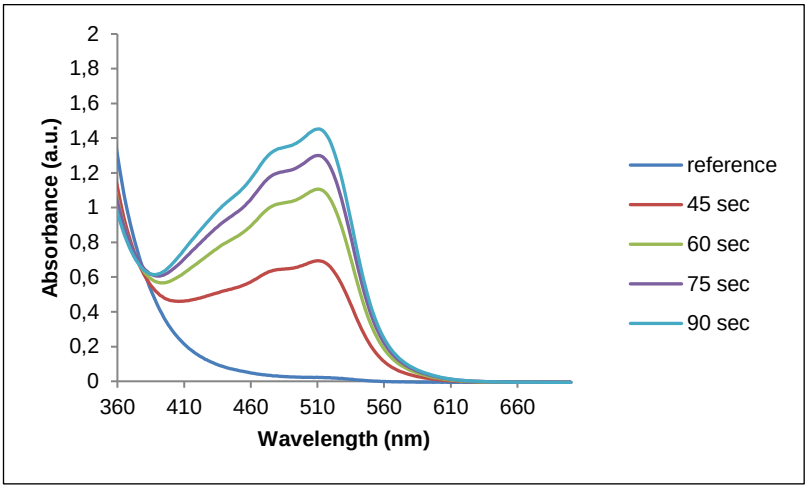

The moles of Fe^{2+} formed for each sample is determined using Beers' Law (Eq. 3.3):

$$\text{Mols of Fe(II)} = \frac{V_1 \times V_3 \times \Delta A(510\text{ nm})}{10^3 \times V_2 \times l \times \varepsilon(510\ nm)} \quad \text{(Eq. 3.3)}$$

where V_1 is the irradiated volume (1 mL), V_2 is the aliquot of the irradiated solution taken for the determination of the ferrous ions (1 mL), V_3 is the final volume after complexation with phenanthroline (10 mL), l is the optical path-length of the irradiation cell (1 cm), $\Delta A(510\text{ nm})$ is the optical difference in absorbance between the irradiated solution and the one stored in the dark, $\varepsilon(510\text{ nm})$ is the extinction coefficient the complex $Fe(phen)_3^{2+}$ at 510 nm (11100 L mol^{-1} cm^1).

The moles of Fe^{2+} formed (x) are plotted as a function of time (t). The slope of this line was correlated to the moles of incident photons by unit of time ($q^0_{n,p}$) by the use of the following Equation 3.4:

$$\Phi(\lambda) = \frac{dx/dt}{q^0_{n,p}[1-10^{-A(\lambda)}]} \quad \text{(Eq. 3.4)}$$

where dx/dt is the rate of change of a measurable quantity (spectral or any other property), the quantum yield (Φ) for Fe^{2+} at 400 nm is 1.13^{22}, $[1\text{-}10^{-A(\lambda)}]$ is the ratio of absorbed photons by the solution, and $A(\lambda)$ is the absorbance of the actinometer at the wavelength used to carry out the experiments (400 nm). The absorbance at 400 nm $A(400)$ was measured using a Shimadzu

2401PC UV-Vis spectrophotometer in a 10 mm path quartz cuvette, obtaining an absorbance of 2.54.

$q^0_{n,p}$, which is the photon flux, was determined to be 1.32×10^{-8} einstein s^{-1}

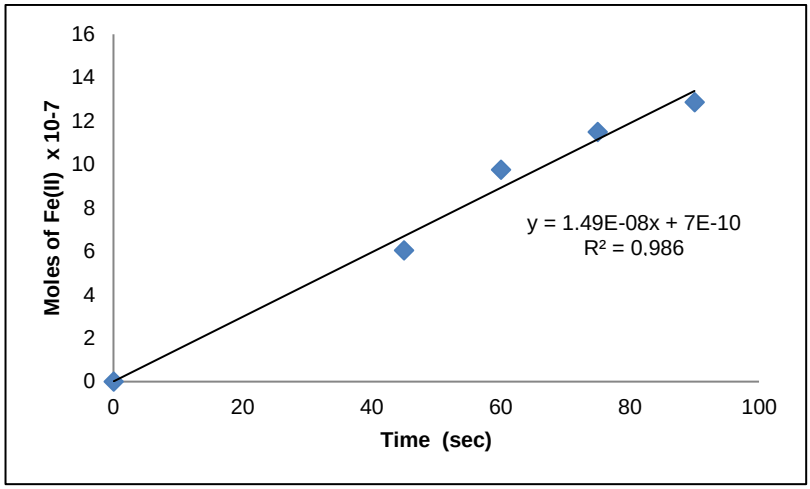

The moles of product **4a** formed for the model reaction were determined by GC measurement (MS detector) using 1,3,5-trimethoxybenzene as internal standard.

The moles of product per unit of time are related to the number of photons absorbed. The photons absorbed are correlated to the number of incident photons by the use of Equation 3. According to this, if we plot the moles of product (x) versus the moles of incident photons ($q^0_{n,p} \cdot dt$), the slope is equal to: $\mathbf{\Phi \cdot (1-10^{-A(400\ nm)})}$, where Φ is the quantum yield to be determined and *A*(400 nm) is the absorption of the reaction under study.

A(400 nm) was measured using a Shimadzu 2401PC UV-Vis spectrophotometer in 10 mm path quartz. An absorbance of 1.29 was determined for the model reaction mixture.

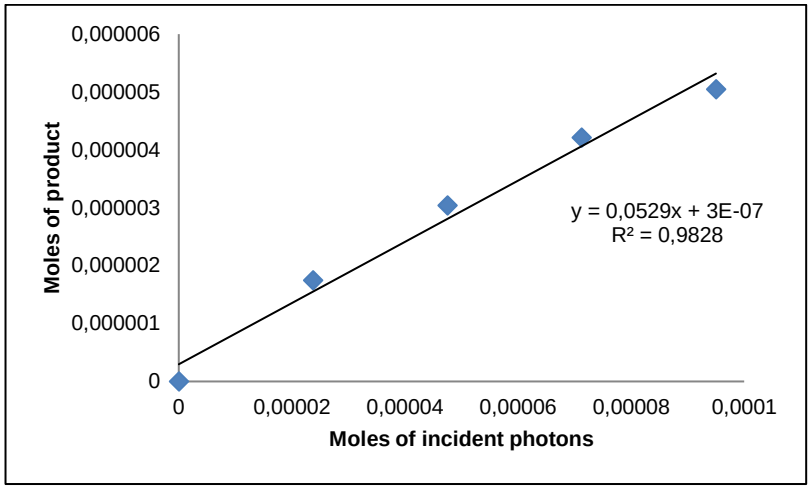

The quantum yield (Φ) of the photochemical benzylation of cinnamaldehyde **15a** with benzyl trimethylsilane **3a** catalyzed by **K** was calculated to be **0.05**.

The procedure was repeated a second time to provide a similar value: quantum yield (Φ) at 400 nm of **0.06**.

Single Crystal X-ray Diffraction Data for the chiral amine 1c

Crystals of the compound **K** were obtained by slow evaporation of a methanol/dichloromethane solution. *Data Collection*. Measurements were made on a Bruker-Nonius diffractometer equipped with an APPEX 2 4K CCD area detector, a FR591 rotating anode with $Mo_{K\alpha}$ radiation, Montel mirrors and a Cryostream Plus low temperature device (*T* = 100K). Full-sphere data collection was used with ω and φ scans.

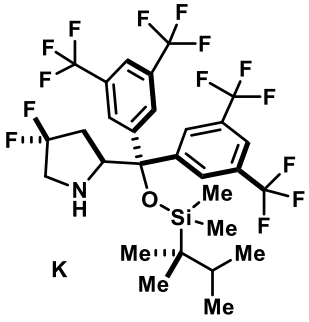

≡

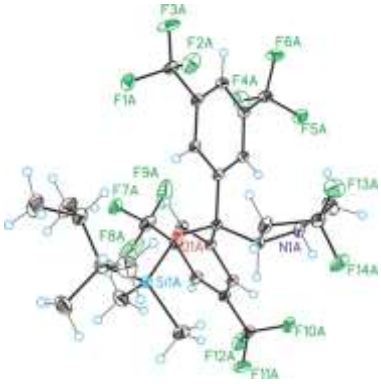

Empirical formula	C29 H31 F14 N O Si
Formula weight	703.64
Temperature	100(2) K
Wavelength	0.71073 Å
Crystal system	Triclinic
Space group	P1
Unit cell dimensions	a = 8.62410(10)Å α= 80.469(2)°. b = 9.7969(2)Å β = 83.3140(10)°. c = 18.9232(3)Å γ = 76.243(2)°.
Volume	1526.55(5) $Å^3$
Z	2
Density (calculated)	1.531 Mg/m^3
Absorption coefficient	0.188 mm^{-1}
F(000)	720
Crystal size	0.3 x 0.2x 0.2 mm^3
Theta range for data collection	2.162 to 45.294°.
Index ranges	-17<=h<=12,-13<=k<=14,-37<=l<=26
Reflections collected	64450
Independent reflections	22188[R(int) = 0.0334]
Completeness to theta =45.294°	54.1%
Absorption correction	Multi-scan
Max. and min. transmission	0.963 and 0.741
Refinement method	Full-matrix least-squares on F^2
Data / restraints / parameters	22188/ 3/ 849

Goodness-of-fit on F^2	1.059
Final R indices [I>2sigma(I)]	R1 = 0.0413, wR2 = 0.1220
R indices (all data)	R1 = 0.0439, wR2 = 0.1242
Flack parameter	x =0.00(3)
Largest diff. peak and hole	1.221 and -0.666 e.Å^{-3}

Single Crystal X-ray Diffraction Data for the Iminium Ion IIc.

Crystals of the iminium ion **IIc** were obtained by slow diffusion of hexane into a saturated solution of **IIc** in tetrahydrofuran. *Data Collection*. Measurements were made on a Bruker-Nonius diffractometer equipped with an APPEX 2 4K CCD area detector, a FR591 rotating anode with $Mo_{K\alpha}$ radiation, Montel mirrors and a Cryostream Plus low temperature device (*T* = 100K). Full-sphere data collection was used with ω and φ scans.

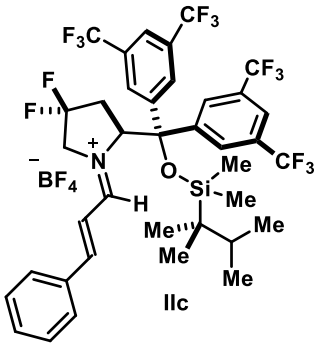

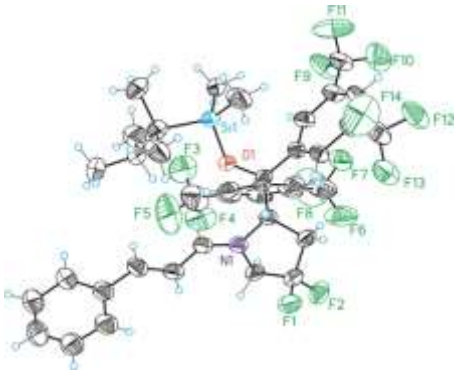

–

Empirical formula	C42 H46 B F18 N O2 Si
Formula weight	977.70
Temperature	90(2) K
Wavelength	0.71073 Å
Crystal system	Orthorhombic
Space group	P2(1)2(1)2(1)
Unit cell dimensions	a = 10.6934(3)Å α= 90°. b = 17.4932(4)Å β = 90°. c = 24.2485(6)Å γ = 90°.
Volume	4535.98(19) Å^3
Z	4
Density (calculated)	1.432 Mg/m^3
Absorption coefficient	0.162 mm^{-1}
F(000)	2008
Crystal size	0.40 x 0.20 x 0.15 mm^3
Theta range for data collection	2.044 to 31.066°.

Index ranges	-15<=h<=14,-23<=k<=25,-26<=l<=34
Reflections collected	59593
Independent reflections	13385[R(int) = 0.0413]
Completeness to theta =31.066°	94.3%
Absorption correction	Multi-scan
Max. and min. transmission	0.976 and 0.751
Refinement method	Full-matrix least-squares on F^2
Data / restraints / parameters	13385/ 792/ 965
Goodness-of-fit on F^2	1.579
Final R indices [I>2sigma(I)]	R1 = 0.0783, wR2 = 0.2159
R indices (all data)	R1 = 0.1037, wR2 = 0.2302
Flack parameter	x =0.05(5)
Largest diff. peak and hole	0.778 and -0.473 e.$Å^{-3}$

Single Crystal X-ray Diffraction Data for a Derivative of Compound 22a

Crystals of compound **22a'**, obtained after NaBH4 aldehyde reduction and subsequent esterification with pyrene carbonyl chloride of compound **22a** (see details in the Experimental Section), were obtained by slow evaporation of a hexane solution. *Data Collection*. Measurements were made on a Bruker-Nonius diffractometer equipped with an APPEX 2 4K CCD area detector, a FR591 rotating anode with $Mo_{K\alpha}$ radiation, Montel mirrors and a Cryostream Plus low temperature device (*T* = 100K). Full-sphere data collection was used with ω and φ scans.

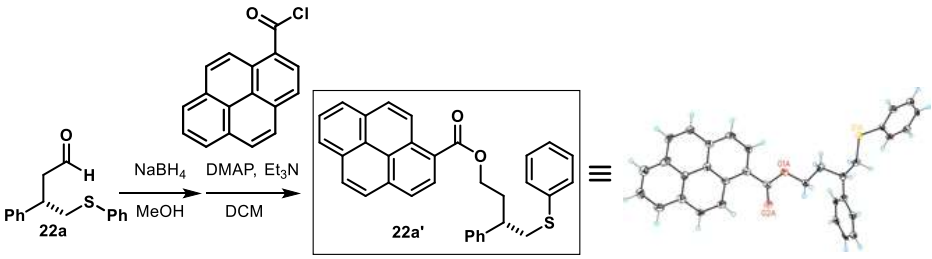

Empirical formula	C33 H26 O2 S
Formula weight	486.60
Temperature	100(2) K
Wavelength	0.71073 Å
Crystal system	Monoclinic
Space group	P2(1)
Unit cell dimensions	a = 29.4752(19)Å α= 90°. b = 8.8183(6)Å β = 97.4465(18)°. c = 37.823(2)Å γ = 90°.
Volume	9748.0(11) $Å^3$
Z	16
Density (calculated)	1.326 Mg/m^3

Absorption coefficient	0.163 mm^{-1}
F(000)	4096
Crystal size	0.25 x 0.08 x 0.03 mm^3
Theta range for data collection	0.697 to 25.470°.
Index ranges	-35<=h<=35,-10<=k<=10,-38<=l<=45
Reflections collected	90192
Independent reflections	34785[R(int) = 0.0445]
Completeness to theta =25.470°	99.2%
Absorption correction	Multi-scan
Max. and min. transmission	0.995 and 0.927
Refinement method	Full-matrix least-squares on F^2
Data / restraints / parameters	34785/ 213/ 2593
Goodness-of-fit on F^2	1.070
Final R indices [I>2sigma(I)]	R1 = 0.0862, wR2 = 0.1829
R indices (all data)	R1 = 0.1100, wR2 = 0.1935
Flack parameter	x =0.02(2)
Largest diff. peak and hole	0.479 and -0.626 e.$Å^{-3}$

Chapter IV

Extending the Reactivity of Excited-State Iminium Ions

Target

Applying the excited-state reactivity of catalitically generated chiral iminium ions to develop novel asymmetric β-functionalization of α,β-unsaturated aldehydes.

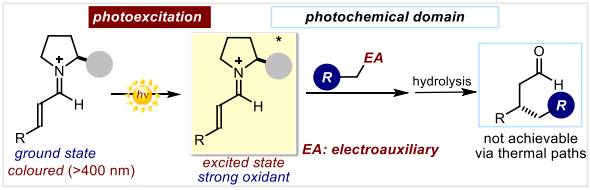

Tools

Analysis of the electrochemical features of molecules to identify suitable electron-donor substrates. Exploiting the highly oxidative properties of excited-state iminium ions to generate alkyl radicals from ready available precursors.[1]

4.1 Introduction

The excited-state reactivity of transiently generated chiral iminium ions has been discussed in the previous Chapter. The investigations led to the development of an unprecedented photochemical methodology for the asymmetric β-benzylation of enals.[2] We used excited-state iminium ions **I*** as chiral oxidants to activate alkyl silane derivatives *via* SET oxidation. The 5π-electron β-enaminyl radical intermediates **II** obtained after the electron transfer could effectively control the stereoselectivity of the ensuing radical coupling, enabling the asymmetric formation of new C–C bonds (Figure 4.1).

Motivated by these results, we anticipated the wide possibilities for reactions invention that this novel mode of activation could provide, combining the powerful tools of organocatalysis with the unique pathways offered by photoinduced reactions.

[1] Part of the projects discussed in this Chapter have been conducted in collaboration with Dr Charlie Verrier, Nurtalya Alandini, Cristofer Pezzetta, Dr Mauro Moliterno, Dr Hamish Hepburn, Dr Alberto Vega-Peñaloza and Dr Mattia Silvi. Part of the work has been published, see: Verrier, C., Alandini, N., Pezzetta, C., Moliterno, M., Buzzetti, L., Hepburn, H. B., Vega-Peñaloza, A., Silvi, M., Melchiorre, P., "Direct Stereoselective Installation of Alkyl Fragments at the β-Carbon of Enals via Excited Iminium Ion Catalysis" *ACS Catal.* **2018**.

[2] Silvi, M., Verrier, C., Rey, Y. P., Buzzetti, L., Melchiorre, P., "Visible-light excitation of iminium ions enables the enantioselective catalytic β-alkylation of enals" *Nat. Chem.* **2017**, *9*, 868.

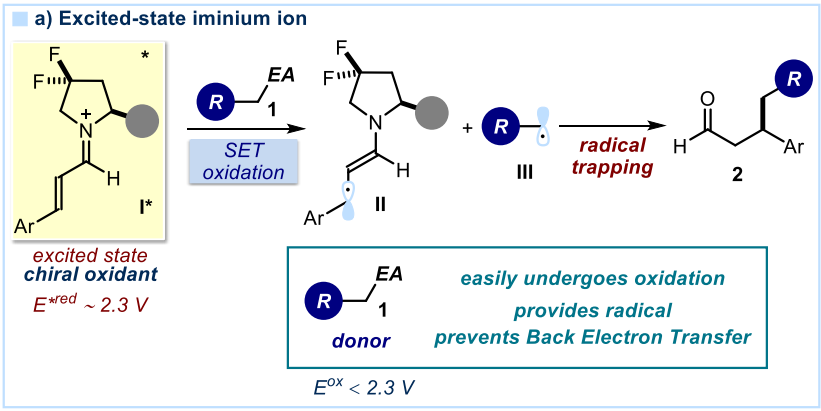

Figure 4.13: a) Photoexcitation of iminium ion provides a chiral oxidant capable to trigger the SET oxidation of suitable donors; EA: electroauxiliary group.

This Chapter describes our efforts to extend the scope of the excited-state iminium ion chemistry to develop novel enantioselective transformations, which could not be achieved through classical ground-state reactivity. The photophysical characterization of the iminium ion, discussed in the previous chapter, provided a solid starting point for the selection of possible reaction partners **1**. Simply relying on physical properties, such as redox potentials, we identified new classes of radical sources which can successfully engage in excited-state iminium ion-mediated reactions. These substrates are characterized by suitable redox properties that match with the oxidative capability of excited-state iminium ions. Following this scheme, we could activate epoxide derivatives, acetals and, ultimately, develop an operationally simple procedure that allows the enantioselective β-alkylation of α,β-unsaturated aldehydes with 4-alkyl dihidropyridines (4-alkyl-DHPs). This transformation overcame the need for stabilized benzyl and α-heteroatom radicals and we could introduce unfunctionalized alkyl fragments at the β-positions of enals with high level regio- and stereo-selectivity.

4.2 Strategies to Prevent the Back Electron Transfer (BET).

Photoinduced electron transfer (PET) occurs between an excited-state species and a ground-state redox partner, namely a donor (D) or an acceptor (A). The frequent thermodynamic feasibility of PET is generally dictated by the high energetic content of the photoexcited species, which displays an enhanced redox potential compared to the corresponding ground state. After the SET event, the donor and the acceptor are in their ground states though in a different oxidation level. Back electron transfer (BET) is the thermal process that, overriding the effect of PET, restores the donor and the acceptor in their original oxidation level. This

step is thermodynamically favored due to the high energy difference between of the HOMO and the LUMO of the species involved (Figure 4.2).[3]

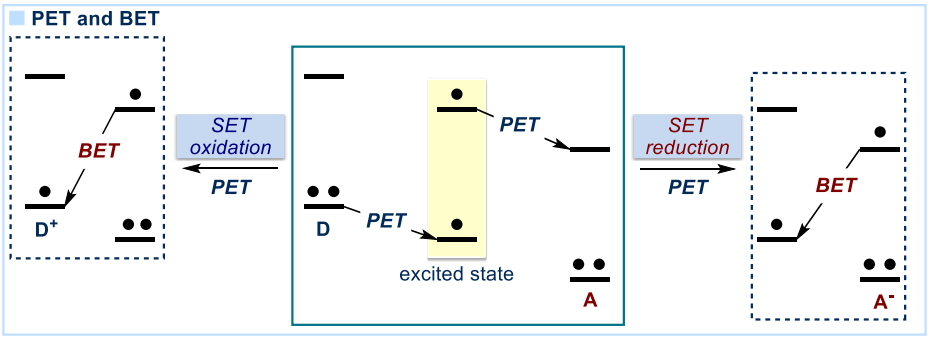

Figure 4.14: Photoinduced electron transfer (central rectangle) occurs between an excited-state species and a suitable donor (D) or acceptor (A). Back electron transfer (dashed rectangles) occurs between the ground-state species obtained after PET and restores the original oxidation level of the substrates. BET is thermodynamically favorable due to the high energy difference between HOMO and LUMO of the species involved.

BET strongly affects the efficiency of light-induced reactions. In fact, it restores the starting materials in their pre-excitation states, thus preventing the occurrence of any further chemical transformations. For this reason, finding a way to inhibit BET is crucial for the development of any electron-transfer-mediated photochemical processes.

Many strategies can be applied in order to obviate BET. In general, these rely on the induction of a quick transformation that sequestrates one of the species obtained after PET. Among these, the *fragmentation* of one of the open-shell intermediates is often exploited (Figure 4.3a). This strategy generally requires the introduction of fragmenting groups (FG) within the donors or the acceptors. These groups are prone to undergo fast fragmentation from the corresponding charged species. The most exploited FGs for donor compounds, which undergoes SET oxidations, are alkylstannanes ($-SnR_3$)[4], alkylsilanes ($-SiR_3$), trifluoroborates ($-BF_3^-$)[5] and carboxylates ($-COO^-$).[6] On the other hand, halides, nitrile, and redox active esters are generally exploited as fragmenting groups that prevents the BET in PET reductions. This approach is efficient when the rate of the fragmentation is higher or comparable with the rate of the BET. Accordingly, a low energetic barrier for the fragmentation step is necessary.[7]

---

[3] Fox, M. A., "Photoinduced electron transfer in organic systems: control of back electron transfer" *Advances in photochemistry* **1986**, *13*, 237.

[4] Kyushin, S., Masuda, Y., Matsushita, K., Nakadaira, Y., Ohashi, M., "Novel alkylation of aromatic nitriles via photo-induced electron transfer of group 14 metal-carbon σ donors" *Tetrahedron Lett.* **1990**, *31*, 6395.

[5] Nishigaichi, Y., Orimi, T., Takuwa, A., "Photo-allylation and photo-benzylation of carbonyl compounds using organotrifluoroborate reagents" *J. Organomet. Chem.* **2009**, *694*, 3837.

[6] Capaldo, L., Buzzetti, L., Merli, D., Fagnoni, M., Ravelli, D., "Smooth Photocatalyzed Benzylation of Electrophilic Olefins via Decarboxylation of Arylacetic Acids" *J. Org. Chem.* **2016**, *81*, 7102.

[7] Albini, A., Mella, M., Freccero, M., "A new method in radical chemistry: generation of radicals by photo-induced electron transfer and fragmentation of the radical cation" *Tetrahedron* **1994**, *50*, 575.

Despite the extensive application of this strategy, the requirement of a fragmenting group limits its applicability to pre-functionalized substrates and affects the overall atom economy of the process.

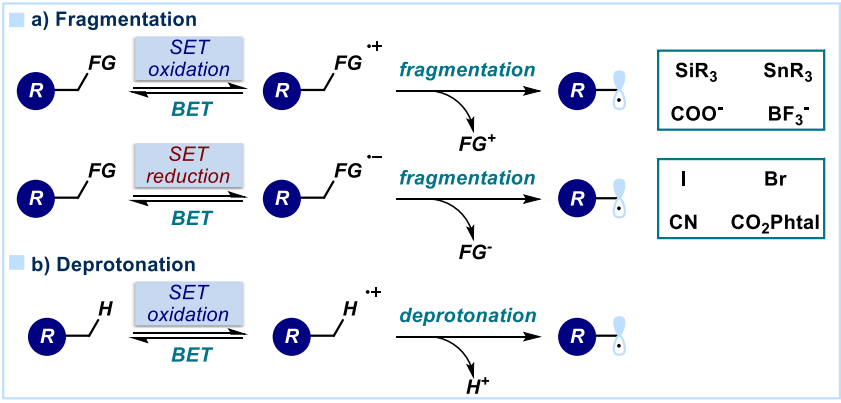

Figure 4.3: a) Fragmentation strategies and common fragmenting groups used to prevent the BET in SET oxidation or SET reduction. b) Deprotonation of the radical cation inhibit the BET providing a neutral radical.

A similar approach for the inhibition of BET relies on the *deprotonation* of the radical cations obtained after SET oxidation of the substrates (Figure 4.3b). These intermediates generally exhibit a strongly increased acidity compared to the parent substrates and they can easily deliver a proton to a suitable base, furnishing a neutral C-centered radical. This scenario falls under the definition of multisite proton-coupled electron transfer (MS-PCET) and it was recently exploited by our group for the excited-state iminium ion-mediated direct functionalization of toluene derivatives.[8] In this reaction, the excited-state iminium ion oxidized toluene to generate benzyl radical after the deprotonation of the corresponding radical cation.

Another strategy that has been widely exploited for the prevention of BET is based on the *strain release* in small rings (Figure 4.4a). Strained radical cations, generated upon oxidation of cyclopropanes, cyclobutanes, or small heterocycles, are susceptible to C–C bond fragmentation and rapidly provide the corresponding open-ring structures. Also this approach was exploited by our group to develop a photochemical organocascade (Figure 4.4b).[9] In this method, the excited-state iminium ion **I*** promotes the oxidation of cyclopropanol **3**. The consequential ring opening furnishes the linear β-keto radical cation **IV** that undergoes a stereocontrolled radical combination with the 5π-electron β-enaminyl radical intermediates

[8] Mazzarella, D., Crisenza, G. E. M., Melchiorre, P., "Asymmetric Photocatalytic C–H Functionalization of Toluene and Derivatives" *J. Am. Chem. Soc.* **2018**, *140*, 8439.
[9] Woźniak, Ł., Magagnano, G., Melchiorre, P., "Enantioselective Photochemical Organocascade Catalysis" *Angew. Chem.* **2018**, *130*, 1080.

II. The resulting enamine intermediate **V** promotes an intramolecular aldol cyclization step by reacting with the electrophilic ketone moiety, affording the enantioenriched cyclopentanol derivative **4** after hydrolysis of the catalyst.

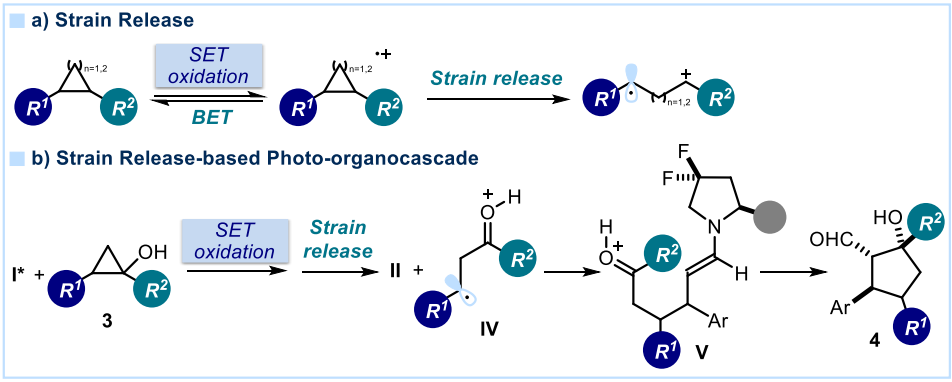

Figure 15.4: a) Strained radical cations rapidly undergo ring opening, thus inhibiting the BET. b) Development of a photo-organocascade process that exploits the oxidation of cyclopropanol derivatives and the strain release approach.

4.3 Results and Discussion

4.3.1 Oxiranes as Radical Precursors

Intrigued by the strain release strategy, we wondered if we could exploit the properties of excited-state iminium ions to promote the SET oxidation of small heterocycles and generate C-centered radicals upon ring opening of the corresponding radical cations. A strategically similar approach was reported in 1978 by Arnold and Albini (Scheme 4.1).[10] In this work, the photoexcited dicyanonaphtalene photocatalyst (DCN*) triggers the SET oxidation of *trans*-stilbene oxide **5** providing the corresponding radical cation $\mathbf{5}^{\cdot+}$. This radical ion intermediate rapidly undergoes ring opening to provide the linear radical intermediate $\mathbf{VI}^{\cdot+}$. A SET event is then taking place between the DCN radical anion and $\mathbf{VI}^{\cdot+}$ giving access to the carbonyl ylide **VI** while regenerating the photocatalyst in its neutral form. **VI** undergoes [3+2] dipolar cycloadditions with electron poor olefins of type **6** providing the tetrahydrofuran derivative **7**.

[10] Albini, A., Arnold, D. R., "Radical ions in photochemistry. 6. The photosensitized (electron transfer) ring opening of aryloxiranes" *Can. J. Chem.* **1978**, *56*, 2985.

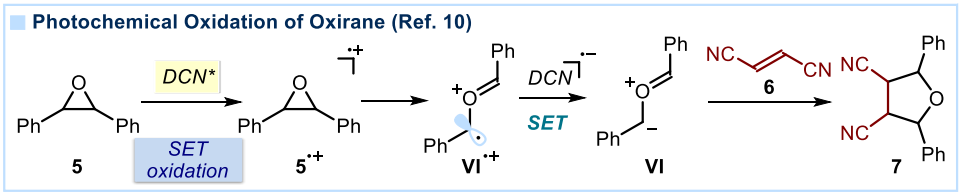

Scheme 4.1: Photochemical oxidation of oxirane.

Inspired by this literature precedent, we anticipated that excited-state iminium ion **I*** can act as the photocatalyst to promote the SET oxidation of the epoxide derivative **5** (Figure 4.5). Additionally, we hypothesized that the 5π-electron β-enaminyl radical intermediates **II** could rapidly intercept the intermediate **VI**$^{\bullet+}$ via a stereoselective radical coupling, forging a C–C bond and setting the first two stereocenters. The so-formed enamine intermediate **VII** would then promote a stereoselective intramolecular aldol cyclization with the highly activated oxonium ion, leading to the enantioenriched tetrahydrofuran derivative **8** with four consecutive stereogenic centers.

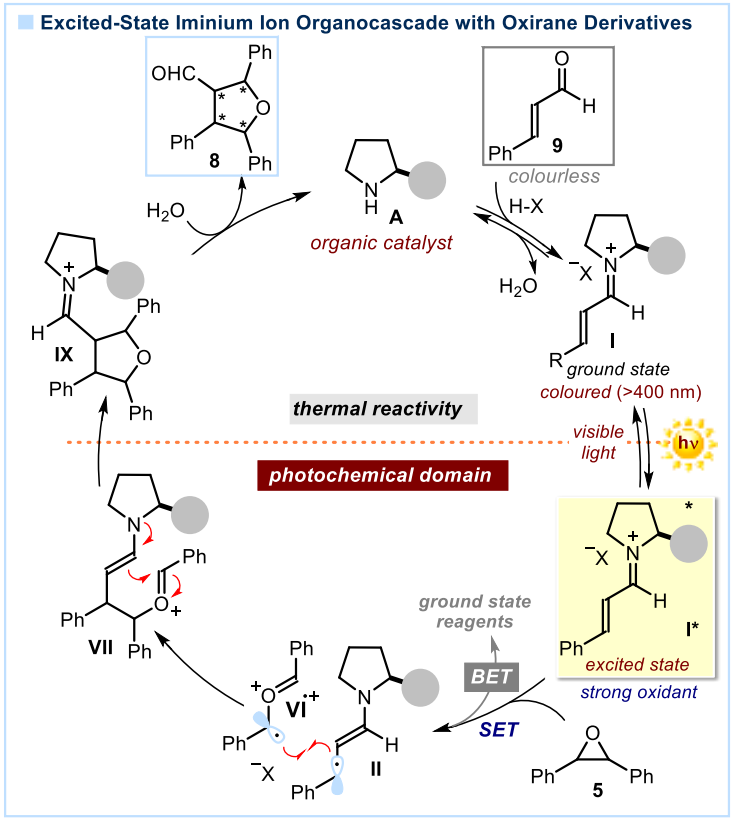

Figure 4.5: Design of the excited-state iminium ion-mediated organocascade with oxirane derivatives.

The thermodynamic feasibility of the SET between the excited iminium ion **I*** and *trans*-stilbene oxide **5** is secured by their electrochemical properties. **5** has a redox potential E^{ox} ($\mathbf{5}^{\cdot+}/\mathbf{5}$) of +1.86 V (vs Ag/AgCl)[11], a value which falls below the oxidative capability of the excited-state iminium ion ($E^{red}(\mathbf{I^*}/\mathbf{I}^{\cdot-})$ ~ +2.3 V vs Ag/AgCl).

Encouraged by this observation, we subjected *trans*-stilbene oxide **5** to the reaction conditions previously developed for the benzylation reaction. We reacted it under 420 nm irradiation, in the presence of 3 equiv. of cinnamaldehyde, using 20 mol% of the difluorinated chiral amine catalyst **A** and in the presence of 40 mol% of TFA as acid co-catalyst (Scheme 4.2).

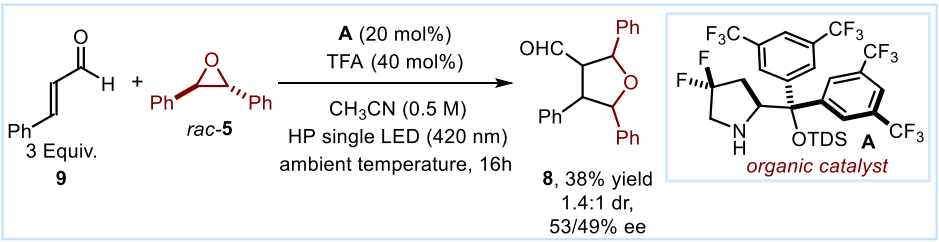

Scheme 4.2: Proof-of-principle reaction.

After 16 h of irradiation, the desired heterocyclic product **8** was obtained in 38% overall yield. Even though the product contains four stereogenic centers, we observed the formation of only two major diasteroisomers in a 1.4:1 diasteromeric ratio. However, the reaction displayed a low level of enantioselectivity, since the two diasteroisomers were obtained with enantiomeric excesses as low as 53% and 49%, respectively.[12]

To optimize the reaction in terms of efficiency and stereocontrol, we screened some of the most commonly used secondary amine catalysts. Amines **B-E** demonstrated good applicability in the excited-state iminium ion chemistry (Scheme 4.3).

[11] Miyashi, T., Kamata, M., Mukai, T., "Simultaneous capture of two distinct radical-ion intermediates generated from the EDA complexes of three-membered compounds with TCNE by photoexcitation and in the dark" *J. Am. Chem. Soc.* **1987**, *109*, 2780.

[12] The enantiomeric excesses were measured on the corresponding alcohols. For further information see Experimental Section.

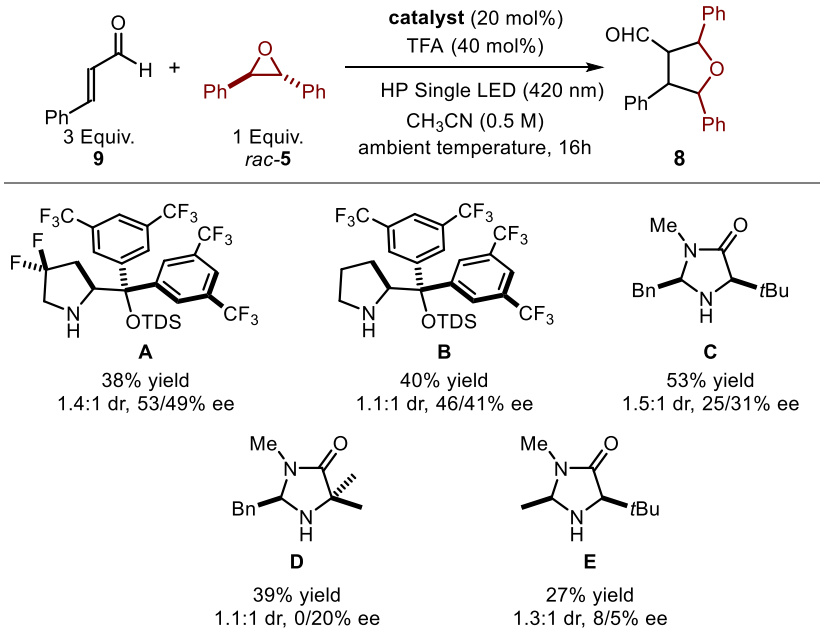

Scheme 4.3: Screening of the catalyst in the excited-state iminium ion oxidation of *trans*-stilbene oxide.

The best results in terms of yield were obtained using the second generation imidazolidinone catalyst **C**, which provided product **8** in 53% yield with a 1.5:1 dr. However, the stereocontrol was poor and the two major diasteroisomers were obtained in 25% and 31% ee. The imidazolidinone-based catalysts **D** and **E** were competent for this transformation, but they provided the tetrahydrofuran derivative with poor ee. Proline-based catalysts **A** and **B** inferred a better control the stereoselectivity to the process. In particular, the difluorinated catalyst **A** was confirmed as the best catalyst.

Unfortunately, the screening of other standard reaction parameters, including solvents, acidic co-catalysts, and stoichiometry of the regents, did not lead to any improvement. Only increasing the loading of catalyst **A** to 40 mol% we observed an enhancement of the enantiomeric excess (60/50%) although with a similar dr (1.4:1) and a lower yield 29%.

However, a peculiar behavior was observed in the evaluation of the reaction temperature. Generally, this parameter can strongly affect the results of an asymmetric photochemical transformation, suppressing parasitic pathway and enhancing the stereoselectivity of the process. For this reason, the two best-performing catalysts **A** and **B** were tested in the model reaction at -10 ºC (Scheme 4.4).

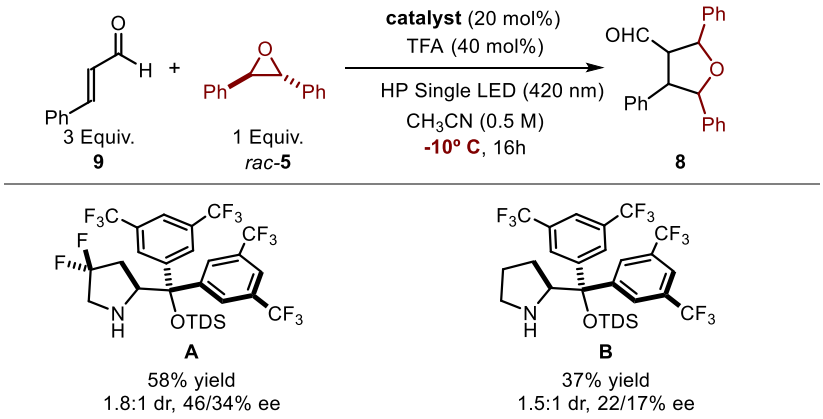

Scheme 4.4: Reactions with catalyst **A** and **B** under cryogenic conditions.

In these conditions, the difluorinated catalyst **A** provided the desired product in 58% yield, 20 points % better than the reaction conducted at ambient temperature. Also the diasteromeric distribution was enhanced to 1.8:1. Conversely, the proline-derived catalyst **B** furnished the tetrahydrofuran derivative in a similar yield and slightly better dr compared to the room temperature reaction. Surprisingly, in contrast with our prediction, both catalysts furnished the desired heterocycle with a substantial erosion of the enantiomeric excess.

These results prompted us to hypothesize the competition of a non-catalyzed, racemic background pathway. As depicted in Figure 4.6, we propose that, in analogy with the mechanism suggested by Albini and Arnold,[10], after the ring-opening event, the radical cation **VI**$^{\cdot+}$ would undergo a SET with the 5π-electron β-enaminyl radical intermediates **II** regenerating the ground-state iminium ion **I** and the carbonyl ylide **VI**. The latter would then engage in a non-catalyzed [3+2] dipolar cycloaddition with the superstoichiometric cinnamaldehyde **9**, which serves as an electron-poor olefin. This step would take place without any catalyst control, leading to the formation of the racemic product *rac*-**8** and competing with the stereoselective radical manifold, which furnish the enantioenriched tetrahydrofuran derivative **8**. Lowering the temperature might help the stabilization of the radical pair **VI**$^{\cdot+}$ + **II**, overall favoring the SET against the radical coupling which provides **VII**. Moreover, at low temperatures, the condensation between the enal and the catalysts might be slower. This would decrease the amount of iminium ion in solution while increasing the concentration of free enal, which triggers the racemic pathway

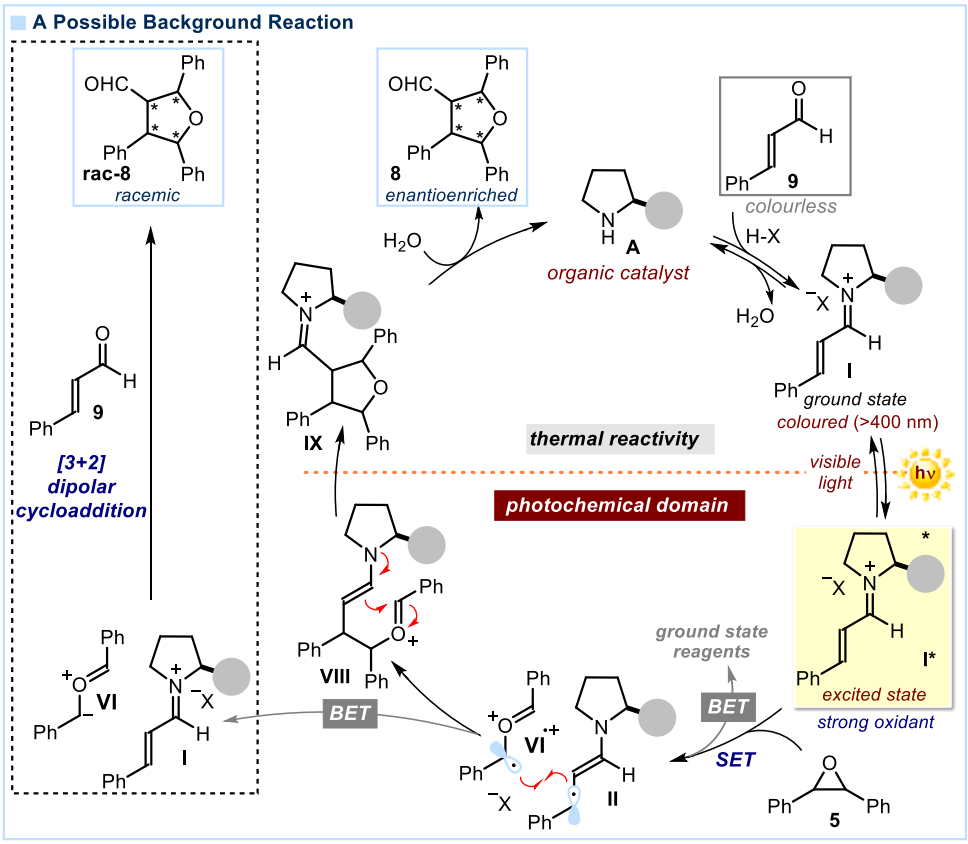

Figure 4.6: A plausible non-catalyzed background [3+2] cycloaddition between the carbonyl ylide **VI** and the cinnamaldehyde **9**.

To gain insights on the synthetic utility of this reaction, we synthesized different epoxide derivatives and we tested them as substrates. Unfortunately, only *trans*-stilbene oxide delivered the desired product. Other substituted oxiranes, cyclopropanes, and aziridines did not participate in the transformation (Figure 4.7). For this reason, we decided to temporary quit this project and to focus on other applications of the excited-state properties of iminium ions for the development of asymmetric transformations.

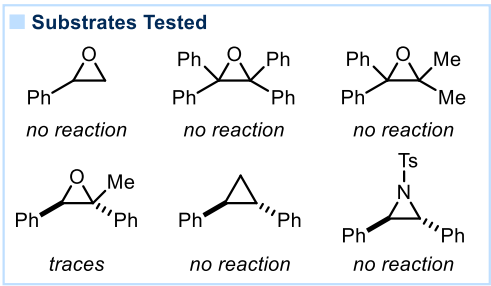

Figure 4.7: Oxirane, cyclopropane, and aziridine derivatives tested in the excited iminium ion-mediated organocascade.

4.3.2 Generation of Alkyl Radicals through C–C Bond Fragmentation

The formation of alkyl radicals through SET oxidation of a substrate followed by C–C bond fragmentation of the resulting radical cations is a synthetically appealing strategy because it does not require the introduction of fragmenting groups withing the substrates. However, this approach has often been limited to the opening of strained rings. In addition, it requires in most of the cases strong oxidants, due to the stability of simple C–C bonds towards SET. After establishing the strong oxidative capability of excited iminium ions, we evaluated the possibility to exploit them for the generation of alkyl radicals through C–C bond fragmentation. This approach would extend the scope of the β-functionalization of enals to other radical precursors. In particular, we identified acetals and 4-alkyl dihydropyridines (4-alkyl DHPs) as suitable radical precursors.

4.3.3 Acetals as Radical Sources: a "Half Failed" Approach

Acetals are carbonyl derivatives having the structure $R_2C(OR^1)_2$. They are diether of geminal diols[13] often used as protecting groups for aldehydes and ketones. They can be easily accessed by condensation of alcohols with the parent carbonyl compounds (Figure 4.8a). Acetals can serve as electron donors in SET oxidations and the ensuing radical cations can undergo C–C bond fragmentations to release alkyl radicals (Figure 4.8b). This behavior was observed by Albini in 1992, when he reported the use of cyclic acetals as alkyl radical sources in a photochemical protocol (Figure 4.8c).[14] In this methodology, the tetracyanobenzene in the excited-state (TCB*), which is an extremely strong oxidant (E^{red} (TCB*/TCB$^{\cdot-}$) = +3.15 V), promotes the SET oxidation of the acetal **10** affording the corresponding radical cation **X**. The fragmentation of this intermediate releases an alkyl radical, which undergoes aromatic *ipso*-substitution with the reduced form of the aromatic nitrile providing the alkylated arene

[13] IUPAC. Compendium of Chemical Terminology, 2nd ed. (the "Gold Book")
[14] Mella, M., Fasani, E., Albini, A., "Electron transfer photoinduced cleavage of acetals. A mild preparation of alkyl radicals" *J. Org. Chem.* **1992**, *57*, 3051.

product **11**. The cation **XI**, obtained after the C–C bond fragmentation, is sequestered by the attack of a nucleophile (in this case the water present as moisture in the solvent). The selectivity and the direction of the cleavage of the acetal radical cations is predictable on the basis of the stability of the formed radical. Stable radicals are released at a faster rate (tertiary > primary > methyl).

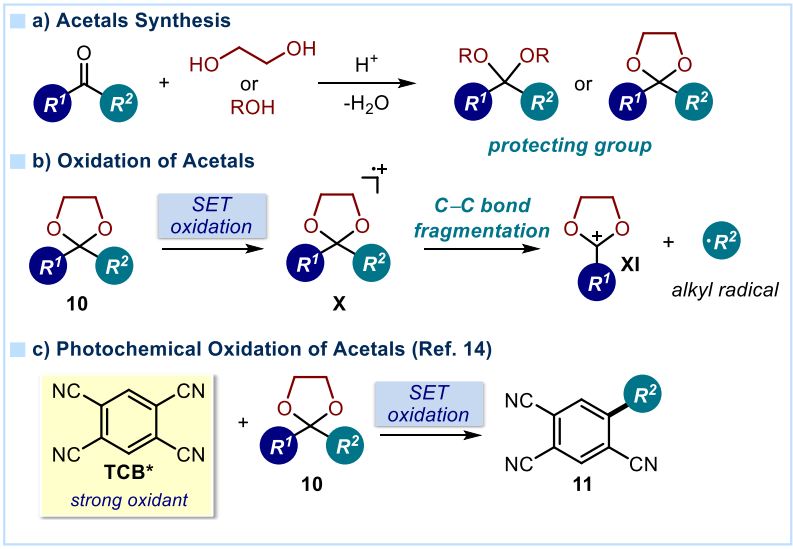

Figure 4.8: a) Synthesis of acetals via condensation of alcohol with carbonyl compounds. b) The SET oxidation of acetals provides a radical cation that undergoes C–C bond fragmentation releasing and alkyl radical. c) A photochemical reaction between acetal and tetracyanobenzene reported by Albini (Ref. 14).

Inspired by this seminal report, we tested the possibility to exploit acetals as donors and radical sources in a photochemical iminium ion-mediated β-alkylation of enals. In our reaction design, the iminium in the excited-state ion would oxidize the acetals and the 5π-electron β-enaminyl radical intermediate **II** would then trap the released alkyl radicals in an enantioselective fashion. We started out our investigation submitting the two commercially available cyclic acetals **10a** and **10b** to the conditions optimized for the β-benzylation protocol (Scheme 4.5). Unfortunately, in none of the cases we observed the formation of the desired β-alkylated product **11**. We ascribed the lack of reactivity to the high oxidation potential of these substrates (E^{ox} (**10**$^{\cdot+}$/**10**) ~ +2.8-3.1 V), which falls above the limit of the oxidative ability of excited iminium ions. Moreover, the low stability of the alkyl radicals released by these substrates might hamper the fragmentation step, thus enhancing the BET pathway.

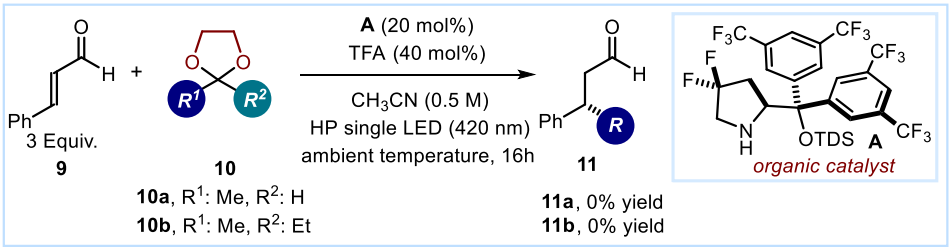

Scheme 4.5: Test reactions with acetals as radical sources.

To overcome these limitations, we designed an acetal decorated with two groups that can modulate its reactivity (Figure 4.9a). In particular, we reasoned that the introduction of a phenyl group would decrease the oxidation potential of the acetal while stabilizing the corresponding radical cation. Additionally, we selected a benzyl fragment as the second group, knowing the tendency of benzyl radicals towards this transformation. The acetal **10c** was easily synthesized by condensation of ethylene glycol **13** with the commercially available benzyl phenyl ketone **12** (Figure 4.9b).

In order to verify our hypothesis, we measured the oxidation potential of 10c and we observed an irreversible oxidation wave wich relates with a potential of E^{ox} (**10c**$^{\cdot+}$/**10c**) = 1.8 V, a value that fall in the operative range of the excited-state iminium ion.

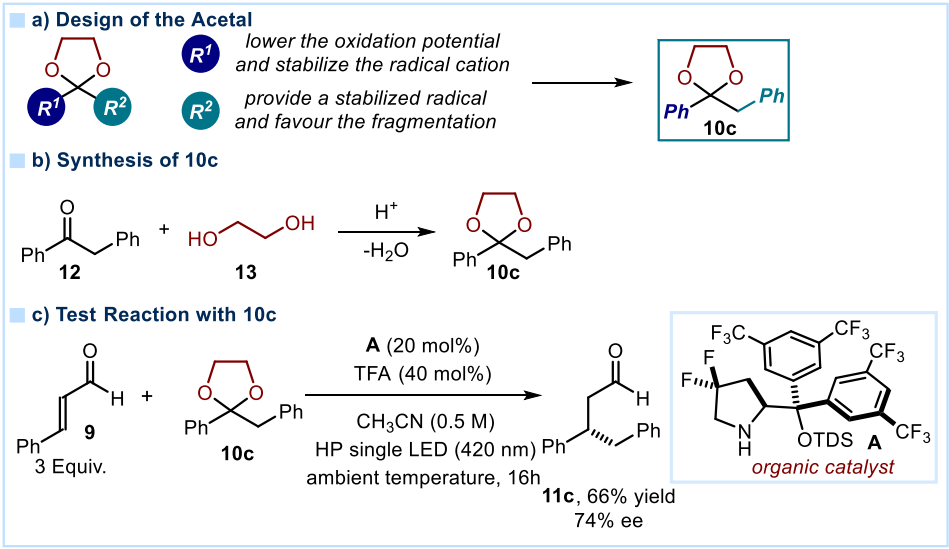

Figure 4.9: a) Design of the acetal substrate **10c**: the groups can modulate the electrochemical properties. b) Synthesis of the acetal **10c**. c) **10c** as substrate for the excited iminium ion-mediated β-alkylation of enals.

When we submitted substrate **10c** to the optimized conditions, we obtained the desired β-benzylation product **11c** in 66% yield and 74% ee (Figure 4.9c). Even though this result is

wors, both in terms of yield and ee, compared to the one obtained in the previously developed benzylation protocol with benzyl trimethyl silane, it provided the evidence that acetals can successfully engage in excited iminium ion-mediated transformations. We could further improve the reaction outcome to 71% yield and 74% ee when performing the reaction in a glass vial instead of a Schlenk tube. Motivated by this proof-of-concept, we tried to extend the scope of the reaction to different alkyl fragments. We synthesized three acetals bearing isopropyl, *tert*-Butyl and allyl groups (Figure 4.10). Despite the stability of the radicals delivered by these substrates, we did not observe any conversion of the starting materials when we submitted them to the reaction conditions.

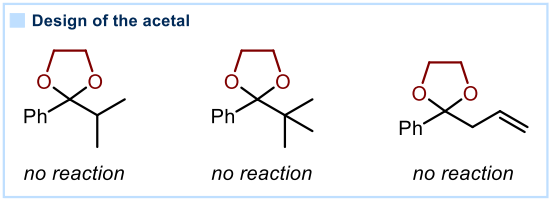

Figure 4.10: Acetals tested in the excited-state iminium ion-mediated β-alkylation.

At this stage, we wondered if the rate of the attack of the nucleophile to the carbocation intermediate **XIc** would affect the reactivity of the acetals towards this photochemical transformation. After the SET oxidation of **10c** the obtained radical cation **Xc** can undergo C–C bond fragmentation delivering the alkyl radical and the carbocationic intermediate **XIc** in close proximity. A reverse radical recombination would then reform **Xc** hampering the reactivity of the alkyl radical species. Conversely, the attack of a nucleophile on **XIc**, would enhance the productive escape of the alkyl radical removing **XIc** and thus shifting the equilibrium (Figure 4.11a).

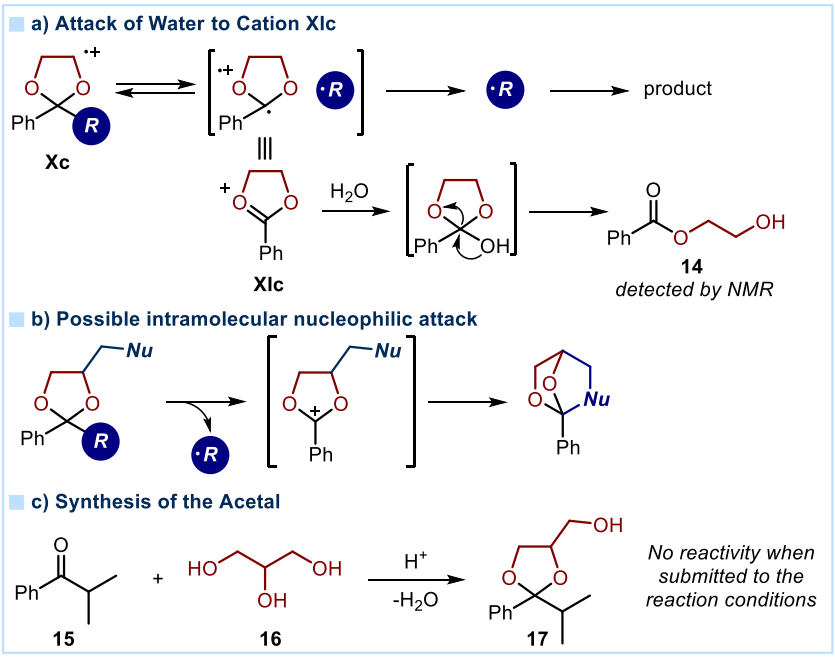

Figure 16: a) The attack of a nucleophile (water in this case) on the cationic intermediate **XIc** might affect the efficientcy of the C–C bond cleavage. b) Design of an acetal that allows a faster intramolecular nucleophilic attack. c) Synthesis of acetal **17**, which did not provide any desired product.

Analyzing the crude of the reactions by NMR spectroscopy, we detected the presence of compound **14**, which derives from the addition of adventitious water (present in the solvent as moisture) to **XIc**. Unfortunately, the addition of water or other nucleophiles as co-solvent did not lead to any improvement in the reactivity. We believed that a faster intramolecular nucleophilic attack, within the carbocation intermediate **XIc**, would enhance the fragmentation of the substrates and the release of the alkyl radicals (Figure 4.11b). Therefore, the isopropyl-containing acetal analogue **17** was prepared (Figure 4.11c), in which the ethylene glycol moiety was substituted with glycerol **16**. This substrates presents a nucleophilic hydroxyl group appended to the acetal backbone that could engage in the intramolecular nucleophilic attack. Unfortunately, when we submitted substrate **17** to the optimized reaction condition we could not detect any product formation.

Considering the limited scope and the lack of reactivity we observed using acetals as alternative alkyl radical sources, we decided to look for other suitable substrates. Therefore, we focused our investigation on the use of 4-alkyl dihydropyridines.

4.3.4 Alkyl Dihydropyridines as Radical Sources: a Successful Approach

4-alkyl dihydropyridines **20** (4-alkyl DHPs) can be easily accessed in one step from the corresponding aldehydes **18**. This synthesis mimics the first step of the venerable Hantzsch pyridine synthesis[15] and proceeds through the multicomponent condensation of an aldehyde **18** with two equivalent of a β-ketoester **19** in the presence of an ammonium salt (Figure 4.12a). These compounds, often referred to as Hantzsch esters, are known to release alkyl radicals upon SET oxidation (Figure 4.12b). This reactivity was first reported in 2001 by Wu,[16] who detected by electron spin resonance (ESR) spectroscopy the formation of isopropyl and isobutyl radicals upon oxidation of 4-isopropy and 4-isobutyl- DHP with nitrosonium tetrafluoroborate $NOBF_4$. The aromatization of the dihydropyridine scaffold, which leads to the pyridine derivative **21**, provides a strong driving force for the C–C bond fragmentation and the consequent release of the radical.

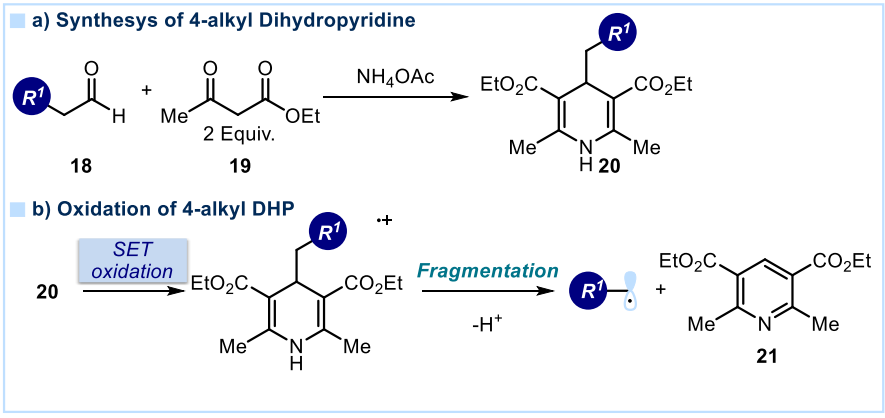

Figure 4.12: a) Synthesis of 4-alkyl-DHP. b) The SET oxidation of 4-alkyl-DHP, followed by C-C bond fragmentation, releases an alkyl radical.

The oxidation potentials of 4-alkyl DHPs fall in the operative range of the most common photocatalysts, rendering them appealing substrates for the generation of C(sp^3)-centered radicals in photocatalytic reactions. For instance, Nishibayashi and Sakata recently reported the use of 4-benzyl DHP for the photoredox construction of C(sp^3)- C(sp^2) bonds (Figure 4.13a).[17] An excited photocatalyst (PC*) promotes the SET oxidation of the 4-benzyl DHP **20**. The resulting benzyl radical **XII** is then trapped by the radical anion of dicyanobenzene

[15] Hantzsch, A., "Condensationsprodukte aus Aldehydammoniak und Ketonartigen Verbindungen" *Chem. Ber.* **1881**, *14*, 1637.
[16] Wu, L.-M., Chen, W., Liu, Z.-L., "Stable free radicals generated during the oxidation of 4-alkyl Hantzsch 1, 4-dihydropyridines with nitrosonium—EPR evidence" *Res. Chem. Intermed.* **2001**, *27*, 219.
[17] Nakajima, K., Nojima, S., Sakata, K., Nishibayashi, Y., "Visible-Light-Mediated Aromatic Substitution Reactions of Cyanoarenes with 4-Alkyl-1, 4-dihydropyridines through Double Carbon–Carbon Bond Cleavage" *ChemCatChem* **2016**, *8*, 1028.

(DCB$^{\bullet-}$), generated upon SET reduction of DCB. This net aromatic *ipso*-substitution process affords the alkylated cyanoarene derivative **22**. The first use of 4-alkyl DHPs as radical sources for the construction of all-carbon quaternary centers was documented by Ma and Cheng (Figure 4.13b).[18] Herein, the photocatalytic SET oxidation and fragmentation of benzyl-DHP **20** furnished the benzyl radical **XII** that underwent radical-radical coupling with the open-shell intermediates **XIII**, obtained upon reductive debromination of α-bromo-isobutyrophenone **23**. The overall process provided the desired congested ketone derivative **24**.

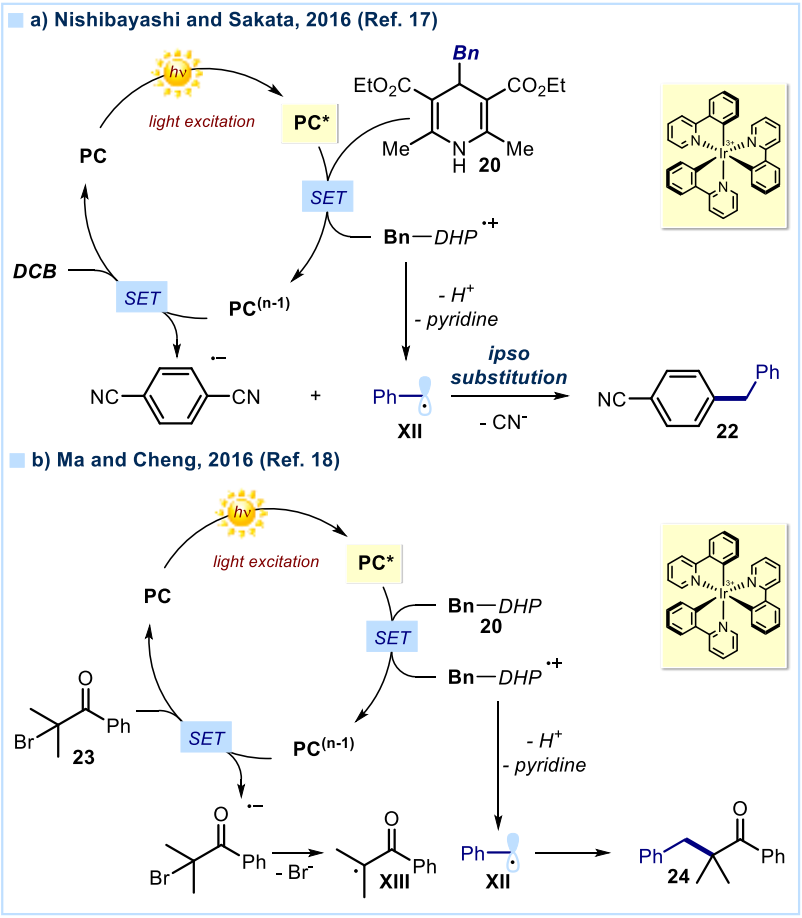

Figure 4.13: a) 4-Benzyl-DHP as radical sources in a photocatalyzed benzylation of cyanoarenes. b) 4-Alkyl-DHP as radical sources in the photocatalyzed synthesis of congested ketones.

[18] Chen, W., Liu, Z., Tian, J., Li, J., Ma, J., Cheng, X., Li, G., "Building congested ketone: substituted hantzsch ester and nitrile as alkylation reagents in photoredox catalysis" *J. Am. Chem. Soc.* **2016**, *138*, 12312.

These literature precedents prompted us to consider 4-alkyl-DHPs as suitable candidates for the development of novel excited iminium ion-mediated transformations. We started our investigation synthesizing 4-benzyl DHP, following a modification of the classical Hantzsch procedure (Figure 4.14a). The substrate was obtained reacting phenylacetaldehde with ethyl acetoacetate and ethyl aminocrotonate in the presence of a catalytic amount of tetrabutylammonium hydrogensulfate. When substrate **20** was submitted to the previously developed reaction conditions, we obtained the desired β-benzylation product **11c** in 55% yield and 74% ee.

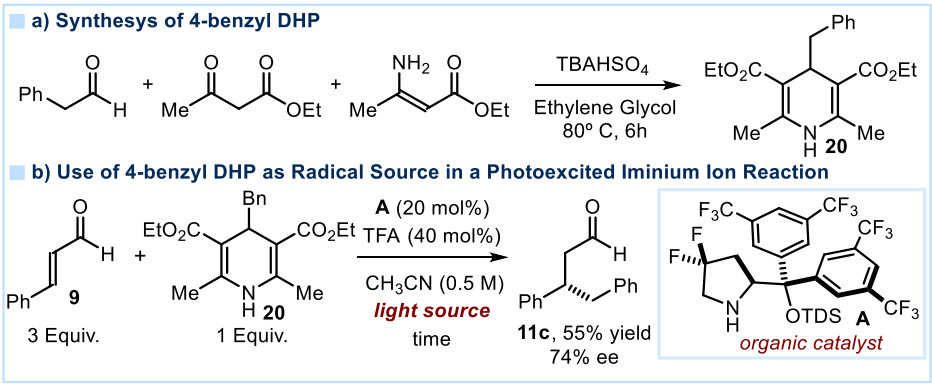

Figure 4.14: a) Modified Hantzsch procedure for the synthesis of 4-benzyl DHP. b) 4-Benzyl DHP as the radical precursor in a photoexcited iminium ion-mediated β-benzylation of enals.

Cyclic voltammetry (CV) measurement of substrate **20** revealed an irreversible oxidation peak with $E_p^A = E_{ox}$ (**20**$^{\bullet+}$/**20**) = +1.00 V. This value confirmed the capability of 4-alkyl DHP to serve as donor for iminium ions in their excited state.

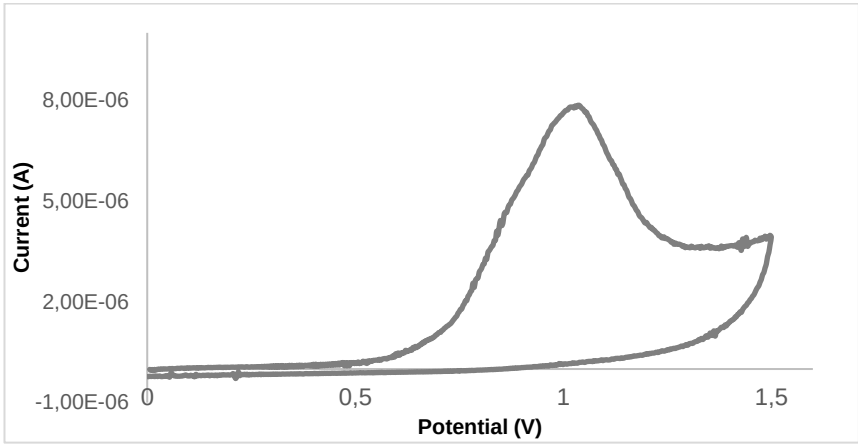

Figure 4.15: Cyclic voltammogram of benzyl dihydropyridine **20** [0.01 M] in [0.1 M] $TBAPF_6$ in CH_3CN. Sweep rate: 20 mV/s. Pt electrode working electrode, Ag/AgCl (KCl 3.5M) reference electrode, Pt wire auxiliary electrode. Irreversible oxidation. $E_p^A = E_{ox}$ (**20**$^{\bullet+}$**/20**) = +1.00 V; E_p^A is the anodic peak potential, while E^{ox} value describes the electrochemical properties of **20**.

4.3.5 Target of the Project

Encouraged by these preliminary results, we wondered if we could exploit 4-alkyl DHPs to stereoselectively install simple and not stabilized alkyl fragments at the β-position of enals via the excited iminium ion activation. The enantioselective β-alkylation of enals with simple alkyl fragments is a difficult target for many reasons. Despite the major progress achieved in the development of asymmetric conjugate addition reactions, the addition of hard carbon nucleophiles to α,β-unsaturated aldehydes has proven difficult. The main complication stems from the high reactivity of the aldehyde moiety, which enables a competing addition to the carbonyl, ultimately leading to a mixture of 1,2- and 1,4- addition adducts (Figure 4.16a). This regioselectivity issue was highlighted by Bräse, who reported that the catalytic addition of diethyl zinc to enals could proceed with high enantioselectivity but poor 1,4/1,2 selectivity (ranging from 4:1 to 1:1).[19] Subsequent studies by Alexakis demonstrated that a chiral copper catalyst could promote the addition of both dialkylzinc and Grignard reagents to enals.[20]

[19] a) Bräse, S., Höfener, S., "Asymmetric Conjugate Addition of Organozinc Compounds to α, β-Unsaturated Aldehydes and Ketones with [2.2] Paracyclophaneketimine Ligands without Added Copper Salts" *Angew. Chem. Int. Ed.* **2005**, *44*, 7879. b) Ay, S., Nieger, M., Bräse, S., "Co-Metal-Free Enantioselective Conjugate Addition Reactions of Zinc Reagents" *Chem. Eur. J.* **2008**, *14*, 11539.

[20] a) Palais, L., Babel, L., Quintard, A., Belot, S., Alexakis, A., "Copper-catalyzed enantioselective 1, 4-addition to α, β-unsaturated aldehydes" Org. Lett. 2010, 12, 1988. b) Goncalves-Contal, S., Gremaud, L., Palais, L., Babel, L., Alexakis, A., "Copper-Catalyzed Enantioselective Conjugate Addition to α, β-Unsaturated Aldehydes with Various Organometallic Reagents" *Synthesis* **2016**, *48*, 3301.

While the former reacted with high 1,4 regioselectivity but moderate stereocontrol, Grignard reagents afforded highly enantioenriched β-substituted enals along with a large amount of 1,2 addition adducts.

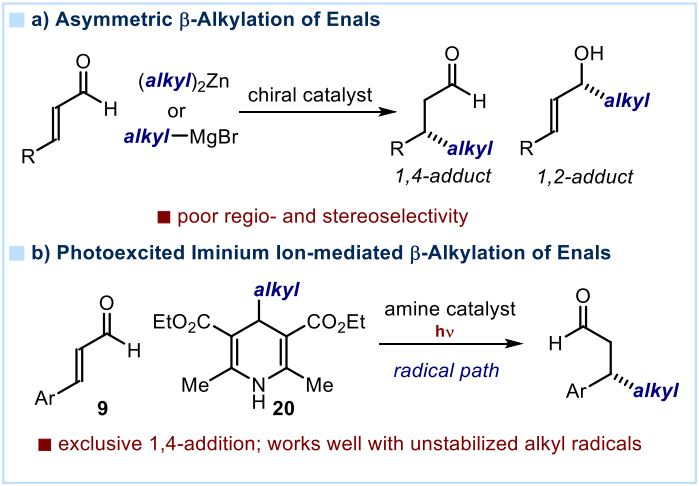

Figure 4.16: a) The previous catalytic asymmetric β-alkylation of enals. b) This work: the excited iminium ion-mediated β-alkylation of enals with 4-alkyl DHP as alkyl sources.

4.3.6 Reaction Optimization[21]

The screening of different reaction parameters led to the optimal reaction conditions for this transformation (Scheme 4.6).

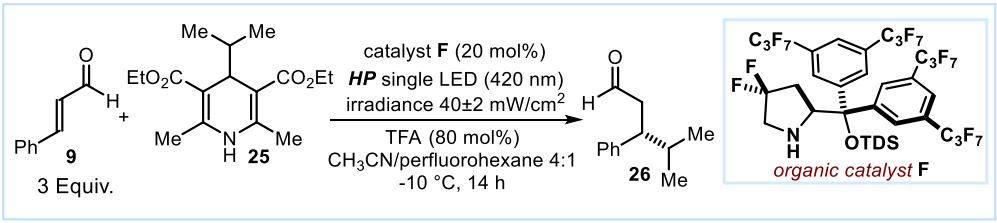

Scheme 4.6: Optimal condition for the β-alkylation of enals.

The reaction proceeded under 420 nm LED irradiation in the presence of the previously developed chiral organic catalyst **F**. 80 mol% of the acid co-catalyst were required to facilitate the formation of the active iminium ion intermediate, while a combination of acetonitrile/perfluorohexane 4:1 served as the best solvent mixture. Decreasing the temperature to -10° C secured a better stereoselectivity.

[21] The optimization process and the evaluation of the scope were conducted by Dr Charlie Verrier, Ms Nurtalya Alandini and Mr Cristopher Pezzetta.

4.3.7 Scope of the Reaction

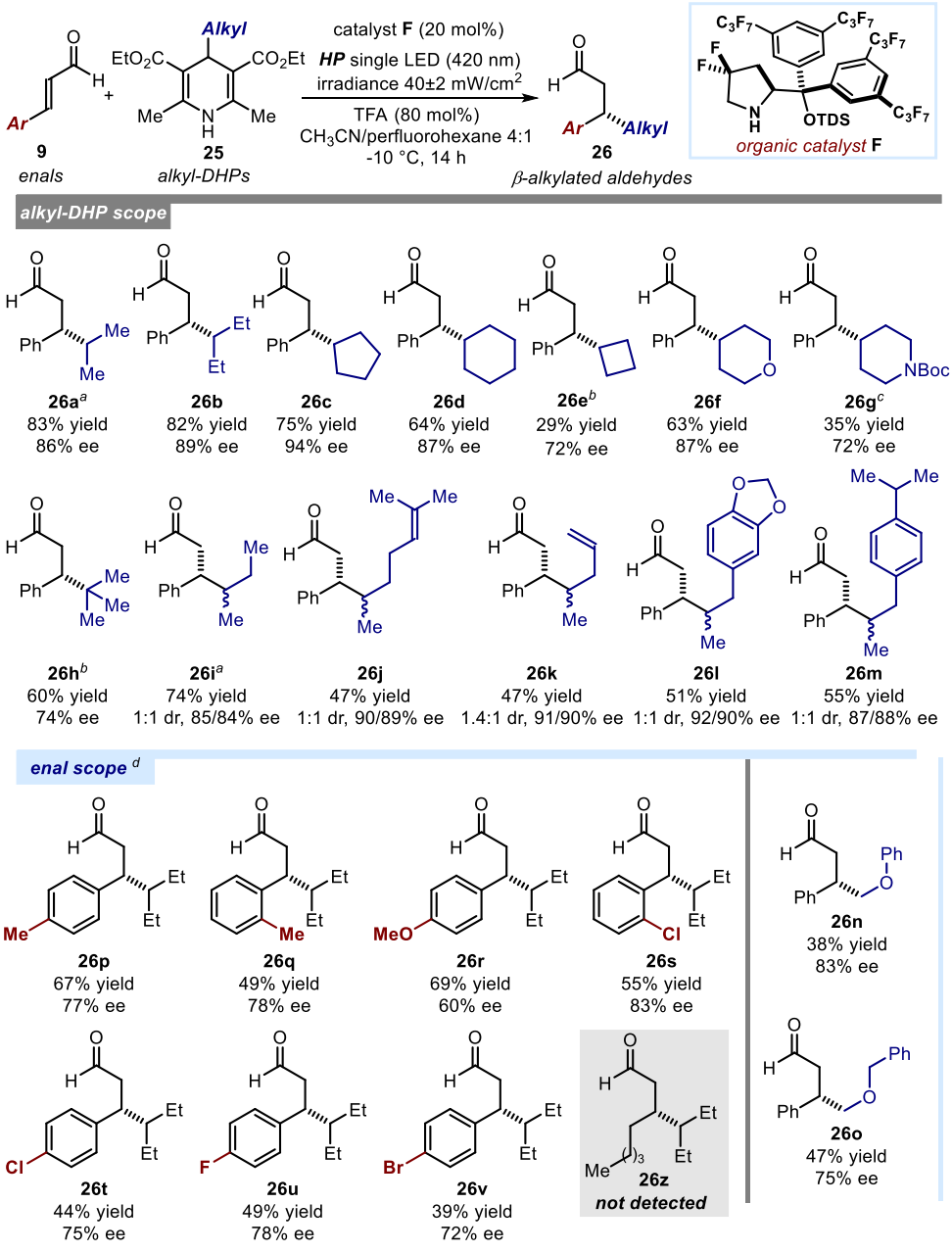

Figure 17: Survey of the enals **9** and the 4-alkyl-1,4-dihyyydropyridines **25** that can participate in the photochemical catalytic strategy for the asymmetric installation of alkyl fragments at the β position of enals. Reactions performed on a 0.1 mmol scale over 14 hours in a 4:1 CH_3CN/perfluorohexane (C_6F_{14}) solvent mixture (0.5 mL) using 3 Equiv. of **9** and an irradiance of 40 mW/cm². Yields and enantiomeric excesses of the isolated products are indicated below each entry. [a] Performed using 100 mol% of TFA in a 2:1 CH_3CN/C_6F_{14} solvent mixture (0.3 mL). [b] Performed using 40 mol% of TFA and the corresponding tetrabutylammonium trifluoroborate as the radical precursor. [c] Performed in dichloromethane using catalyst

F and 100 mol% of TFA. [d] Performed in a 2:1 CH_3CN/C_6F_{14} solvent mixture (0.3 mL); TDS: thexyl-dimethylsilyl.

With the best reaction conditions in hand, we next evaluated the scope of the transformation reacting different enals and alkyl DHPs. The results are summarized in Figure 4.17. Both linear and cyclic fragments could be successfully introduced at the β carbon of cinnamaldehyde **9**, exclusively leading to the 1,4-adducts with good yields and stereocontrol (products **26a-26m**). An oxygen-containing heterocyclic motif did not hamper the reaction (**26f**), while a piperidine moiety could be installed at the β position of **9** with good stereocontrol but a poor yield (product **26g**). Sterically demanding fragments were accommodated well, as demonstrated with the *tert*-butyl moiety. In this case, we used the corresponding *tert*-butyl trifluoroborate salt as radical source,[22] due to the difficulty to access sterically hindered dihydropyridines. The use of alkyl-DHPs bearing a chiral fragment afforded the formation of adducts **26i-26j**, that have two vicinal stereogenic centers, with high enantiomeric purity, albeit with a poor diastereomeric ratio. Interestingly, alkyl fragments adorned with both alkene and aromatic moieties could be installed, leading to the corresponding products **26k-26m**. Also primary radicals could successfully participate in this stereoselective coupling reaction when adorned with a stabilizing α-oxygen atom, leading to adducts **26n** and **26o**.

As for the scope of the α,β-unsaturated aldehydes **9**, different substituents at the β aromatic moiety could be accommodated well, regardless of their electronic and steric properties and position on the phenyl ring. The β-alkylation products **26p-26v** were formed with exclusive 1,4-selectivity, in moderate to good chemical yields and with good stereocontrol. As a limitation of the method, the presence of a linear β-alkyl fragment in **9** completely inhibited the reaction (product **26z**). Conversely, the desired product was obtained in 12% yield when *tert*-butyl acrolein was submitted to the optimized condition.

4.3.8 Functionalization of Glucosides

To further expand the synthetic utility of the methodology, the optimized conditions were applied to the stereocontrolled preparation of saccharide-containing aldehydes **28** (Figure 4.17). The 1,4-dihydropyridine **27**, which contains a galactosyl moiety, was easily prepared from the corresponding protected sugar.[23] **27** was used as radical precursor to access the target adducts **28** in fairly good yields and high stereocontrol. The reactions were performed with both the enantiomers of the chiral organic catalyst **A**, which provided access to different

[22] Trifluoroborates salts are widely used as radical precursor in SET oxidative reactions. Tellis, J. C., Primer, D. N., Molander, G. A., "Single-Electron Transmetalation in Organoboron Cross-coupling by Photoredox/Nickel Dual Catalysis" *Science* **2014**, *345*, 433.

[23] Tewari, N., Dwivedi, N., Tripathi, R. P., "Tetrabutylammonium hydrogen sulfate catalyzed eco-friendly and efficient synthesis of glycosyl 1, 4-dihydropyridines" *Tetrahedron Lett.* **2004**, *45*, 9011.

diastereoisomers of the galactose derivatives (adduct **28a** and **28b**). These results indicate that the chiral organic catalyst governs the stereoselectivity of the process, and can overwrite the inherent stereochemical information encoded within the chiral substrate **27**. A crystal of the galactose derivative **28a** was obtained and submitted to X-ray crystallographic analysis, thus establishing the absolute stereochemistry of the adduct.

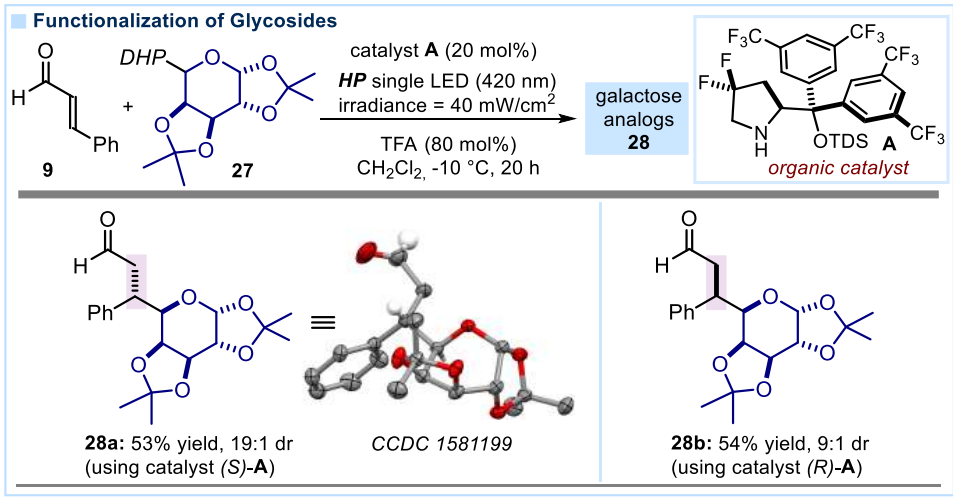

Figure 4.17: Stereocontrolled synthesis of saccharide-containing aldehydes.

4.3.9 Reaction Mechanism

The mechanism for this transformation is similar to the one proposed for the previously discussed β-benzylation reaction and it is depicted in Figure 4.18. The condensation of the chiral secondary amine catalyst **14** with the enal **9**, in the presence of the acid co-catalyst, furnishes the iminium ion **II**. Visible-light excitation gives access to an electronically excited **II***, which promotes the SET oxidation of the 4-alkyl dihydropyridine. This redox event affords the 5π-electron β-enaminyl radical intermediate **II** along with the radical cation **IX**, which undergoes irreversible fragmentation to provide the key alkyl radical **X**. The stereoselective intermolecular coupling of the chiral β-enaminyl radical **II** with **X** forms a new C–C bond while forging the stereogenic center. Hydrolysis of the resulting enamine intermediate **XI** regenerates the catalyst **14** while liberating the β-alkylated aldehyde product **4**.

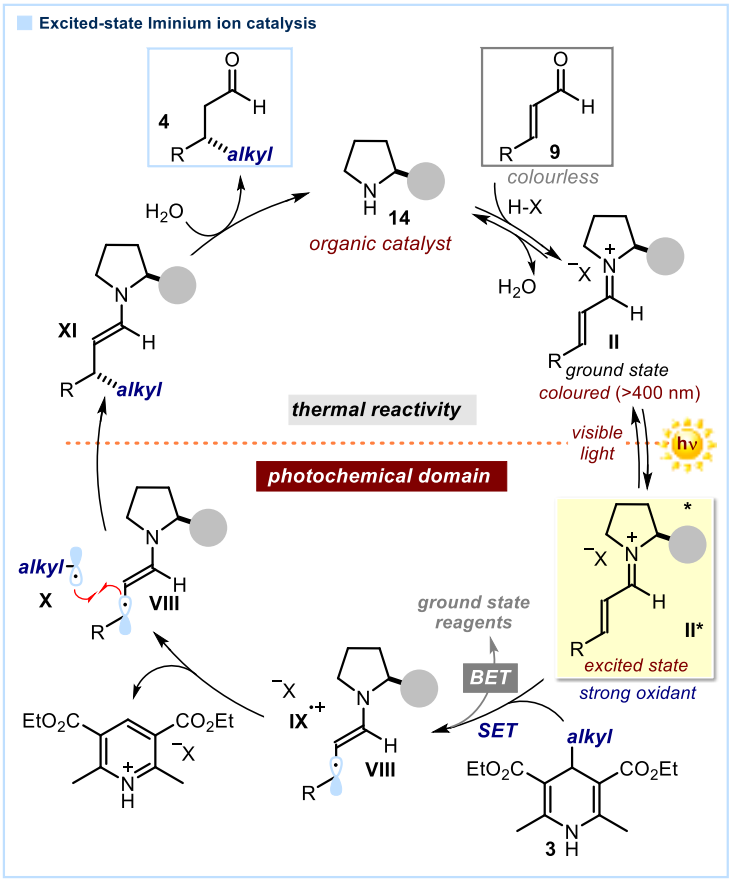

Figure 4.18: Proposed mechanism for the excited iminium ion-mediated β-alkylation of enals.

4.4 Conclusions

This investigation led to the identification of several donor compounds that can productively participate in the excited iminium ion chemistry. Relying on the analysis of the redox potential of the substrates, we evaluated the possibility to generate alkyl radicals from various precursors, including oxiranes, acetals, and 4-alkyl-dihydropyridines. The radical generation strategy relied on the C–C bond fragmentation, which was crucial to prevent the back electron transfer.

Ultimately, we developed a method for the direct regio- and stereoselective installation of alkyl fragments at the β position of α,β–unsaturated aldehydes. The chemistry relies on the visible light excitation of chiral iminium ions, which turns them into strong oxidants able to generate C(sp^3)-centered radicals from readily available 4-alkyl-1,4-dihydropyridines. The reaction protocol is operationally simple and allows the synthesis of several enantioenriched

β-alkylated aldehydes. Moreover, it is amenable to the asymmetric functionalization of saccharides.

4.5 Experimental Section

General Information. The NMR spectra were recorded at 400 MHz and 500 MHz for ^{1}H or at 100 MHz and 125 MHz for ^{13}C, respectively. The chemical shifts (δ) for ^{1}H and ^{13}C are given in ppm relative to residual signals of the solvents ($CHCl_3$ @ 7.27 ppm ^{1}H NMR, 77.00 ppm ^{13}C NMR). Coupling constants are given in Hz. The following abbreviations are used to indicate the multiplicity: s, singlet; d, doublet; t, triplet; q, quartet; m, multiplet; br s, broad signal.

High-resolution mass spectra (HRMS) were obtained from the ICIQ High Resolution Mass Spectrometry Unit on MicroTOF Focus and Maxis Impact (Bruker Daltonics) with electrospray ionization. X-ray data were obtained from the ICIQ X-Ray Unit using a Bruker-Nonius diffractometer equipped with an APPEX 2 4K CCD area detector. Optical rotations were measured on a Polarimeter Jasco P-1030 and are reported as follows: $[\alpha]_D$ rt (c in g per 100 mL, solvent).

UV-vis measurements were carried out on a Shimadzu UV-2401PC spectrophotometer equipped with photomultiplier detector, double beam optics and D_2 and W light sources. Cyclic voltammetry studies were carried out on a Princeton Applied Research PARSTAT 2273 potentiostat offering compliance voltage up to ± 100 V (available at the counter electrode), ± 10 V scan range and ± 2 A current range.

General Procedures. All reactions were set up under an argon atmosphere in oven-dried glassware using standard Schlenk techniques, unless otherwise stated. Synthesis grade solvents were used as purchased. Anhydrous solvents were taken from a commercial SPS solvent dispenser. Chromatographic purification of products was accomplished using force-flow chromatography (FC) on silica gel (35-70 mesh). For thin layer chromatography (TLC) analysis throughout this work, Merck precoated TLC plates (silica gel 60 GF_{254}, 0.25 mm) were used, using UV light as the visualizing agent and and either phosphomolybdic acid in EtOH, dinitrophenylhydrazine in $EtOH/H_2O$ or basic aqueous potassium permangante ($KMnO_4$), and heat as developing agents. Organic solutions were concentrated under reduced pressure on a Büchi rotary evaporator (in vacuo at 40 ºC, ~5 mbar).

Determination of Diastereomeric Ratio. The diastereomeric ratio was determined by ^{1}H NMR analysis of the crude reaction mixture through integration of diagnostic signals.

Determination of Enantiomeric Purity: HPLC analysis on chiral stationary phase was performed on an Agilient 1200 series HPLC, using a Daicel Chiralpak IC-3 column with *i*PrOH:hexane as the eluent. UPC^2 analysis on chiral stationary phase was performed on a Waters Acquity instrument using a CEL1, CEL2, ID3 or IE3 chiral colums. The exact conditions for the analyses are specified within the characterization section. HPLC/ UPC^2

traces were compared to racemic samples prepared by running the reaction in the presence of a catalytic amount (20 mol%) of racemic 2-tert-butyl-3-methyl-5-benzyl-4-imidazolidinone, which is commercially available form Sigma Aldrich.

Materials: Commercial grade reagents and solvents were purchased at the highest commercial quality from Sigma Aldrich, Fluka, Acros Organics, Fluorochem or Alfa Aesar and used as received, unless otherwise stated. Chiral secondary amine catalysts **A** and **F** were prepared as described in the previous chapter. The majority of enals **9** are commercially available, cinnamaldehyde **9a** was distilled prior to use. Enals **9o** and **9q** were prepared according to the procedures described in the previous chapter. All the alkyl trifluoroborate salts and the majority of 4-alkyl-1,4-dihydropyridine derivatives (Hantzsch esters) were prepared according to known literature procedures.[24]

Synthesis of 4-Alkyl-1,4-Dihydropyridines 20

Many 4-alkyl-1,4-dihydropyridines were synthesized using procedure reported in the literature. The following Hantzsch esters were prepared from the corresponding aldehydes.

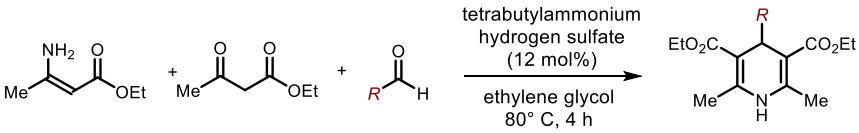

In accordance to the reported procedure[24a] ethyl-3-aminocrotonate (1.0 equiv) and ethylene glycol (2.5M) were added to a flask under nitrogen. Next, ethyl acetoacetate (1.0 equiv) was added followed by aldehyde (1.0 equiv) and tetrabutylammonium hydrogen sulfate (12 mol%). The resultant solution was heated at 80 °C for 4 hours, then cooled and diluted with ethyl acetate. The solution was added to a solution of brine and separated using ethyl acetate (3 x 50 mL). The organic layers were combined, dried ($MgSO_4$) and concentrated. The crude material was purified by flash column chromatography to furnish the desired 4-alkyl-1,4-dihydropyridine.

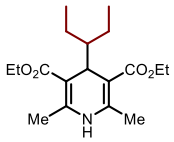

Diethyl 4-(3-pentyl)-2,6-dimethyl-1,4-dihydropyridine-3,5-dicarboxylate.

Prepared according to the procedure described above using 2-ethyl butanal (1.23 mL, 10.0 mmol). The crude material was purified by flash column chromatography (95:5 cyclohexane.EtOAc) to give the corresponding product (1.21 g, 36% yield) as a yellow solid.

---

[24] a) Gutiérrez-Bonet, A. l., Tellis, J. C., Matsui, J. K., Vara, B. A., Molander, G. A., "1, 4-Dihydropyridines as Alkyl radical Precursors: Introducing the Aldehyde Feedstock to Nickel/Photoredox Dual Catalysis" *ACS Catal.* **2016**, *6*, 8004. b) Dreher, S. D., Dormer, P. G., Sandrock, D. L., Molander, G. A., "Efficient Cross-Coupling of Secondary Alkyltrifluoroborates with Aryl Chlorides-Reaction Discovery Using Parallel Microscale Experimentation" *J. Am. Chem. Soc.* **2008**, *130*, 9257.

^{1}H NMR (500 MHz, $CDCl_3$) δ 5.51 (1H, s, N**H**), 4.25-4.11 (5H, m, 2 x OC**H**$_2$CH$_3$ + C**H**$_{(pyridyl)}$), 2.29 (6H, s, 2 x C**H**$_3$), 1.31 (6H, td, *J* = 7.1, 0.5 Hz, 2 x OCH$_2$C**H**$_3$), 1.23-1.02 (5H, m, C**H**(C**H**$_2$CH$_3$)$_2$), 0.87 (6H, t, *J* = 7.3 Hz, CH(CH$_2$C**H**$_3$)$_2$);
^{13}C NMR (125.6 MHz, $CDCl_3$) δ 168.8 (2 x C), 144.6 (2 x C), 102.1 (2 x C), 59.6 (2 x CH_2), 49.8 (CH), 34.6 (CH), 21.2 (2 x CH_2), 19.3 (2 x CH_3), 14.3 (2 x CH_3), 11.8 (2 x CH_3).
HRMS (ESI) Exact mass calculated for $C_{18}H_{28}NO_4$ $[M-H]^-$: 322.2024, found: 322.2012.

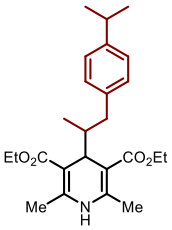

Diethyl 4-(1-(4-*iso*-propyl)phenylpropan-2-yl)-2,6-dimethyl-1,4-dihydropyridine-3,5-dicarboxylate.

Prepared according to the procedure described above using 3-(4-isopropylphenyl)isobutyraldehyde (2.00 mL, 10.0 mmol). The crude material was purified by flash column chromatography (98:2 cyclohexane/EtOAc) to give the corresponding product (1.56 g, 38% yield) as a yellow oil.

^{1}H NMR (500 MHz, $CDCl_3$) δ 7.12-7.07 (2H, m, Ar**H**), 7.05-6.98 (2H, m, Ar**H**), 5.57 (1H, s, N**H**), 4.29-4.06 (5H, m, OC**H**$_2$CH$_3$ + C=CC**H**), 2.86 (1H, app p, *J* = 6.9 Hz, C**H**(CH$_3$)$_2$), 2.77 (1H, dd, *J* = 13.3, 3.6 Hz, C**H**CH$_2$Ar), 2.32 (6H, app d, *J* = 1.7 Hz, 2 x NCC**H**$_3$), 2.09 (1H, dd, *J* = 13.3, 11.2 Hz, C**H**$_2$Ar), 1.75 (1H, ddd, *J* = 11.1, 7.5, 4.2 Hz, C**H**$_2$Ar), 1.31 (6H, dt, *J* = 12.2, 7.1 Hz, OCH$_2$C**H**$_3$), 1.23 (6H, d, *J* = 6.9 Hz, CH(C**H**$_3$)$_2$), 0.65 (3H, d, *J* = 6.8 Hz, CHC**H**$_3$).
^{13}C NMR (125.6 MHz, $CDCl_3$) δ 168.7 (C=O), 168.4 (C=O), 145.9 (C), 144.71 (C), 144.65 (C), 139.4 (C), 128.9 (2 x CH), 126.0 (2 x CH), 102.0 (C), 101.6 (C), 59.7 (2 x CH_2), 43-1 (CH), 38.84 (CH_3), 39.76 (CH_3), 33.7 (CH_2), 24.1 (2 x CH_3), 19.5 (CH), 19.4 (CH), 14.5 (CH_3), 14.44 (CH_3), 14.38 (CH_3).
HRMS (ESI) Exact mass calculated for $C_{25}H_{34}NO_4$ $[M-H]^-$: 412.2493, found: 412.2481.

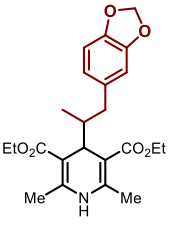

Diethyl 4-(1-(benzo[*d*][1,3]dioxol-5-yl)propan-2-yl)-2,6-dimethyl-1,4-dihydropyridine-3,5-dicarboxylate.

Prepared according to the procedure described above using 3-(benzo[*d*][1,3]dioxol-5-yl)-2-methylpropanal (1.92 g, 10.0 mmol). The crude material was purified by flash column chromatography (80:20 cyclohexane/EtOAc) to give the corresponding product (2.05 g, 49% yield) as a yellow oil.

^{1}H NMR (500 MHz, $CDCl_3$) δ 6.68 (1H, d, *J* = 7.9 Hz, Ar**H**), 6.58 (1H, d, *J* = 1.5 Hz, Ar**H**), 6.53 (1H, dd, *J* = 7.9, 1.5 Hz), 5.89 (2H, app q, *J* = 1.5 Hz, OC**H**$_2$O), 5.66 (1H, br s, N**H**), 4.28-4.13 (4H, m, OC**H**$_2$CH$_3$), 4.11 (1H, d, *J* = 4.8 Hz, C=CC**H**), 2.72 (1H, dd, *J* = 13.3, 3.5 Hz, ArC**H**$_2$), 2.32 (6H, app d, *J* = 1.6, NCC**H**$_3$), 2.03 (1H, dd, *J* = 13.3, 11.3 Hz, ArC**H**$_2$),

1.72-1.65 (1H, m, C**H**CH_2Ar), 1.32 (3H, t, *J* = 7.1 Hz, $OCH_2C\mathbf{H}_3$), 1.30 (3H, t, *J* = 7.1 Hz, $OCH_2C\mathbf{H}_3$), 0.63 (3H, d, *J* = 6.8 Hz, $CHC\mathbf{H}_3$);

^{13}C NMR (125.6 MHz, $CDCl_3$) δ 168.6 (C=O), 168.4 (C=O), 147.3 (C), 145.2 (C), 144.8 (C), 144.7 (C), 136.0 (C), 121.7 (CH), 109.3 (CH), 107.8 (CH), 101.9 (C), 101.5 (C), 100.6 (CH_2), 59.7 (CH_2), 43.3 (CH), 39.0 (CH_2), 38.7 (CH), 19.5 (CH_3), 19.4 (CH_3), 14.4 (CH_3), 14.3 (CH_3).

HRMS (ESI) Exact mass calculated for $C_{29}H_{29}NNaO_6$ $[M+Na]^+$: 438.1887, found: 438.1885.

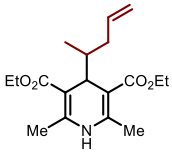

Diethyl 2,6-dimethyl-4-(pent-4-en-2-yl)-1,4-dihydropyridine-3,5-dicarboxylate

Prepared according to the procedure described above using 2-methylpent-4-enal (473 mg, 4.8 mmol). The crude material was purified by flash column chromatography (80:20 hexane/EtOAc) to give the corresponding product (713 mg, 46% yield) as a light yellow oil that solidified upon standing.

^{1}H NMR (500 MHz, $CDCl_3$) δ 5.77-5.68 (1H, m, $CH_2C\mathbf{H}=CH_2$), 5.60 (1H, s, N**H**), 4.97-4.91 (2H, m, CH=$C\mathbf{H}_2$), 4.26-4.13 (4H, m, $OC\mathbf{H}_2CH_3$), 4.04 (1H, d, *J* = 4.8 Hz, C=CC**H**), 2.31 (6H, s, $NCC\mathbf{H}_3$), 2.18-2.11 (1H, m, $C\mathbf{H}_2CH=CH_2$), 1.72-1.64 (1H, m, $C\mathbf{H}_2CH=CH_2$), 1.54-1.46 (1H, m, CC**H**CH), 1.30 (6H, t, *J* = 7.1 Hz, $OCH_2C\mathbf{H}_3$), 0.73 (3H, d, *J* = 6.9 Hz, $CHCHC\mathbf{H}_3$);

^{13}C NMR (125.6 MHz, $CDCl_3$) δ 168.6 (C=O), 168.4 (C=O), 144.6 (C), 138.6 (CH), 115.0 (CH_2), 102.0 (C), 101.5 (C), 59.6 (CH_2), 40.9 (CH), 38.1 (CH), 37.1 (CH_2), 19.5 (CH_3), 19.4 (CH_3), 14.9 (CH_3), 14.4 (CH_3).

HRMS (ESI) Exact mass calculated for $C_{18}H_{27}NNaO_4$ $[M+Na]^+$: 344.1832, found: 344.1834.

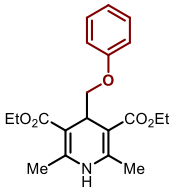

Diethyl 2,6-dimethyl-4-(phenoxymethyl)-1,4-dihydropyridine-3,5-dicarboxylate.

Prepared according to the procedure described above using 2-phenoxyacetaldehyde (1.3 g, 9.55 mmol). The crude material was purified by flash column chromatography (hexane/EtOAc 80:20) to give the corresponding product (2.2 g, 64% yield) as a light yellow solid.

^{1}H NMR (500 MHz, $CDCl_3$) δ 7.22 (dd, *J* = 8.8, 7.0 Hz, 2H, Ar**H**), 6.90 – 6.86 (m, 3H, Ar**H**), 5.77 (bs, 1H, N**H**), 4.42 (t, *J* = 5.8 Hz, 1H, C=CC**H**), 4.12 (qq, *J* = 10.8, 7.1 Hz, 4H, $OC\mathbf{H}_2CH_3$), 3.86 (d, *J* = 5.8 Hz, 2H, $OC\mathbf{H}_2$), 2.30 (s, 6H, $NCC\mathbf{H}_3$), 1.24 – 1.18 (m, 6H, $OCH_2C\mathbf{H}_3$).

^{13}C NMR (125.6 MHz, $CDCl_3$) δ 167.9 (2 x C=O), 159.4 (C), 146.2 (2 x C), 129.4 (2 x CH), 120.3 (CH), 114.6 (2 x CH), 100.1 (2 x C), 70.5 (CH_2), 60.0 (2 x CH_2), 33.9 (CH), 19.6 (2 x CH_3), 14.4 (2 x CH_3).

Synthesis of the Chiral Amine Catalyst ((*R*)-A)

The chiral amine catalyst (*R*)-**A** was synthesized according to the procedure reported in the previous chapter.

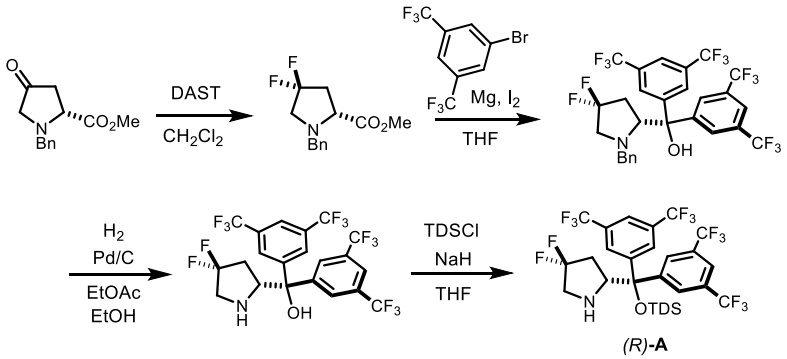

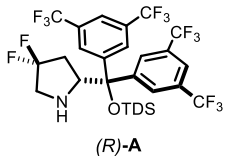

(*R*)-2-(Bis-(3,5-bis-(trifluoromethyl)-phenyl)-(((2,3-dimethylbutan-2-yl)-dimethylsilyl)-oxy)-methyl)-4,4-difluoropyrrolidine ((*R*)-A).

^{1}H NMR (400 MHz, $CDCl_3$): δ 8.10 (s, 2H, *ortho*), 8.01 (s, 2H, *para* and *para*'), 7.92 (s, 2H, *ortho*'), 4.47 (br t, *J* = 8.3 Hz, 1H, C2**H**), 3.21-3.09 (m, 1H, C5**H**H), 2.69-2.55 (m, 1H, C5H**H**), 2.31-2.11 (m, 2H, C3**H**H and N**H**), 1.95-1.69 (m, 2H, C3H**H** and SiCC**H**), 0.95 (d, *J* = 3.0 Hz, 3H, SiCCHC**H**$_3$), 0.94 (d, *J* = 3.0 Hz, 3H, SiCCHC**H**$_3$'), 0.89 (s, 3H, SiCC**H**$_3$), 0.87 (s, 3H, SiCC**H**$_3$'), -0.13 (s, 3H, SiC**H**$_3$), -0.47 (s, 3H, SiC**H**$_3$).

^{13}C NMR (101 MHz, $CDCl_3$): δ 146.3 (*ipso*), 144.8 (*ipso*'), 131.9 (2C, q, J_{CF} = 32.0 Hz, *meta*), 131.2 (2C, q, J_{CF} = 33.2 Hz, *meta'*), 129.7 (dd, J_{CF} = 254.0 Hz, 246.9 Hz, *C4*), 129.5 (2C, q, J_{CF} = 4.1 Hz, *ortho*), 128.8 (2C, q, J_{CF} = 4.1 Hz, *ortho*'), 123.4 (2C, q, J_{CF} = 272.8 Hz, Ar**C**F$_3$), 123.2 (2C, q, J_{CF} = 272.9 Hz, Ar'**C**F$_3$), 122.6 (apparent p, J_{CF} = 3.8 Hz, *para*), 122.4 (apparent p, J_{CF} = 3.8 Hz, *para*'), 82.2 (*C6*), 62.8 (dd, J_{CF} = 6.5 Hz, 1.3 Hz, *C2*), 53.9 (t, J_{CF} = 28.8 Hz, *C3*), 37.6 (t, J_{CF} = 25.0 Hz, *C5*), 33.9 (SiC**C**H), 26.0 (Si**C**CH), 20.4 (SiC**C**H$_3$), 20.2 (SiC**C**H$_3$'), 18.7 (2C, SiCCH**C**H$_3$), -0.03 (Si**C**H$_3$), -0.80 (Si**C**H$_3$').

^{19}F NMR (376 MHz, $CDCl_3$): δ -63.01 (s, 6F, ArCF$_3$), -63.05 (s, 6F, Ar'CF$_3$), -97.7 (dp, J_{FF} = 231.5 Hz, J_{HF} = 18.7 Hz, 1F, C4*F*F), -104.1 (br d, J_{FF} = 228.7 Hz, 1F, C4F*F*).

HRMS: calculated for $C_{29}H_{32}F_{14}NOSi$: 704.2024, found: 704.2052.

$[\alpha]_D^{26}$ = –2.2 (c= 0.62, $CHCl_3$). Lit: $[\alpha]_D^{26}$ = +1.9 (c= 0.5 CH_2Cl_2, for (*S*) enantiomer.

General Procedure for the Photochemical β-Alkylation of Enals

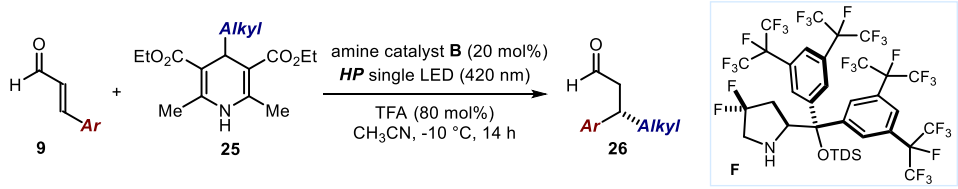

General Procedure: To a 5 mL argon-purged glass vial, containing the amine catalyst **F** (22.1 mg, 0.02 mmol, 20 mol%) and the desired 4-alkyl-1,4-dihydropyridine **2** (0.1 mmol, 1 equiv.), was added enal **9** (0.3 mmol, 3 equiv.) Then 400 µL of an argon-sparged 0.2 M acetonitrile solution of TFA (6.2 µL, 0.08 mmol, 80 mol%) and perfluorohexane (100 µL) were added. The vial was sealed with Parafilm, and then placed into an aluminium block on a 3D-printed holder, fitted with a 420 nm high-power single LED. The irradiance was fixed at 40±2 mW/cm^2, as controlled by an external power supply and measured using a photodiode light detector at the start of each reaction. This setup secured a reliable irradiation while keeping a distance of 1 cm between the reaction vessel and the light source.

The temperature was kept at -10 °C with a chiller connected to the irradiation plate (the setup is detailed in Figure S1). The reaction was stirred for the indicated time (generally 14 hours), then the solvent was evaporated and the crude mixture was purified by flash column chromatography on silica gel to furnish the product **26.**

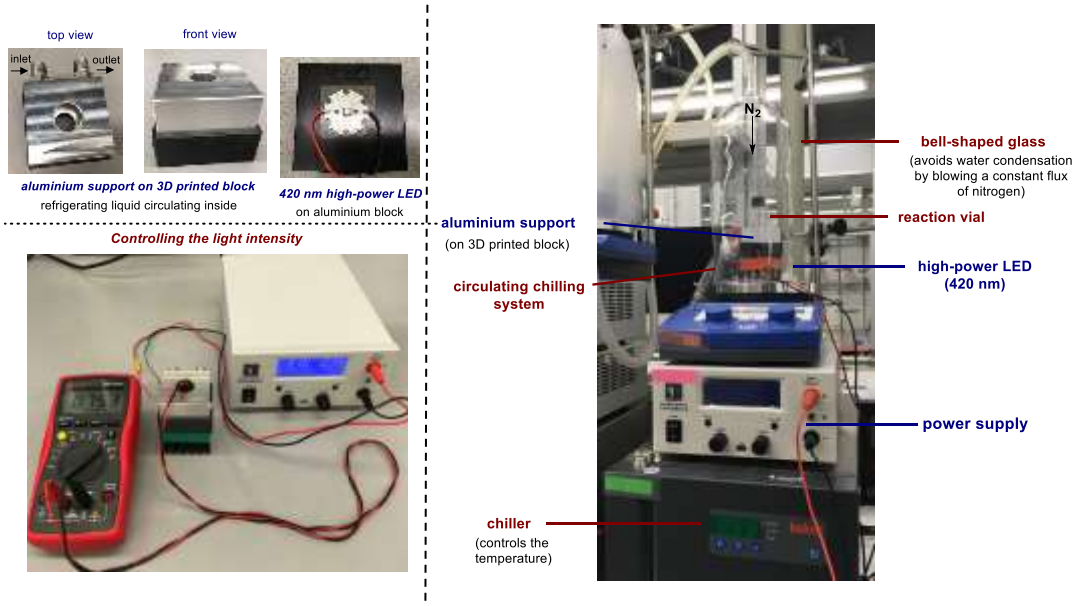

Characterization of Products

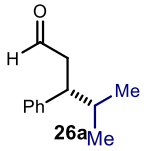

(*R*)-4-Methyl-3-phenylpentanal (26a)

Prepared according to the general procedure using cinnamaldehyde (39.6 mg, 0.3 mmol), aminocatalyst **F** (22.1 mg, 20 mol%), the corresponding dihydropyridine (29.5 mg, 0.1 mmol), trifluoroacetic acid (7.6 µL, 0.1 mmol), acetonitrile (200 µL) and perfluorohexane (100 µL). The crude material was purified by flash column chromatography (pentane/diethyl ether 99.7:0.3) to give the product **26a** (14.6 mg, 83% yield, 86% ee, average of two runs) as a colourless oil that displayed spectroscopic data consistent with those reported previously.[3,6] The enantiomeric excess of the corresponding alcohol (obtained upon reduction with sodium borohydride) was determined by UPC[2] analysis using a CEL2 chiral column: after 1 min of 100% CO_2, gradient up to 60:40 CO_2/isopropanol over 5 minutes, curve 6), flow rate 2 mL/min. τ_{minor} = 3.31 min, τ_{major} = 3.51 min (86% ee); $[\alpha]_D^{26}$ = –14.3 (c = 0.57, CH_2Cl_2, 86% ee), Lit: $[\alpha]_D^{26}$ = +14.9 (c = 1.04 CH_2Cl_2, 83% ee, for (*S*) enantiomer).[25]

^{1}H NMR (400 MHz, $CDCl_3$) δ 9.61 (1H, t, *J* = 2.2 Hz, C**H**O), 7.33-7.28 (2H, m, Ar**H**), 7.25-7.18 (1H, m, Ar**H**), 7.18-7.13 (2H, m, Ar**H**), 2.96 (1H, ddd, *J* = 9.5, 7.5, 5.5 Hz, PhC**H**), 2.84-2.71 (2H, m, CHOC**H**$_2$), 1.95-1.81 (1H, m, C**H**$(CH_3)_2$), 0.96 (3H, d, *J* = 6.7 Hz, C**H**$_3$), 0.79 (3H, d, *J* = 6.7 Hz, C**H**$_3$);

^{13}C NMR (101 MHz, $CDCl_3$) δ 202.4 (C=O), 142.5 (C), 128.3 (CH), 128.2 (CH), 126.5 (CH), 47.2 (CH_2), 46.9 (CH), 33.4 (CH), 20.5 (CH_3), 20.2 (CH_3).

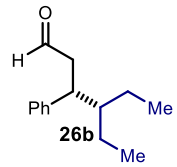

(*R*)-4-ethyl-3-phenylhexanal (26b) Prepared according to the general procedure using cinnamaldehyde (39.6 mg, 0.3 mmol), aminocatalyst **F** (22.1 mg, 20 mol%), the corresponding dihydropyridine (32.3 mg, 0.1 mmol), trifluoroacetic acid (6.2 µL, 0.08 mmol), acetonitrile (400 µL) and perfluorohexane (100 µL). The crude material was purified by flash column chromatography (pentane/diethyl ether 99.7:0.3) to give the product **26b** (17.6 mg, 86% yield, 88% ee, average of two runs) as a colourless oil. The enantiomeric excess of the corresponding alcohol (obtained upon reduction with sodium borohydride) was determined by HPLC analysis on a Agilent IC-3 column, 95:05 hexane/*i*-PrOH, flow rate 0.6 mL/min, 20 °C. λ = 215 nm. τ_{minor} = 16.0 min, τ_{major} = 20.1 min (88% ee). $[\alpha]_D^{26}$ = –4.49 (c = 0.79, $CHCl_3$, 88% ee).

^{1}H NMR (500 MHz, $CDCl_3$) δ 9.60 (1H, t, *J* = 2.3 Hz, C**H**O), 7.32-7.27 (2H, m, Ar**H**), 7.23-7.18 (3H, m, Ar**H**), 3.25 (1H, q, *J* = 7.4 Hz, PhC**H**), 2.77-2.74 (2H, m, CHOC**H**$_2$), 1.51-1.39 (1H, m, CH(C**H**$_2$CH$_3$)$_2$), 1.37-1.23 (3H, m, CH(C**H**$_2$CH$_3$)$_2$), 1.11 (1H, dp, *J* = 14.5 Hz, 7.4 Hz, PhCHC**H**), 0.90 (3H, t, *J* = 7.4 Hz, CH(CH_2C**H**$_3$)$_2$), 0.83 (3H, t, *J* = CH(CH_2C**H**$_3$)$_2$);

[25] Tanaka, K., Fu, G. C., "A Versatile new Catalyst for the Enantioselective Isomerization of Allylic Alcohols to Aldehydes: Scope and Mechanistic Studies" *J. Org. Chem.* **2001**, *66*, 8177.

^{13}C NMR (125.8 MHz, $CDCl_3$) δ 202.6 (C=O), 142.8 (C), 128.4 (2 x CH), 128.3 (2 x CH), 126.4 (CH), 46.7 (CH_2), 46.0 (CH), 41.9 (CH), 22.3 (CH_2), 21.9 (CH_2), 11.1 (CH_3), 10.8 (CH_3).
HRMS (ESI) Exact mass calculated for $C_{14}H_{20}NaO$ $[M+Na]^+$: 227.1406, found: 227.1399.

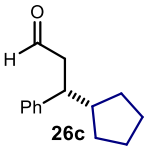

(*R*)-3-cyclopentyl-3-phenylpropanal (26c)

Prepared according to the general procedure using cinnamaldehyde (39.6 mg, 0.3 mmol), aminocatalyst **F** (22.1 mg, 0.02 mmol), the corresponding dihydropyridine (32 mg, 0.1 mmol), trifluoroacetic acid (6.2 µL, 0.08 mmol), acetonitrile (400 µL) and perfluorohexane (100 µL). The crude material was purified by flash column chromatography (pentane/diethyl ether 99.7:0.3) to give the product **26c** (15.1 mg, 75% yield, 94% ee, average of two runs) as a colourless oil. The enantiomeric excess of the corresponding alcohol (obtained upon reduction with sodium borohydride) was determined to be 94% by HPLC analysis on a Daicel Chiralpack IC-3 column: 90:10 hexane/*i*-PrOH, flow rate 0.6 mL/min, 20 °C, λ = 215 nm. τ_{minor} = 11.5 min, τ_{major} = 14.5 min. $[\alpha]_D^{26}$ = +15.1 (c= 0.40, $CHCl_3$, 94% ee).
^{1}H NMR (500 MHz, $CDCl_3$) δ 9.60 (1H, t, *J* = 2.3 Hz, C**H**O), 7.31-7.25 (2H, m, Ar**H**), 7.21-7.17 (3H, m, Ar**H**), 2.94 (1H, td, *J* = 9.7, 5.0 Hz, ArC**H**), 2.83-2.72 (2H, m, C**H**$_2$CHO), 2.10-2.02 (1H, m, C**H**CHCH$_2$CHO), 1.91-1.84 (1H, m, cyclopentyl**H**), 1.73-1.62 (1H, m, cyclopentyl**H**), 1.63-1.52 (2H, m, cyclopentyl**H**), 1.49-1.35 (2H, m, cyclopentyl**H**), 1.26-1.16 (1H, m, cyclopentyl**H**), 1.09-1.00 (1H, m, cyclopentyl**H**);
^{13}C NMR (125.8 MHz, $CDCl_3$) δ 202.4 (C=O), 143.8 (C), 128.5 (2 x CH), 127.8 (2 x CH), 126.5 (CH), 49.5 (CH_2), 46.4 (CH), 46.2 (CH), 31.4 (CH_2), 31.3 (CH_2), 25.2 (CH_2), 24.8 (CH_2);
HRMS (ESI) Exact mass calculated for $C_{15}H_{22}NaO_2$ $[M+MeOH+Na]^+$: 257.1512, found: 257.1513.

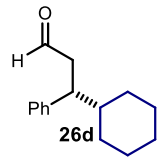

(*R*)-3-cyclohexyl-3-phenyl-propanal (26d)

Prepared according to the general procedure using cinnamaldehyde (39.6 mg, 0.3 mmol), aminocatalyst **F** (22.1 mg, 0.02 mmol), the corresponding dihydropyridine (33.5 mg, 0.1 mmol), trifluoroacetic acid (6.2 µL, 0.08 mmol), acetonitrile (400 µL) and perfluorohexane (100 µL). The crude material was purified by flash column chromatography (pentane/diethyl ether 99.7:0.3) to give the product **26d** (13.8 mg, 64% yield, 87% ee, average of two runs) as a colourless oil that displayed spectroscopic data consistent with those reported previously.[4] The enantiomeric excess of the corresponding alcohol (obtained upon reduction with sodium borohydride) was determined by HPLC analysis on a Agilent IC-3 column, 90:10 hexane/*i*-PrOH, flow rate 0.6 mL/min, 20

°C. λ = 215 nm. τ_{minor} = 12.6 min, τ_{major} = 15.3 min (87% ee). $[\alpha]_D^{26}$ = -3.7 (c= 0.66, $CHCl_3$, 87% ee).

^{1}H NMR (400 MHz, $CDCl_3$) δ 9.61 (1H, t, *J* =2,2 Hz, C**H**O), 7.32-7.26 (2H, m, Ar**H**), 7.23-7.18 (1H, m, Ar**H**), 7.16-7.12 (2H, m, Ar**H**), 3.02-2.94 (1H, m, ArC**H**), 2.87-2.68 (2H, m, C**H**$_2$CHO), 1.85- 1.71 (2H, m, cyclohexyl**H**), 1.69-1.59 (2H, m, cyclohexyl**H**), 1.54-1.44 (2H, m, cyclohexyl**H**), 1.25-1.02 (3H, m, cyclohexyl**H**), 1.00-0.77 (2H, m, cyclohexyl**H**).

^{13}C NMR (101 MHz, $CDCl_3$) δ 202.6 (C=O), 142.7 (C), 128.3 (CH), 128.2 (CH), 126.4 (CH), 47.1(CH_2), 46.1 (CH), 43.1 (CH), 31.0 (CH), 30.7 (CH_2), 26.4 (CH_2), 26.3 (CH).

(*R*)-3-cyclobutyl-3-phenyl-propanal (26e)

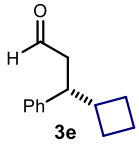

3e

Prepared according to the general procedure using cinnamaldehyde (39.6 mg, 0.3 mmol), aminocatalyst **F** (22.1 mg, 0.02 mmol), tetrabutylammonium cyclobutyltrifluoroborate (36.5 mg, 0.1 mmol), trifluoroacetic acid (3.1 µL, 0.04 mmol), acetonitrile (200 µL) and perfluorohexane (100 µL). The crude material was purified by flash column chromatography (pentane/diethyl ether 99:1) to give the product **26e** (5.5 mg, 29% yield, 72% ee, average of two runs) as a colourless oil. The enantiomeric excess of the corresponding alcohol (obtained upon reduction with sodium borohydride) was determined to be 72% by HPLC analysis on a Daicel Chiralpack IC-3 column: 90:10 hexane/*i*-PrOH, flow rate 0.6 mL/min, 20 °C, λ = 215 nm. τ_{minor} = 11.5 min, τ_{major} = 13.1 min (72% ee). $[\alpha]_D^{26}$ = -12.1 (c= 0.3,$CHCl_3$, 72%ee).

^{1}H NMR (500 MHz, $CDCl_3$) δ 9.65 (1H, t, *J* = 2.3 Hz, C**H**O), 7.32-7.27 (2H, m, Ar**H**), 7.23-7.16 (3H, m, Ar**H**), 3.13-3.06 (1H, m, ArC**H**), 2.68-2.63 (2H, m, CHOC**H**$_2$), 2.59-2.48 (1H, m, cyclobutyl**H**), 2.16-2.06 (1H, m, cyclobutyl**H**), 1.84-1.70 (3H, m, cyclobutyl**H**), 1.66-1.58 (1H, m, cyclobutyl**H**), 1.35-1.26 (1H, m, cyclobutyl**H**).

^{13}C NMR (125.8 MHz, $CDCl_3$) δ 202.2 (C=O), 142.1 (C), 128.5 (CH), 127.6 (CH), 126.6 (CH), 47.8 (CH_2), 47.0 (CH), 41.4 (CH), 27.5 (CH_2), 26.8 (CH_2), 17.3 (CH_2).

HRMS (ESI) Exact mass calculated for $C_{14}H_{20}NaO_2$ $[M+Na+MeOH]^+$: 243.1356, found: 243.1357.

This entry was performed using tetrabutylammonium cyclobutyltrifluoroborate as the radical precursor because of the photochemical inactivity of the corresponding dihydropyridine, which failed to deliver the corresponding radical upon excitation.

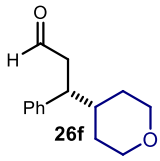

26f

(*R*)-3-phenyl-3-(tetrahydro-2H-pyran-4-yl)propanal (26f)

Prepared according to the general procedure using cinnamaldehyde (39.6 mg, 0.3 mmol), aminocatalyst **F** (22.1 mg, 0.02 mmol), the corresponding dihydropyridine (33.7 mg, 0.1 mmol), trifluoroacetic acid (6.2 µL, 0.08 mmol), acetonitrile (400 µL) and perfluorohexane (100 µL). The crude

material was purified by flash column chromatography (hexane/diethyl ether, gradient from 90:10 to 70:30) to give the product **26f** (13.7 mg, 63% yield, 87% ee, average of two runs) as a yellow oil. The enantiomeric excess of the corresponding alcohol (obtained upon reduction with sodium borohydride) was determined by HPLC analysis on a Agilent IC-3 column,70:30 hexane/*i*-PrOH, flow rate 0.6 mL/min, 20 °C, λ = 215 nm. τ_{minor} = 13.8 min, τ_{major} = 15.5 min (87% ee). $[\alpha]_D^{26}$ = –17.9 (c = 0.30, $CHCl_3$, 87% ee).

^{1}H NMR (500 MHz, $CDCl_3$) δ 9.62 (1H, t, *J* =2,1 Hz, C**H**O), 7.35-7.28 (2H, m, Ar**H**), 7.22 (1H, tt, *J* = 6.7, 1.2 Hz, Ar**H**), 7.18-7.13 (2H, m, Ar**H**), 4.01 (1H, ddd, *J* = 11.4, 4.0 2.3 Hz,- C**H**$_2$OCH$_2$-), 3.92-3.84 (1H, m, - C**H**$_2$OCH$_2$-), 3.36 (1H, td, *J* = 11.9, 2.2 Hz,- CH$_2$OC**H**$_2$-), 3.26 (1H, td, *J* = 11.5, 2.9 Hz,- CH$_2$OC**H**$_2$-), 2.98 (1H, ddd, *J* = 9.7, 8.4, 5.2 Hz, ArC**H**), 2.85 (1H, ddd, *J* = 16.5, 5.2, 1.8 Hz, CHOC**H**$_2$), 2.75 (1H, ddd, *J* = 16.5, 9.6, 2.5 Hz, CHOC**H**$_2$), 1.78-1.66 (2H, m, CHC**H**$_2$CH$_2$O), 1.37 (1H, dtd, *J* = 13.1, 12.0, 11.6, 4.5 Hz, CH$_2$C**H**CH$_2$), 1.31-1.19 (2H, m, CHC**H**$_2$CH$_2$O);

^{13}C NMR (125.8 MHz, $CDCl_3$) δ 201.9 (C=O), 141.8 (C), 128.6 (2 x CH), 128.2 (2 x CH), 126.8 (CH), 68.0 (CH_2), 67.9 (CH_2), 46.8 (CH_2), 45.9 (CH), 40.5 (CH), 31.2 (CH_2), 30.9 (CH_2);

HRMS (ESI) Exact mass calculated for $C_{15}H_{22}NaO_3$ $[M+MeOH+Na]^+$: 273.1461, found: 273.1470;

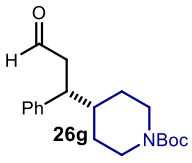

3*R*, 4*RS*)-5-(benzo[*d*][1,3]dioxol-5-yl)-4-methyl-3-phenylpentanal (26g)

The compound was prepared according to the general procedure using cinnamaldehyde (39.6 mg, 0.3 mmol), aminocatalyst **A** (14 mg, 0.02 mmol), the corresponding dihydropyridine (44 mg, 0.1 mmol) trifluoroacetic acid (7.6 µL, 0.1 mmol) and dichloromethane (400 µL). The crude material was purified by flash column chromatography (hexane/diethyl ether 80:20) to give the product **26g** (11.2 mg, 35% yield, 72% ee, average of two runs) as a colourless oil. The enantiomeric excess of the corresponding alcohol (obtained upon reduction with sodium borohydride) was determined to be 72% by HPLC analysis on a Daicel Chiralpack IC-3 column: 80:20 hexane/*i*-PrOH, flow rate 0.6 mL/min, 20 °C, λ = 215 nm. τ_{minor} = 24.2 min, τ_{major} = 32.3 min (72% ee). $[\alpha]_D^{26}$ = –3.7 (c = 0.55, $CHCl_3$, 72% ee).

^{1}H NMR (500 MHz, $CDCl_3$) δ 9.61 (1H, t, *J* = 2.0 Hz, C**H**O), 7.33-7.29 (2H, m, Ar**H**), 7.23 (1H, tt, *J* = 7.3, 1.3 Hz, Ar**H**), 7.16-7.13 (2H, m, Ar**H**), 4.15 (1H, br s, NC**H**$_2$), 4.03 (1H, br s, NC**H**$_2$), 3.03-2.97 (1H, m, ArC**H**), 2.88-2.73 (2H, m, CHOC**H**$_2$), 2.66 (1H, br m, NC**H**$_2$), 2.55 (1H, br m, NC**H**$_2$), 1.75 (1H, bd, *J* = 12.2 Hz, NCH$_2$C**H**$_2$), 1.68-1.59 (1H, m, ArCHC**H**), 1.43 (9H, s, CC**H**$_3$), 1.40-1.32 (1H, m, NCH$_2$C**H**$_2$), 1.21-1.13 (1H, m, NCH$_2$C**H**$_2$), 1.08-0.98 (1H, m, NCH$_2$C**H**$_2$);

^{13}C NMR (125.8 MHz, $CDCl_3$) δ 201.8 (CHO), 154.7 (CO_2), 141.9 (C), 128.6 (CH), 128.2 (CH), 126.8 (CH), 79.4 (C), 47.0 (CH_2), 45.5 (CH), 41.6 (CH), 28.4 (CH_2). Due to rotamers, the N**C**H$_2$ carbon signal is not visible in the ^{13}C-NMR spectrum, but an HSQC signal at 44 Hz is coupled to the corresponding protons.

HRMS (ESI) Exact mass calculated for $C_{19}H_{27}NNaO_3$ $[M+Na]^+$: 340.1883, found: 340.1894.

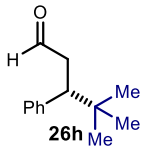

26h

(*R*)-4,4-dimethyl-3-phenylpentanal (26h)

Prepared according to the general procedure using cinnamaldehyde (39.6 mg, 0.3 mmol), aminocatalyst **F** (22.1 mg, 0.02 mmol), tetrabutylammonium *tert*-butyltrifluoroborate (36.7 mg, 0.1 mmol), trifluoroacetic acid (3.1 µL, 0.04 mmol), acetonitrile (200 µL) and perfluorohexane (100 µL). The crude material was purified by flash column chromatography (pentane/diethyl ether 99.7:0.3) to give the product **26h** (13.1 mg, 60% yield, 74 % ee, average of two runs) as a colourless oil that displayed spectroscopic data consistent with those reported previously.[4,6] The enantiomeric excess of the corresponding alcohol (obtained upon reduction with sodium borohydride) was determined by HPLC analysis on a Agilent IC-3 column, 90:10 hexane/*i*-PrOH, flow rate 0.6 mL/min, 20 °C. λ = 215 nm. τ_{minor} = 10. 5 min, τ_{major} = 11.2 min (74 % ee). $[\alpha]_D^{26}$ = –67.3 (c = 0.45, CH_2Cl_2, 74% ee); Lit: $[\alpha]_D^{26}$ = +44.0 (c = 1.29, CH_2Cl_2, 91% ee, for (*S*)-enantiomer).[6]

^{1}H NMR (500 MHz, $CDCl_3$) δ 9.54 (1H, dd, *J* = 2.9, 1.7 Hz, C**H**O), 7.31 – 7.15 (5H, m, Ar**H**), 3.05 (1H, dd, *J* = 10.7, 4.6 Hz, ArC**H**), 2.94 – 2.77 (2H, m, C**H**$_2$CHO), 0.93 (9H, s, C**H**$_3$).

^{13}C NMR (126 MHz, $CDCl_3$) δ 202.7 (C=O), 141.1 (C), 129.4 (CH), 127.9 (CH), 126.6 (CH), 50.3 (CH), 44.6 (CH_2), 33.7 (C), 27.8 (CH_3).

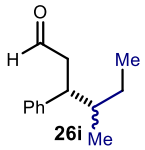

26i

(3*R*, 4*RS*)-4-methyl-3-phenylhexanal (26i)

Prepared according to the general procedure using cinnamaldehyde (39.6 mg, 0.3 mmol), aminocatalyst **F** (22.1 mg, 0.02 mmol), the corresponding dihydropyridine (30.9 mg, 0.1 mmol), trifluoroacetic acid (7.6 µL, 0.1 mmol), acetonitrile (200 µL) and perfluorohexane (100 µL). The crude material was purified by flash column chromatography (hexane/diethyl ether 99.7:0.3) to give the product **26i** (14.1 mg, 74% yield, 1:1 mixture of diastereoisomers) as a colourless oil. The enantiomeric excess of the corresponding alcohol (obtained upon reduction with sodium borohydride) was determined to be 84% for the first diastereoisomer and 83% for the second by UPC^2 analysis using CEL1 chiral column: 99.4:0.6 CO_2/ethanol, curve 6), flow rate 1.8 mL/min, λ = 215 nm. First diastereoisomer: τ_{minor} = 4.39 min, τ_{major} = 5.50 min (83% ee); second diastereoisomer: τ_{minor} = 4.75 min, τ_{major} = 5.16 min (84% ee). $[\alpha]_D^{26}$ = –4.3 (c= 0.43, $CHCl_3$, dr 1:1, 84% ee / 83% ee).

^{1}H NMR *1:1mixture of diastereoisomers* (500 MHz, $CDCl_3$) δ 9.63 (2H, q, *J* = 4.4, 2.2 Hz, 2 x C**H**O), 7.31 (4H, td, *J* = 7.6, 1.9 Hz, Ar**H**), 7.26-7.20 (2H, m, Ar**H**), 7.18 (4H, ddd, *J* = 7.9, 4.9, 1.3 Hz, Ar**H**), 3.13 (2H, dq, *J* = 21.7, 7.3 Hz, 2 x C**H**Ph), 2.84-2.76 (4H, m, 2 x C**H**$_2$CHO), 1.67 (2H, dddd, *J* = 13.0, 8.9, 6.3, 4.3 Hz, 2 x C**H**CH$_3$), 1.51 (1H, ddd, *J* = 13.5, 7.4, 4.4 Hz,

C**H**$_2$CH3), 1.37 (1H, ddd, *J* = 13.5, 7.5, 4.0 Hz, C**H**$_2$CH$_3$), 1.11 (1H, dt, *J* = 13.5, 8.4, 7.2 Hz, C**H**$_2$CH$_3$), 1.02 (1H, dddd, *J* = 16.8, 13.6, 8.5, 7.2 Hz, C**H**$_2$CH$_3$), 0.96-0.92 (6H, m, CHC**H**$_3$ + CH$_2$C**H**$_3$), 0.87 (3H, t, *J* = 7.4 Hz, CH$_2$C**H**$_3$), 0.78 (3H, d, *J* = 6.8 Hz, CHC**H**$_3$);

^{13}C NMR (125.8 MHz, $CDCl_3$) δ 202.6 (C=O), 202.5 (C=O), 143.0 (C), 142.1 (C), 128.5 (2 x CH), 128.4 (2 x CH), 128.3 (2 x CH), 128.2 (2 x CH), 126.50 (CH), 126.46 (CH), 47.2 (CH$_2$), 46.4 (CH$_2$), 45.3 (CH), 44.8 (CH), 40.1 (CH), 39.7 (CH), 26.84 (CH$_2$), 26.76 (CH$_2$), 16.2 (CH$_3$), 16.1 (CH$_3$), 11.5 (CH$_3$), 11.4 (CH$_3$);

HRMS (ESI) Exact mass calculated for $C_{14}H_{22}NaO_2$ $[M+MeOH+Na]^+$: 245.1512, found: 245.1506.

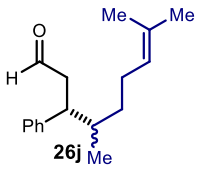

(3*R*, 4*RS*)-4,8-dimethyl-3-phenylnon-8-enal (26j)

Prepared according to the general procedure using cinnamaldehyde (39.6 mg, 0.3 mmol), aminocatalyst **F** (22.1 mg, 0.02 mmol), the corresponding dihydropyridine (36 mg, 0.1 mmol), trifluoroacetic acid (6.2 µL, 0.08 mmol), acetonitrile (400 µL) and perfluorohexane (100 µL). The crude material was purified by flash column chromatography (hexane/diethyl ether 99.7:0.3) to give the product **26j** (11.5 mg, 47% yield, 1:1 mixture of diastereoisomers) as a colourless oil. The enantiomeric excess of the corresponding alcohol (obtained upon reduction with sodium borohydride) was determined to be 89% for the *major* diastereoisomer and 90% for the *minor* by UPC^2 analysis using CEL2 chiral column: 94:6 CO_2/isopropanol, curve 6), flow rate 1.8 mL/min, λ = 215 nm. *Major diastereoisomer*: τ_{minor} = 3.65 min, τ_{major} = 3.90 min (89% ee); m*inor diastereoisomer*: τ_{minor} = 3.42 min, τ_{major} = 4.60 min (90% ee). $[\alpha]_D^{26}$ = –10.6 (c = 0.40, $CHCl_3$, dr 1:1, 90% ee / 89% ee).

^{1}H NMR *1:1mixture of diastereoisomers* (400 MHz, $CDCl_3$) δ 9.61 (2H, app q, *J* = 2.2 Hz, 2x C**H**O), 7.33-7.26 (4H, m, Ar**H**), 7.24-7.13 (6H, m, Ar**H**), 5.07 (1H, ddt, *J* = 8.5, 5.6, 1.4 Hz, C**H**=C), 4.99 (1H, ddt, *J* = 8.5, 5.6, 1.4 Hz, C**H**=C), 3.12 (2H, app dq, *J* = 14.6, 7.3 Hz, 2x C**H**Ar), 2.82-2.73 (4H, m, 2x C**H**$_2$CHO), 1.97 (4H, m, 2x C**H**$_2$CH=C), 1.77-1.68 (2H, m, 2x C**H**$_2$CH$_2$CH=C), 1.68 (3H, d, *J* = 1.4 Hz, CH=C(C**H**$_3$)$_2$), 1.65 (3H, d, *J* = 1.4 Hz, CH=C(C**H**$_3$)$_2$). 1.60 (3H, d, *J* = 1.3 Hz, CH=C(C**H**$_3$)$_2$), 1.55 (3H, t, *J* = 1.3 Hz, CH=C(C**H**$_3$)$_2$), 1.50-1.39 (1H, m, C**H**$_2$CH$_2$CH=C), 1.37-1.19 (1H, m, C**H**$_2$CH$_2$CH=C), 1.12-0.97 (2H, m, 2x C**H**CHPh), 0.91 (3H, d, *J* = 7.2 Hz, CHC**H**$_3$), 0.78 (3H, d, *J* = 6.8 Hz, CHC**H**$_3$);

^{13}C NMR *Diastereomer 1* (125.8 MHz, $CDCl_3$) δ 202.5 (C=O), 142.8 (C), 131.6 (CH), 128.4 (2 x CH), 128.2 (2 x CH), 126.5 (CH), 124.3 (CH), 46.2 (CH$_2$), 45.4 (CH), 38.0 (CH), 34.1 (CH$_2$), 25.7 (CH$_3$), 25.5 (CH$_2$), 17.6 (CH$_3$), 16.7 (CH$_3$);

^{13}C NMR *Diastereomer 2* (125.8 MHz, $CDCl_3$) δ 202.4 (C=O), 141.9 (C), 131.5 (CH), 128.5 (2 x CH), 128.3 (2 x CH), 126.5 (CH), 124.3 (CH), 47.2 (CH$_2$), 45.0 (CH), 37.7 (CH), 34.4 (CH$_2$), 25.7 (CH$_3$), 25.6 (CH$_2$), 17.7 (CH$_3$), 16.4 (CH$_3$);

HRMS (ESI) Exact mass calculated for $C_{17}H_{24}NaO$ $[M+Na]^+$: 267.1719, found: 267.1711.

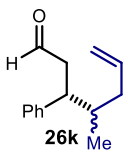

(3*R*, 4*RS*)-4-methyl-3-phenylhept-6-enal (26k)

Prepared according to the general procedure using cinnamaldehyde (39.6 mg, 0.3 mmol), aminocatalyst **F** (22.1 mg, 0.02 mmol), the corresponding dihydropyridine (32.1 mg, 0.1 mmol) trifluoroacetic acid (6.2 µL, 0.08 mmol), acetonitrile (400 µL) and perfluorohexane (100 µL). The crude material was purified by flash column chromatography (pentane/diethyl ether 99:1) to give the product **26k** (9.5 mg, 47% yield, 1.4:1 mixture of diastereoisomers) as a colourless oil. The enantiomeric excess of the corresponding alcohol (obtained upon reduction with sodium borohydride) was determined to be 91% for the *major* diastereoisomer and 90% for the *minor* by UPC^2 analysis using CEL2 chiral column: 93:7 CO_2/isopropanol, curve 6), flow rate 1 mL/min, $\lambda = 215$ nm. *Major diastereoisomer*: $\tau_{minor} = 4.39$ min, $\tau_{major} = 5.50$ min (91% ee); *minor diastereoisomer*: $\tau_{minor} = 4.75$ min, $\tau_{major} = 5.16$ min (90% ee). $[\alpha]_D^{26} = -24.0$ (c = 0.23, $CHCl_3$, dr 1.4:1, 91% ee / 90% ee).

^{1}H NMR *1.4:1mixture of diastereoisomers* (500 MHz, $CDCl_3$) δ 9.61 (2H, m, 2x C**H**O), 7.33-7.38 (4H, m, Ar**H**), 7.24-7.15 (6H, m, Ar**H**), 5.85-5.66 (2H, m, 2x H_2C=C**H**), 5.08-4.92 (4H, m, 2x **H**$_2$C=CH), 3.21-3.07 (2H, m, 2x ArC**H**), 2.84-2.76 (4H, m, 2x CHOC**H**$_2$), 2.25-2.16 (1H, m, H_2C=CHC**H**$_2$), 2.10-2.03 (1H, m, H_2C=CHC**H**$_2$), 1.90-1.79 (3H, m, 1x H_2C=CHC**H**$_2$ + 2x ArCHC**H**), 1.78-1.69 (1H, m, H_2C=CHC**H**$_2$), 0.94 (3H, d, *J* = 6.6 Hz, C**H**$_3$), 0.78 (3H, d, *J* = 6.6 Hz, C**H**$_3$).

^{13}C NMR (125.8 MHz, $CDCl_3$) δ 202.3 (CHO), 202.1 (CHO), 142.7 (C), 141.6 (C), 136.8 (CH), 128.6 (CH), 128.5 (CH), 128.3 (CH), 128.2 (CH), 126.6 (CH), 116.5 (CH_2), 116.4 (CH_2), 47.2 (CH_2), 46.4 (CH_2), 45.0 (CH), 44.3 (CH), 38.8 (CH_2), 38.7 (CH_2), 38.3 (CH), 37.9 (CH), 16.7 (CH_3), 16.4 (CH_3).

HRMS (ESI) Exact mass calculated for $C_{15}H_{22}NaO_2$ $[M+Na+MeOH]^+$: 257.1512, found: 257.1505.

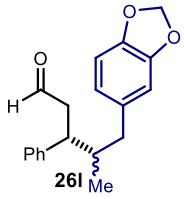

(3*R*, 4*RS*)-5-(benzo[*d*][1,3]dioxol-5-yl)-4-methyl-3-phenylpentanal (26l)

Prepared according to the general procedure using cinnamaldehyde (39.6 mg, 0.3 mmol), aminocatalyst **F** (22.1 mg, 0.02 mmol), the corresponding dihydropyridine (41.5 mg, 0.1 mmol), trifluoroacetic acid (6.2 µL, 0.08 mmol), acetonitrile (400 µL) and perfluorohexane (100 µL). The crude material was purified by flash column chromatography (hexane/diethyl ether 90:10, two consecutive purifications) to give the product **26l** (15.1 mg, 51% yield, 1:1 mixture of diastereoisomers) as a colourless oil. The enantiomeric excess of the corresponding alcohol (obtained upon reduction with sodium borohydride) was determined to be 92% for the *major* diastereoisomer and 90% for the *minor* by UPC^2 analysis using ID-3 chiral column: after 1 min of 100% CO_2, gradient up to 60:40 CO_2/acetonitrile over 5 minutes, curve 6), flow rate 3

mL/min, λ = 287 nm. *Major diastereoisomer*: τ_{minor} = 5.13 min, τ_{major} = 4.47 min (92% ee); *minor diastereoisomer*: τ_{minor} = 4.73 min, τ_{major} = 4.03 min (90% ee). $[\alpha]_D^{26}$ = –7.7 (c = 0.38, $CHCl_3$, dr 1:1, 90% ee / 90% ee).

^{1}H NMR *1:1mixture of diastereoisomers* (500 MHz, $CDCl_3$) δ 9.65 (1H, t, *J* = 2.1 Hz, C**H**O), 9.63 (1H, t, *J* = 2.1 Hz, C**H**O), 7.37-7.31 (4H, m, 2x Ar**H**), 7.25-7.18 (6H, m, 2x Ar**H**), 6.74 (1H, d, *J* = 7.9 Hz, Ar**H**), 6.72 (1H, d, *J* = 7.9 Hz, Ar**H**), 6.63-6.50 (4H, m, Ar**H**), 5.92 (2H, s, OC**H₂**O), 5.91 (2H, s, OC**H₂**O), 3.26 (1H, td, *J* = 8.2, 6.8 Hz, ArC**H**), 3.13 (1H, td, *J* = 8.2, 6.8 Hz, ArC**H**), 2.91-2.87 (2H, m, CHOC**H₂**), 2.86-2.82 (2H, m, CHOC**H₂**), 2.74 (1H, dd, *J* = 13.4, 4.8 Hz, ArC**H₂**), 2.61 (1H, dd, *J* = 13.3, 4.2 Hz, ArC**H₂**), 2.16-2.03 (2H, m, ArC**H₂**), 2.06-1.92 (2H, m, C**H**CH_3), 0.88 (3H, d, *J* = 6.6 Hz, CHC**H₃**), 0.75 (3H, d, *J* = 6.6 Hz, CHC**H₃**);

^{13}C NMR (125.8 MHz, $CDCl_3$) δ 202.2 (C=O), 202.0 (C=O), 147.6 (C), 147.5 (C), 145.7 (C), 145.6 (C), 142.7 (C), 141.3 (C), 134.7 (C), 134.5 (C), 128.7 (CH), 128.6 (CH), 128.4 (CH), 128.2 (CH), 126.7 (CH), 121.9 (CH), 121.8 (CH), 109.3 (CH), 109.2 (CH), 108.1 (CH), 108.0 (CH), 100.8 (CH_2), 100.7 (CH_2), 47.2 (CH_2), 46.3 (CH_2), 45.2 (CH), 44.6 (CH), 41.0 (CH), 40.7 (CH_2), 40.5 (CH_2), 40.2 (CH), 16.5 (CH_3), 16.0 (CH_3);

HRMS (ESI) Exact mass calculated for $C_{19}H_{20}NaO_3$ $[M+Na]^+$: 319.1305, found: 319.1313.

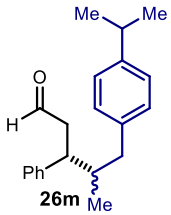

(3*R*, 4*RS*)-4,8-dimethyl-3-phenylnon-8-enal (26m)

Prepared according to the general procedure using cinnamaldehyde (39.6 mg, 0.3 mmol), aminocatalyst **F** (22.1 mg, 0.02 mmol), the corresponding dihydropyridine (41.4 mg, 0.1 mmol), trifluoroacetic acid (6.2 µL, 0.08 mmol), acetonitrile (400 µL) and perfluorohexane (100 µL). The crude material was purified by flash column chromatography (hexane/diethyl ether 96:4) to give the product **26m** (16.2 mg, 55% yield, 1:1 mixture of diastereoisomers) as a colourless oil. The enantiomeric excess of the corresponding alcohol (obtained upon reduction with sodium borohydride) was determined to be 88% for the *major* diastereoisomer and 87% for the *minor* by UPC^2 analysis on a using IE-3 chiral column: after 1 min of 100% CO_2, gradient up to 60:40 CO_2/acetonitrile over 5 minutes, curve 6), flow rate 3 mL/min, λ = 220 nm. *Major diastereoisomer*: τ_{minor} = 5.37 min, τ_{major} = 4.92 min (88% ee); *minor diastereoisomer*: τ_{minor} = 5.09 min, τ_{major} = 5.22 min (87% ee). $[\alpha]_D^{26}$ = –5.9 (c = 0.8, $CHCl_3$, dr 1:1, 88% ee/87% ee).

^{1}H NMR *1:1mixture of diastereoisomers* (500 MHz, $CDCl_3$) δ 9.63 (2H, app dt, *J* = 6.4, 2.1 Hz, 2x C**H**O), 7.37-7.30 (4H, m, Ar**H**), 7.26-7.18 (6H, m, Ar**H**), 7.16-7.11 (4H, m, Ar**H**), 7.07-7.03 (2H, m, Ar**H**), 6.99 (2H, d, *J* = 8.1 Hz, Ar**H**), 3.29-3.22 (1H, m, $CHOCH_2C$**H**), 3.18-3.11 (1H, m, $CHOCH_2C$**H**), 2.92-2.82 (6H, m, 2x CHOC**H₂** + 2x ArC**H**$(CH_3)_2$), 2.78 (1H, dd, *J* = 13.6, 4.9 Hz, ArC**H₂**), 2.66 (1H, dd, *J* = 13.4, 4.2 Hz, ArC**H₂**), 2.23-2.11 (2H, m, 2x ArC**H₂**), 2.10-

1.98 (1H, m, 2x PhCHC**H**), 1.25 (12H, dd, *J* = 6.9, 6.0 Hz, 2x CH(C**H**$_3$)$_2$), 0.88 (3H, d, *J* = 6.6 Hz, CHC**H**$_3$), 0.74 (3H, d, *J* = 6.7 Hz, CHC**H**$_3$);

^{13}C NMR (125.8 MHz, $CDCl_3$) δ 202.3 (C=O), 202.2 (C=O), 146.5 (C), 146.4 (C), 142.7 (C), 141.4 (C), 138.1 (C), 137.9 (C), 129.0 (2 x CH), 128.9 (2 x CH), 128.7 (2 x CH), 128.6 (2 x CH), 128.34 (2 x CH), 128.25 (2 x CH), 126.7 (2 x CH), 126.32 (2 x CH), 126.27 (2 x CH), 47.3 (CH_2), 46.2 (CH_2), 45.3 (CH), 44.7 (CH), 40.8 (CH), 40.6 (CH_2), 40.3 (CH_2), 40.1 (CH), 33.68 (CH), 33.66 (CH), 24.1 (4 x CH_3), 16.6 (CH_3), 16.2 (CH_3);

HRMS (ESI) Exact mass calculated for $C_{21}H_{26}NaO$ $[M+Na]^+$: 317.1876, found: 317.1877.

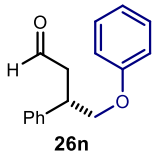

26n

(S)-4-phenoxy-3-phenylbutanal (26n)

Prepared according to the general procedure using cinnamaldehyde (39.6 mg, 0.3 mmol), aminocatalyst **F** (22.1 mg, 0.02 mmol), the correspondin dihydropyridine (35.9 mg, 0.1 mmol), trifluoroacetic acid (6.2 µL, 0.08 mmol), acetonitrile (400 µL) and perfluorohexane (100 µL). The crude material was purified by flash column chromatography (two consecutive columns, first hexane/toluene gradient from 100:0 to 0:100, then hexane/diethyl ether 9:1) to give the product **26n** (9.1 mg, 38% yield, 83 % ee, average of two runs) as a colourless oil. The enantiomeric excess was determined by HPLC analysis on a Agilent IC-3 column, 90:10 hexane/*i*-PrOH, flow rate 0.8 mL/min, 20 °C. λ = 215 nm. τ_{major} = 12. 0 min, τ_{minor} = 13.1 min (83 % ee).

^{1}H NMR (500 MHz, $CDCl_3$) δ 9.80 (t, 1H, J = 1.8 Hz C**H**O), 7.38 – 7.24 (m, 7H, Ar**H**), 6.97 – 6.93 (m, 1H, Ar**H**), 6.87 (dt, *J* = 7.8, 1.1 Hz, 2H, Ar**H**), 4.18 (dd, *J* = 9.2, 5.0 Hz, 1H, C**H**$_2$O), 4.03 (dd, *J* = 9.3, 8.3 Hz, 1H, C**H**$_2$O), 3.76 (qd, *J* = 7.4, 5.0 Hz, 1H, ArC**H**), 3.10 (ddd, *J* = 17.1, 6.9, 2.0 Hz, 1H, C**H**$_2$CHO), 2.87 (ddd, *J* = 17.1, 7.4, 1.8 Hz, 1H, C**H**$_2$CHO)

^{13}C NMR (126 MHz, $CDCl_3$) δ 200.2 (C=O), 157.6 (C), 139.6 (C), 128.7 (CH), 128.0 (CH), 127.0 (CH), 126.5 (CH), 120.3 (CH), 113.7 (CH), 70.7 (CH_2), 46.1 (CH_2), 39.11 (CH).

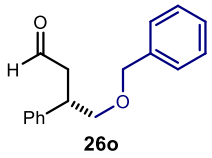

26o

(S)-4-(benzyloxy)-3-phenylbutanal (26o)

Prepared according to the general procedure using cinnamaldehyde (39.6 mg, 0.3 mmol), aminocatalyst **F** (22.1 mg, 0.02 mmol), the correspondin dihydropyridine (37.3 mg, 0.1 mmol), trifluoroacetic acid (6.2 µL, 0.08 mmol), acetonitrile (400 µL) and perfluorohexane (100 µL). The crude material was purified by flash column chromatography (two consecutive columns, first hexane/dichloromethane 1:1, then hexane /diethyl ether 9:1) to give the product **26o** (12 mg, 47% yield, 75 % ee, average of two runs) as a colourless oil. The enantiomeric excess was determined by HPLC analysis on a Agilent IC-3 column, 90:10 hexane/*i*-PrOH, flow rate 0.8 mL/min, 20 °C. λ = 215 nm. τ_{major} = 11. 8 min, τ_{minor} = 12.6 min (75 % ee).

^{1}H NMR (500 MHz, $CDCl_3$) δ 9.74 (t, 1H, J = 2Hz, C**H**O), 7.35 – 7.20 (m, 10H, Ar**H**), 4.50 (s, 2H, PhC**H**$_2$O), 3.69 – 3.65 (m, 1H, C**H**$_2$O), 3.61 – 3.52 (m, 2H, C**H**$_2$O + PhC**H**), 2.96 (ddd, *J* = 16.6, 6.8, 2.3 Hz, 2H, C**H**$_2$CHO), 2.74 (ddd, *J* = 16.7, 7.0, 1.8 Hz, 2H, C**H**$_2$CHO).
^{13}C NMR (126 MHz, $CDCl_3$) δ 200.6 (C=O), 140.2 (C), 137.2 (C), 130.5 (CH), 127.9 (CH), 127.6 (CH), 126.9 (CH), 126.8 (CH), 126.2 (CH), 73.5 (CH_2), 72.3 (CH_2), 46.4 (CH_2), 39.7 (CH).

(*R*)-4-ethyl-3-(*p*-tolyl)hexanal (26p)

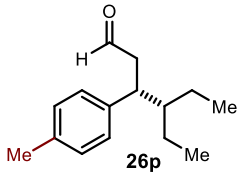

26p

Prepared according to the general procedure using 3-(*p*-tolyl)acrylaldehyde (44 mg, 0.3 mmol), aminocatalyst **F** (22.1 mg, 0.02 mmol), the corresponding dihydropyridine (32.3 mg, 0.1 mmol), trifluoroacetic acid (6.2 µL, 0.08 mmol), acetonitrile (200 µL) and perfluorohexane (100 µL). The crude material was purified by flash column chromatography (hexane/diethyl ether 99:1) to give the product **26p** (14.6 mg, 67% yield, 77% ee, average of two runs) as a colourless oil. The enantiomeric excess of the corresponding alcohol (obtained upon reduction with sodium borohydride) was determined to be 77% by UPC^2 analysis using CEL2 chiral column: after 1 min of 100% CO_2, gradient up to 60:40 CO_2/methanol over 5 minutes, curve 6), flow rate 2 mL/min, λ = 220 nm. τ_{minor} = 2.71 min, τ_{major} = 2.61 min.$[\alpha]_D^{26}$ = –6.3 (c = 0.7, $CHCl_3$, 77% ee).
^{1}H NMR (500 MHz, $CDCl_3$) δ 9.59 (1H, t, *J* = 2.3 Hz, C**H**O), 7.12-7.04 (4H, m, Ar**H**), 3.21 (1H, q, *J* = 7.4 Hz, ArC**H**), 2.75-2.71 (2H, m, CHOC**H**$_2$), 2.32 (3H, s, ArC**H**$_3$), 1.49-1.22 (4H, m, C**H**$(CH_2CH_3)_2$ + 3 x C**H**$_2CH_3$), 1.17-1.05 (1H, m, CH(C**H**$_2CH_3)_2$), 0.90 (3H, t, *J* = 7.4 Hz, CH_2C**H**$_3$), 0.83 (3H, t, *J* = 7.4 Hz, CH_2C**H**$_3$);
^{13}C NMR (125.8 MHz, $CDCl_3$) δ 202.8 (C=O), 139.6 (C), 135.9 (C), 129.1 (CH), 128.1 (CH), 46.8 (CH_2), 46.0 (CH), 41.5 (CH), 22.3 (CH_2), 21.9 (CH_2), 21.0 (CH_3), 11.1 (CH_3), 10.8 (CH_3);
HRMS (ESI) Exact mass calculated for $C_{15}H_{22}NaO$ $[M+Na]^+$: 241.1563, found: 241.1573.

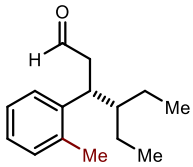

26q

(*R*)-4-ethyl-3-(*o*-tolyl)hexanal (26q)

Prepared according to the general procedure using 3-(*o*-tolyl)acrylaldehyde (44 mg, 0.3 mmol), aminocatalyst **F** (22.1 mg, 0.02 mmol), the corresponding dihydropyridine (32.3 mg, 0.1 mmol), trifluoroacetic acid (6.2 µL, 0.08 mmol), acetonitrile (200 µL) and perfluorohexane (100 µL). The crude material was purified by flash column chromatography (hexane/diethyl ether 99:1) to give the product **26q** (10.7 mg, 49% yield, 78% ee, average of two runs) as a colourless oil. The enantiomeric excess of the corresponding alcohol (obtained upon reduction with sodium borohydride) was determined to be 78% by UPC^2 analysis using CEL2 chiral column: after 1 min of 100% CO_2, gradient up to 60:40 CO_2/isopropanol over 5

minutes, curve 6), flow rate 2 mL/min, λ = 215 nm. τ_{minor} = 3.59 min, τ_{major} = 3.35 min.$[\alpha]_D^{26}$ = +6.5 (c = 0.5, $CHCl_3$, 78% ee).

^{1}H NMR (500 MHz, $CDCl_3$) δ 9.54 (1H, t, *J* = 2.3 Hz, C**H**O), 7.19-7.08 (4H, m, Ar**H**), 3.49 (1H, q, *J* = 7.6 Hz, ArC**H**), 2.76-2.74 (2H, m, CHOC**H**$_2$), 2.38 (3H, s, ArC**H**$_3$), 1.61-1.49 (2H, m, C**H**$(CH_2CH_3)_2$ + C**H**$_2CH_3$), 1.37-1.23 (2H, m, C**H**$_2CH_3$), 1.21-1.12 (1H, m, C**H**$_2CH_3$), 0.86 (3H, t, *J* = 7.4 Hz, CH_2CH_3), 0.84 (3H, t, *J* = 7.4 Hz, CH_2CH_3);

^{13}C NMR (125.8 MHz, $CDCl_3$) δ 202.6 (CHO), 141.7 (C), 136.2 (C), 130.6 (CH), 126.8 (CH), 126.1 (CH), 126.0 (CH), 46.6 (CH_2), 45.2 (CH), 36.9 (CH), 22.3 (CH_2), 21.4 (CH_2), 20.0 (CH_3), 11.3 (CH_3), 10.3 (CH_3).

HRMS (ESI) Exact mass calculated for $C_{16}H_{26}NaO_2$ $[M+Na+MeOH]^+$: 273.1825, found: 273.1822.

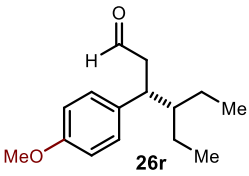

26r

(*R*)-4-ethyl-3-(4-methoxyphenyl)hexanal (26r)

Prepared according to the general procedure using 4-methoxycinnamaldehyde (48.7 mg, 0.3 mmol), aminocatalyst **F** (22.1 mg, 0.02 mmol), the corresponding dihydropyridine (32.3 mg, 0.1 mmol), trifluoroacetic acid (7.6 µL, 0.1 mmol), acetonitrile (200 µL) and perfluorohexane (100 µL). The crude material was purified by flash column chromatography (hexane/diethyl ether 90:10) to give the product **26r** (16.2 mg, 69% yield, 60% ee, average of two runs) as a colourless oil. The enantiomeric excess of the corresponding alcohol (obtained upon reduction with sodium borohydride) was determined by HPLC analysis on a Agilent IC-3 column, 90:10 hexane/*i*-PrOH, flow rate 0.6 mL/min, 20 °C. λ = 215 nm. τ_{minor} = 13.7 min, τ_{major} = 15.9 min (60% ee). $[\alpha]_D^{26}$ = –4.65 (c = 0.82, $CHCl_3$, 60% ee).

^{1}H NMR (500 MHz, $CDCl_3$) δ 9.58 (1H, t, *J* = 2.3 Hz, , C**H**O), 7.10-7.05 (2H, m, Ar**H**), 6.85-6.81 (2H, m, Ar**H**), 3.79 (3H, s, ArOC**H**$_3$), 3.20 (1H, q, *J* = 7.2 Hz, ArC**H**), 2.74-2.70 (2H, m, CHOC**H**$_2$), 1.48-1.22 (4H, m C**H**$(CH_2CH_3)_2$ + 3 x C**H**$_2CH_3$), 1.15-1.04 (1H, m, C**H**$_2CH_3$), 0.90 (3H, t, *J* = 7.3 Hz, CH_2CH_3), 0.82 (3H, t, *J* = 7.4 Hz, CH_2CH_3);

^{13}C NMR (126 MHz, $CDCl_3$) δ 202.8 (C=O), 158.0 (C), 134.6 (C), 129.1 (CH), 113.7 (CH), 55.1 (CH_3), 46.8 (CH_2), 46.1 (CH), 41.0 (CH), 22.2 (CH_2), 21.9 (CH_2), 11.1 (CH_3), 10.8 (CH_3).

HRMS (ESI) Exact mass calculated for $C_{15}H_{22}NaO_2$ $[M+Na]^+$: 257.1512, found: 257.1515.

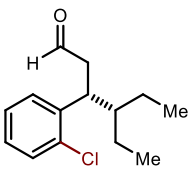

26s

(*R*)-3-(2-chlorophenyl)-4-ethylhexanal (26s)

Prepared according to the general procedure using 3-(2-chlorophenyl)acrylaldehyde (50 mg, 0.3 mmol), aminocatalyst **F** (22.1 mg, 0.02 mmol) the corresponding dihydropyridine (32.3 mg, 0.1 mmol), trifluoroacetic acid (0.08 mmol, 6.2 µL), acetonitrile (200 µL) and perfluorohexane (100 µL). The crude material was purified by flash column chromatography (hexane/diethyl ether 99:1) to give the product **26s** (13.1 mg, 55% yield, 83% ee, average of two runs) as a colourless oil. The enantiomeric excess of the corresponding alcohol (obtained upon reduction with sodium borohydride) was determined to be 83% by UPC^2 analysis using CEL2 chiral column: after 1 min of 100% CO_2, gradient up to 60:40 CO_2/ethanol over 5 minutes, curve 6), flow rate 2 mL/min, λ = 215 nm. τ_{minor} = 3.23 min, τ_{major} = 3.04 min. $[\alpha]_D^{26}$ = –12.6 (c = 0.33, $CHCl_3$, 83% ee).

^{1}H NMR (500 MHz, $CDCl_3$) δ) 9.57 (1H, dd, *J* = 3.1, 1.7 Hz, C**H**O), 7.37 (1H, dd, *J* = 7.9, 1.2 Hz, Ar**H**), 7.25-7.12 (3H, m, Ar**H**), 3.88-3.81 (1H, m, ArC**H**), 2.82-2.66 (2H, m, CHOC**H**$_2$), 1.67-1.61 (1H, m, C**H**(CH_2CH_3)$_2$), 1.57-1.46 (1H, m, C**H**$_2$$CH_3$), 1.37-1.27 (2H, m, C**H**$_2$$CH_3$), 1.25-1.14 (1H, m, C**H**$_2$$CH_3$), 0.87 (6H, t, *J* = 7.4 Hz, CH_2C**H**$_3$);

^{13}C NMR (125.8 MHz, $CDCl_3$) δ 202.1 (CHO), 140.6 (C), 134.4 (C), 129.9 (CH), 128.8 (CH), 127.6 (CH), 126.9 (CH), 45.8 (CH_2), 44.5 (CH), 37.9 (CH), 22.5 (CH_2), 21.6 (CH_2), 10.9 (CH_3), 10.6 (CH_3).

HRMS (ESI) Exact mass calculated for $C_{15}H_{23}ClNaO_2$ $[M+Na+MeOH]^+$: 293.1279, found: 293.1268.

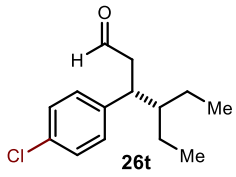

26t

(*R*)-3-(4-chlorophenyl)-4-ethylhexanal (26t)

Prepared according to the general procedure using 3-(4-chlorophenyl)acrylaldehyde (50 mg, 0.3 mmol), aminocatalyst **F** (22.1 mg, 0.02 mmol) the corresponding dihydropyridine (32.3 mg, 0.1 mmol), trifluoroacetic acid (6.2 µL, 0.08 mmol), acetonitrile (200 µL) and perfluorohexane (100 µL). The crude material was purified by flash column chromatography (hexane/diethyl ether 98.5:1.5) to give the product **26t** (10.5 mg, 44% yield, 75% ee, average of two runs) as a colourless oil. The enantiomeric excess of the corresponding alcohol (obtained upon reduction with sodium borohydride) was determined to be 74% by UPC^2 analysis using CEL2 chiral column: after 1 min of 100% CO_2, gradient up to 60:40 CO_2/isopropanol over 5 minutes, curve 6), flow rate 2 mL/min, λ = 221 nm. τ_{minor} = 3.53 min, τ_{major} = 3.42 min. $[\alpha]_D^{26}$ = +3.2 (c= 0.55, $CHCl_3$, 75% ee).

^{1}H NMR (500 MHz, $CDCl_3$) δ 9.62 (1H, t, *J* = 2.3 Hz, C**H**O), 7.30-7.26 (2H, m, Ar**H**), 7.15-7.10 (2H, m, Ar**H**), 3.28-3.22 (1H, m, ArC**H**), 2.82-2.71 (2H, m, CHOC**H**$_2$), 1.49-1.22 (4H, m, C**H**(CH_2CH_3)$_2$ + 3 x C**H**$_2$$CH_3$), 1.16-1.05 (1H, m, C**H**$_2$$CH_3$), 0.91 (3H, t, *J* = 7.4 Hz, CH_2C**H**$_3$), 0.84 (3H, t, *J* = 7.4 Hz, CH_2C**H**$_3$);

^{13}C NMR (125.8 MHz, $CDCl_3$) δ 201.9 (CHO), 141.4 (C), 132.1 (C), 129.6 (CH), 128.5 (CH), 46.7 (CH_2), 45.9 (CH), 41.2 (CH), 22.3 (CH_2), 21.9 (CH_2), 11.0 (CH_3), 10.8 (CH_3).
HRMS (ESI) Exact mass calculated for $C_{15}H_{23}ClNaO_2$ $[M+Na+MeOH]^+$: 293.1279, found: 293.1280.

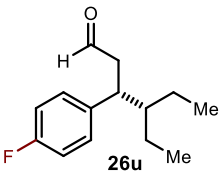

26u

(*R*)-4-ethyl-3-(4-fluorophenyl)hexanal (26s)

Prepared according to the general procedure using 4-fluoro cinnamaldehyde (45.0 mg, 0.3 mmol), aminocatalyst **F** (22.1 mg, 0.02 mmol the corresponding dihydropyridine (32.3 mg, 0.1 mmol), trifluoroacetic acid (6.2 µL, 0.08 mmol), acetonitrile (200 µL) and perfluorohexane (100 µL). The crude material was purified by flash column chromatography (hexane/diethyl ether 99:1) to give the product **26u** (10.7 mg, 48% yield, 78% ee, average of two runs) as a colourless oil. The enantiomeric excess of the corresponding alcohol (obtained upon reduction with sodium borohydride) was determined by HPLC analysis on a Agilent IC-3 column, 95:05 hexane/*i*-PrOH, flow rate 0.6 mL/min, 20 °C. λ = 215 nm. τ_{minor} = 12.9 min, τ_{major} = 13.8 min (78% ee).$[\alpha]_D^{26}$ = –3.70 (c = 0.47, $CHCl_3$, 78% ee).
^{1}H NMR (500 MHz, $CDCl_3$) δ 9.62 (1H, t, *J* = 2.6 Hz, C**H**O), 7.16-7.10 (2H, m, Ar**H**), 7.01-6.95 (2H, m, Ar**H**), 3.25 (1H, q, *J* = 7.2 Hz, ArC**H**), 2.79-2.69 (2H, m, CHOC**H**$_2$), 1.47-1.22 (4H, m, C**H**(CH_2CH_3)$_2$ + 3 x C**H**$_2$$CH_3$), 1.14-1.04 (1H, m, C**H**$_2$$CH_3$), 0.89 (3H, t, *J* = 7.3 Hz, CH_2C**H**$_3$), 0.82 (3H, t, *J* = 7.4 Hz CH_2C**H**$_3$);
^{13}C NMR (126 MHz, $CDCl_3$): δ 202.1 (CHO), 161.3 (d, J_{CF} = 244.9 Hz, Ar^{para}), 138.4 (d, J_{CF} = 3.4 Hz, Ar^{ipso}), 129.6 (2C, d, J_{CF} = 7.8 Hz, Ar^{ortho}), 115.2 (2C, d, J_{CF} = 21.2 Hz, Ar^{meta}), 46.9 (CH_2), 46.01 (CH), 41.1 (CH), 22.2 (CH_2), 21.9 (CH_2), 11.0 (CH_3), 10.8 (CH_3).
^{19}F NMR (376 MHz, $CDCl_3$): δ -116.7.
HRMS (ESI) Exact mass calculated for $C_{15}H_{23}FNaO_2$ $[M+MeOH+Na]^+$: 277.1574, found: 277.1569.

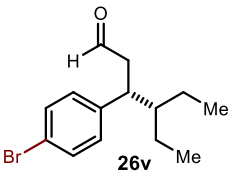

26v

(*R*)-3-(4-bromophenyl)-4-ethylhexanal (26v)

Prepared according to the general procedure using 4-bromocinnamaldehyde (63.3 mg, 0.3 mmol), aminocatalyst **F** (22.1 mg, 0.02 mmol), the corresponding dihydropyridine (32.3 mg, 0.1 mmol), trifluoroacetic acid (6.2 µL, 0.08 mmol), acetonitrile (200 µL) and perfluorohexane (100 µL). The crude material was purified by flash column chromatography (hexane/diethyl ether 99:1) to give the product **26v** (11.0 mg, 39% yield, 72% ee, average of two runs) as a colourless oil. The enantiomeric excess of the corresponding alcohol (obtained upon reduction with sodium borohydride) was determined by UPC^2 analysis using CEL2 chiral column: after 1 min of 100% CO_2, gradient up to 60:40 CO_2/isopropanol

over 5 minutes, curve 6), flow rate 2 mL/min. λ = 215 nm. τ_{minor} = 3.76 min, τ_{major} = 3.64 min (72% ee). $[\alpha]_D^{26}$ = –84.7 (c= 0.48, $CHCl_3$, 72% ee).

^{1}H NMR (500 MHz, $CDCl_3$) δ 9.60 (1H, t, *J* = 2.4 Hz, C**H**O), 7.45-7.39 (2H, m, Ar**H**), 7.09-7.02 (2H, m, Ar**H**), 3.23 (1H, q, *J* = 7.1 Hz, ArC**H**), 2.81-2.67 (2H, m, CHOC**H**$_2$), 1.49-1.18 (4H, m, C**H**$(CH_2CH_3)_2$ + 3 x C**H**$_2CH_3$), 1.14-1.03 (1H, m, C**H**$_2CH_3$), 0.89 (3H, t, *J* = 7.4 Hz, CH_2C**H**$_3$), 0.82 (3H, t, *J* = 7.4 Hz CH_2C**H**$_3$);

^{13}C NMR (101 MHz, $CDCl_3$) δ 201.8 (CHO), 141.9 (C), 131.4 (CH), 129.9 (CH), 120.19 (C), 46.6 (CH_2), 45.8 (CH), 41.2 (CH), 22.28 (CH_2), 21.88 (CH_2), 11.01 (CH_3), 10.81 (CH_3).

HRMS (ESI) Exact mass calculated for $C_{15}H_{23}BrNaO_2$ $[M+MeOH+Na]^+$: 337.0774, found: 337.0774

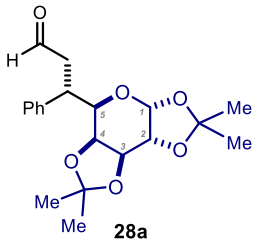

28a

(*S*)-3-phenyl-3-((3a*R*,5*R*,5a*S*,8a*S*,8b*R*)-2,2,7,7-tetramethyltetrahydro-5H-bis([1,3]dioxolo)[4,5-b:4',5'-d]pyran-5-yl)propanal (28a)

Prepared according to the general procedure using cinnamaldehyde (39.6 mg, 0.3 mmol), aminocatalyst (*S*)-**A** (14 mg, 20 mol%), and the corresponding dihydropyridine (48.2 mg, 0.1 mmol) in DCM (400 µL) . The crude material was purified by flash column chromatography (hexane/diethyl ether 4:1) to give the product (19.1 mg, 53% yield, 19:1 mixture of diastereoisomers, average of two runs) as a white solid. *Characterization of the major diastereoisomer*: ^{1}H NMR (400 MHz, $CDCl_3$) δ 9.62 (1H, t, *J* = 2.1 Hz C**H**O),7.37-7.22 (5H, m, Ar**H**), 5.56 (1H, d, *J* = 5.0 Hz, C1**H**), 4.43 (1H, dd, *J* = 8.0, 2.3 Hz, C3**H**), 4.28 (1H, dd, *J* = 5.1, 2.3 Hz, C2**H**), 3.82 (1H, dd, *J* = 10.3, 1.6 Hz, (C5**H**), 3.76 (1H, dd, *J* = 8.0, 1.6 Hz, C4**H**), 3.70 (1H, ddd, *J* = 10.3, 7.9, 6.3 Hz, ArC**H**), 3.11 (1H, ddd, *J* = 16.7, 6.3, 2.0 Hz, C**H**$_2$CHO), 2.65 (1H, ddd, *J* = 16.7, 7.9, 2.2 Hz, C**H**$_2$CHO), 1.56 (3H, s, C**H**$_3$), 1.50 (3H, s, C**H**$_3$), 1.34 (3H, s, C**H**$_3$), 1.25 (3H, s, C**H**$_3$).

^{13}C NMR (126 MHz, $CDCl_3$) δ 201.7 (CHO), 140.1 (C), 128.6 (CH), 128.4 (CH), 127.1 (CH), 109.0 (C), 108.5 (C), 96.7 (CH), 71.1 (CH), 70.8 (CH), 70.7 (CH), 70.5 (CH), 47.0 (CH_2), 40.2 (CH), 26.1 (CH_3), 26.0 (CH_3), 24.9 (CH_3), 24.3 (CH_3).

HRMS (ESI) Exact mass calculated for $C_{20}H_{26}NaO_{76}$ $[M+Na]^+$: 385.1622, found: 385.1617

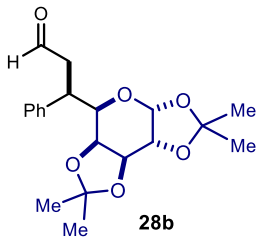

28b

(*R*)-3-phenyl-3-((3a*R*,5*R*,5a*S*,8a*S*,8b*R*)-2,2,7,7-tetramethyltetrahydro-5H-bis([1,3]dioxolo)[4,5-b:4',5'-d]pyran-5-yl)propanal (28b)

Prepared according to the general procedure using cinnamaldehyde (39.6 mg, 0.3 mmol), aminocatalyst (*R*)-**A** (14 mg, 20 mol%), and the corresponding dihydropyridine (48.2 mg, 0.1 mmol) in DCM (400 µL). The crude material was purified by flash column chromatography (hexane/diethyl ether 4:1) to give the product (19.8 mg, 54% yield, 10:90

mixture of diastereoisomers, average of two runs) as a white solid. C*haracterization of the major diastereoisomer*: ^{1}H NMR (400 MHz, $CDCl_3$) δ 9.62 (1H, dd, *J* = 2.6, 1.9 Hz C**H**O),7.35-7.19 (5H, m, Ar**H**), 5.47 (1H, d, *J* = 5.1 Hz, C1**H**), 4.58 (1H, dd, *J* = 8.0, 2.4 Hz, C3**H**), 4.28 (1H, dd, *J* = 5.1, 2.4 Hz, C2**H**), 4.22 (1H, dd, *J* = 8.0, 1.8 Hz, C4**H**), 4.01 (1H, dd, *J* = 8.5, 1.8 Hz, C5**H**), 3.64 (1H, td, *J* = 8.9, 5.2 Hz, ArC**H**), 3.02 (1H, ddd, *J* = 16.6, 5.2, 1.9 Hz, C**H**$_2$CHO), 2.82 (1, ddd, *J* = 16.6, 9.2, 2.6 Hz, C**H**$_2$CHO), 1.52 (3H, s, C**H**$_3$), 1.49 (3H, s, C**H**$_3$), 1.35 (3H, s, C**H**$_3$), 1.29 (3H, s, C**H**$_3$).

^{13}C NMR (101 MHz, $CDCl_3$) δ 201.9 (C=O), 140.3 (C), 128.5 (CH), 128.2 (CH), 126.9 (CH), 109.3 (C), 108.4 (C), 96.6 (CH), 71.0 (CH), 70.9 (CH), 70.4 (CH), 69.6 (CH), 45.30 (CH_2), 41.6 (CH), 26.0 (CH_3), 25.9 (CH_3), 24.8 (CH_3), 24.3 (CH_3).

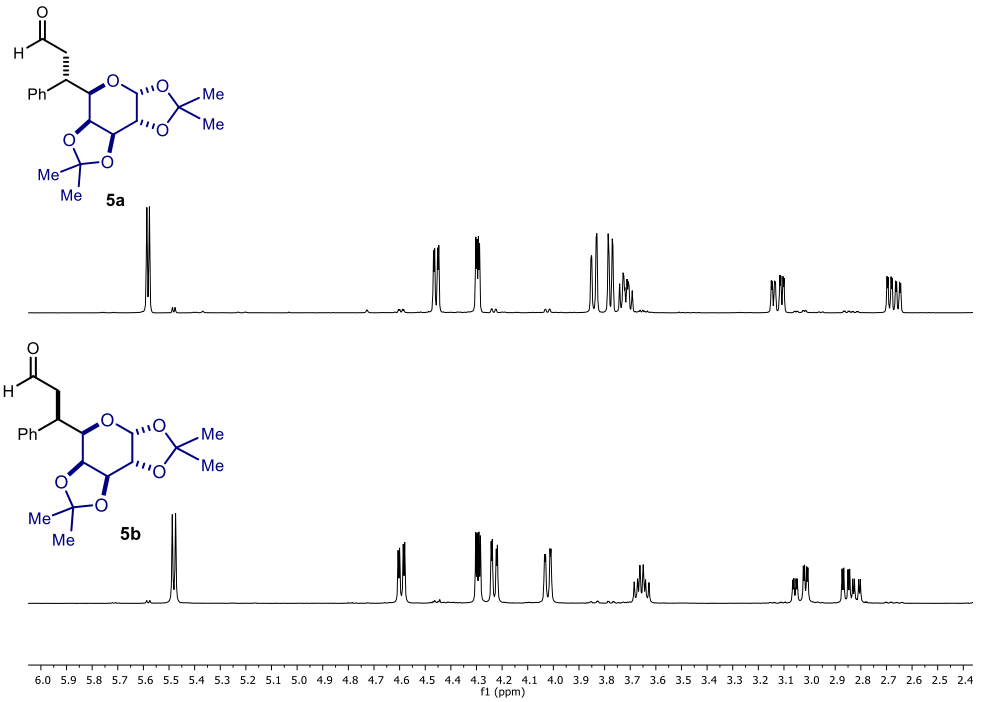

Acid Screening and Control Experiments

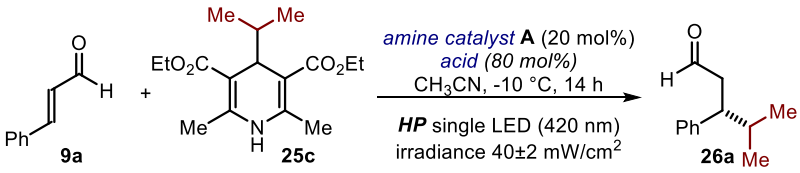

entry	Acid	yield (%)[a]	ee (%)
1	Benzoic Acid	< 5	-
2	Acetic Acid	< 5	-
3	Triflic Acid	6	-
4	Perchloric Acid	65 (58)[b]	63
5	Tosylic Acid	66 (55)[b]	68
6	Tetrafluoroboric Acid	73 (67)[b]	67
7	Trifluoroacetic Acid	91	80

[a] NMR yield of **3a** determined using trichloroethylene as the internal standard.[b] Number in parenthesis indicates the yield of the isolated 3a after chromatographic purification on silica gel.

Benzoic acid, acetic acid and triflic acid are not competent acids while the desired product **26a** was formed with moderate yield and selectivity when using perchloric, *p*-toluenesulfonic, and tetrafluoroboric acid. Clearly, trifluoroacetic acid provided the best results in terms of both reactivity and enantiocontrol.

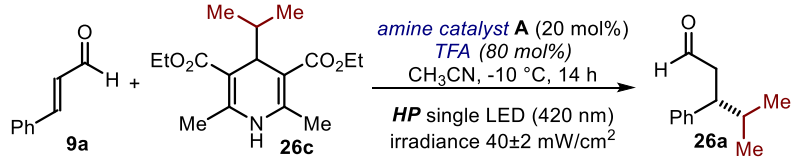

entry	TFA	Catalyst	Light	Conversion **2c** (%)[a]	Yield **3a** (%)[b]
1	×	✓	✓	< 10	0
2	×	×	✓	< 10	0
3	✓	×	✓	74	8
4	✓	✓	×	0	0

[a] Conversion of **2c** determined using trichloroethylene as the internal standard.[b] NMR yield of 3a determined using trichloroethylene as the internal standard.

In order to exclude the direct photoactivity of the 1,4 dihydropyridine, control experiments were conducted in the absence of catalyst, acid and light irradiation.

The reaction does not proceed in the absence of the acid, even in the presence of the catalyst (entries 1 and 2). In these cases, the conversion of the dihydropyridine derivatives is less than 10% confirming the absence of a direct absorption of the substrate 25c (see also Section E.1.) and ruling out a possible cinnamaldehyde photoactivity at this wavelength. The reaction does not proceed in the absence of light confirming the photochemical nature of the transformation (entry 4).

When adding TFA but in the absence of the amine catalyst A (entry 3), we did observe the formation the alkylation product 26a in 8% yield along with 74% of conversion of dihydropyridine 25c. This result suggests that TFA, by means of Brønsted acid activation of cinnamaldehyde 9a, may enable a bathochromic shift. The selective excitation of the TFA-9a adduct at 420 nm may trigger the photooxidation of the dihydropyridine 25c.

Single Crystal X-ray Diffraction Data for compound 28a

Crystals of the compound **28a** were obtained by slow evaporation of a hexane/ethyl acetate solution.

Data Collection. Measurements were made on a Bruker-Nonius diffractometer equipped with an APPEX 2 4K CCD area detector, a FR591 rotating anode with MoKα radiation. Montel mirrors and a Cryostream Plus low temperature device (T = 100K). Full-sphere data collection was used with ω and φ scans.

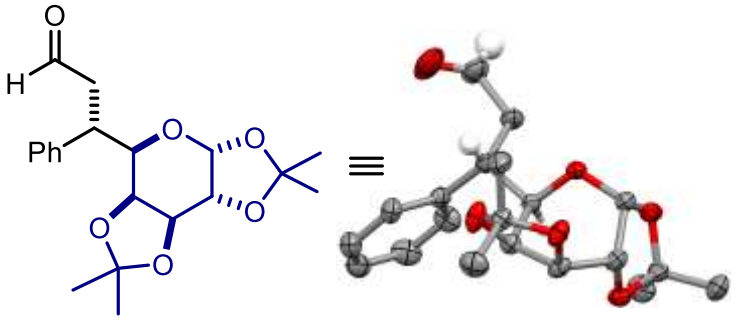

28a *CCDC 1581199*

Empirical formula	C20 H26 O6
Formula weight	362.41
Temperature	100(2) K
Wavelength	0.71073 Å
Crystal system	Monoclinic
Space group	P2(1)
Unit cell dimensions	a = 20.0688(3)Å α= 90°.
	b = 9.57471(12)Å β = 113.3147(18)°.

	c = 21.8114(3)Å γ = 90°.
Volume	3848.90(11) $Å^3$
Z	8
Density (calculated)	1.251 Mg/m^3
Absorption coefficient	0.091 mm^{-1}
F(000)	1552
Crystal size	? x ? x ? mm^3
Theta range for data collection	1.891 to 40.249°.
Index ranges	-36<=h<=36,-16<=k<=17,-39<=l<=39
Reflections collected	201662
Independent reflections	47414[R(int) = 0.0361]
Completeness to theta =40.249°	100.0%
Absorption correction	Multi-scan
Max. and min. transmission	0.995 and 0.765
Refinement method	Full-matrix least-squares on F^2
Data / restraints / parameters	47414/ 25/ 981
Goodness-of-fit on F^2	0.990
Final R indices [I>2sigma(I)]	R1 = 0.0503, wR2 = 0.1298
R indices (all data)	R1 = 0.0722, wR2 = 0.1462
Flack parameter	x =-0.08(9)
Largest diff. peak and hole	0.477 and -0.260 $e.Å^{-3}$

Chapter V

Reactivity of 1,4-Dihydropyridines in the Excited State

Target

Investigation of the excited-state properties of 4-alkyl-1,4-dihydropyridines and development of a photochemical methodology for the nickel-catalyzed radical alkylation of arenes and acyl chlorides.

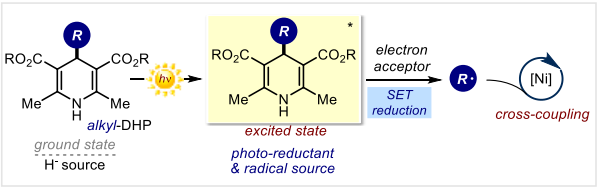

Tools. Using the properties of of 4-alkyl-1,4-dihydropyridines in the excited state to generate alkyl radicals and develop photochemical nickel-catalyzed cross-coupling processes.[1]

5.1 Introduction

The electronic reorganization associated with light excitation turns excited-state species into better reductants and oxidants than in the ground state. Light absorption turns electron-deficient chiral iminium ions into strong oxidants capable to trigger a variety of enantioselective radical transformations. In the last part of my Ph.D. studies, I investigated the excited-state reactivity of 4-alkyl dihydropyridines (4-alkyl-DHPs), which become strong reducing agents upon visible-light irradiation.

Within our group, we have already shown that electron-rich enamines **I**, which act as nucleophiles in the ground state, could become strong reductants upon light excitation and trigger the formation of radicals through SET reduction of electron-poor organic halides (Figure 5.1a). In the same vein, 1,4-dihydropyridine derivatives (H-DHP) **1** are primarily understood as hydride (H^-) sources in their ground-state. It was recently demonstrated that exciting them with visible light affords strong photoreductants that can productively engage in single electron transfer (SET) manifolds (Figure 5.2b).

[1] Part of the projects discussed in this Chapter has been conducted in collaboration with Dr Alexis Prieto, Dr Sudipta Raha Roy, Nurtalya Alandini and Dr Thomas van Leeuwen. Part of the work has been published, see: Buzzetti, L., Prieto, A., Roy, S. R., Melchiorre, P., "Radical-Based C−C Bond-Forming Processes Enabled by the Photoexcitation of 4-Alkyl-1,4-dihydropyridines" *Angew. Chem. Int. Ed.* **2017**, *56*, 15039.

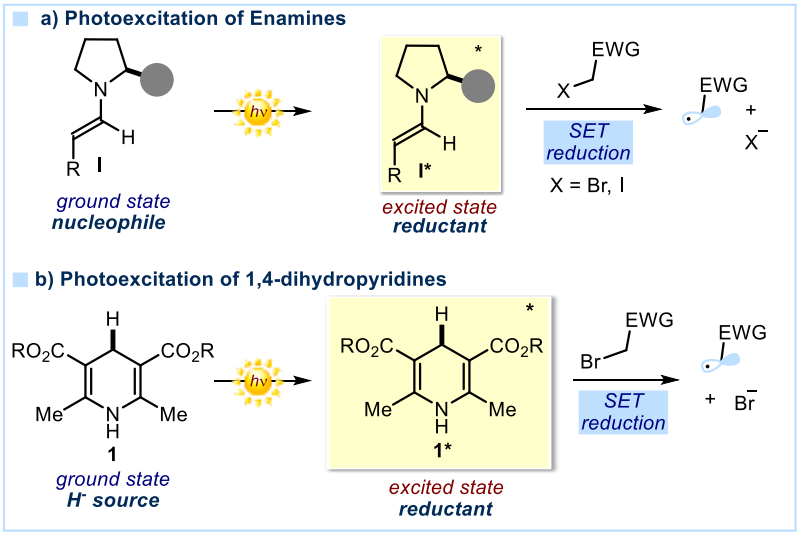

Figure 5.1: Radical generation strategies enabled by the excited-state reactivity of organic molecules. Previous studies demonstrating that light excitation turns a) enamines and b) 1,4-dihydropyridines **1** (H-DHP) into strong reductants and the resulting SET-based radical generation mechanisms.

In this chapter, we details our efforts in the evaluation of the excited-state properties of 4-alkyl-DHPs, previously exploited in their ground states only as alkyl radical sources.[2] After establishing the dual ability of photo-excited alkyl-DHP to generate C(sp^3)-centered radicals and to act as strong reducing agents, we demonstrated the possibility to use them in photochemical nickel-catalyzed C(sp^2)-C(sp^3) cross-coupling reactions in the absence of an external photoredox catalyst.

[2] a)Verrier, C., Alandini, N., Pezzetta, C., Moliterno, M., Buzzetti, L., Hepburn, H. B., Vega-Peñaloza, A., Silvi, M., Melchiorre, P., "Direct Stereoselective Installation of Alkyl Fragments at the β-Carbon of Enals via Excited Iminium Ion Catalysis" *ACS Catal.* **2018**. b) Gutiérrez-Bonet, A. l., Tellis, J. C., Matsui, J. K., Vara, B. A., Molander, G. A., "1,4-Dihydropyridines as Alkyl radical Precursors: Introducing the Aldehyde Feedstock to Nickel/Photoredox Dual Catalysis" *ACS Catal.* **2016**, *6*, 8004. c) Nakajima, K., Nojima, S., Sakata, K., Nishibayashi, Y., "Visible-Light-Mediated Aromatic Substitution Reactions of Cyanoarenes with 4-Alkyl-1,4-dihydropyridines through Double Carbon–Carbon Bond Cleavage" *ChemCatChem* **2016**, *8*, 1028.

5.2 Metalla-photoredox Catalysis

The combination of transition-metal catalysis with photochemistry, named metallaphotocatalysis, has recently emerged as a powerful technology for the development of novel synthetic methodologies (Figure 5.2).[3] Photoredox catalysis gives access to highly reactive open shell intermediates from a variety of substrates through SET manifolds. In addition, the transition-metal catalysts activate different classes of electrophiles and direct their reactivity towards the coupling with the radical intermediates, thus promoting the formation of new chemical bonds. The photocatalyst is also responsible of the modulation of the oxidation states of the transition-metal center, helping the organometallic steps of the transformation and closing the catalytic cycle. The metallaphotoredox approach provides a new activation mode that is complementary to the classical transition-metal catalyzed reactions. Molecules, which are generally inert in polar pathways, can be activated via SET providing radical intermediates that engage in metal-mediated cross-coupling reactions.

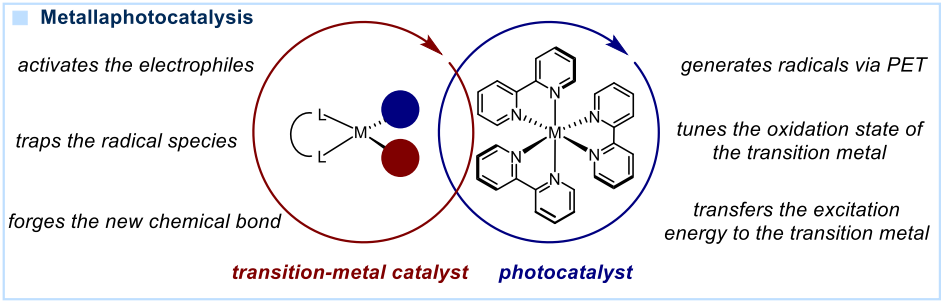

Figure 5.2: The benefit of combining transition metal catalysis and photocatalysis.

The seminal works that set the foundation of the metallaphotocatalysis field were published independently in 2014 by Molander[4] and MacMillan and Doyle.[5] In the first report, the activity of an iridium based photocatalyst in combination with nickel catalysis allowed the direct coupling between aryl halides **2** and alkyl potassium trifluoroborate salts **3** (Figure 5.3a). Despite the wide use of trifluoroborate salts in classical Suzuki-Miyaura cross-coupling reactions for the formation of C(sp^2)-C(sp^2) bonds[6], alkyl trifluoroborate derivatives are generally recalcitrant towards classical two-electron nickel catalyzed protocols, due to their low rates in the transmetallation steps. This long standing problem was overcome using a

[3] Twilton, J., Zhang, P., Shaw, M. H., Evans, R. W., MacMillan, D. W., "The merger of transition metal and photocatalysis" *Nat. Rev. Chem.* **2017**, *1*, 0052.
[4] Tellis, J. C., Primer, D. N., Molander, G. A., "Single-Electron Transmetalation in Organoboron Cross-coupling by Photoredox/Nickel Dual Catalysis" *Science* **2014**, *345*, 433.
[5] Zuo, Z., Ahneman, D. T., Chu, L., Terrett, J. A., Doyle, A. G., MacMillan, D. W., "Merging photoredox with nickel catalysis: Coupling of α-carboxyl sp3-carbons with aryl halides" *Science* **2014**, *345*, 437.
[6] Molander, G. A., Brown, A. R., "Suzuki− Miyaura cross-coupling reactions of potassium vinyltrifluoroborate with aryl and heteroaryl electrophiles" *J. Org. Chem.* **2006**, *71*, 9681.

radical approach. Specifically (Figure 5.3b), the Ni(0) complex **II** undergoes oxidative addition with the bromoarene **2** generating the Ni(II) complex **III**. Concomitantly, the iridium based photocatalyst triggers the thermodynamically feasible SET oxidation of the benzylic potassium trifluoroborate salt **3** upon light-excitation. The benzyl radical **IV**, generated upon fragmentation of the leaving group, is then trapped by the nickel complex **III** forming the high-valent Ni(III) intermediate **V**. The rapid reductive elimination from this species yields the desired cross-coupling product **4** and the Ni(I) complex **VI**. The reduction of the latter from the reduced photocatalyst Ir(II) regenerates both the Ni(0) catalyst and the Ir photocatalyst in the original oxidation state, thus closing both catalytic cycles.

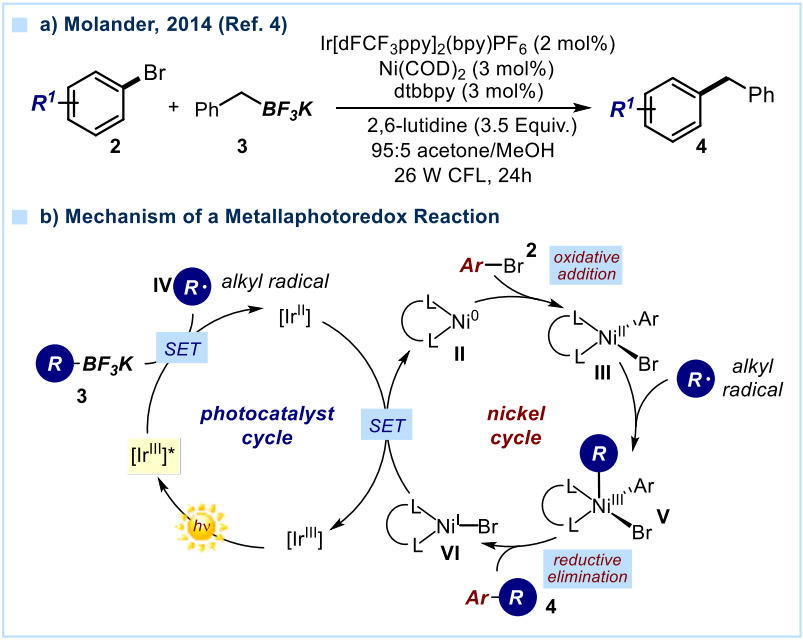

Figure 5.3: a) Metallaphotocatalytic reaction between aryl bromide **2** and alkyl trifluoroborate salts **3**. b) Proposed reaction mechanism.

In the conceptually similar MacMillan and Doyle's approach, the radical is generated upon light-triggered SET oxidation and decarboxylation of carboxylic acid derivatives **5** (Figure 5.4a). Also in this case the combination of a nickel catalyst and an iridium-based photocatalyst is crucial for successfully implementing the cross-coupling method. Benzylic, α-oxy, α-amino, and simple alkyl carboxylic acids were used as suitable substrates. The use of a chiral ligand for binding the nickel catalyst allowed the development of an asymmetric version of this transformation. MacMillan and Fu reported a metallaphotocatalytic protocol for the

enantioselective decarboxylative arylation of α-amino acids (Figure 5.4b).[7] In this protocol, the use of a substituted C_2-symmetric semiccorin-like ligand **8**[8] furnishes the chiral Ni(0) complex, which can undergo oxidative addition with the bromoarene **2** and trap the radical generated upon photocatalytic SET oxidation and decarboxylation of the amino acid derivative **7**. The chiral complex delivers the desired chiral arylated product **9** in high enantioselectivity after reductive elimination.

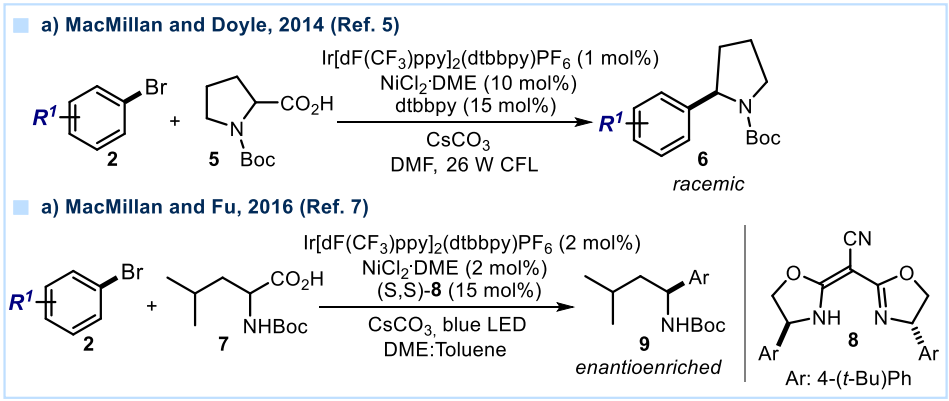

Figure 5.4: a) The use of carboxylic acids as radical precursor for metallaphotocatalytic protocols. b) An enantioselective metallaphotocatalytic reaction enabled by the use of a chiral ligand.

The transition metal with the widest application in metallo-photoredox catalysis is, without any doubts, nickel (Figure 5.5). The main reason can be found in the redox properties of this metal. In addition to the oxidation states (0) and (II), which are typical of the catalytic cycles of classical metal-catalyzed cross-coupling reactions, nickel can also easily access the oxidation states (I) and (III), which are peculiar of radical and one-electron based radical protocols.[9] Additionally, the redox potential associated to the reduction of Ni(II) to Ni(0) and Ni(I) to Ni(0), which are crucial redox steps of the metallaphotoredox catalytic cycles, are relatively low (E(Ni(II)/(Ni(I) ~ -1.2 V)[10] and compatible with the redox properties of the most common photoredox catalysts.

---

[7] Zuo, Z., Cong, H., Li, W., Choi, J., Fu, G. C., MacMillan, D. W., "Enantioselective decarboxylative arylation of α-amino acids via the merger of photoredox and nickel catalysis" *J. Am. Chem. Soc.* **2016**, *138*, 1832.

[8] This class of ligands was first reported by Pfaltz and exploited in asymmetric transition-metal catalyzed transformation: Fritschi, H., Leutenegger, U., Pfaltz, A., "Chiral Copper-Semicorrin Complexes as Enantioselective Catalysts for the Cyclopropanation of Olefins by Diazo Compounds" *Angew. Chem. Int. Ed.* **1986**, *25*, 1005.

[9] Tasker, S. Z., Standley, E. A., Jamison, T. F., "Recent advances in homogeneous nickel catalysis" *Nature* **2014**, *509*, 299.

[10] a) Cannes, C., Labbé, E., Durandetti, M., Devaud, M., Nédélec, J. Y., "Nickel-catalyzed electrochemical homocoupling of alkenyl halides: Rates and mechanisms" *J. Electroanal. Chem.* **1996**, *412*, 85. The reduction of (bpy)$NiBr_2$ is observed as a two-electron wave at -1.1 V, implying that reduction of (bpy)NiBr to (bpy)Ni(0) occurs at a more positive potential.

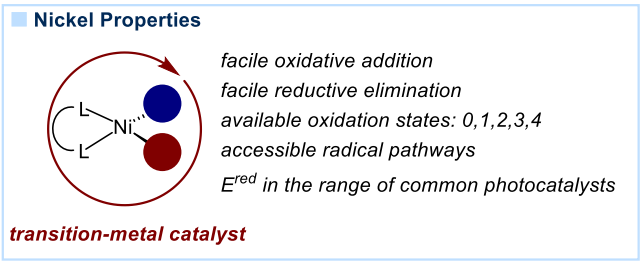

Figure 5.5: The peculiar features of nickel make it the most suitable transition metal for the metallaphotoredox methodologies.

In addition to the SET-based metallaphotoredox reactions, transition-metal catalyzed transformations based on energy transfer events have been recently disclosed. This is the case of the nickel-catalyzed photocatalytic acylation of bromo arenes recently reported by MacMillan (Figure 5.6).[11] In this reaction, the nickel catalyst undergoes oxidative addition with the bromoarene **10** providing the aryl-Ni(II) complex **VII**, which can coordinate the carboxylate obtained by deprotonation of the carboxylic acid derivative **11**. The reductive elimination from the so formed aryl-Ni(II) carboxylate complex **VIII** is known to be difficult in the ground state. Here, this difficult step is achieved thanks to the interaction with the excited-state photocatalyst. The iridium-based photocatalyst harvests the energy of the light and transfer it to the nickel complex **VIII**, which reaches the electronically-excited state **VIII***. From this state, the reductive elimination can easily take place delivering the desired acylated arene **12** and restoring the Ni(0) catalyst. Control experiments confirmed that the aryl-Ni(II) carboxylate complex **VIII** in the ground state is recalcitrant towards reductive elimination and proved that the photocatalyst is not participating in an electron-transfer event but is acting as an antenna, transferring its excitation energy to the nickel-complex.

[11] Welin, E. R., Le, C., Arias-Rotondo, D. M., McCusker, J. K., MacMillan, D. W., "Photosensitized, energy transfer-mediated organometallic catalysis through electronically excited nickel (II)" *Science* **2017**, *355*, 380.

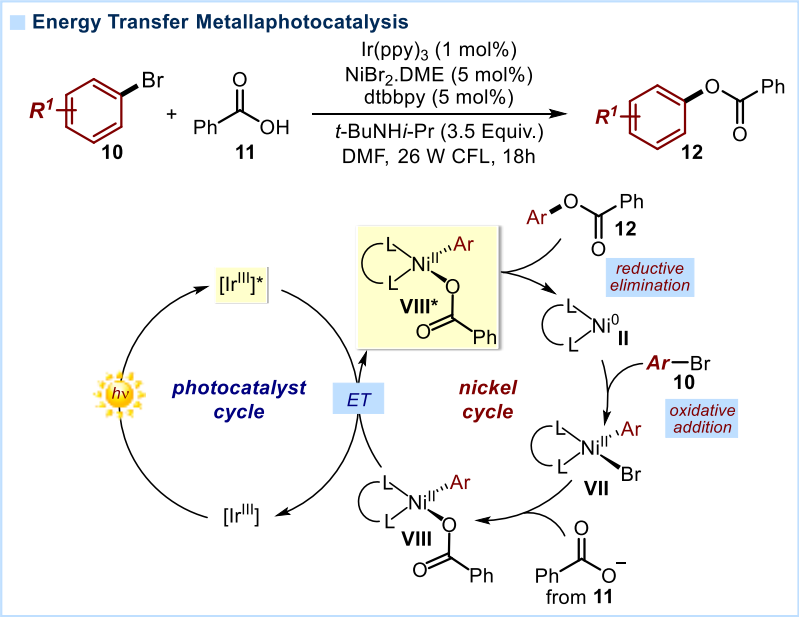

Figure 5.6: A metallaphotocatalysis methodology based on an energy-transfer interaction between the photocatalyst and the nickel complex.

5.3 1,4-Dihydropyridines: Ground-State Properties and Reactivity

1,4-dihydropyridines (DHPs) are versatile scaffolds found in several biologically active and pharmaceutically relevant compounds. For instance, many calcium channel blockers, used in the treatment of hypertension and others cardiovascular diseases, are based on this scaffold (Figure 5.7a). Nicotinamide adenine dinucleotide (NAD) is the most abundant biomolecule containing this moiety (Figure 5.7b). This coenzyme is present in all living cells and plays a crucial role in the cell metabolism, acting as redox mediator and carrying electrons from one reaction to another. This process is often referred to as *transfer hydrogenation*. This task is accomplished by the coexistence of this molecule in two oxidation states: the oxidized form NAD^+, which can accept electrons from a reductant, and the reduced form NADH, which can donate electrons to an acceptor.

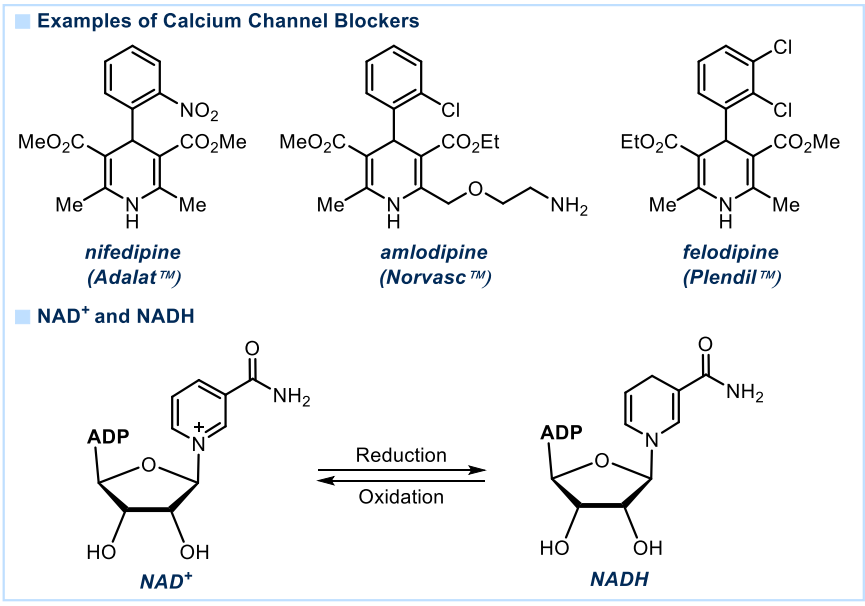

Figure 5.7: a) Examples of drugs containing the DHP scaffold. b) The two oxidation states of the coenzyme NAD.

In the realm of organic chemistry, 1,4-dihydropyridines, namely Hantzsch esters, were first synthesized in 1881 by Arthur Hantzsch through a multicomponent condensation of β-keto esters with ammonium acetate.[12] Concerning the ground-state reactivity of 1,4 dihydropyridines, they are mainly intended as hydride sources. In fact, these compounds can easily donate a hydride (H^-) to a suitable electrophile. The aromatization of the dihydropyridine scaffold provides the driving force to trigger these reactions. This feature was exploited in the 1970s for the development of bioinspired metal-free reductions of electron-poor olefins and iminium salts, using DHP **1** as reducing agents.[13] Recently, with the advent of organocatalysis, asymmetric versions of these transfer hydrogenations were independently reported by List and MacMillan.[14] List exploited a chiral Brønsted acid to develp a biomimetic enantioselective reduction of imines (Figure 5.8a).[15] In this reaction, the chiral Brønsted acid **14** protonates and activates the imine derivatives **13** towards the stereoselective nucleophilic

[12] Hantzsch, A., "Condensationsprodukte aus Aldehydammoniak und Ketonartigen Verbindungen" *Chem. Ber.* **1881**, *14*, 1637.
[13] Selected examples: Pandit, U. K., Cabré, F. R. M., Gase, R. A., de Nie-Sarink, M. J., "Biomimetic stereospecific reduction of αβ-unsaturated iminium salts" *J. Chem. Soc., Chem. Commun.* **1974**, 627b.
[14] Selected reviews about asymmetric transfer hydrogenation: a) Zheng, C., You, S.-L., "Transfer hydrogenation with Hantzsch esters and related organic hydride donors" *Chem. Soc. Rev.* **2012**, *41*, 2498. b) You, S. L., "Recent developments in asymmetric transfer hydrogenation with Hantzsch esters: a biomimetic approach" *Chem. Asian J.* **2007**, *2*, 820.
[15] Hoffmann, S., Seayad, A. M., List, B., "A powerful Brønsted acid catalyst for the organocatalytic asymmetric transfer hydrogenation of imines" *Angew. Chem.* **2005**, *117*, 7590.

attack of the hydride, delivering the enantioenriched amine product **15**. MacMillan exploited the iminium ion activation strategy for the enantioselective reduction of cinnamaldehyde derivatives (Figure 5.8b).[16] In this approach, the condensation of the chiral secondary amine catalyst **17** with the enal **16** generates an electrophilic iminium ion **IX**, which undergoes the stereoselective attack of the hydride affording the enantioenriched reduced aldehyde **18**.

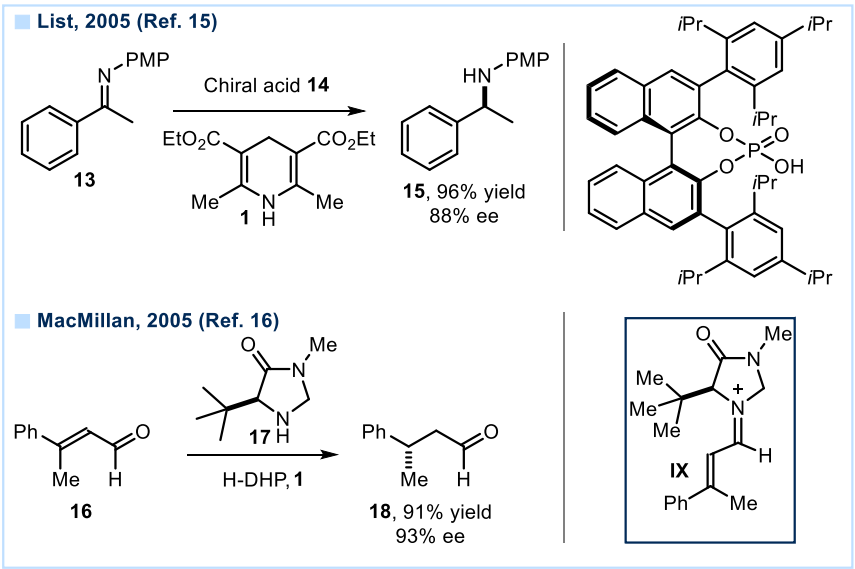

Figure 5.8: a) Hantzsch ester as hydride source in a Brønsted acid catalyzed enantioselective reduction of imines. b) An iminium-ion mediated asymmetric reduction of enal exploiting Hantzsch ester as hydride source.

With the advent of photoredox catalysis, the search for suitable electron-donors that can participate in the reductive quenching of the photocatalysts led to the identification of 1,4-dihydropyridines as valid alternatives to the commonly used tertiary amines.[17] In fact, the redox potential of these species (E^{ox}~0.8-0.9V) falls in the operative range of the excited-state photocatalysts and is comparable with the ones of alkyl tertiary amines (E^{ox} ~0.8-1V). The ability of DHP to donate electrons to excited-state photocatalysts, thus generating a highly reducing photocatalyst, was exploited by Stephenson in the reductive dehalogenation of unactivated organic halides (Figure 5.9a).[18] In this report, a combination of tributyl amine Bu_3N and Hantzsch ester (H-DHP) **1** is responsible for the reductive quenching of the

[16] Ouellet, S. G., Tuttle, J. B., MacMillan, D. W., "Enantioselective organocatalytic hydride reduction" *J. Am. Chem. Soc.* **2005**, *127*, 32.
[17] Zhu, X. Q., Li, H. R., Li, Q., Ai, T., Lu, J. Y., Yang, Y., Cheng, J. P., "Determination of the C4-H Bond Dissociation Energies of NADH Models and Their Radical Cations in Acetonitrile" *Chem. Eur. J.* **2003**, *9*, 871.
[18] Nguyen, J. D., D'amato, E. M., Narayanam, J. M., Stephenson, C. R., "Engaging unactivated alkyl, alkenyl and aryl iodides in visible-light-mediated free radical reactions" *Nat. Chem.* **2012**, *4*, 854.

photoexcited $Ir(ppy)_3$ photocatalyst (PC). The so formed Ir(II) intermediate (PC^-) acts as strong reductant and triggers the reductive deiodination of alkyl iodides **19**. Other variants of Hantzsch ester derivatives, bearing not-fragmenting groups at the 4 position (i.e. Ph, Me, Et) were synthesized and exploited as electron donors in photoredox methodologies.

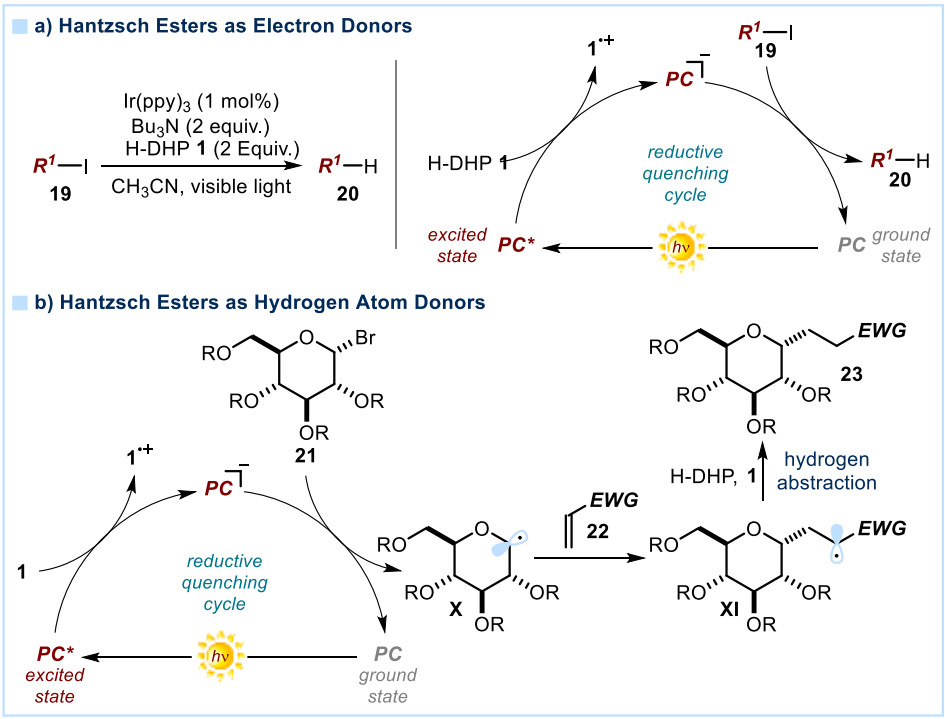

Figure 5.9: a) Hantzsch ester as electron donors in a photoredox methodology. b) Hantzsch esters can act both as electron donor and hydrogen atom donor.

In addition to the electron-donor capability of these compounds, DHPs can also deliver hydrogen atom and can be used as hydrogen sources in radical processes. This feature was exploited by Gagné to achieve the photocatalytic addition of glycosides to Michael acceptors (Figure 5.9b).[19] The excited-state $[Ru(bpy)_3(BF_4)_2]$ photocatalyst (PC) is reduced by a combination of Hünig's base and H–DHP, providing the Ru(I) intermediate (PC^-). This is responsible of the reduction of a glycosyl bromide **21** that ultimately generates the alkyl radical intermediate **X** after mesolytic cleavage. The radical is trapped by the Michael acceptor **22** delivering the radical intermediate **XI**, which can abstract a hydrogen atom from another molecule of Hantzsch ester **1** affording the desired hydroalkylation product **23**.

As already discussed in Chapter IV, section 4.3.4, when the DHPs are decorated with easily fragmenting alkyl groups in the C4-position, the oxidation of these compounds generates unstable radical cations, which can easily undergo C–C fragmentation delivering alkyl

[19] Andrews, R. S., Becker, J. J., Gagné, M. R., "Intermolecular addition of glycosyl halides to alkenes mediated by visible light" *Angew. Chem.* **2010**, *122*, 7432.

radicals. We relied on this concept for the development of the photoexcited iminium ion-mediated β-alkylation of enals. In addition to this example, the use of 4-alkyl DHPs as radical sources has been recently reported by Molander in a metallaphotoredox protocol (Figure 5.10).[20] In this reaction, the organic photocatalyst 4CzIPN (PC) reaches an excited state upon visible-light absorption and triggers the SET oxidation of the 4-alkyl dihydropyridine **25** generating the alkyl radical after C–C fragmentation. Concomitantly, the Ni(0) catalyst **XII** traps this open-shell species and the resulting Ni(I) complex **XIII** undergoes oxidative addition with the aryl bromide **24**. Reductive elimination from the emerging Ni(III) species **XIV** delivers the desired products **26** and the Ni(I) complex **XV**, which readily accepts an electron from the reduced photocatalyst closing the catalytic cycles. Recently, a similar reactivity was exploited for the functionalization of glycosides starting from easily accessible 4-glycosyl-DHPs.[21]

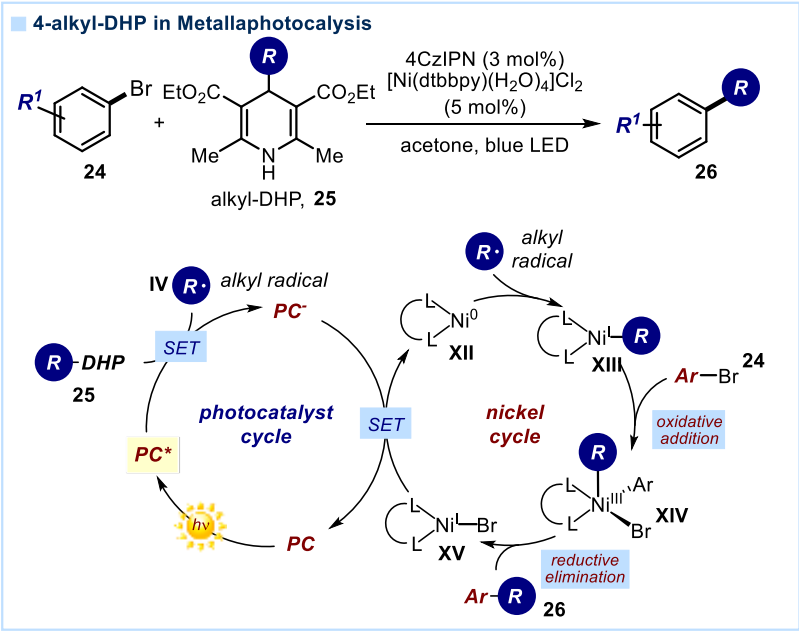

Figure 5.10: Use of 4-alkyl-DHP as radical sources in a metallaphotocatalysis methodology.

[20] Gutiérrez-Bonet, A. l., Tellis, J. C., Matsui, J. K., Vara, B. A., Molander, G. A., "1,4-Dihydropyridines as Alkyl radical Precursors: Introducing the Aldehyde Feedstock to Nickel/Photoredox Dual Catalysis."

[21] a) Badir, S. O., Dumoulin, A., Matsui, J. K., Molander, G. A., "Synthesis of Reversed C-Acyl Glycosides through Ni/Photoredox Dual Catalysis" *Angew. Chem. Int. Ed.* **2018**, *57*, 6610. b) Dumoulin, A., Matsui, J. K., Gutiérrez-Bonet, Á., Molander, G. A., "Synthesis of Non-Classical Arylated C-Saccharides Through Nickel/Photoredox Dual Catalysis" *Angew. Chem.* **2018**, *130*, 6724.

5.4 1,4-Dihydropyridines: Excited-state Properties and Reactivity

After the discovery of the biological role of NADH, several model systems which emulate this coenzyme were studied and exploited in biomimetic transfer hydrogenation reactions.[22] However, the researchers soon realized that these transformations are strongly dependent on the high electrophilicity of the substrates. Only electrophilic compounds are prone to accept the hydride ion (H^-) from the dihydropyridine scaffold. To expand the scope of these reactions, the excited-state properties of 1,4-dihydropyridine have been investigated. In particular, in 1961 Kurtz serendipitously discovered a photoinitiated reaction between Hantzsch esters **1** and bromotrichloromethane **27** (Figure 5.11a).[23] The reaction proceeds through light-excitation of H-DHP and delivers the corresponding pyridine **28** and chloroform **29** as products. The author did not propose any reasonable mechanism for this transformation, which still laid the basis for the investigation of the excited-state chemistry of DHPs.

20 years later, Fukuzumi carefully investigated the light-induced dehalogenation of organic halides in the presence of NADH. Using a combination of spectroscopic techniques and kinetic analysis, he postulated that the excited states of the electron-rich dihydropyridines can act as photoreductants and trigger the SET reduction of suitable acceptors.[24] In the following years, this discovery fostered the development of several methodologies in which the excited-state properties of H–DHP are exploited for the reduction of various acceptors.[25] These precedents inspired Cho and co-workers to assess the reductive capability of photoexcited H–DHP through a combination of spectroscopic and electrochemical analysis (Figure 5.11b).[26] The estimated high reducing power ($E(\mathbf{1}^{\cdot+}/\mathbf{1}^{*})$= -2.28V vs SCE) confirmed the feasibility of triggering the photochemical reductive debromination of α-bromo ketones **30** providing products **31**.

[22] Eisner, U., Kuthan, J., "Chemistry of dihydropyridines" *Chem. Rev.* **1972**, *72*, 1.
[23] Kurz, J. L., Hutton, R., Westheimer, F., "The photochemical reduction of bromotrichloromethane by derivatives of 1, 4-dihydropyridine" *J. Am. Chem. Soc.* **1961**, *83*, 584.
[24] Fukuzumi, S., Hironaka, K., Tanaka, T., "Photoreduction of alkyl halides by an NADH model compound. An electron-transfer chain mechanism" *J. Am. Chem. Soc.* **1983**, *105*, 4722.
[25] Selected examples: a) Jin, M.-Z., Yang, L., Wu, L.-M., Liu, Y.-C., Liu, Z.-L., "Novel photoinduced aromatization of Hantzsch 1, 4-dihydropyridines" *Chem. Commun.* **1998**, 2451. b) Zhang, J., Jin, M.-Z., Zhang, W., Yang, L., Liu, Z.-L., "Photoinduced transformation of α, β-epoxyketones to β-hydroxyketones by Hantzsch 1, 4-dihydropyridine" *Tetrahedron Lett.* **2002**, *43*, 9687.
[26] Jung, J., Kim, J., Park, G., You, Y., Cho, E. J., "Selective Debromination and α-Hydroxylation of α-Bromo Ketones Using Hantzsch Esters as Photoreductants" *Adv. Synth. Catal.* **2016**, *358*, 74.

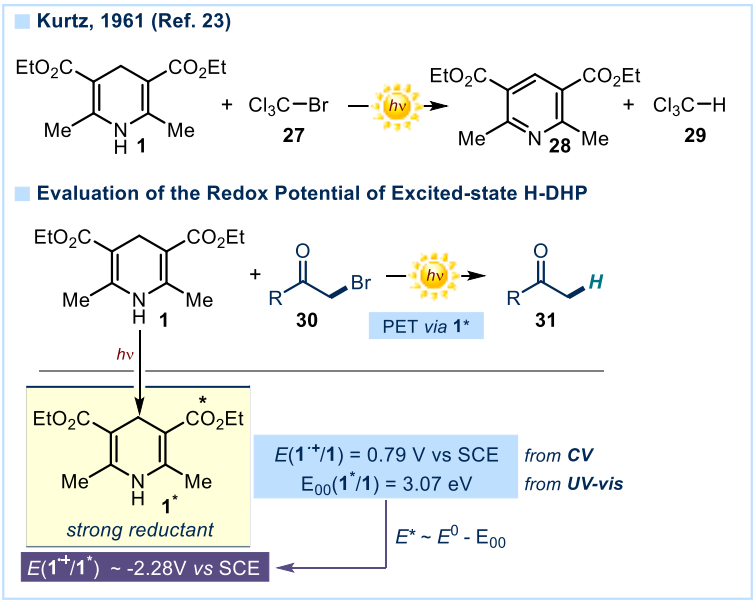

Figure 5.11: a) Serendipitous discovery of the excited-state chemistry of Hantzsch esters. b) Evaluation of the redox properties of photoexcited Hantzsch esters.

Recently, the photochemistry of NADPH (NADH Phosphate) was exploited by Hyster in combination with enzymatic catalysis for the development of a highly enantioselective radical debromination of racemic halolactones (Figure 5.12).[27] The racemic starting material **32** and the NADPH are seated in the active site of a ketoreductase (KRED). Visible-light excitation of the NADPH affords the excited-state NADPH*, which triggers the SET reduction of the halolactone providing the prochiral radical **XVI** after mesolytic cleavage of the C–Br bond. At this stage, a conformational change within the enzymatic task enables an asymmetric hydrogen atom transfer to the radical **XVI** to form the enantioenriched product **33**.

[27] Emmanuel, M. A., Greenberg, N. R., Oblinsky, D. G., Hyster, T. K., "Accessing non-natural reactivity by irradiating nicotinamide-dependent enzymes with light" *Nature* **2016**, *540*, 414.

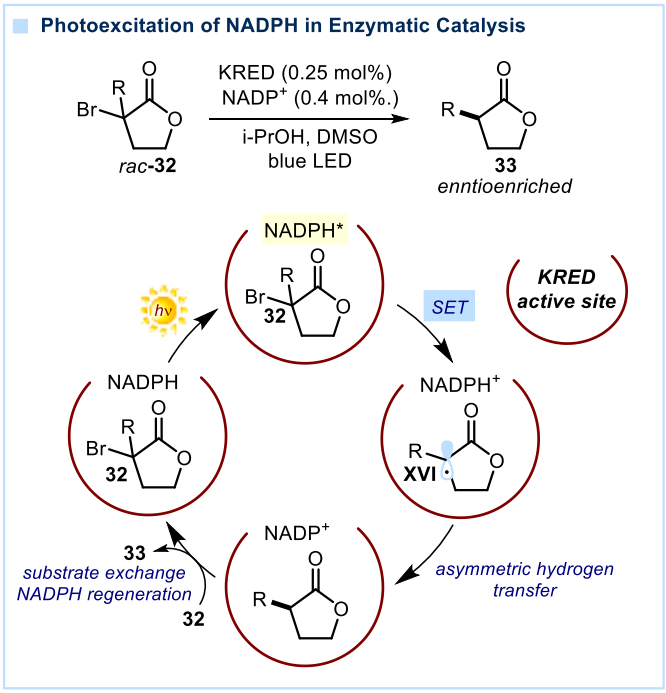

Figure 5.12: Excited-state DHP and enzymatic catalysis for the asymmetric dehalogenation of racemic halolactones. KRED: Ketoreductase.

5.5 Design and Target of the Project

Intrigued by the reductive properties of excited-state NADH and Hantzsch esters, we planned to extend this reactivity to 4-alkyl-1,4-dihydropyridines. The literature precedents and the extensive work conducted during the development of the photoexcited iminium ion-mediated β-alkylation of enals allowed us to gain an extensive knowledge on the behavior of these compounds in SET reactions. We hypothesized that, upon light irradiation, 4-alkyl-DHPs can reach an electronically excited state that can trigger a SET reduction of a suitable electron acceptor, thus forming the unstable radical cation **XVII**. As already demonstrated,[2] **XVII** would undergo a fast C–C bond fragmentation releasing the alkyl radical and forming the corresponding pyridine upon deprotonation (Figure 5.13)

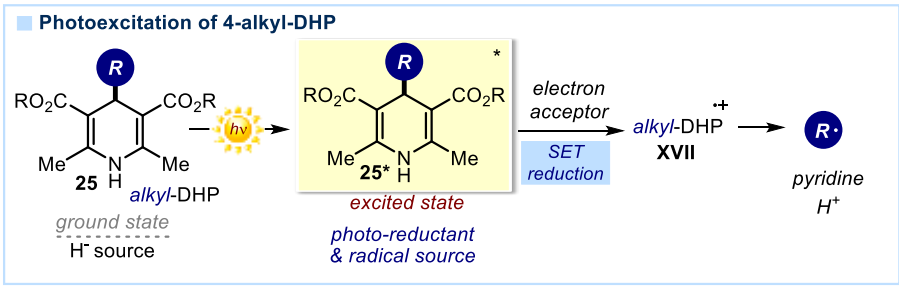

Figure 5.13: Design plan for exploiting the excited-state chemistry of 4-alkyl-DHPs.

In particular, we envisioned that the photochemistry of 4-alkyl-DHPs and their dual role could enable a nickel-catalyzed C(sp^2)–C(sp^3) cross-coupling, which reminds a metallaphotoredox protocol but without the need for any external photocatalyst. In our reaction design, depicted in Figure 5.14, the photoexcitation of a sacrificial amount of alkyl-DHP **25** provides the excited state intermediate **25***, which is responsible of the reduction (via two consecutive discrete SET events) of the Ni(II) precatalyst to afford the active Ni(0) intermediate (E^{red} = -1.2V vs SCE in DMF).[10] The concomitant formation of the radical cation **XVII** would secure the formation of the alkyl radical, which is then intercepted by the Ni(0) complex **XVIII**. The emerging Ni(I) organometallic species **XIX** would then undergo oxidative addition with the aromatic bromide **32**. This would lead to the Ni(II) intermediate **XX**, which, after reductive elimination, forges the desired C(sp^2)–C(sp^3) bond in the cross-coupled product **33**. Finally, the SET reduction of the generated Ni(I) complex **XXI** by the excited-DHPs **25*** would complete the nickel catalytic cycle while regenerating the C(sp^3) centered radical.

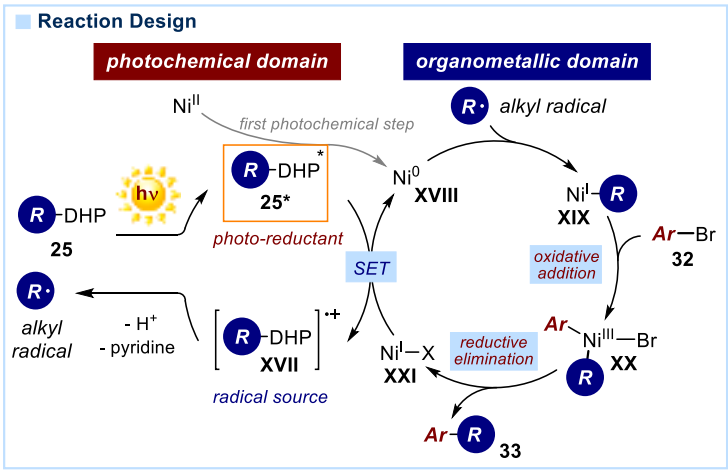

Figure 5.14: Our reaction design for the use of photoexcited alkyl-DHP in a nickel-catalyzed radical cross-coupling.

5.6 Results and Discussion

5.6.1 Photophysical Characterization of 4-alkyl-DHPs

As for many of the photochemical processes developed in our group, the color of 4-alkyl-DHPs was a wake-up call for starting the investigations. The 4-alkyl-DHPs synthesized and exploited for the previous project display a pale-yellow color, indicating their ability to absorb in the visible range (Figure 5.15).

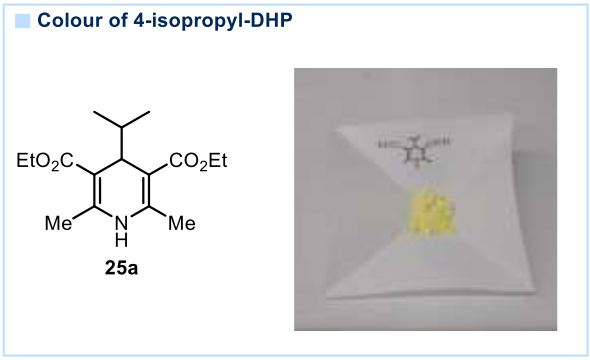

Figure 5.15: Empirical evaluation of the ability of 4-alkyl-DHP to absorb visible light.

To gain useful insights on the photochemical reactivity of these species, we conducted an extensive photophysical characterization of the model 4-benzyl-1,4-dihydropyridine **25b** (Bn-DHP.) We first recorded the optical absorption spectrum of **25b** dissolved in CH_3CN, confirming its ability to absorb in the visible frequency region, until 420 nm. The linearity of the Lambert-Beer correlation further confirmed the stability of these species under the condition of the photophysical investigation (Figure 5.16).

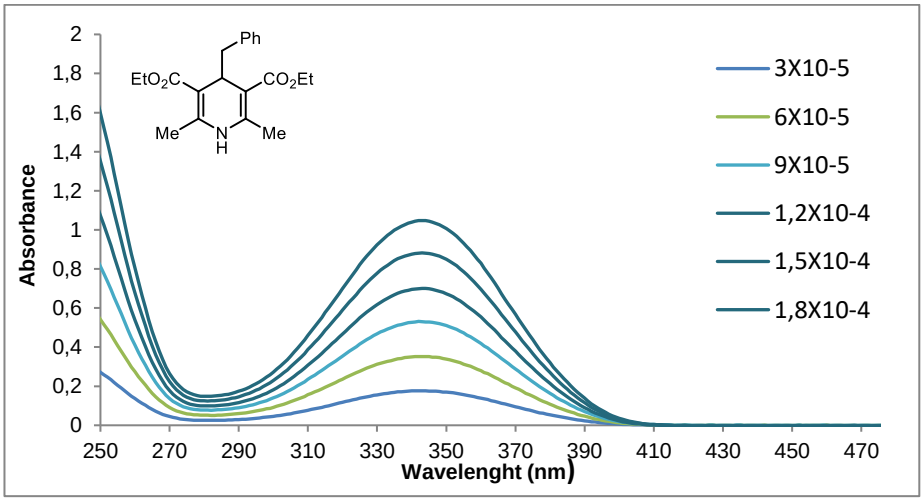

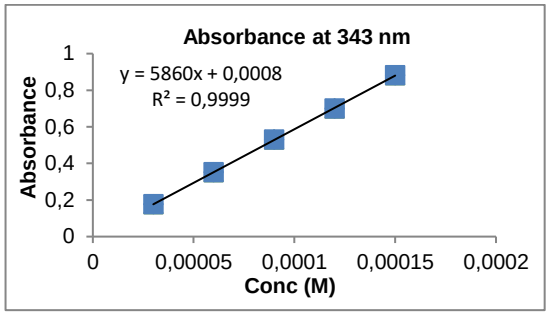

Figure 5.16: UV-Vis absorption spectra of **25b** at different concentration and Lambert-Beer linear correlation between absorbance and concentration at 343 nm.

We later focused on the electrochemical-characterization of substrate **25b**. Cyclic voltammetry (CV) measurement revealed an irreversible oxidation peak with $E_p^A = E_{ox}$ (**25b**$^{\cdot+}$/**25b**) = +1.00 V. This value confirmed the propensity of 4-alkyl DHP towards SET oxidation.

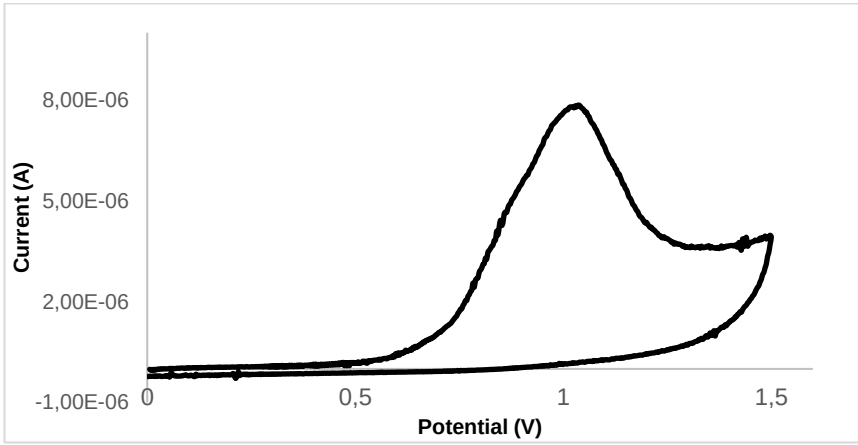

Figure 5.17: Cyclic voltammogram of 4-benzyl dihydropyridine **25b** [0.01 M] in [0.1 M] $TBAPF_6$ in CH_3CN. Sweep rate: 20 mV/s. Pt electrode working electrode, Ag/AgCl (KCl 3.5M) reference electrode, Pt wire auxiliary electrode. Irreversible oxidation. $E_p^A = E^{ox}$ (**25b**$^{\cdot+}$/**25b**) = +1.00 V; E_p^A is the anodic peak potential, while E^{ox} value describes the electrochemical properties of **25b**.

On the basis of the spectroscopic and electrochemical measurement and exploiting the Rehm-Weller theory, we estimated the reduction potential of the excited Bn-DHP E^{red} (**25b**$^{\cdot+}$/**25b***) = -2.0 V vs Ag/AgCl. This value confirms the reducing properties of the photoexcited alkyl-DHP.

We found that **25b** was fluorescent when excited at 405 nm, which allowed us to record the emission spectrum (Figure 5.18) and to measure the fluorescence lifetime in CH_3CN using a

picosecond pulsed laser (Figure 5.18, insert).[28] The reconvolution fitting showed a double exponential decay, affording the following values: τ_0=0.28 ns (below the instrument's detection limit) and τ_0=4.1 ns (see the Experimental Section for further details). Interestingly, the excited-state lifetime of Bn-DHP **25b** is comparable with the lifetime of unsubstituted 1,4-dihydropyridine of type **1** (H-DHP), which was measured to be 320 ps.[25] This result suggests that the excited-state alkyl-DHPs are long-lived enough to engage in photochemical process.

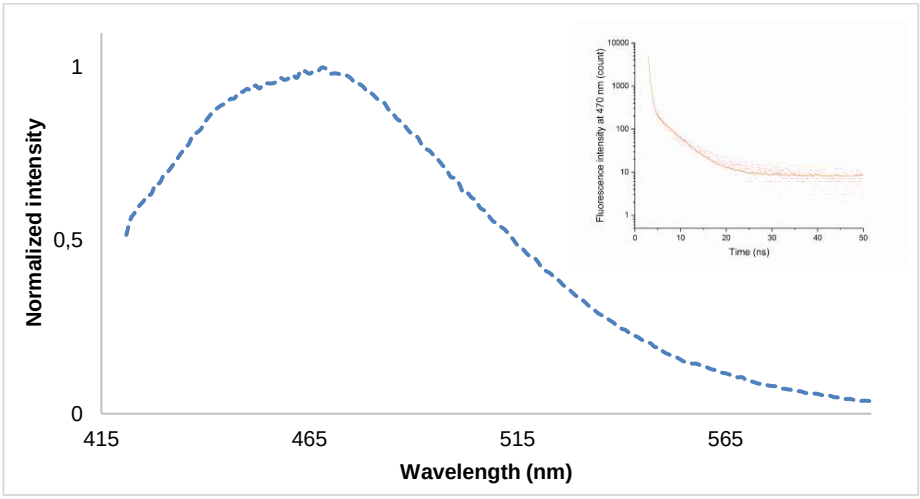

Figure 5.18: Emission spectrum of Bn-DHP **25b** (excitation wavelength at 405 nm). Insert: Fluorescence decay trace of 600 μM of **25b** in CH_3CN after nanosecond photoexcitation of 405 nm laser.

The thermodynamic and kinetic data we collected prompted us to further evaluate the photochemistry of the excited Bn-DHP.

5.6.2 Proving the Dual Role of 4-alkyl DHPs as Photoreductants and Radical Sources

At this stage, we wanted to prove the ability of 4-alkyl-DHP to act both as photoreductant and radical sources at the same time. We conducted a series of spectroscopic analysis and tailored control experiments. We started evaluating their behavior under visible light irradiation. Direct illumination of a CH_3CN solution of **25b** led to the complete disappearance of the DHP and to the formation of toluene, 1,2-diphenylethane, and the corresponding pyridine (Figure 5.19). Repeating the reaction in the presence of 2,2,6,6-tetramethyl-1-piperidinyloxy (TEMPO, 1 equiv.), a radical scavenger, we detected the formation of the benzyl-TEMPO adduct in 55% yield.

[28] The fluorescence lifetime measurement were conducted exploiting the Time-Correlated Single Photon Counting (TCSPC) technique. For more information: Lakowicz, J. R. Ed. *Principles of Fluorescence Spectroscopy* Plenum Press, New York, 1983

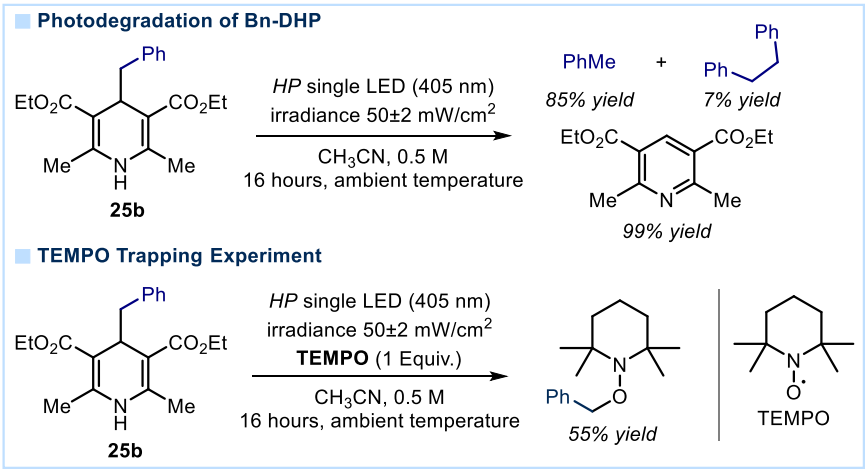

Figure 5.19: a) Photochemical behavior of a solution of **25b** in CH_3CN under 405 nm irradiation. b) Trapping of the benzyl radical in the presence of TEMPO as radical scavenger.

Overall, these experiments indicate that the simple photoexcitation of **25b** can trigger the formation of benzyl radicals. This notion was further corroborated by EPR studies of a solution of **25b** in CH_3CN, conducted at 77 K and with the same illumination system used in the previous control experiments (Figure 5.20). The EPR spectrum showed a strong isotropic X-band absorption and afforded a g-values of 2.0035, which is consistent with literature data for the characterization of benzyl radicals.[29]

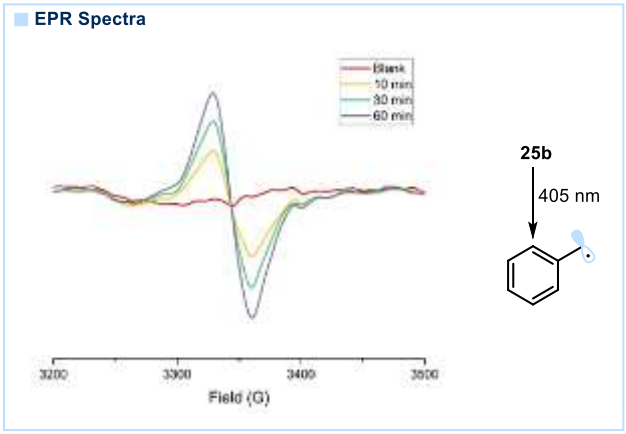

Figure 5.20: EPR experiment of 25b at different time intervals. EPR spectra were recorded after 0, 10, 30, and 60 min of irradiation.

[29] Kim, K. H., Bai, X., Brown, R. C., "Pyrolysis mechanisms of methoxy substituted α-O-4 lignin dimeric model compounds and detection of free radicals using electron paramagnetic resonance analysis" *J. Anal. Appl. Pyrolysis* **2014**, *110*, 254.

After establishing the ability of **25b** to generate C(sp^3)-centered radicals upon excitation, we evaluated its propensity to act as a strong reducing agent in the excited state. To test this possibility, we selected the aromatic *ipso*-substitution of cyanoarenes as the model reaction (Figure 5.21a).[30] Indeed, this process classically proceeds through a radical coupling mechanism that requires the concomitant formation of a C(sp^3)-centered radical and a persistent cyanoarene radical anion **XXII** obtained upon reduction of **34**. The ensuing C–C bond formation affords a cyclohexadienyl anion **XXIII** that is prone to rapid rearomatization *via* elimination of cyanide to afford the alkylated arene product **35**. When mixing either 4-cyanopyridine **34a** or tetracyanobenzene **34b**, two substrates largely used in aromatic *ipso*-substitution, with **25b** under light irradiation, the corresponding products **35a** and **35b** were generated in fairly good yields (Figure 5.21b). These results are consonant with the excited state of **25b** acting as both a strong reducing agent, affording the cyanoarene radical anion of type **XXII** upon SET reduction of substrate **34**, and as a source of benzyl radical, generated upon C–C bond fragmentation from the unstable radical cation **XVII**, emerging from SET. The thermodynamic feasibility of the SET reduction of both **34a** (E^{red} = -1.87 V *vs* SCE) and **34b** (E^{red} = -0.64V *vs* SCE)[31] is secured by the estimated reduction potential of the photoexcited **25b***.

[30] For a review: Bonesi, S. M., Fagnoni, M., "The Aromatic Carbon–Carbon ipso-Substitution Reaction" *Chem. Eur. J.* **2010**, *16*, 13572. For selected examples: a) McNally, A., Prier, C. K., MacMillan, D. W., "Discovery of an α-amino C–H arylation reaction using the strategy of accelerated serendipity" *Science* **2011**, *334*, 1114. b) Nakajima, K., Nojima, S., Sakata, K., Nishibayashi, Y., "Visible-Light-Mediated Aromatic Substitution Reactions of Cyanoarenes with 4-Alkyl-1,4-dihydropyridines through Double Carbon–Carbon Bond Cleavage."

[31] a) Mcdevitt, P., Vittimberga, B. M., "The electron transfer reactions of cyano substituted pyridines and quinolines with thermally generated diphenyl ketyl" *Journal of heterocyclic chemistry* **1990**, *27*, 1903. b) Bagnato, J. D., Shum, W. W., Strohmeier, M., Grant, D. M., Arif, A. M., Miller, J. S., "The Structure of Fractionally Charged Tetracyanobenzene n− Present in [TCNB]3 2−" *Angew. Chem.* **2006**, *118*, 5448.

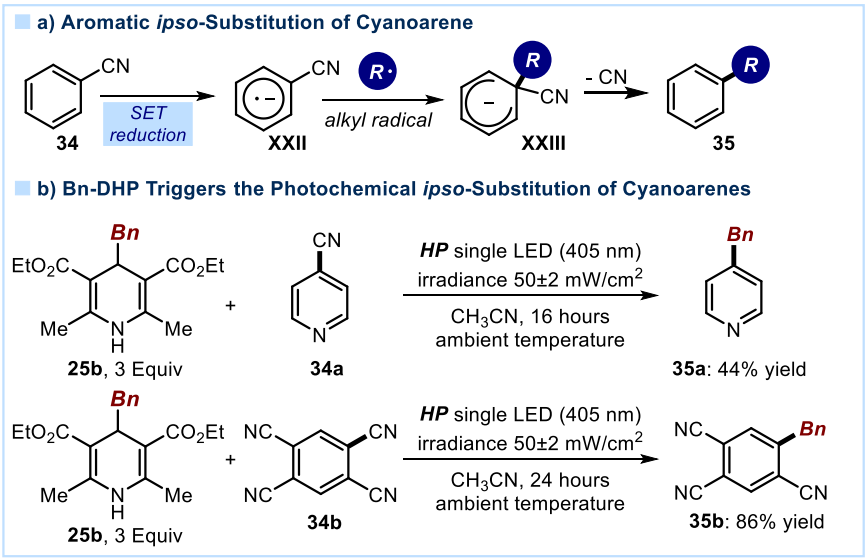

Figure 5.21: a) Mechanism of the aromatic substitution of cyanoarenes, governed by the radical coupling of an alkyl radical and the persistent cyanoarene radical anion **XXII**. b) Benzylation of 4-cyanopyridine **34a** and tetracyanobenzene **34b** enabled by the direct photoexcitation of **25b**.

These studies confirmed that alkyl-DHPs **25** possess a dual reactivity profile, since excitation with a violet-light-emitting diode turns them into strong reducing agents, capable to activate reagents via SET manifold, while undergoing a homolytic cleavage to directly generate alkyl radicals.

5.6.3 Preliminary Results and Optimization

After establishing the photochemical behavior of 4-alkyl-DHP, we tested their reactivity in the light-induced nickel-catalyzed radical cross-coupling. We began our investigation reacting 4-benzyl-DHP **25b** with 4-bromobenzonitrile **36** in the presence of $NiCl_2$·DME as nickel source and bipyridine as ligand (Scheme 5.1).

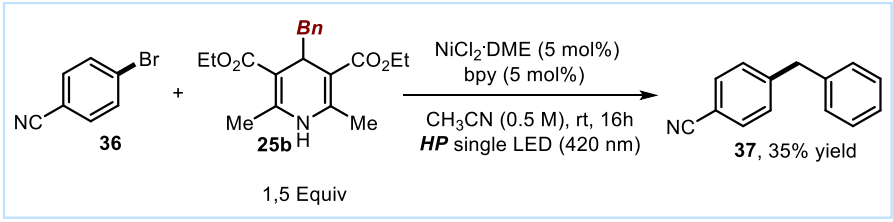

Scheme 5.1: Proof of concept reaction.

After 16 hours of irradiation with a 420 nm high power (HP) single LED, the desired product **37** was obtained in 35% yield proving the feasibility of the designed reaction. Control

experiments established the necessity of light irradiation and the nickel source. We then run a reaction optimization to increase the efficiency of the process. Relying on the analysis of the absorption spectra of **25b** (Figure 5.16), we found that changing to 405 nm HP single LED as light source provided better results. Additionally, an increase in the ratio metal/ligand to 1:2 resulted in a cleaner reaction with lower formation of metallic nickel. Finally, the use of 2,6-lutidine as the base helped to quench the formation of HBr, one of the byproducts of this transformation. With these optimized conditions, we could obtain the desired product **37** in 89% yield (Scheme 2). Screening of other reaction parameters, including solvents, ligands, nickel sources, dilution, and stoichiometry, did not lead to any further improvement.

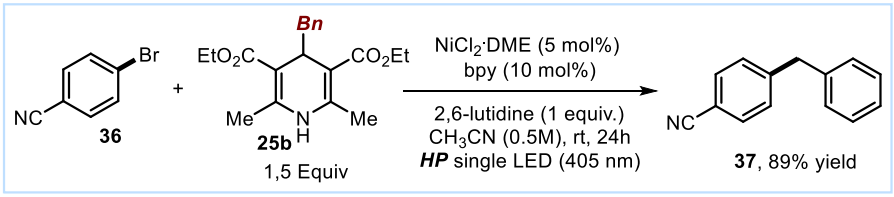

Scheme 5.2: Optimized condition for the light-induced nickel-catalyzed radical cross-coupling.

5.6.4 Scope of the Process

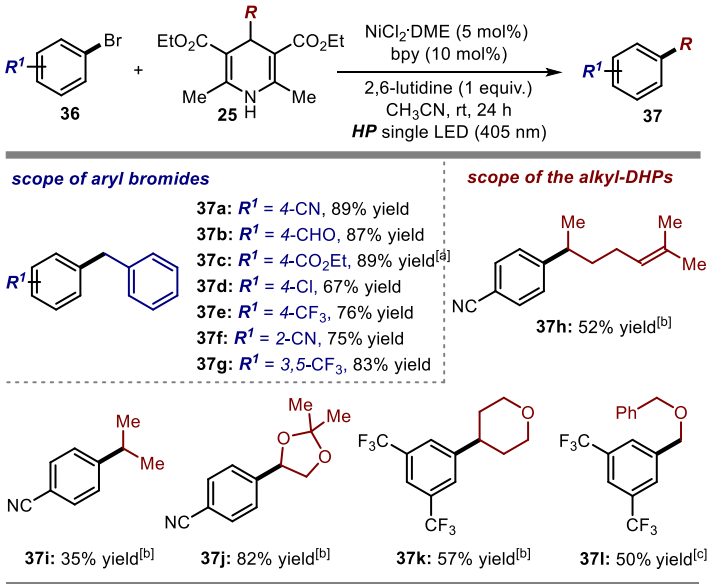

Figure 5.22: Survey of the aryl bromides **36** and the 4-alkyl-1,4-dihydropyridines **25** that can participate in the nickel-catalyzed cross-coupling process enabled by the photochemical activity of **25**. Reactions performed on a 0.5 mmol scale using 1.5 Equiv. of **25** and an irradiance of 50 mW/cm^2. Yields refer to isolated products. [a]The NMR yield is given, since the compound was isolated together with 10% of a by-product. [b] 0.1 mmol scale reaction performed over 16 hours (average of two runs). [c] Reaction time: 72 hours.

With the best condition in hand, we evaluated the scope of this transformation. As depicted in Figure 5.22, a variety of aryl bromides **36** could be successfully coupled with Bn-DHP **25b**, affording the corresponding benzylated product **37a**-**37g** with good to excellent yields. The process tolerated a wide range of functional groups, including cyano, aldehyde, ester, and chloride moieties. Moreover, an *ortho*-substituent did not hinder the reaction, yielding the coupling product **37f** in good yield. We then evaluated the possibility of using alkyl-DHP substrates **25** bearing different alkyl fragments than benzyl at the C4-position. Both linear and cyclic fragments could be successfully coupled with aryl bromides (adducts **37h**-**37l**). An alkene, an acetal moiety, and an oxygen-based heterocycle were all well-tolerated, leading to the corresponding product **37h**, **37j** and **37k**, respectively. In addition, a primary radical could successfully engage in this coupling protocol when adorned with a stabilizing α-oxygen atom (adduct **37l**). These results are mechanistically relevant since they demonstrate that different 4-alkyl-1,4-dihydropyridines **25** can be excited upon visible-light irradiation and their photochemical activity successfully integrated in a nickel catalytic cycle to enable C(sp^3)–C(sp^2) cross-coupling processes.

We then wondered if the same photochemical protocol could be successfully translated to the photochemical nickel-mediated cross-coupling of **25** with acyl chlorides **38**. The use of acyl

chlorides as electrophile in nickel-catalyzed radical cross couplings was inspired by two recent literature precedents by Molander.[32] As shown in Figure 5.23, an array of dialkyl ketones **39** could be efficiently prepared under mild conditions and relying only on the visible-light excitation of alkyl-DHP substrates **25.**

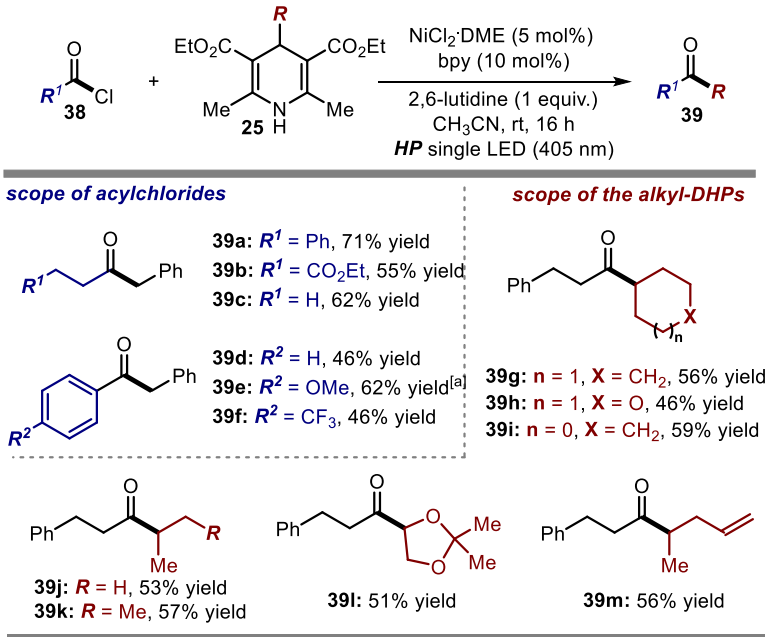

Figure 5.23: Survey of the acyl chlorides **38** and the 4-alkyl-1,4-dihydropyridines **25** that can participate in the nickel-catalyzed cross-coupling process to afford dialkyl ketones **39**. Reactions performed on a 0.1 mmol scale using 1.5 Equiv. of **25** and an irradiance of 50 mW/cm^2. Yields refer to isolated products (average of two runs). [a] 0.5 mmol scale reaction performed over 24 hours.

Also in this case, a variety of acyl chlorides can be successfully reacted with Bn-DHP including benzoyl chloride derivatives (**39d**-**39f**) providing the desired ketones in good yields. Concerning the DHP substrate, both linear and cyclic secondary fragments could be successfully coupled with the acyl chlorides including oxygenated heterocycles (**39h** and **39l**).

[32] a) Amani, J., Sodagar, E., Molander, G. A., "Visible light photoredox cross-coupling of acyl chlorides with potassium alkoxymethyltrifluoroborates: synthesis of α-alkoxyketones" *Org. Lett.* **2016**, *18*, 732. b) Amani, J., Molander, G. A., "Synergistic Photoredox/Nickel Coupling of Acyl Chlorides with Secondary Alkyltrifluoroborates: Dialkyl Ketone Synthesis" *J. Org. Chem.* **2017**, *82*, 1856.

5.6.5 Mechanistic Considerations

Ni(II)-bipyridine complexes were recently reported to be photoactive and to participate in light-induced processes.[33] To exclude the participation of these species in the developed photochemical reaction, we compared the absorption profiles of Bn-DHP with the one of a solution containing $NiCl_2$·DME and bipyridine in a 1:1 ratio. The UV-Vis spectra are depicted in Figure 5.24.

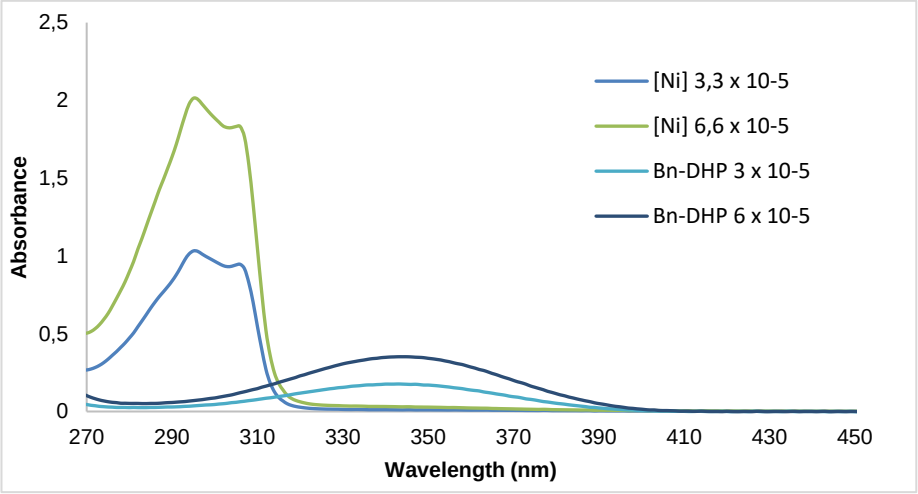

Figure 5.24: Comparison of the absorption profile of a Ni(II)bpy complex and Bn-DHP **25b**.

At the same concentration, for wavelengths > 350nm, the DHP derivative presents a higher absorbance compared to the Ni(II) complex. Additionally, it is worth to notice that in the reaction mixture the amount of Bn-DHP present in solution is 30 times higher compared to the amount of the catalytic Ni(II) complex, thus presumably overriding the absorption capability of the latter.

To study the interaction of the excited-state alkyl-DHP, we tried to perform luminescence quenching experiments. Unfortunately, all our attempts to perform Stern-Volmer studies using different electron acceptors, including electron-poor cyano substrates **34a** and **34b**, met with failure. For all the tested 4-alkyl-1,4-dihydropyridines, including Bn-DHP, we observed an increase of fluorescent intensity upon multiple irradiation of the substrate alone, within the spectrofluorometer. This phenomenon is likely ascribable to the formation of a strongly emitting compound, which is generated upon photo-degradation of **25b** (most probably the

[33] Selected examples: a) Ishida, N., Masuda, Y., Ishikawa, N., Murakami, M., "Cooperation of a Nickel–Bipyridine Complex with Light for Benzylic C− H Arylation of Toluene Derivatives" *Asian J. Org. Chem.* **2017**, *6*, 669. b) Shields, B. J., Kudisch, B., Scholes, G. D., Doyle, A. G., "Long-lived charge-transfer states of Nickel (II) aryl halide complexes facilitate bimolecular photoinduced electron transfer" *J. Am. Chem. Soc.* **2018**, *140*, 3035.

correspondin pyridine) and hampers any possibility to perform accurate collisional-quenching experiments.

Finally, to gain further insights into this process, we measured the quantum yield (Φ) of the photochemical cross-coupling reaction. A value of 0.0034 (λ=405 nm in CH_3CN, average of three runs) was determined, which is consonant with the mechanism proposed in Figure 5.14, and discards the occurrence of any chain-propagation manifold.

5.7 Future Directions

After studying and establishing the excited-state reactivity of alkyl-DHPs, we evaluated the possibility to exploit the peculiar behavior of this scaffold for the development of other radical-based transformations. In particular, we investigated the trapping of the radicals, delivered via photoexcitation of alkyl-DHP, with different substrates (SOMOphiles). Additionally, we tried to develop a Giese-type radical conjugate addition and a nickel-catalyzed radical transfer amidation.

5.7.1 Trapping of the Radicals with SOMOphiles

We demonstrated the ability of alkyl-DHPs to release alkyl radicals upon photoexcitation. We wondered if we could exploit this feature for enabling a variety of functionalizations relying on the trapping of the photogenerated radicals with different SOMOphiles (Figure 5.25).[34]

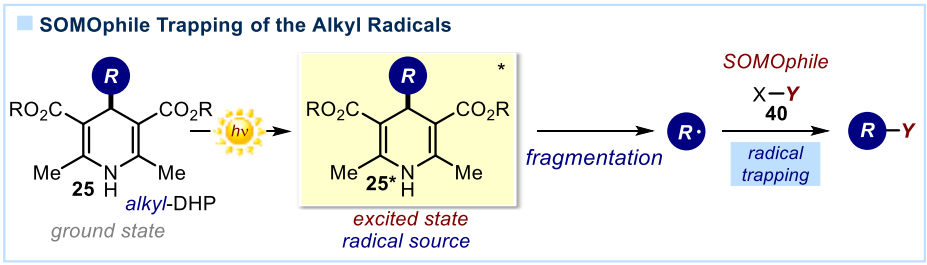

Figure 5.25: Trapping of the alkyl radicals generated upon photoexcitation of **25**.

We checked the feasibility of this idea irradiating DHPs bearing different alkyl substituents at the C4-position in the presence of various commonly-used radical traps (Table 5.1).

[34] Davies, J., Sheikh, N. S., Leonori, D., "Photoredox Imino Functionalizations of Olefins" *Angew. Chem.* **2017**, *129*, 13546.

Table 5.1: Attempted SOMOphilic trappings of the radicals generated upon light-excitation of alkyl-DHP **25**. NMR yields were determined using trichloroethylene as internal standard.

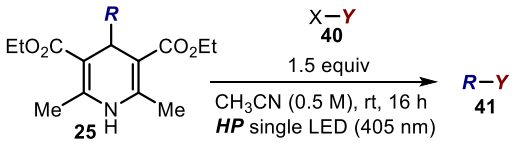

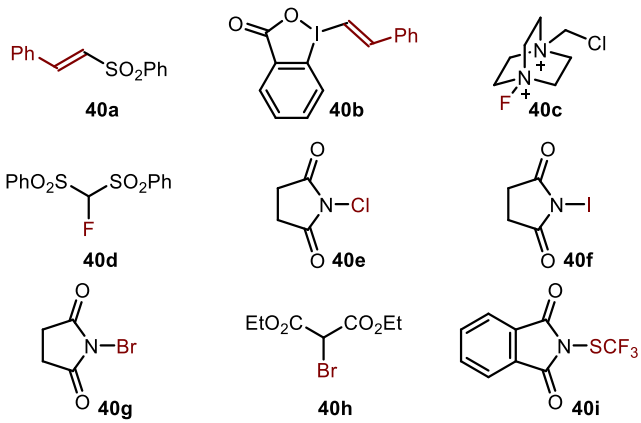

Entry	Radical Trap	R	Yield (NMR)	Reaction
1	**40a**	-CH_2OBn	-	Vinylation
2	**40b**	-CH_2OBn	Traces	Vinylation
3	**40b**	Bn	Traces	Vinylation
4	**40b**	iPr	21%	Vinylation
5	**40c**	Bn	-	Fluorination
6	**40d**	Bn	-	Fluorination
7	**40e**	Bn	12%	Chlorination
8	**40f**	Bn	40%	Iodination
9	**40g**	Bn	-	Bromination
10	**40h**	Bn	13%	Bromination
11	**40i**	Bn	32%	Thiotrifluoromethylation

A vinylation reaction proceeded in the presence of the hypervalent iodine reagent **40b**, providing 21% of the desired product when the isopropyl-DHP was used as the radical source. Other DHPs delivered only traces of the olefin product. Bn-DHP, which provides a benzyl

radical, was tested in various functionalizations. Fluorination reactions conducted with Selectfluor **40c** and NFSI **40d** as source of SOMOphilic fluorine met with failure. N-Chloro succinimide (NCS, **40e**) provided the desired benzyl chloride in 12% NMR yield while N-Iodo succinimide (NIS, **40f**) yielded 40% of benzyl iodide. in contrast, N-Bromo succinimide (NBS, **40g**) did not provide the desired benzyl bromide, which was obtained in 13% NMR yield when using dimethyl bromomalonate **40h** as the bromine source. Finally, the use of N-thiotrifluoro phtalamide **40i** provided the desired thioether product in 32% NMR yield.
These preliminary results confirmed the possibility to use 4-alkyl-DHP as radical sources for various functionalization. Further studies in this direction are currently ongoing.

5.7.2 Giese-type Radical Conjugate Additions

The conjugate addition of alkyl radicals to Michael acceptors, termed the Giese reaction, is a powerful technology for the construction of C(sp^3)–C(sp^3) bonds.[35] This reaction was first reported using tributyltin hydride as radical initiator to generate alkyl radicals from alkyl halides (Figure 5.26a). The radical is then trapped by the Michael acceptor providing a radical intermediate that abstracts a hydrogen atom from the tributyltin hydride to afford the desired product.
Radical conjugate addition (RCA) procedures have been extensively implemented during the last three decades and they have become a classic in the repertoire of radical chemists. Our group recently reported an enantioselective catalytic version of RCA for the construction of all-carbon quaternary stereocenters (Figure 5.26b).[36] In this protocol, the photoexcitation of a tetrabutylammonium decatungstate (TBADT) photocatalyst triggers the hydrogen abstraction and the formation of a C(sp^3) centered radical **XXIV** from a benzodioxole precursor **43**. The radical undergoes RCA to an iminium ion, formed upon condensation of a chiral primary amine catalyst **45** with a cyclohexanone derivative **42**, to afford the enanantioenriched addition product **44** after hydrolysis of the catalyst. Recently, Baran extended the scope of this transformation reporting redox-active esters **46** as radical sources for RCAs (Figure 5.26c).[37] In this methodology, a combination of stoichiometric zinc and a catalytic nickel salt is responsible for the reduction of the redox-active ester. The subsequent decarboxylation delivers the alkyl radical, which is trapped by a Michael acceptor **47** delivering the addition product **48**.

---

[35] a) Giese, B., Dupuis, J., "Diastereoselective Syntheses of C-Glycopyranosides" *Angew. Chem. Int. Ed.* **1983**, *22*, 622. b) Giese, B., González-Gómez, J. A., Witzel, T., "The Scope of Radical CC-Coupling by the "Tin Method"" *Angew. Chem. Int. Ed.* **1984**, *23*, 69.
[36] Murphy, J. J., Bastida, D., Paria, S., Fagnoni, M., Melchiorre, P., "Asymmetric catalytic formation of quaternary carbons by iminium ion trapping of radicals" *Nature* **2016**, *532*, 218.
[37] Qin, T., Malins, L. R., Edwards, J. T., Merchant, R. R., Novak, A. J., Zhong, J. Z., Mills, R. B., Yan, M., Yuan, C., Eastgate, M. D., "Nickel-Catalyzed Barton Decarboxylation and Giese Reactions: A Practical Take on Classic Transforms" *Angew. Chem. Int. Ed.* **2017**, *56*, 260.

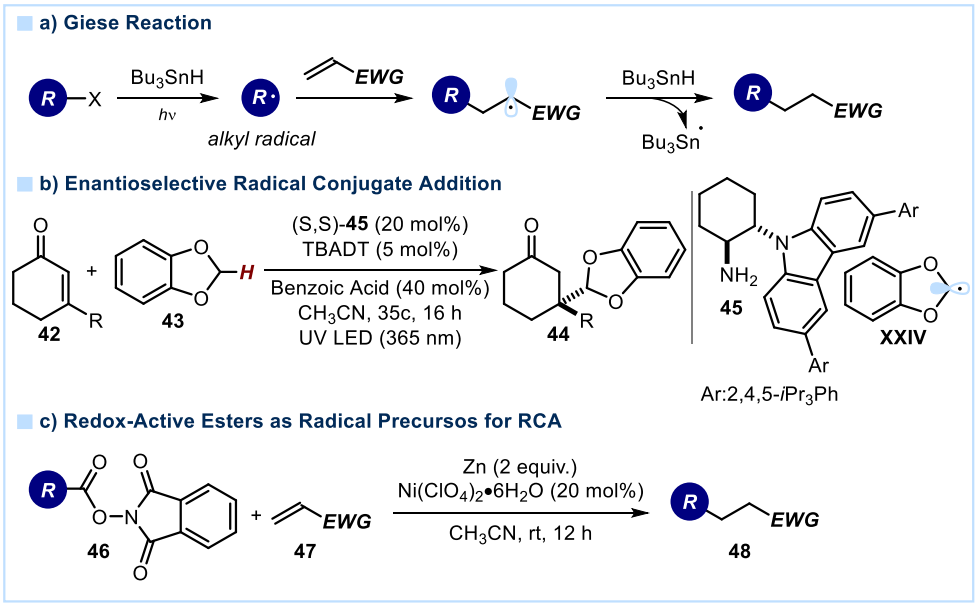

Figure 5.26: a) The Gyese reaction. b) Iminium-ion activation for a light-driven enantioselective radical conjugate addition. c) Redox-active esters as radical precursors for nickel-catalyzed radical conjugate additions.

Intrigued by this reactivity, we evaluated the possibility to exploit the photoexcitation of 4-alkyl-DHPs for the generation of alkyl radicals, which can be used in RCA reactions. We started out our investigation reacting Bn-DHP **25b** with dimethyl fumarate **49a** under 405 nm irradiation in acetonitrile (Scheme 5.3). After 16 hours, we could not detect any desired benzylation product **50**, despite the full conversion of the DHP to the corresponding pyridine. However, toluene and bibenzyl were formed, thus proving the efficient generation of benzyl radicals under the reaction conditions.

Scheme 5.3: RCA reaction using photoexcited Bn-DHP as the radical source.

We rationalized the lack of reactivity with *i*) the low nucleophilicity of benzyl radicals towards addition to polarized olefins and *ii*) a competitive β-scission from the radical intermediate **XXV**, generated after the RCA, which reforms the original open-shell species and the Michael acceptor (Figure 5.27a). In contrast, in the Baran's report, the addition of various non-

nucleophilic radicals to Michael acceptors was successfully achieved using nickel to mediate the process. This observation led us to investigate the role that nickel can play in such transformations: specifically, we wondered whether this redox active transition metal might trap the radical intermediate **XXV** avoiding the β-scission and enabling the formation of the desired RCA product (Figure 5.27b).

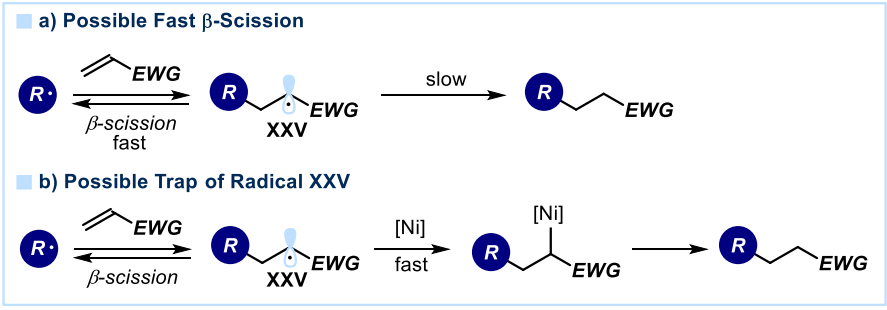

Figure 5.27: a) A fast β-scission may hamper the radical conjugate addition of non-nucleophilic radicals. b) Nickel might be involved in the stabilization of radical **XXV**.

Following this reasoning, we repeated the reaction with Bn-DHP and dimethyl fumarate **49a** in the presence of 10 mol% of $NiCl_2$·DME as nickel catalyst and 20 mol% of bipyridine as ligand (Scheme 5.4).

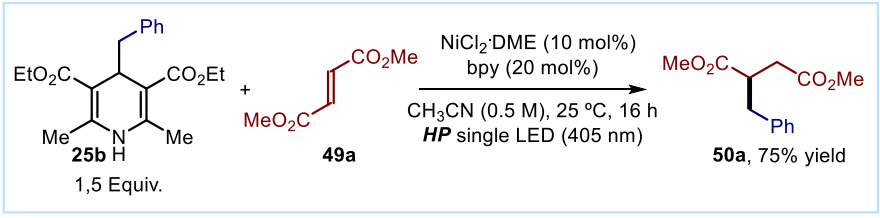

Scheme 5.4: RCA reaction using the photoexcited Bn-DHP as the radical source in the presence of nickel.

In this case, the desired product **50a** was obtained in 75% yield, which confirmed the involvement of a nickel species in the reaction mechanism. Without any further optimization, we evaluated a preliminary scope of this reaction, screening various alkyl-DHPs and Michael acceptors (Scheme 5.5)

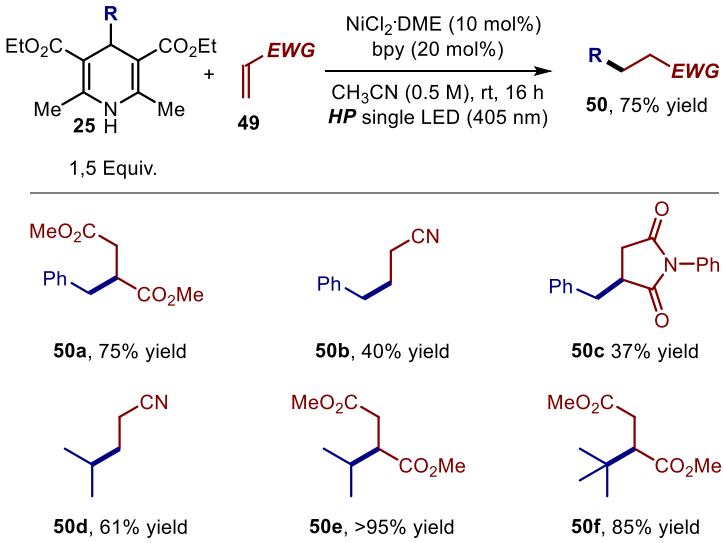

Scheme 5.5: Preliminary scope of the nickel-catalyzed RCA reaction.

Using this methodology, we could add benzyl radicals to fumarates, acrylonitrile, and N-phenyl maleimide **50a**, **50b**, and **50c**. Also simple alkyl radicals, including *iso*-propyl and *tert*-butyl[38], are competent for this transformation (**50d-50f**).

To elucidate the role of nickel, we performed some control experiments using a catalytic amount of preformed $[Ni(II)(bpy)_3](BF_4)_2$ complex. Performing the reaction using this complex as the nickel source, we obtained comparable results. This stable nickel complex, because of the coordination by three bipyridines, is not prone to trap open-shell species. We therefore rationalized its efficiency in the RCA reaction with the ability to act as a redox mediator. In the proposed mechanism depicted in Figure 5.28, the excited alkyl-DHP **25b*** reduces the Ni(II) complex **XXVI** to the highly reducing Ni(I) complex **XXVII** (E(Ni(II)/Ni(I) = -1.26 V).[39] The unstable radical cation **XVII** releases an alkyl radical, which is trapped by the Michael acceptor **49** in a RCA manifold. The resulting radical intermediate **XXV** is then reduced by the Ni(I) complex **XXVII** forming the radical anion **XXVIII** (E^{red} > -1.26 V),[40] which delivers the desired product **50** upon protonation while regenerating the Ni(II) catalyst.

[38] The *tert*-butyl radical was generated from 4-(*tert*-butyl)-2,6,dimethyl-1,4-dihydropyridine-3,5-dicarbonitrile, bearing two nitrile groups instead of the carboxylates, due to the difficulty in obtaining Hantzsch ester derivative with bulky substituent at the C4.

[39] Henne, B. J., Bartak, D. E., "Metal-vapor synthesis and electrochemistry of bis (bipyridyl) nickel (0)" *Inorg. Chem.* **1984**, *23*, 369.

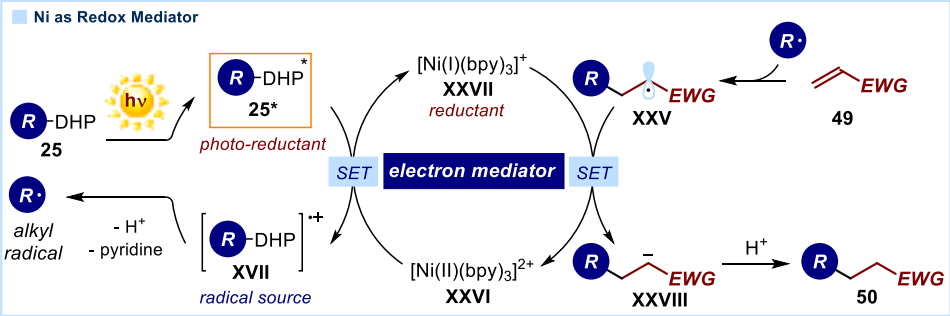

Figure 5.28: Proposed mechanism for the nickel-mediated RCA, where nickel acts as an electron mediator.

These preliminary results confirmed the possibility to use 4-alkyl-DHPs as radical sources in Giese-type reactions. The evaluation of a comprehensive scope for this reaction and further mechanistic studies are currently underway in the group.

5.7.3 Dihydropyridines for Amidation Reactions

The large occurrence of amide bonds in biologically relevant compounds, in particular in peptides and proteins, and their peculiar properties make the synthesis of amides one of the most frequently performed transformations in medicinal chemistry (Figure 5.29).[41]

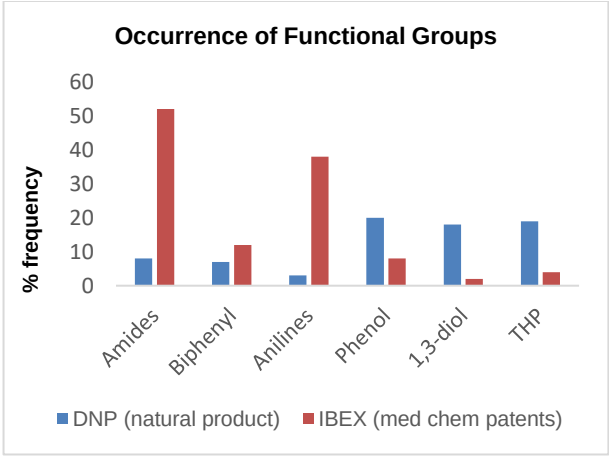

[41] Brown, D. G., Bostrom, J., "Analysis of Past and Present Synthetic Methodologies on Medicinal Chemistry: Where Have All the New Reactions Gone? Miniperspective" *Journal of medicinal chemistry* **2015**, *59*, 4443.

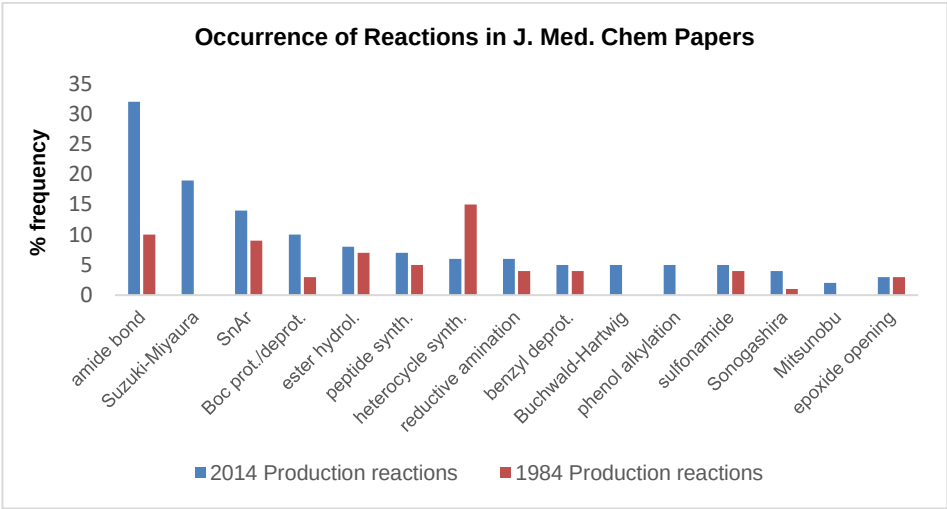

Figure 5.29: The occurrence of the amide bond in biologically active compounds and the occurrence of amidation reactions in J. Med. Chem. papers.

The most common way to forge an amide bond relies on the acylation of amines with activated carboxylic acids (Figure 5.30, top left). This methodology relies on the use of coupling reagents (i.e. carbodiimide derivatives) which convert the unreactive carboxylic acids into an activated carboxylates.[42] In the absence of such coupling reagents, the amines and the acids simply form ammonium-carboxylate salts. The coupling agents are generally used in stoichiometric amounts and produce a large amount of chemical waste. Other strategies for amide synthesis are based on the transition-metal catalyzed aminocarbonylation (Figure 5.30, top right).[43] This three-component reaction, firstly reported by Heck[44], allows the direct coupling of electrophiles, such as aryl or alkyl halides, with amines and carbon monoxide. Despite the good atom economy of this process, the use of toxic carbon monoxide represents a safety issue, especially when performed on an industrial scale. Moreover, this coupling reaction often relies on the expensive and limited palladium as the transition-metal catalyst. Recently, the use of isocyanates as building blocks for amide synthesis have been reported (Figure 5.30, bottom left).[45] These substrates can participate in transition-metal catalyzed reductive couplings with electrophiles to forge amide bonds. This transformation overcomes the requirement of carbon monoxide, typical of aminocarbonylation, but it does not allow the

[42] Dunetz, J. R., Magano, J., Weisenburger, G. A., "Large-scale applications of amide coupling reagents for the synthesis of pharmaceuticals" *Org. Process Res. Dev.* **2016**, *20*, 140.
[43] Roy, S., Roy, S., Gribble, G. W., "Metal-catalyzed amidation" *Tetrahedron* **2012**, *48*, 9867.
[44] Schoenberg, A., Heck, R., "Palladium-catalyzed amidation of aryl, heterocyclic, and vinylic halides" *J. Org. Chem.* **1974**, *39*, 3327.
[45] Serrano, E., Martin, R., "Forging Amides Through Metal-Catalyzed C–C Coupling with Isocyanates" *Eur. J. Org. Chem.* **2018**, *2018*, 3051.

synthesis of tertiary amides, due to the peculiar structure of the isocyanates. Finally, amide bond can be accessed through transamidation reactions (Figure 5.30, bottom right). This methodology, often catalyzed by transition-metals, allows the conversion of an amide into another but it is often hampered by the high chemical stability of amide, which increases the kinetic barrier of the acyl C–N bond cleavage. Another difficulty arises from the thermodynamic of transamidation, since the conversion of an amide into another is almost a thermoneutral process.

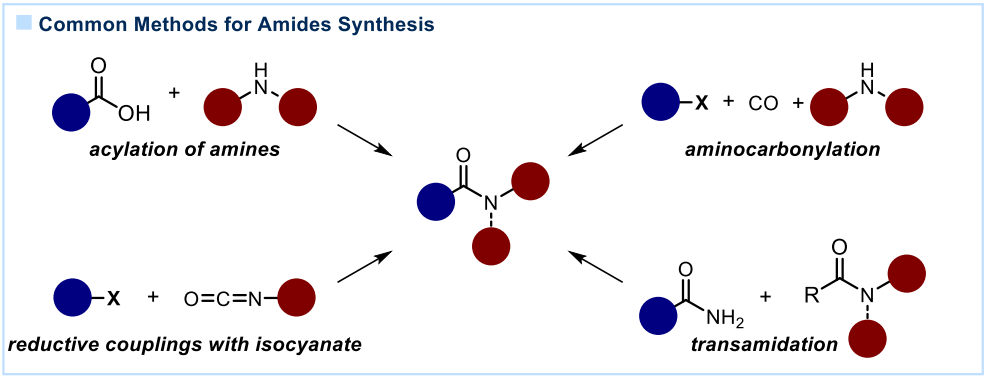

Figure 5.30: Some of the available methods for the synthesis of amides.

Aiming to overcome some of the limitations of the classical polar methods for amide synthesis, we explored the possibility to exploit the photochemical reactivity of dihydropyridines to generate carbamoyl radicals and develop an alternative procedure for forging amide bonds. We hypothesized that a Hantzsch ester derivative **53**, bearing a carboxylic moiety at the C4-position, would represent a suitable handle for the further installation of a carbamoyl group (Figure 5.31a). This compound **53**, which is easily accessible through condensation of glyoxylic acid **51** with amino crotonate **52**, can be condensed with a variety of amines **54** to afford DHP compounds **55** loaded with an amide moiety. Photoexcitation of such carbamoyl-DHPs **55** would then deliver the desired carbamoyl radical **XXIX** (Figure 5.31b). We surmised to exploit the excited-state reactivity of carbamoyl-DHPs to develop a nickel-catalyzed radical cross-coupling with aryl halide derivatives **56** (Figure 5.31c)

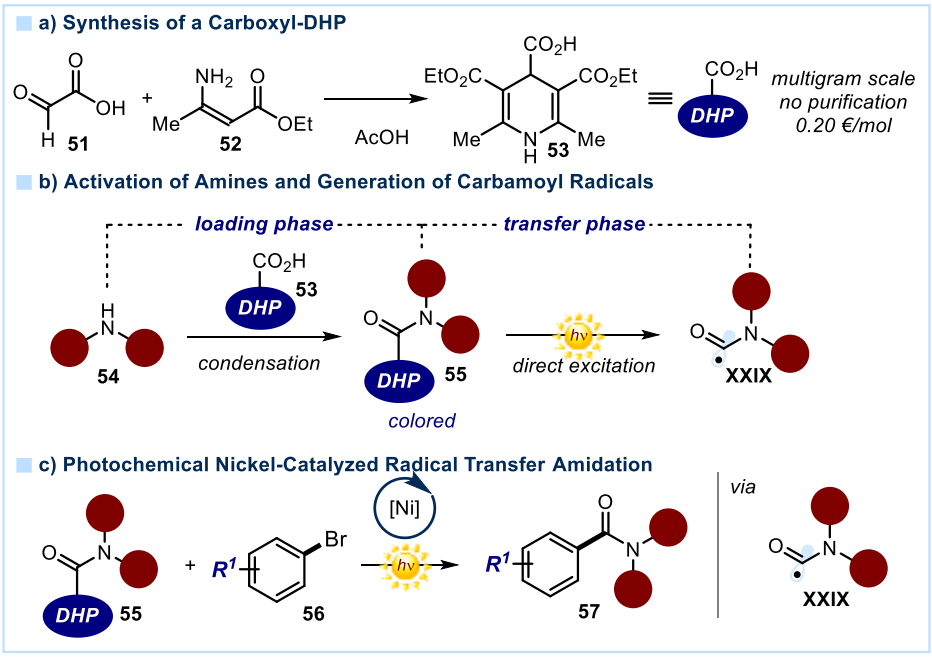

Figure 5.31 a) Synthesis of a DHP bearing a carboxylic moiety at C4. b) Condensation of **53** with amines and generation of carbamoyl radicals under light excitation. c) Use of a carbamoyl-DHP for a photochemical nickel-catalyzed radical transfer amidation.

With this idea in mind, we proceeded with the optimization of the "loading phase", where we synthesized the carbamoyl radical precursors **54**. We found that various amines can easily condense with **55** in the presence of stoichiometric amounts of isobutylchloroformate as the coupling agent (Figure 5.32). This reaction delivers the desired product **55** in quantitive yield, producing CO_2 and isobutyl alcohol as byproducts.

Figure 5.32: Optimal conditions for the synthesis of **55**: the "loading phase".

With the carbamoyl Hantzsch esters **55** in hand, we evaluated the possibility to exploit them in a photochemical nickel-catalyzed radical transfer amidation with aryl halides (Figure 5.33, the "transfer phase").

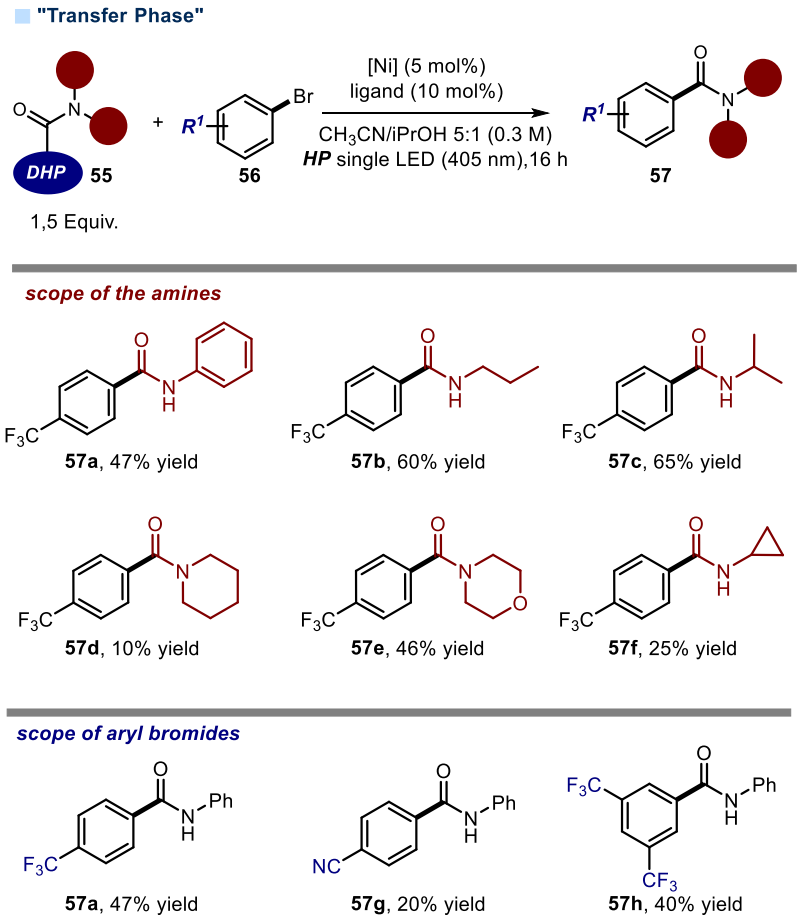

Figure 18.33: Preliminary scope of the photochemical nickel-catalyzed radical transfer amidation.

These preliminary results confirmed that DHP **55** can serve for the photochemical generation of carbamoyl radicals, which can then participate in nickel-catalyzed radical transfer amidation reaction. The optimization of the reaction conditions and the evaluation of a comprehensive scope o this transformation are currently ongoing in our group.

5.8 Conclusions

We have documented that 4-alkyl-1,4-dihydropyiridines can unveil a rich photochemistry upon light excitation. Selective absorption of violet light turns them into strong reducing agents that can activate reagents *via* single-electron transfer manifolds while undergoing a homolytic cleavage to generate C(sp^3)-centered radicals. This light-triggered dual reactivity profile was integrated within a nickel catalytic cycle to enable C(sp^3)–C(sp^2) cross coupling reactions without the need for an external photoredox catalysis. We exploited this reactivity to develop other photochemical radical transformations, including a Giese-type radical conjugate addition and a nickel-catalyzed radical transfer amidation.

5.9 Experimental Section

General Information. The NMR spectra were recorded at 300 MHz and 400 MHz for ^{1}H, 75 or 100 MHz for ^{13}C and 286 or 376 MHz for ^{19}F. The chemical shift (δ) for ^{1}H and ^{13}C are given in ppm relative to residual signals of the solvents ($CHCl_3$ @ 7.26 ppm ^{1}H NMR and 77.16 ppm ^{13}C NMR, and tetramethylsilane @ 0 ppm). Coupling constants are given in Hertz. The following abbreviations are used to indicate the multiplicity: s, singlet; d, doublet; q, quartet; p, pentet; sept, septet; m, multiplet; br, broad signal. NMR yields were determined by adding trichloroethylene (Cl_2=ClH, δ = 6.44 ppm) as an internal standard to the crude reaction mixtures and by integration of diagnostic signals.

High-resolution mass spectra (HRMS) were obtained from the ICIQ High Resolution Mass Spectrometry Unit on MicroTOF Focus and Maxis Impact (Bruker Daltonics) with electrospray ionization.

UV-vis measurements were carried out on a Shimadzu UV-2401PC spectrophotometer equipped with photomultiplier detector, double beam optics and D_2 and W light sources. The emission spectra were recorded in a Fluorolog Horiba Jobin Yvon spectrofluorimeter equipped with a photomultiplier detector, a double monochromator, and a 350W xenon light source.

Cyclic voltammetry studies were carried out on a Princeton Applied Research PARSTAT 2273 potentiostat offering compliance voltage up to ± 100 V (available at the counter electrode), ± 10 V scan range and ± 2 A current range.

Continuous wave (CW) EPR spectra were obtained on a Bruker EMX Micro X-band bridge of 9.1 - 9.9 GHz, using a Bruker ER 1164 HS resonator and equipped with an ESR900 cryostat.

General Procedures. All reactions were set up under an argon atmosphere in oven-dried glassware using standard Schlenk techniques, unless otherwise stated. Synthesis grade solvents were used as purchased. Anhydrous solvents were taken from a commercial SPS

solvent dispenser. Chromatographic purification of products was accomplished using force-flow chromatography (FC) on silica gel (35-70 mesh). For thin layer chromatography (TLC) analysis throughout this work, Merck pre-coated TLC plates (silica gel 60 GF_{254}, 0.25 mm) were employed, using UV light as the visualizing agent and ethanol solution of phosphomolybdic acid or basic aqueous potassium permanganate ($KMnO_4$) stain solutions and heat as developing agents. Organic solutions were concentrated under reduced pressure on a Büchi rotary evaporator (*in vacuo* at 40 ºC, ~5 mbar).

Materials. Commercial grade reagents and solvents were purchased from Sigma-Aldrich, Fluka, Alfa Aesar, Fluorochem, SynQuest at the highest commercial quality and used without further purification, unless otherwise stated. Nickel(II) chloride ethylene glycol dimethyl ether complex ($NiCl_2$·DME) is commercially available and was used as purchased (from Sigma Aldrich). Other starting materials, including all the aryl bromides **36** and acyl chlorides **38**, were purchased from commercial source and used as received. All of the 4-alkyl-1,4-dihydropyridine (Hantzsch esters) derivatives **25** were prepared according to a literature procedure.[46]

[46] Gutiérrez-Bonet, A. l., Tellis, J. C., Matsui, J. K., Vara, B. A., Molander, G. A., "1,4-Dihydropyridines as Alkyl radical Precursors: Introducing the Aldehyde Feedstock to Nickel/Photoredox Dual Catalysis." *ACS Catal.* **2016**, *6*, 8004

Fluorescence Studies of Benzyl- and isopropyl-DHP Derivatives

The emission spectra were recorded in a Fluorolog Horiba Jobin Yvon spectrofluorimeter equipped with a photomultiplier detector, a double monochromator, and a 350W xenon light source. 2 mL of acetonitrile, thoroughly degassed by freeze pump thaw, were placed in a 10x10 mm light path quartz fluorescence cuvette equipped with Silicone/PTFE 3.2 mm septum under an argon atmosphere. Then, 25 µL of a 15 mM solution of benzyl-DHP **25b** in acetonitrile was added to afford a final concentration of **25b** of 150 µM. The excitation wavelength was fixed at 405 nm (incident light slit regulated to 4 mm), while the emission light was acquired from 415 nm to 600 nm (emission light slit regulated to 8 mm). A solvent blank was subtracted from the measurement.

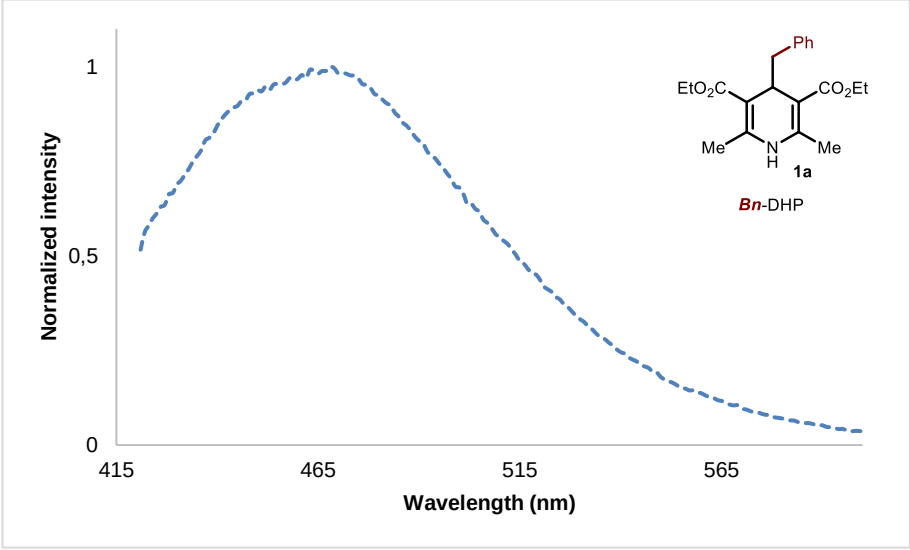

The same procedure was repeated to study the photophysical behavior of the isopropyl-DHP derivative. 25 µL of a 15 mM solution of *i*Pr-DHP in acetonitrile was added to afford a final concentration of 150 µM. The excitation wavelength was fixed at 390 nm (incident light slit regulated to 4 mm), while the emission light was acquired from 410 nm to 600 nm (emission light slit regulated to 8 mm). A solvent blank was subtracted from the measurement.

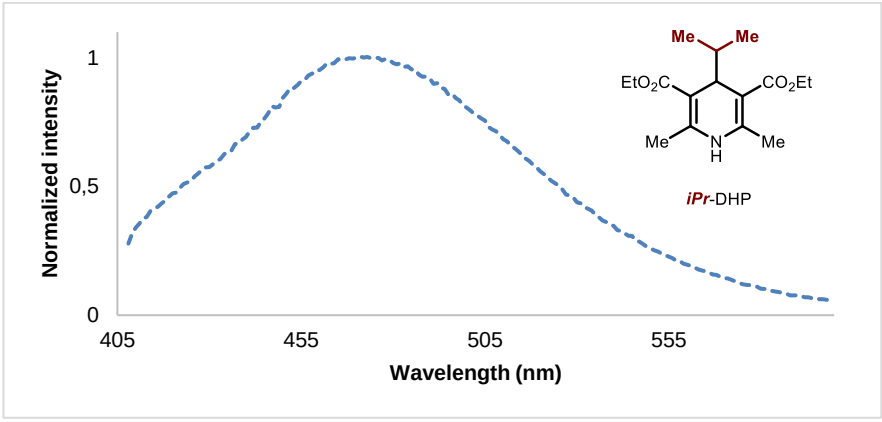

After multiple excitation of solutions of both benzyl- and isopropyl-DHP derivatives (when the DHP substrate was *alone* in the cell), we could observe an increase in the emission intensity. The phenomenon is shown for the isopropyl-DHP derivative, and an identical behaviour was observed with Bn-DHP **25b**. This phenomenon is likely ascribable to the formation of a strongly emitting compound, which is generated upon photo-degradation of **25**. This emission behavior frustrated any attempt to perform reliable Stern-Volmer quenching studies using different electron acceptors.

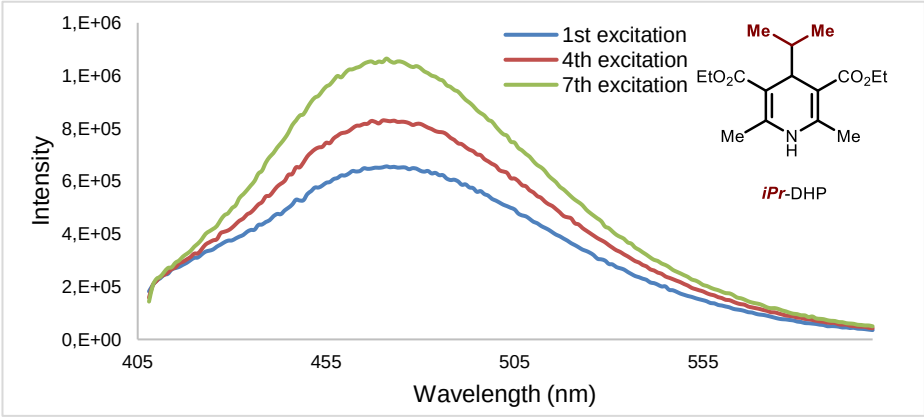

Fluorescence Decay of 4-Benzyl-1,4-dihydropyridine-3,5-dicarboxylate 1a

Lifetime measurements were carried out on an Edinburgh Instruments LifeSpec-II based on the time-correlated single photon counting (TCSPC) technique, equipped with a PMT detector, double subtractive monochromator and picosecond pulsed 405 nm diode laser.

A 600 μM solution of **25b** in acetonitrile was introduced into a 1 cm path length quartz cuvette equipped with a Teflon® septum and the decay was recorded. The reconvolution fitting from the fluorescence decay trace shows a double exponential decay, affording the following values: $\tau_0 = 0.28$ ns (below the limit of the detector) and $\tau_1 = 4.1$ ns.

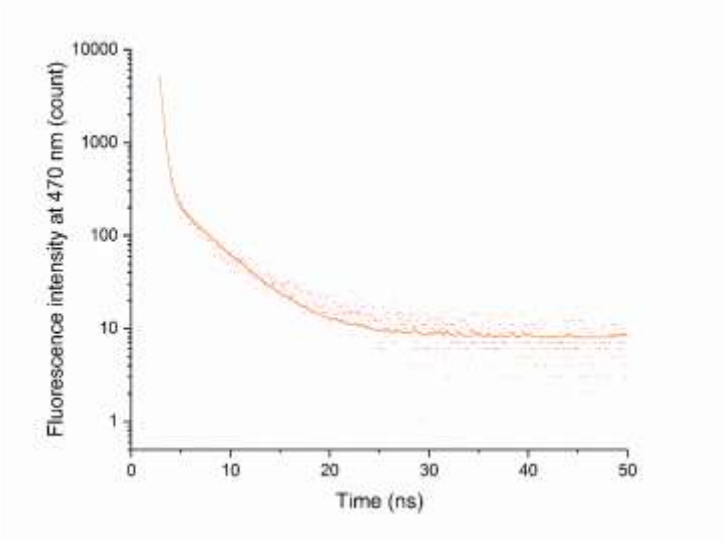

EPR Experiment

Continuous wave (CW) EPR spectra were obtained on a Bruker EMX Micro X-band spectrometer operating at 9.374 GHz using a Bruker ER 1164 HS resonator and equipped with an ESR900 cryostat. The spectral data was collected at 77 K with the following spectrometer settings: microwave power = 0.5 mW; center field = 3348 G, sweep width = 1000 G, sweep time = 30 s, modulation frequency = 100 KHz, modulation amplitude = 10 G, power attenuation = 25 dB, time constant = 0.01 ms.

The samples were prepared as follow: 4-benzyl-1,4-dihydropyridine-3,5-dicarboxylate **25b** (70 mg, 0.2 mmol) was dissolved in CH_3CN (1 mL, [**25b**] = 200 mM). This solution was transferred into EPR Low Pressure/Vacuum Tube. The reaction mixture was degassed *via* a freeze pump thaw procedure, and kept frozen with liquid nitrogen under vacuum in the EPR tube. The tube was then inserted inside the EPR cavity for the EPR measurements.

Before acquiring the spectra, a 405 nm high power LED purchased from LEDENGIN (which is the same light source used in the synthetic experiments) was used to irradiate the samples.

The LED was connected to the EPR cavity using an optical fiber supplied with the equipment from Bruker.

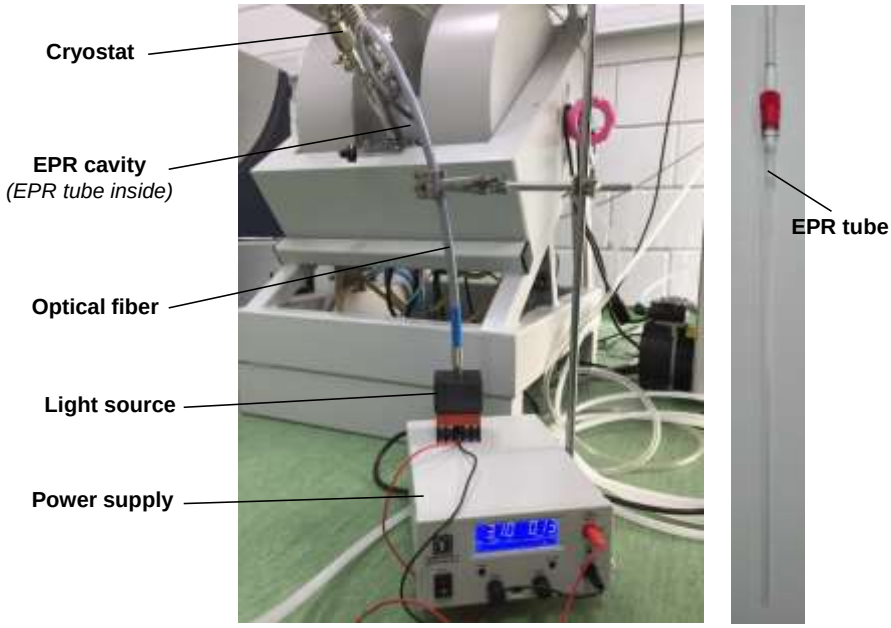

EPR spectra were recorded after 0, 10, 30, and 60 minutes of irradiation (Figure S9). All the spectra, except after 0 minute, showed an isotropic X-band absorption and afforded a g-values of 2.0035, which is consistent with literature data for the characterization of benzyl radicals.

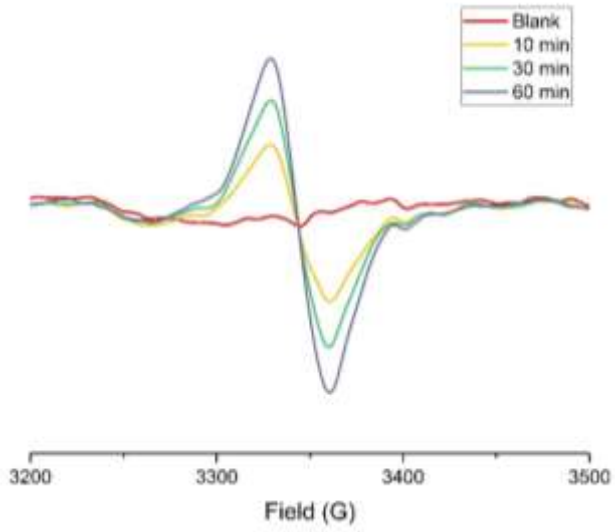

Experimental Procedures

Light illumination system and reaction set-up

The reactions were performed in a 15 mL Schlenk tube that, after addition of reagents and CH_3CN, was placed under an atmosphere of argon, cooled to –78 °C, and degassed via vacuum evacuation (5 min), backfilled with argon, and warmed to room temperature. The freeze-pump-thaw cycle was repeated three times, and then the Schlenk tube was sealed with Parafilm and placed into a 3D-printed plastic support mounted on an aluminium block fitted with a 405 nm high-power single LED (λ = 405 nm). The irradiance was fixed at 50±3 mW/cm^2, as controlled by an external power supply and measured using a photodiode light detector at the start of each reaction.

This setup secured a reliable irradiation while keeping a distance of 1 cm between the reaction vessel and the light source.

top view

front view

3D printed support

Light source

405 nm high-power LED
on an aluminium block

Controlling the light intensity

Photodiode
(measures light intensity)

Power supply
(controls the light intensity)

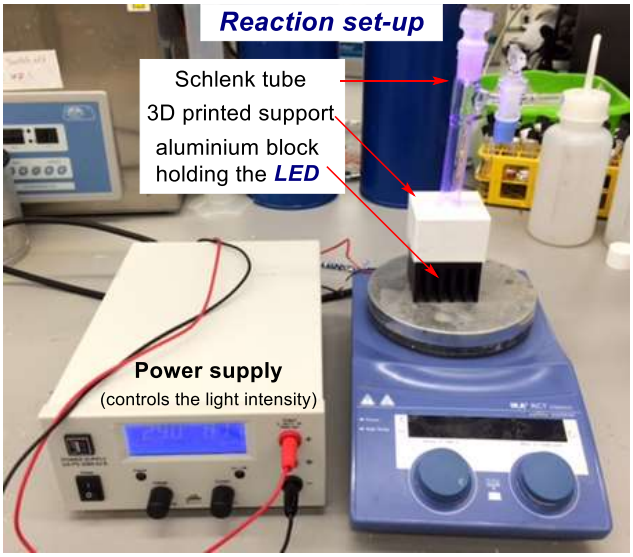

Benzylation of Cyanoarenes

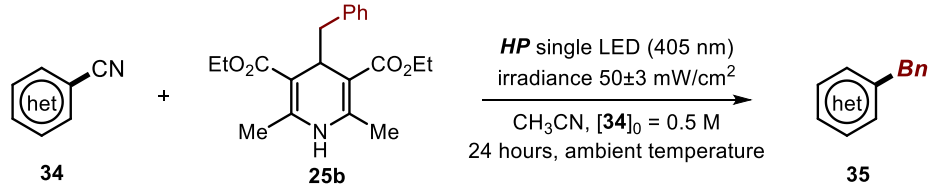

General Procedure A *(0.1 mmol scale reaction).* In a Schlenk tube, the selected cyanoarenes **34** (0.1 mmol, 1 equiv.) and Bn-DHP **25b** (0.15 mmol, 1.5 equiv.) were dissolved in MeCN (200 μL). The reaction mixture was degassed *via* a freeze pump thaw procedure, and then placed on a 405 nm high-power single LED (λ = 405 nm, irradiance = 50±3 mW/cm^2, as controlled by an external power supply; the set-up is detailed in Figure S10). The reaction was stirred under irradiation at ambient temperature over 24 hours. Then the mixture was concentrated in vacuo and the residue was purified by flash chromatography (silica gel, appropriate mixture of hexane/ethyl acetate) to afford the corresponding product **35**.

Characterization of adducts 35

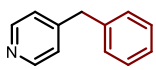

4-Benzylpyridine (35a). Prepared according to the general procedure A, using 4-cyanopyridine **34a** (0.1 mmol, 10 mg, 1 equiv.) and Bn-DHP **25b** (0.15 mmol, 52 mg, 1.5 equiv.); time of irradiation: 24 hours. 44% yield, as determined by ^{1}H NMR analysis of the crude mixture. Data for **35a** from crude analysis: ^{1}H NMR (300 MHz, Chloroform-*d*) δ (selected signals) δ 8.53 (d, J = 6.1 Hz, 2H), 4.00 (s, 2H). The spectroscopic characterization matched with data reported in the literature.[47]

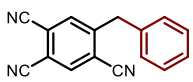

5-Benzylbenzene-1,2,4-tricarbonitrilenitrile (35b). Prepared according to the general procedure A, using tetracyanobenzene **2b** (0.1 mmol, 18 mg, 1 equiv.) and **1a** (0.15 mmol, 52 mg, 1.5 equiv.); time of irradiation: 24 hours. The crude mixture was purified by flash column chromatography (gradient from pure hexane to hexane/ethyl acetate 9:1) to afford the product as a white solid (scale 0.1 mmol : 21 mg, 86% yield). The spectroscopic characterization matched with data reported in the literature.[48] **^{1}H NMR** (300 MHz, Chloroform-*d*) δ 8.07 (s, 1H), 7.67 (s, 1H), 7.56 – 7.32 (m, 3H), 7.28 – 7.02 (m, 2H), 4.32 (s, 2H). **^{13}C NMR** (75 MHz, Chloroform-*d*) δ 151.3, 137.1, 135.6, 135.0, 129.6, 129.2, 128.1, 119.6, 117.8, 114.8, 113.7, 40.4.

[47] Nakajima, K., Nojima, S., Sakata, K., Nishibayashi, Y., "Visible-Light-Mediated Aromatic Substitution Reactions of Cyanoarenes with 4-Alkyl-1,4-dihydropyridines through Double Carbon–Carbon Bond Cleavage." *ChemCatChem* **2016**, *8*, 1028.

[48] Lu, Z.-F., Yue, J.-J., Zhu, Y., Hu, H.-W., Xu, J.-H., "Photo-Multicomponent Reactions Leading to the Construction of Isocoumarins and Large Ring Lactone Precursors" *Photochem. Photobiol. Sci.* **2009**, *8*, 217.

Nickel-catalyzed C(sp^2)-C(sp^3) cross-coupling enabled by the photochemical activity of 25

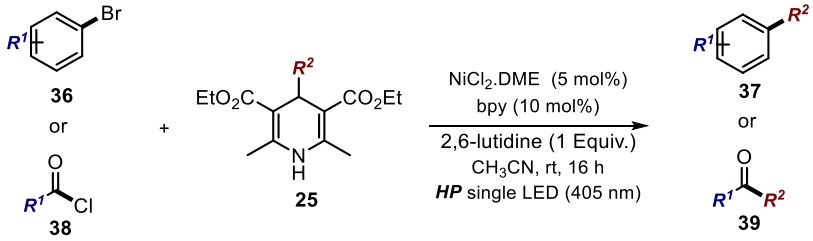

General Procedure B *(0.1 mmol scale reaction).* In a Schlenk tube, the aryl bromide **36** or the acyl chloride **38** (0.1 mmol, 1 equiv.), the selected 4-alkyl-1,4-dihydropyridines **25** (0.15 mmol, 1.5 equiv.), and lutidine (11 µL, 0.1 mmol, 1 equiv.) were successively added to a suspension of $NiCl_2$·DME (1 mg, 5 mol%) and bipyridine (1.5 mg, 10 mol%) in MeCN (200 □L). The reaction mixture was degassed *via* a freeze pump thaw procedure, and then placed on a 405 nm high-power single LED (λ = 405 nm, irradiance = 50±3 mW/cm^2, as controlled by an external power supply; the set-up is detailed in Figure S10). This set-up secured a reliable irradiation while keeping a constant distance of 1 cm between the reaction vessel and the light source. The reaction was stirred under light irradiation at ambient temperature for the appropriate time (generally 16 hours). Then the reaction mixture was concentrated in vacuo and the residue was purified by flash chromatography (silica gel, appropriate mixture of hexane/ethyl acetate) to afford the corresponding product **37** or **39**. Results on a 0.1 mmol scale are average of two runs.

General Procedure C *(0.5 mmol reaction scale)*. In a 100 mL Schlenk tube (this reaction vessel secures a good ratio between the surface area and volume solvent, thus allowing efficient irradiation of the reaction mixture), the aryl bromide **36** or the acyl chloride **38** (0.5 mmol, 1 equiv.), the selected 4-alkyl-1,4-dihydropyridines **25** (0.75 mmol, 1.5 equiv.), and lutidine (58 µL, 0.5 mmol, 1 equiv.) were successively added to a suspension of $NiCl_2$·DME (5.5 mg, 5 mol%) and bipyridine (7.5 mg, 10 mol%) in MeCN (1 mL). The reaction mixture was degassed *via* a freeze pump thaw procedure, and then placed above a 405 nm high-power single LED (λ = 405 nm, irradiance = 50±3 mW/cm^2, as controlled by an external power supply; the set-up is detailed in Figure S11).

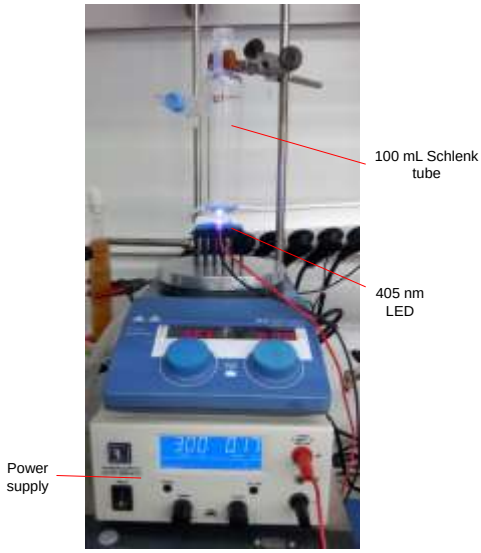

Figure S11. Set-up for 0.5 mmol scale reactions.

This set-up secured a reliable irradiation while keeping a constant distance of 1 cm (using a spacer of 1 cm) between the reaction vessel and the light source.

The reaction was stirred under light irradiation at ambient temperature for the appropriate time (generally 24 hours). Then the reaction mixture was concentrated in vacuo and the residue purified by flash chromatography (silica gel, appropriate mixture of hexane/ethyl acetate) to afford the corresponding products **37** or **39**.

Characterization of products 37

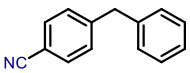

4-Benzylbenzonitrile (37a). Prepared according to the general procedure B, using 4-bromobenzonitrile (0.1 mmol, 18 mg, 1 equiv.) and **25b** (0.15 mmol, 52 mg, 1.5 equiv.); time of irradiation: 16 hours. The crude mixture was purified by flash column chromatography (gradient from pure hexane to hexane/ethyl acetate 9:1) to afford the product as a colorless oil (17 mg, 91% yield, average of two runs).

0.5 mmol scale: Prepared according to the general procedure C, using 4-bromobenzonitrile (0.5 mmol, 90 mg, 1 equiv.) and **25b** (0.75 mmol, 260 mg, 1.5 equiv.); time of irradiation: 24 hours. The crude mixture was purified by flash column chromatography (gradient from pure hexane to hexane/ethyl acetate 9:1) to afford the product as a colorless oil (82 mg, 89% yield). The spectroscopic characterization matched with data reported in the literature.[49]

[49] Vara, B. A., Patel, N. R., Molander, G. A., "O-Benzyl Xanthate Esters under Ni/Photoredox Dual Catalysis: Selective Radical Generation and Csp3–Csp2 Cross-Coupling" *ACS Catal.* **2017**, *7*, 3955.

^{1}H NMR (300 MHz, Chloroform-*d*) δ 7.65 – 7.46 (m, 2H), 7.37 – 7.21 (m, 5H), 7.20 – 7.11 (m, 2H), 4.02 (s, 2H). **^{13}C NMR** (75 MHz, Chloroform-*d*) δ 146.9, 139.4, 132.4, 129.8, 129.1, 128.9, 126.8, 119.1, 110.2, 42.1.

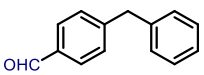

4-Benzylbenzadehyde (37b). Prepared according to general procedure C, using 4-bromobenzaldehyde (0.5 mmol, 90 mg, 1 equiv.) and **25b** (0.75 mmol, 260 mg, 1.5 equiv.); time of irradiation: 24 hours. The crude mixture was purified by flash column chromatography (gradient from pure hexane to hexane/ethyl acetate 9:1) to afford the product as a colorless oil (85 mg, 87% yield). The spectroscopic characterization matched with data reported in the literature.[50]

^{1}H NMR (300 MHz, Chloroform-*d*) δ 9.96 (s, 1H), 7.79 (d, *J* = 8.1 Hz, 2H), 7.39 – 7.26 (m, 4H), 7.23 (d, *J* = 7.0 Hz, 1H), 7.20 – 7.14 (m, 2H), 4.05 (s, 2H). **^{13}C NMR** (75 MHz, Chloroform-*d*) δ 192.1, 148.5, 139.9, 134.8, 130.2, 129.7, 129.1, 128.8, 126.7, 42.2.

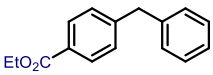

Ethyl 4-benzylbenzoate (37c). Prepared according to the general procedure B, using ethyl 4-bromobenzoate (0.1 mmol, 23 mg, 1 equiv.) and **25b** (0.15 mmol, 52 mg, 1.5 equiv.); time of irradiation: 16 hours. The crude mixture was purified by flash column chromatography (gradient from pure hexane to hexane/ethyl acetate 9:1) to afford the product as a colorless oil (89% NMR yield, the product was isolated with about 10% of ethyl benzoate). The spectroscopic characterization matched with data reported in the literature.[51]

^{1}H NMR (300 MHz, Chloroform-*d*) δ 7.88 (d, *J* = 8.3 Hz, 2H), 7.27 – 7.01 (m, 7H), 4.28 (q, *J* = 7.2 Hz, 2H), 3.94 (s, 2H), 1.29 (t, *J* = 7.1 Hz, 3H). **^{13}C NMR** (75 MHz, Chloroform-*d*) δ 166.7, 146.5, 140.3, 129.9, 129.1, 129.0, 128.7, 128.6, 126.5, 60.9, 42.0, 14.5.

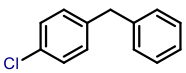

1-Benzyl-4-chlorobenzene (37d). Prepared according to the general procedure C, using 1-bromo-4-chlorobenzene (0.5 mmol, 95 mg, 1 equiv.) and **25b** (0.75 mmol, 260 mg, 1.5 equiv.); time of irradiation: 24 hours. The crude mixture was purified by flash column chromatography (gradient from pure hexane to hexane/ethyl acetate 9:1) to afford the product as a colorless oil (67 mg, 67% yield). The spectroscopic characterization matched with data reported in the literature.[52]

---

[50] Bailey, C. L., Joh, A. Y., Hurley, Z. Q., Anderson, C. L., Singaram, B., "Controlled Reduction of Tertiary Amides to the Corresponding Alcohols, Aldehydes, or Amines Using Dialkylboranes and Aminoborohydride Reagents" *J. Org. Chem.* **2016**, *81*, 3619.

[51] Nakajima, K., Nojima, S., Nishibayashi, Y., "Nickel-and Photoredox-Catalyzed Cross-Coupling Reactions of Aryl Halides with 4-Alkyl-1, 4-dihydropyridines as Formal Nucleophilic Alkylation Reagents" *Angew. Chem. Int. Ed.* **2016**, *55*, 14106.

[52] Vasilopoulos, A., Zultanski, S. L., Stahl, S. S., "Feedstocks to Pharmacophores: Cu-Catalyzed Oxidative Arylation of Inexpensive Alkylarenes Enabling Direct Access to Diarylalkanes" *J. Am. Chem. Soc.* **2017**, *139*, 7705.

^{1}H NMR (300 MHz, Chloroform-*d*) δ 7.72 – 6.88 (m, 9H), 4.00 (s, 2H). **^{13}C NMR** (75 MHz, Chloroform-*d*) δ 140.7, 139.7, 132.0, 130.4, 129.0, 128.7, 128.5, 126.4, 41.4.

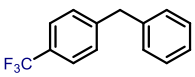

1-Benzyl-4-(trifluoromethyl)benzene (37e). Prepared according to the general procedure C, using 1-bromo-4-(trifluoromethyl)benzene (0.5 mmol, 115 mg, 1 equiv.) and **25b** (0.75 mmol, 260 mg, 1.5 equiv.); time of irradiation: 24 hours. The crude mixture was purified by flash column chromatography (gradient from pure hexane to hexane/ethyl acetate 9:1) to afford the product as a colorless oil (90 mg, 76% yield). The spectroscopic characterization matched with data reported in the literature.[53]

^{1}H NMR (400 MHz, Chloroform-*d*) δ 7.62 (d, *J* = 8.0 Hz, 2H), 7.43 – 7.35 (m, 4H), 7.35 – 7.29 (m, 1H), 7.28 – 7.25 (m, 1H), 4.11 (s, 1H). **^{13}C NMR** (101 MHz, Chloroform-*d*) δ 145.4 (d, *J* = 1.5 Hz), 140.1, 129.3, 129.1, 128.8, 126.6, 125.5 (q, $^{2}J_{C\text{-}F}$ = 3.8 Hz), 124.7 (q, $^{1}J_{C\text{-}F}$ = 271.8 Hz), 41.9. **^{19}F NMR** (376 MHz, Chloroform-*d*) δ -62.4.

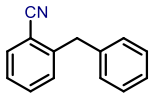

1-Benzyl-3,5-bis(trifluoromethyl)benzene (37f). Prepared according to the general procedure C, using 2-bromobenzonitrile (0.5 mmol, 90 mg, 1 equiv.) and **25b** (0.75 mmol, 260 mg, 1.5 equiv.); time of irradiation: 24 hours. The crude mixture was purified by flash column chromatography (gradient from pure hexane to hexane/ethyl acetate 9:1) to afford the product as a colorless oil (70 mg, 75% yield). The spectroscopic characterization matched with data reported in the literature.[54]

^{1}H NMR (300 MHz, Chloroform-*d*) δ 7.65 (d, *J* = 7.6 Hz, 1H), 7.52 (td, *J* = 7.7, 1.5 Hz, 1H), 7.42 – 7.16 (m, 7H), 4.24 (s, 2H). **^{13}C NMR** (75 MHz, Chloroform-*d*) δ 145.0, 138.8, 133.0, 132.9, 130.1, 129.0, 128.8, 126.9, 126.8, 118.2, 112.6, 40.2.

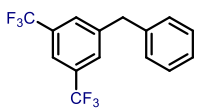

1-Benzyl-3,5-bis(trifluoromethyl)benzene (37g). Prepared according to the general procedure C, using 1-bromo-3,5-bis(trifluoromethyl)benzene (0.5 mmol, 145 mg, 1 equiv.) and **25b** (0.75 mmol, 260 mg, 1.5 equiv.); time of irradiation: 24 hours. The crude mixture was purified by flash column chromatography (gradient from pure hexane to hexane/ethyl acetate 9:1) to afford the product as a colorless oil (126 mg, 83% yield). The spectroscopic characterization matched with data reported in the literature.[55]

---

[53] Nambo, M., Keske, E. C., Rygus, J. P., Yim, J. C.-H., Crudden, C. M., "Development of Versatile Sulfone Electrophiles for Suzuki–Miyaura Cross-Coupling Reactions" *ACS Catal.* **2017**, *7*, 1108.
[54] Liang, F., Ji, X., Zhang, J., Cao, S., "LDA-Mediated Synthesis of ortho-Cyanated Diarylmethanes by Reaction of Fluoroarene with Arylacetonitrile at Room Temperature" *Org. Chem. Front.* **2016**, *3*, 1425.
[55] Chen, C. R., Zhou, S., Biradar, D. B., Gau, H. M., "Extremely Efficient Cross-Coupling of Benzylic Halides with Aryltitanium Tris (isopropoxide) Catalyzed by Low Loadings of a Simple Palladium (II) Acetate/Tris (p-tolyl) phosphine System" *Adv. Synth. Catal.* **2010**, *352*, 1718.

^{1}H NMR (400 MHz, Chloroform-*d*) δ 7.77 (s, 1H), 7.67 (d, *J* = 1.7 Hz, 2H), 7.42 – 7.35 (m, 2H), 7.35 – 7.26 (m, 1H), 7.25 – 7.19 (m, 2H), 4.14 (s, 2H). **^{13}C NMR** (101 MHz, Chloroform-*d*) δ 143.7, 138.9, 131.9 (q, $^{2}J_{C-F}$ = 33.1 Hz), 129.2-129.0 (m), 129.1, 129.1, 129.0, 127.1, 123.5 (d, $^{1}J_{C-F}$ = 272.6 Hz), 120.5 (p, $^{3}J_{C-F}$ = 3.9 Hz), 41.7. **^{19}F NMR** (376 MHz, Chloroform-*d*) δ -62.6.

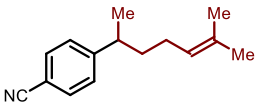

4-(6-Methylhept-5-en-2-yl)benzonitrile (37h). Prepared according to the general procedure C, using 4-bromobenzonitrile (0.5 mmol, 90 mg, 1 equiv.) and diethyl 2,6-dimethyl-4-(6-methylhept-5-en-2-yl)-1,4-dihydropyridine-3,5-dicarboxylate (0.75 mmol, 275 mg, 1.5 equiv.); time of irradiation: 72 hours. The crude mixture was purified by flash column chromatography (gradient from pure hexane to hexane/ethyl acetate 9:1) to afford the product as a (55 mg, 52% yield).

^{1}H NMR (300 MHz, Chloroform-*d*) δ 7.58 (d, *J* = 8.3 Hz, 2H), 7.28 (d, *J* = 8.4 Hz, 2H), 5.05 (tt, *J* = 7.1, 1.4 Hz, 1H), 2.76 (q, *J* = 7.1 Hz, 1H), 2.21 – 1.70 (m, 2H), 1.66 (d, *J* = 1.4 Hz, 3H), 1.65 – 1.52 (m, 2H), 1.50 (d, *J* = 1.3 Hz, 3H), 1.24 (d, *J* = 7.0 Hz, 3H). **^{13}C NMR** (75 MHz, Chloroform-*d*) δ 153.5, 132.3, 132.1, 128.0, 124.0, 119.3, 109.8, 39.8, 38.1, 26.1, 25.8, 22.1, 17.8. **HRMS (ESI):** Calcd for $C_{15}H_{19}NNa$ [M+Na+ , 100 %]: 236.1410, found 236.1405.

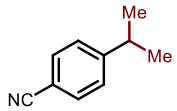

4-isopropylbenzonitrile (37i). Prepared according to the general procedure B, using 4-bromobenzonitrile (0.1 mmol, 18 mg, 1 equiv.) and diethyl 4-isopropyl-2,6-dimethyl-1,4-dihydropyridine-3,5-dicarboxylate (0.15 mmol, 44 mg, 1.5 equiv.); time of irradiation: 16 hours. The crude mixture was purified by flash column chromatography (gradient from pure hexane to hexane/ethyl acetate 9:1) to afford the product as a colorless oil (5 mg, 35% yield, average of two runs). The spectroscopic characterization matched with data reported in the literature.[46]

^{1}H NMR (300 MHz, Chloroform-*d*) δ 7.57 (d, *J* = 8.1 Hz, 2H), 7.32 (d, *J* = 8.1 Hz, 2H), 2.96 (p, *J* = 6.9 Hz, 1H), 1.26 (d, *J* = 6.9 Hz, 6H). **^{13}C NMR** (75 MHz, Chloroform-*d*) δ 154.5, 132.4, 127.4, 119.3, 109.7, 34.5, 23.7.

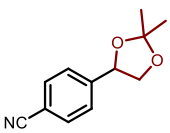

4-(2,2-dimethyl-1,3-dioxolan-4-yl)benzonitrile (37j). Prepared according to the general procedure B, using 4-bromobenzonitrile (0.1 mmol, 18 mg, 1 equiv.) and diethyl 4-(2,2-dimethyl-1,3-dioxolan-4-yl)-2,6-dimethyl-1,4-dihydropyridine-3,5-dicarboxylate (0.15 mmol, 53 mg, 1.5 equiv.); time of irradiation: 16 hours. The crude mixture was purified by flash column chromatography

(gradient from pure toluene to toluene/ethyl acetate 8:2) to afford the product as a colorless oil (15 mg, 77% yield, average of two runs).

^{1}H NMR (300 MHz, Chloroform-*d*) δ 7.65 (d, *J* = 8.3 Hz, 2H), 7.47 (d, *J* = 8.2 Hz, 2H), 5.11 (t, *J* = 7.0 Hz, 1H), 4.35 (dd, *J* = 8.3, 6.4 Hz, 1H), 3.66 (t, *J* = 7.9 Hz, 1H), 1.54 (s, 3H), 1.48 (s, 3H). **^{13}C NMR** (75 MHz, Chloroform-*d*) δ 145.3, 132.5, 126.8, 118.8, 111.9, 110.5, 77.2, 71.4, 26.5, 25.9. **HRMS (ESI):** Calcd for $C_{11}H_{10}NO_2$ [M-Me, 100 %]:188.0717, found 188.0712.

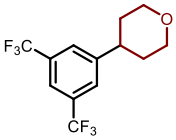

4-(3,5-bis(trifluoromethyl)phenyl)tetrahydro-2*H*-pyran (37k). Prepared according to the general procedure B, using 1-bromo-3,5-bis(trifluoromethyl)benzene (0.1 mmol, 29 mg, 1 equiv.) and diethyl diethyl 2,6-dimethyl-4-(tetrahydro-2H-pyran-4-yl)-1,4-dihydropyridine-3,5-dicarboxylate (0.15 mmol, 51 mg, 1.5 equiv.); time of irradiation: 16 hours. The crude mixture was purified by flash column chromatography (gradient from pure hexane to hexane/ethyl acetate 9:1) to afford the product as a white solid (scale 0.1 mmol: 17 mg, 57% yield, average of two runs). The spectroscopic characterization matched with data reported in the literature.[55]

^{1}H NMR (400 MHz, Chloroform-*d*) δ 7.74 (s, 1H), 7.67 (s, 2H), 4.26 – 3.88 (m, 2H), 3.65 – 3.37 (m, 2H), 3.10 – 2.77 (m, 1H), 1.92 – 1.78 (m 4H). **^{13}C NMR** (101 MHz, Chloroform-*d*) δ 148.3, 132.0 (q, $^{2}J_{C\text{-}F}$ = 33.1 Hz), 127.4 – 126.9 (m), 123.5 (q, $^{1}J_{C\text{-}F}$ = 272.7 Hz), 120.6 (dt, *J* = 7.8, 3.8 Hz), 68.1, 41.5, 33.7. **^{19}F NMR** (376 MHz, Chloroform-*d*) δ -63.0.

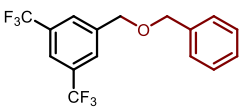

1-((Benzyloxy)methyl)-3,5-bis(trifluoromethyl)benzene (37l). Prepared according to general procedure C, using 1-bromo-3,5-bis(trifluoromethyl)benzene (0.5 mmol, 145 mg, 1 equiv.) and diethyl 2,6-dimethyl-4-(phenoxymethyl)-1,4-dihydropyridine-3,5-dicarboxylate (0.75 mmol, 300 mg, 1.5 equiv.); time of irradiation: 72 hours. The crude mixture was purified by flash column chromatography (gradient from pure hexane to hexane/ethyl acetate 9:1) to afford the product as a colorless oil scale (83 mg, 50% yield).

^{1}H NMR (300 MHz, Chloroform-*d*) δ 7.86 (s, 3H), 7.63 – 7.05 (m, 5H), 4.68 (s, 4H). **^{13}C NMR** (75 MHz, Chloroform-*d*) δ 141.2, 137.5, 131.8 (q, *J* = 33.3 Hz), 128.8, 128.2, 128.1, 127.5, 121.7 – 121.4 (m), 73.2, 70.6. **^{19}F NMR** (376 MHz, Chloroform-*d*) δ -63.0. **HRMS (ESI):** Calcd for $C_9H_5F_6$ [M-OCH_2Ph , 100 %]: 227.0295, found 227.0286.

Characterization of ketones 39

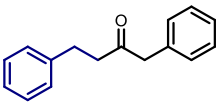

1,4-Diphenylbutan-2-one (39a). Prepared according to the general procedure B, using ethyl 4-chloro-4-oxobutanoate (0.1 mmol, 17 mg, 1 equiv.) and **25b** (0.15 mmol, 52 mg, 1.5 equiv.); time of irradiation: 16 hours. The crude mixture was purified by flash column chromatography (gradient from pure hexane to hexane/ethyl acetate 9:1) to afford the product as a colourless oil (16 mg, 71% yield, average of two runs).

0.5 mmol scale: Prepared according to the general procedure C, using ethyl 4-chloro-4-oxobutanoate (0.5 mmol, 85 mg, 1 equiv.) and **25b** (0.75 mmol, 260 mg, 1.5 equiv.); time of irradiation: 24 hours. The crude mixture was purified by flash column chromatography (gradient from pure hexane to hexane/ethyl acetate 9:1) to afford the product as a colourless liquidcolorless oil (63 mg, 56% yield). The spectroscopic characterization matched with data reported in the literature.[56]

^{1}H NMR (300 MHz, Chloroform-*d*) δ 7.25 – 6.92 (m, 10H), 3.57 (s, 2H), 2.78 (dd, *J* = 8.2, 5.7 Hz, 2H), 2.67 (ddd, *J* = 8.2, 6.5, 1.8 Hz, 2H). **^{13}C NMR** (75 MHz, Chloroform-*d*) δ 207.5, 141.0, 134.2, 129.5, 128.8, 128.6, 128.4, 127.1, 126.2, 50.5, 43.6, 29.9.

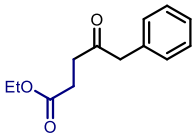

Ethyl 4-oxo-5-phenylpentanoate (39b). Prepared according to the general procedure B, using ethyl 4-chloro-4-oxobutanoate (0.1 mmol, 17 mg, 1 equiv.) and **25b** (0.15 mmol, 52 mg, 1.5 equiv.); time of irradiation: 16 hours. The crude mixture was purified by flash column chromatography (gradient from pure hexane to hexane/ethyl acetate 9:1) to afford the product as a colourless oil (12 mg, 55% yield, average of two runs). The spectroscopic characterization matched with data reported in the literature.[57]

^{1}H NMR (400 MHz, Chloroform-*d*) δ 7.38 – 7.33 (m, 2H), 7.32 – 7.26 (m, 1H), 7.26 – 7.21 (m, 2H), 4.13 (q, *J* = 7.1 Hz, 2H), 3.76 (s, 2H), 2.78 (t, *J* = 6.6 Hz, 2H), 2.57 (dd, *J* = 7.0, 6.2 Hz, 2H), 1.25 (t, *J* = 7.1 Hz, 3H). **^{13}C NMR** (101 MHz, Chloroform-*d*) δ 206.6, 172.8, 134.2, 129.6, 128.9, 127.2, 60.8, 50.2, 36.6, 28.2, 14.3.

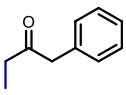

1-Phenylbutan-2-one (39c). Prepared according to the general procedure B, using propionyl chloride (0.1 mmol, 9 mg, 1 equiv.) and **25b** (0.15 mmol, 52 mg, 1.5 equiv.); time of irradiation: 16 hours. The crude mixture was purified

[56] Xiao, L.-J., Fu, X.-N., Zhou, M.-J., Xie, J.-H., Wang, L.-X., Xu, X.-F., Zhou, Q.-L., "Nickel-Catalyzed Hydroacylation of Styrenes with Simple Aldehydes: Reaction Development and Mechanistic Insights" *J. Am. Chem. Soc.* **2016**, *138*, 2957.

[57] Bao, R., Valverde, S., Herradón, B., "The Claisen-Johnson Rearrangement Route to 1, 4-dicarbonyl Compounds: Synthesis of Ethyl 4-ethoxy-4-alkenoates as Masked 4-oxo Esters" *Synlett* **1992**, *1992*, 217.

by flash column chromatography (gradient from pure hexane to hexane/ethyl acetate 9:1) to afford the product as a colourless oil (9 mg, 62% yield, average of two runs). The spectroscopic characterization matched with data reported in the literature.[58]

^{1}H NMR (400 MHz, Chloroform-*d*) δ 7.36 – 7.30 (m, 2H), 7.29 – 7.24 (m, 1H), 7.23 – 7.18 (m, 2H), 3.69 (s, 2H), 2.47 (q, *J* = 7.3 Hz, 2H), 1.03 (t, *J* = 7.3 Hz, 3H). **^{13}C NMR** (101 MHz, Chloroform-*d*) δ 209.1, 134.6, 129.5, 128.8, 127.1, 50.0, 35.4, 7.9.

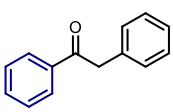

1,2-Diphenylethan-1-one (39d). Prepared according to the general procedure B, using benzoyl chloride (0.1 mmol, 14, mg, 1 equiv.) and **25b** (0.15 mmol, 52 mg, 1.5 equiv.); time of irradiation: 16 hours. The crude mixture was purified by flash column chromatography (gradient from pure hexane to hexane/ethyl acetate 9:1) to afford the product as a white solid (9 mg, 46% yield, average of two runs). The spectroscopic characterization matched with data reported in the literature.[59]

^{1}H NMR (400 MHz, Chloroform-*d*) δ 8.07 – 8.02 (m, 2H), 7.61 – 7.56 (m, 1H), 7.51 – 7.46 (m, 2H), 7.38 – 7.33 (m, 2H), 7.32 – 7.25 (m, 3H), 4.32 (s, 2H). **^{13}C NMR** (101 MHz, Chloroform-*d*) δ 197.7, 136.7, 134.7, 133.3, 129.6, 128.8, 128.8, 128.7, 127.0, 45.6.

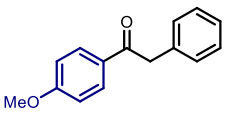

1-(4-Methoxyphenyl)-2-phenylethan-1-one (39e). Prepared according to the general procedure B, using 4-methoxybenzoyl chloride (0.1 mmol, 17 mg, 1 equiv.) and **25b** (0.15 mmol, 52 mg, 1.5 equiv.); time of irradiation: 16 hours. The crude mixture was purified by flash column chromatography (gradient from pure hexane to hexane/ethyl acetate 9:1) to afford the product as a white solid (16 mg, 71% yield, average of two runs).

0.5 mmol scale: Prepared according to general procedure C using 4-methoxybenzoyl chloride (0.5 mmol, 85, mg, 1 equiv.) and **1a** (0.15 mmol, 260 mg, 1.5 equiv.); time of irradiation: 24 hours. The crude mixture was purified by flash column chromatography (gradient from pure hexane to hexane/ethyl acetate 9:1) to afford the product as a white solid (70 mg, 62% yield). The spectroscopic characterization matched with data reported in the literature.[60]

^{1}H NMR (300 MHz, Chloroform-*d*) δ 8.09 – 7.79 (m, 2H), 7.31 (dtt, *J* = 8.0, 6.0, 2.9 Hz, 5H), 7.02 – 6.75 (m, 2H), 4.25 (s, 2H), 3.87 (s, 3H). **^{13}C NMR** (75 MHz, Chloroform-*d*) δ 196.3, 163.6, 135.1, 131.0, 129.7, 129.5, 128.7, 126.9, 113.9, 55.6, 45.4.

---

[58] Zhang, G., Hu, X., Chiang, C.-W., Yi, H., Pei, P., Singh, A. K., Lei, A., "Anti-Markovnikov Oxidation of β-alkyl Styrenes with H2O as the Terminal Oxidant" *J. Am. Chem. Soc.* **2016**, *138*, 12037.

[59] Simmons, B. J., Weires, N. A., Dander, J. E., Garg, N. K., "Nickel-Catalyzed Alkylation of Amide Derivatives" *ACS Catal.* **2016**, *6*, 3176.

[60] Amani, J., Molander, G. A., "Direct Conversion of Carboxylic Acids to Alkyl Ketones" *Org. Lett.* **2017**, *19*, 3612.

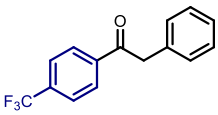

2-Phenyl-1-(4-(trifluoromethyl)phenyl)ethan-1-one (39f). Prepared according to the general procedure B, using 4-(trifluoromethyl)benzoyl chloride (21 mg, 1 equiv.) and **25b** (0.15 mmol, 52 mg, 1.5 equiv.); time of irradiation: 16 hours. The crude mixture was purified by flash column chromatography (gradient from pure hexane to hexane/ethyl acetate 9:1) to afford the product as a white solid (12 mg, 46% yield, average of two runs). The spectroscopic characterization matched with data reported in the literature.[60]

^{1}H NMR (400 MHz, Chloroform-*d*) δ 8.10 (dp, *J* = 7.7, 0.9 Hz, 2H), 7.75 – 7.69 (m, 2H), 7.38 – 7.31 (m, 2H), 7.30 – 7.25 (m, 3H), 4.31 (s, 2H). **^{13}C NMR** (101 MHz, Chloroform-*d*) δ 196.8, 139.4, 134.6 (d, $^2J_{C\text{-}F}$ = 32.9 Hz), 133.9, 129.5, 129.1, 129.0, 127.3, 125.9 (q, $^3J_{C\text{-}F}$ = 3.7 Hz), 123.7 (d, $^1J_{C\text{-}F}$ = 272.7 Hz), 46.0. **^{19}F NMR** (376 MHz, Chloroform-*d*) δ -62.9.

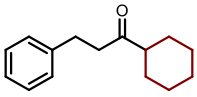

1-Cyclohexyl-3-phenylpropan-1-one (39g). Prepared according to general procedure B, using 3-phenylpropanoyl chloride (0.1 mmol, 17 mg, 1 equiv.) and diethyl 4-cyclohexyl-2,6-dimethyl-1,4-dihydropyridine-3,5-dicarboxylate (0.15 mmol, 50 mg, 1.5 equiv.); time of irradiation: 16 hours. The crude mixture was purified by flash column chromatography (gradient from pure hexane to hexane/ethyl acetate 9:1) to afford the product as a colorless oil (12 mg, 56% yield, average of two runs). The spectroscopic characterization matched with data reported in the literature.[60]

^{1}H NMR (500 MHz, Chloroform-*d*) δ 7.30 – 7.24 (m, 2H), 7.22 – 7.16 (m, 3H), 2.86 – 2.90 (m, 2H), 2.79 – 2.70 (m, 2H), 2.31 (tt, *J* = 11.3, 3.4 Hz, 1H), 1.84 – 1.73 (m, 4H), 1.64 – 1.67 (m, 1H), 1.41 – 1.14 (m, 5H). **^{13}C NMR** (126 MHz, Chloroform-*d*) δ 213.3, 141.6, 128.6, 128.5, 126.1, 51.1, 42.4, 29.9, 28.6, 26.0, 25.8.

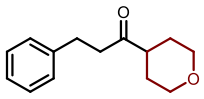

3-Phenyl-1-(tetrahydro-2H-pyran-4-yl)propan-1-one (39h). Prepared according to the general procedure B, using 3-phenylpropanoyl chloride (0.1 mmol, 17 mg, 1 equiv.) and diethyl diethyl 2,6-dimethyl-4-(tetrahydro-2H-pyran-4-yl)-1,4-dihydropyridine-3,5-dicarboxylate (0.15 mmol, 51 mg, 1.5 equiv.); time of irradiation: 16 hours. The crude mixture was purified by flash column chromatography (gradient from pure hexane to hexane/ethyl acetate 9:1) to afford the product as a colorless oil (10 mg, 46% yield, average of two runs). The spectroscopic characterization matched with data reported in the literature.[60]

^{1}H NMR (500 MHz, Chloroform-*d*) δ 7.30 – 7.24 (m, 2H), 7.21 – 7.15 (m, 3H), 3.97 (ddd, *J* = 11.4, 4.2, 2.6 Hz, 2H), 3.39 (td, *J* = 11.4, 2.9 Hz, 2H), 2.92 – 2.88 (m, 2H), 2.83 – 2.72 (m, 2H), 2.53 – 2.47 (m, 1H), 1.80 – 1.57 (m, 4H). **^{13}C NMR** (126 MHz, Chloroform-*d*) δ 211.1, 141.3, 128.6, 128.5, 126.3, 67.4, 47.9, 42.1, 29.8, 28.2.

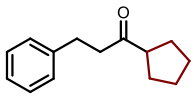

1-Cyclopentyl-3-phenylpropan-1-one (39i). Prepared according to the general procedure B, using 3-phenylpropanoyl chloride (0.1 mmol, 17 mg, 1 equiv.) and diethyl 4-cyclopentyl-2,6-dimethyl-1,4-dihydropyridine-3,5-dicarboxylate (0.15 mmol, 48 mg, 1.5 equiv.); time of irradiation: 16 hours. The crude mixture was purified by flash column chromatography (gradient from pure hexane to hexane/ethyl acetate 9:1) to afford the product as a colourless liquid (12 mg, 59% yield, average of two runs). The spectroscopic characterization matched with data reported in the literature.[61]

^{1}H NMR (500 MHz, Chloroform-*d*) δ 7.30 – 7.25 (m, 2H), 7.21 – 7.16 (m, 3H), 2.92 – 2.89 (m, 2H), 2.84 (ddd, *J* = 16.0, 8.6, 7.3 Hz, 1H), 2.80 – 2.74 (m, 2H), 1.82 – 1.51 (m, 8H). **^{13}C NMR** (126 MHz, Chloroform-*d*) δ 212.4, 141.5, 128.6, 128.5, 126.1, 51.7, 43.5, 30.0, 28.9, 26.1.

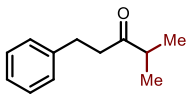

4-Methyl-1-phenylpentan-3-one (39j). Prepared according to the general procedure B, using 3-phenylpropanoyl chloride (0.1 mmol, 17 mg, 1 equiv.) and diethyl 4-isopropyl-2,6-dimethyl-1,4-dihydropyridine-3,5-dicarboxylate (0.15 mmol, 44 mg, 1.5 equiv.); time of irradiation: 16 hours. The crude mixture was purified by flash column chromatography (gradient from pure hexane to hexane/ethyl acetate 9:1) to afford the product as a colourless oil (10 mg, 57% yield, average of two runs). The spectroscopic characterization matched with data reported in the literature.[61]

^{1}H NMR (400 MHz, Chloroform-*d*) δ 7.31 – 7.25 (m, 2H), 7.23 – 7.15 (m, 3H), 2.93 – 2.85 (m, 2H), 2.79 – 2.75 (m, 2H), 2.57 (sept, *J* = 6.9 Hz, 1H), 1.07 (d, *J* = 6.9 Hz, 6H). **^{13}C NMR** (101 MHz, Chloroform-*d*) δ 213.9, 141.5, 128.6, 128.5, 126.2, 42.1, 41.2, 30.0, 18.3.

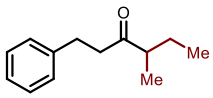

4-Methyl-1-phenylhexan-3-one (39k). Prepared according to the general procedure B, using 3-phenylpropanoyl chloride (0.1 mmol, 17 mg, 1 equiv.) and diethyl 4-(sec-butyl)-2,6-dimethyl-1,4-dihydropyridine-3,5-dicarboxylate (0.15 mmol, 46 mg, 1.5 equiv.); time of irradiation: 16 hours. The crude mixture was purified by flash column chromatography (gradient from pure hexane to hexane/ethyl acetate 9:1) to afford the product as a colourless oil (10 mg, 53% yield, average of two runs). The spectroscopic characterization matched with data reported in the literature.[61]

^{1}H NMR (500 MHz, Chloroform-*d*) δ 7.30 – 7.25 (m, 2H), 7.21 – 7.16 (m, 3H), 2.92 – 2.86 (m, 2H), 2.78 – 2.72 (m, 2H), 2.43 (h, *J* = 6.8 Hz, 1H), 1.71 – 1.61 (m, 1H), 1.42 – 1.31 (m,

[61] Amani, J., Molander, G. A., "Synergistic Photoredox/Nickel Coupling of Acyl Chlorides with Secondary Alkyltrifluoroborates: Dialkyl Ketone Synthesis." *J. Org. Chem.* **2017**, *82*, 1856

1H), 1.04 (d, *J* = 6.9 Hz, 3H), 0.84 (t, *J* = 7.4 Hz, 3H). **^{13}C NMR** (126 MHz, Chloroform-*d*) δ 213.9, 141.5, 128.6, 128.5, 126.2, 48.2, 42.9, 29.9, 26.0, 15.9, 11.8.

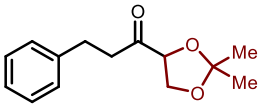

1-(4,4-Dimethyl-1,3-dioxolan-2-yl)-3-phenylpropan-1-one (39l). Prepared according to the general procedure B, using 3-phenylpropanoyl chloride (0.1 mmol, 17 mg, 1 equiv.) and diethyl 4-(2,2-dimethyl-1,3-dioxolan-4-yl)-2,6-dimethyl-1,4-dihydropyridine-3,5-dicarboxylate (0.15 mmol, 53 mg, 1.5 equiv.); time of irradiation: 16 hours. The crude mixture was purified by flash column chromatography (gradient from pure hexane to hexane/ethyl acetate 9:1) to afford the product as a colourless oil (12 mg, 51% yield, average of two runs). The spectroscopic characterization matched with data reported in the literature.[62]

^{1}H NMR (500 MHz, Chloroform-*d*) δ 7.31 – 7.26 (m, 2H), 7.21 – 7.18 (m, 3H), 4.42 (dd, *J* = 7.8, 5.6 Hz, 1H), 4.17 (dd, *J* = 8.7, 7.8 Hz, 1H), 3.92 (dd, *J* = 8.7, 5.6 Hz, 1H), 2.98 – 2.88 (m, 4H), 1.45 (s, 3H), 1.38 (s, 3H). **^{13}C NMR** (126 MHz, Chloroform-*d*) δ 210.1, 141.1, 128.6, 128.5, 126.3, 111.1, 80.4, 66.6, 40.4, 29.1, 26.2, 25.1.

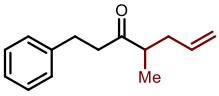

4-Methyl-1-phenylhept-6-en-3-one (39m). Prepared according to the general procedure B, using 3-phenylpropanoyl chloride (0.1 mmol, 17, mg, 1 equiv.) and diethyl 4-(hex-5-en-2-yl)-2,6-dimethyl-1,4-dihydropyridine-3,5-dicarboxylate (0.15 mmol, 50 mg, 1.5 equiv.); time of irradiation: 16 hours. The crude mixture was purified by flash column chromatography (gradient from pure hexane to hexane/ethyl acetate 9:1) to afford the product as a colourless oil (12 mg, 56% yield, average of two runs). The spectroscopic characterization matched with data reported in the literature.[63]

^{1}H NMR (400 MHz, Chloroform-*d*) δ 7.32 – 7.25 (m, 2H), 7.23 – 7.14 (m, 3H), 5.77 – 5.60 (m, 1H), 5.08 – 4.95 (m, 2H), 2.91 – 2.87 (m, 2H), 2.78 – 2.73 (m, 2H), 2.57 (h, *J* = 6.9 Hz, 1H), 2.42 – 2.32 (m, 1H), 2.14 – 2.03 (m, 1H), 1.05 (d, *J* = 7.0 Hz, 3H). **^{13}C NMR** (101 MHz, Chloroform-*d*) δ 213.0, 141.4, 135.8, 128.6, 128.5, 126.2, 117.0, 46.3, 43.1, 37.2, 29.8, 16.1.

---

[62] Vellakkaran, M., Andappan, M. M., Kommu, N., "Replacing a Stoichiometric Silver Oxidant with Air: Ligated Pd (II)-catalysis to β-aryl Carbonyl Derivatives with Improved Chemoselectivity" *Green Chem.* **2014**, *16*, 2788.

[63] Gazzard, L., Motherwell, W., Sandham, D., "Rhodium Promoted Isomerisation of Allylic Alkoxides: a new Method for Enolate Anion Formation" *J. Chem. Soc. Perkin Trans. 1* **1999**, 979.

Mechanistic Experiments

Irradiation of 25b

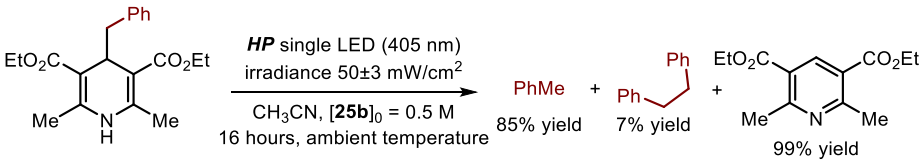

In a Schlenk tube, diethyl 4-benzyl-1,4-dihydropyridine-3,5-dicarboxylate **25b** (0.1 mmol, 1 equiv.) was dissolved in CH_3CN (200 □L). The reaction mixture was degassed *via* a freeze pump thaw procedure, and then placed above a 405 nm high-power single LED (λ = 405 nm, irradiance = 50 mW/cm^2, as controlled by an external power supply). The reaction was stirred under visible light irradiation at ambient temperature for 16 hours. Then, the reaction mixture was analyzed by NMR, and GC-MS specstroscopic analysis, confirming the formation toluene, 1,2-diphenyltehane, and the corresponding pyridine. Yields were determined by ^{1}H NMR analysis of the crude mixture using trichloroethylene as the internal standard.

Studies on the effect of the light irradiance

The photodegradation of **25b**, discussed in Section D1, was used as the test reaction to evaluate the effect of the light intensity, which can directly influence the photochemistry of Bn-DHP **25b**.

A solution of **25b** was irradiated with a high power LED emitting at 405 nm, while the power supplier was used to modulate the irradiance. We measured the formation of the pyridine, formed from the photochemical activity of **25b**, to calculate the reactivity.

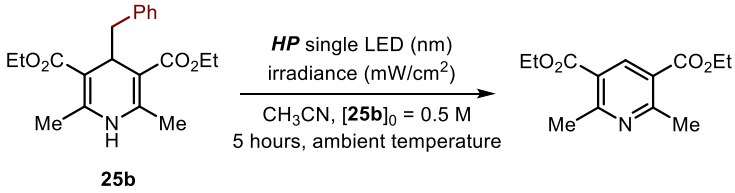

entry	wavelength (nm)	irradiance (mW/cm^2)	yield (%)
1	405	10	30
2	405	30	53
3	405	40	66
4	405	50	88

Reaction conditions: DHP **25b** (34 mg, 0.1 mmol) was dissolved in MeCN (200 µL) and irradiated with a HP single LED for 5 hours. Yields determined by ^{1}H NMR spectroscopy analysis using trichloroethylene as the internal standard; incomplete reaction returned unreacted **25b**.

Radical trapping experiment

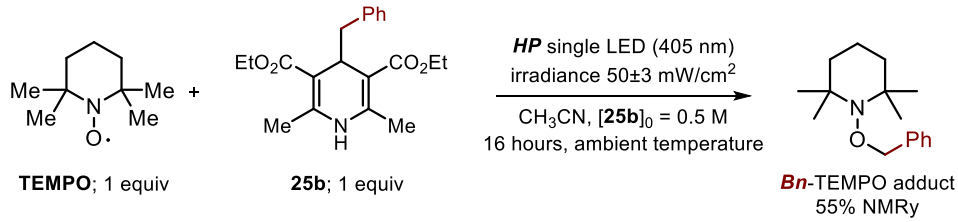

In a Schlenk tube, **25b** (0.1 mmol, 1 equiv) and TEMPO (0.1 mmol, 1 equiv) were dissolved in CH_3CN (200 □L). The reaction mixture was degassed *via* a freeze pump thaw procedure, and then placed above a 405 nm high-power single LED (λ = 405 nm, irradiance = 50 mW/cm^2, as controlled by an external power supply). The reaction was stirred under light irradiation at ambient temperature for 16 hours. Then, the reaction mixture was analyzed by NMR and GC-MS specstroscopic analysis, confirming the formation of the Bn-TEMPO adduct. The ^1H NMR yield was determined using trichloroethylene as the internal standard. Diadnotic signals: **^1H NMR** (400 MHz, Chloroform-*d*) δ 7.41 – 7.34 (m, 5H), 4.83 (s, 2H), 1.87 – 1.47 (m, 6H), 1.26 (s, 6H), 1.15 (s, 6H). The spectroscopic characterization of the Bn-TEMPO adduct matched with data reported in the literature.[64]

A control experiment performed in the absence of light did not lead to the formation of the Bn-TEMPO adduct while returning the unreacted starting substrates.

Quantum Yield Measurement

Determination of the quantum yield[65] was achieved running the reactions using an Osa-Optoelectronic 405nm high power LED. Reactions were carried out in an argon purged flat bottom vial keeping the distance between the light source and vessel at 1 cm with a 3D printed spacer. Specifications from the supplier allowed the determination of the photon flux. The supplier provides the radiant intensity value, regulating the inlet current at 350 mA with a power supply.

The radiant intensity **Ie,Ω**(mW/sr) for the 405 nm LED with an inlet current of 350 mA corresponds to:

$$\mathbf{I_{e,\Omega} = 110\ mW/sr}$$

With a distance between the light source and the vessel of 1 cm, the irradiance **Ee** (mW/cm2) can be calculated:

$$\mathbf{E_e = I_{e,\Omega} * 1\ sr/cm^2 = 110\ mW/cm^2}$$

[64] Nomura, M., Takayama, C., Kajitani, M., "Electrochemical Behavior of Nickeladithiolene S, S '-Dialkyl Adducts: Evidence for the Formation of a Metalladithiolene Radical by Electrochemical Redox Reactions" *Inorg. Chem.* **2003**, *42*, 6441.

[65] Murov, S. L., Carmichael, I., Hug, G. L., "Handbook of photochemistry". 1993; CRC Press.

The surface of the vial is:

$$\mathbf{A=1{,}5386\ cm^2}$$

The power received by the reaction mixture is:

$$\mathbf{P= 110\ mW/cm^2 * 1{,}5386\ cm^2 = 169.246\ mW}$$

Since W corresponds to J/s and knowing that at 405 nm the energy of the photons is:[66]

$$\mathbf{Ep,_{405} = 295370\ J/mol}$$

the photon flux can be calculated:

$$\textbf{\textit{photon flux}} = \mathbf{F= P/Ep,_{405} = 5.73x10^{-7}\ ens/s}$$

The absorbance of the reaction mixture at 405 nm, measured using a Shimadzu 2401PC UV-Vis spectrophotometer in 10 mm path quartz, was: *A*(405 nm) >3. Since the transmittance of photons at is sufficiently small, it can be assumed that all of the photons which pass through the cell are absorbed.

The moles of product **37** formed for the model reaction were determined by GC measurement (FID detector) using 4-methylbenzonitrile as the internal standard.
The moles of product per unit of time are related to the number of incident photons. According to this, if the moles of product (x) are plotted versus the moles of incident photons ($q^0_{n,p}\cdot dt$), the slope gives the overall quantum yield (Φ) of the process under study.

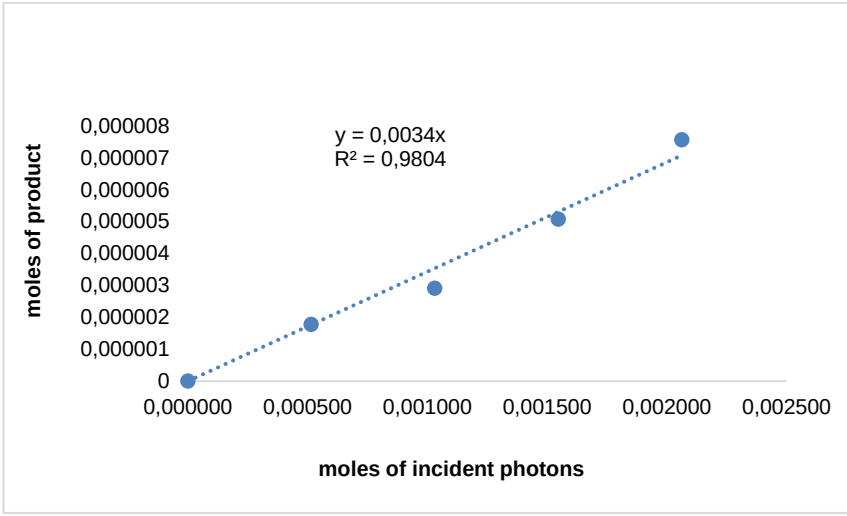

[66] The emission from the HP LED is symmetric, with a maximum centered at 405 nm and an emission band of 30 nm; as an approximation, we considered the LED emission at 405 nm as monochromatic.

The quantum yield (Φ) of the photochemical benzylation of the 4-bromobenzonitrile **36a** with Bn-DHP **25b** was calculated to be **0.0034**.

Chapter VI

General Conclusions

Photochemistry is the branch of chemistry that deals with the interaction between light and molecules. The chemical reactivity of electronically excited species differs fundamentally from that in the ground state. An excited-state molecule is both a better electron donor and a better electron acceptor than in the ground state and behaves respectively as a better reductant and a better oxidant.

Within this doctoral thesis, we demonstrated that transiently generated chiral iminium ions, which are key intermediates in polar enantioselective organocatalytic processes, can enable previously inaccessible reactivities when reaching an excited state upon visible-light absorption, while inducing effective stereochemical control over the ensuing C–C bond-forming event. We applied this photochemical mode of substrate activation to develop an enantioselective β-benzylations of enals (Chapter III).

We were also able to extend the excited iminium ion chemistry to several donor compounds. Relying on the analysis of the redox potential of the substrates, we evaluated the possibility to generate alkyl radicals from various precursors. This investigation resulted in the development of a method for the direct regio- and stereoselective installation of alkyl fragments at the β position of α,β–unsaturated aldehydes. The chemistry relies on the visible light excitation of chiral iminium ions, which turns them into strong oxidants able to generate C(sp^3)-centered radicals from readily available 4-alkyl-1,4-dihydropyridines (Chapter IV).

Ultimately, in Chapter V we have documented that 4-alkyl-1,4-dihydropyiridines can unveil a rich photochemistry upon light excitation. Selective absorption of violet light turns them into strong reducing agents that can activate reagents *via* single-electron transfer manifolds while undergoing a homolytic cleavage to generate C(sp^3)-centered radicals. This light-triggered dual reactivity profile was integrated within a nickel catalytic cycle to enable C(sp^3)–C(sp^2) cross coupling reactions without the need for an external photoredox catalysis. We exploited this reactivity to develop other photochemical radical transformations, including a Giese-type radical conjugate addition and a nickel-catalyzed radical transfer amidation.

Overall, this doctoral thesis demonstrates that the photoexcitation of chemical species is powerful tool to unlock reactivities that are not achievable through the classical ground-state chemistry.

UNIVERSITAT ROVIRA I VIRGILI
PHOTOCHEMICAL STRATEGIES FOR CARBON–CARBON FORMING PROCESSES
Luca Buzzetti

UNIVERSITAT ROVIRA I VIRGILI
PHOTOCHEMICAL STRATEGIES FOR CARBON–CARBON FORMING PROCESSES
Luca Buzzetti

UNIVERSITAT ROVIRA I VIRGILI
PHOTOCHEMICAL STRATEGIES FOR CARBON–CARBON FORMING PROCESSES
Luca Buzzetti

UNIVERSITAT
ROVIRA i VIRGILI